THE UNIVERSITY
of EDINBURGH

Defining the role of Notch Signalling in Intrahepatic Cholangiocarcinoma

Rachel Guest

Doctor of Philosophy

Stem Cell Biology and Regenerative Medicine

University of Edinburgh

2014

ABSTRACT

Intrahepatic cholangiocarcinoma (ICC) is an aggressive malignancy with a dismal prognosis. Few patients present with disease amenable to resection and chemotherapy is not curative. The incidence of ICC is rising worldwide and new therapeutic approaches are urgently required. Notch signalling is critical for the embryological development and regeneration of the biliary tree in the mammalian liver. Dysregulation of Notch is known to drive tumorigenesis in a range of solid and haematological malignancies and the aim of this work was to define its contribution to the pathogenesis of ICC.

Transgenic overexpression of Notch1 has been described to result in the formation of biliary lineage tumours in the liver. I have used resected human tissue, a chemically-induced model of ICC in rat and a novel transgenic murine model in which the tumour suppressor p53 is conditionally deleted from biliary epithelia, to demonstrate that endogenous Notch signalling is acting via the Notch3 receptor to drive tumorigenesis. I use multiple independent methods of Notch3 blockade to establish that Notch3 promotes epithelial cell survival and self-renewal in ICC and demonstrate that Notch3 inhibition significantly attenuates tumour growth *in vivo*.

My data suggest that Notch3 promotes activity through the PI3K/AKT cell survival cascade via a mechanism independent of the effector of canonical Notch, RBPJκ. Given the significant toxicity associated with gamma-secretase inhibitors these findings offer a novel and specific target for further investigation and future therapeutic development in ICC.

DECLARATION

This dissertation has been written by me and represents my own work. All experiments described herein were performed by me, but where I have collaborated with other researchers this is stated within the text. These data have not been submitted for any other degree or professional qualification.

ACKNOWLEDGMENTS

I would like to offer my heartfelt thanks to my supervisor Stuart Forbes for his unwavering support and encouragement throughout the PhD. Without him I would never have had the courage to even start this endeavour. I am indebted to my second supervisor Owen Sansom. His guidance and advice have been invaluable and his insatiable knowledge of cancer biology a true inspiration. I extend a special thanks to the department of surgery in Edinburgh for supporting my forays into science; particularly Steve Wigmore who has been a mentor and kindred spirit in believing surgeons have a contribution to make to biological understanding. I would also like to thank Luke Boulter, Wei-Yu Lu and Sarah Minnis-Lyons for being such excellent and good-humoured companions for scientific discovery. I thank Davina Wotjacha for teaching me so much about the practicalities of work at the bench and the Wellcome Trust for funding the project so generously. Lastly, I would like to thank my family for bringing so much joy to my life. This thesis is dedicated to Bob Philp.

List of Tables

List of Figures

List of Abbreviations

αSMA	Alpha Smooth Muscle Actin
ALT	Alanine Transaminase
ALP	Alkaline Phosphatase
AST	Aspartate Aminotransferase
BNF	Betanapthoflavone
BrdU	5-bromo-2-deoxyuridine
BTC	Biliary Tract Cancer
CCL_4	Carbon Tetrachloride
CK	Cytokeratin
CSC	Cancer Stem Cell
DAB	Diaminobenzidine
DAPI	4',6-diamidino-2-phenylindole
DAPT	N-[N-(3,5-Difluorophenacetyl)-L-alanyl]-S-phenylglycine t-butyl ester (a gamma-secretase inhibitor)
DDC	3,5-diethoxycarbonyl-1,4-dihydrocollidine Diet
DMSO	Dimethyl Sulphoxide
ECC	Extrahepatic Cholangiocarcinoma
EGF	Epidermal Growth Factor
eYFP	Enhanced Yellow Fluorescent Protein
FACS	Fluorescence-Activated Cell Sorting
FCS	Fetal Calf Serum

GAPDH	Glyceraldehyde 3-phosphate dehydrogenase
HAT	Histone acetyltransferase
HCC	Hepatocellular Carcinoma
HDAC	Histone deacetylase
HET	Heterozygote
HOM	Homozygote
HPC	Hepatic Progenitor Cell
HRP	Horseradish Peroxidase
ICC	Intrahepatic Cholangiocarcinoma
I.P.	Intraperitoneal
LB	Lysogeny broth
NEXT	Notch Extracellular Truncation
N-ICD	Notch Intracellular Domain
NRR	Negative Regulatory Region
NSCLC	Non-Small Cell Lung Cancer
PanCK	PanCytokeratin
PanIN	Pancreatic Intraepithelial Neoplasia
PBS	Phosphate Buffered Saline
PCR	Polymerase Chain Reaction
PDA	Pancreatic Ductal Adenocarcinoma
RAM	RBPJk Association Molecule

RBPJκ	Recombination signal Bindin Protein for immunoglobulin kappa J region
RNAi	RNA Interference
Rt-qPCR	Reverse Transcription Quantitative Polymerase Chain Reaction
SDS-PAGE	Sodium dodecyl sulphate polyacrylamide gel electrophoresis
SEM	Standard Error of the Mean
siRNA	Short Interfering RNA
TAA	Thioacetamide
TM	Tamoxifen
TSA	Trichostatin A
TUNEL	Terminal deoxynucleotidyl transferase dUTP nick end labelling
WT	Wild Type

Chapter 1: Introduction

Biliary Tract Cancer

Classification

Biliary tract cancer (BTC) can be defined as a malignant lesion arising from the biliary epithelium lining the gallbladder or extra or intrahepatic biliary tree. Historically these tumours have been divided into three clinical phenotypes according to anatomical location: those arising from the intrahepatic ductular network within the liver (Intrahepatic Cholangiocarcinoma (ICC)); those arising from the large distal ducts outwith the liver (Extrahepatic Cholangiocarcinoma (ECC)) and gallbladder cancers. This has been a clinically useful classification due to differences in presentation and clinical behaviour. Intrahepatic tumours present as mass lesions within the liver parenchyma in contrast to extrahepatic tumours which typically cause biliary obstruction. Furthermore these cancers demonstrate differing responses to therapy and therefore management and outcomes differ (1). The most frequently involved site is the confluence of the right and left hepatic ducts (2). The boundary between intra and extrahepatic ducts at this site is often unclear and surgical management of these tumours is similar so consequently the two types have been grouped together (hilar cholangiocarcinoma). An eponymous classification of these tumours by Gerald Klatskin in 1965 (3) has led to inconsistencies in the diagnostic classification of the two tumour phenotypes and a misrepresentation of outcome data for these cancers (4). This has been compounded by inconsistencies between the second and third editions of the International Classification of Diseases for Oncology (ICD-O), which recommended hilar tumours be cross-referenced as intrahepatic (ICD-O-2) and later either intrahepatic or extrahepatic (ICD-O-3) (4).

Nomenclature

In light of low prevalence rates, individual epidemiological data for ECC, ICC and gallbladder cancers are frequently grouped together. Where this has occurred or no distinction has been made in the literature, I have used the encompassing nomenclature biliary tract cancer (BTC) in this text. This introduction attempts to present an overview of the current understanding and statistics for all these tumour subgroups; however the scientific focus of the primary data presented in this dissertation is on ICC. There is evidence that gallbladder cancer and cancers of the distal extrahepatic ducts as a group have a distinct tumour biology and differing responses to treatment to intrahepatic tumours (1). Such distinctions between intrahepatic and hilar tumours are as yet unclear, and in fact immunoreactivity between these two subsets is similar (5). Where human specimens have been used in this research, in the interests of including statistically relevant cohorts, I have included both intrahepatic and hilar tumours, which are herein referred to as ICC. Where this is not the case, this is specifically referred to in the text.

The global health burden

In the USA and Western Europe biliary tract cancers are uncommon, with a reported incidence of 1-2 per 100,000, accounting for 3% of all gastrointestinal tumours (6, 7). In contrast in regions of South East Asia where infestation with the liver fluke parasites *Opisthorchis viverrini* and *Clonorchis sinensis* is endemic, age-standardised incidence rates of BTC can reach as high as 94.8 and 39.4 per 100,000 males and females respectively (8). Incidence and mortality rates of intrahepatic cholangiocarcinoma (ICC) in industrialised nations however have been substantially increasing over the last 20 years, (9-11). In the UK following 1993 ICC became the most commonly recorded cause of malignant liver tumour-related death in females in England and Wales (12, 13). This prompted examination as to whether misclassification of 'Klatskin' or perihilar tumours as intrahepatic rather than

extrahepatic cholangiocarcinoma by the International Classification of Diseases for Oncology, 2nd Edition (ICD-O-2) had skewed such trends. However when diagnoses were re-classified to an extrahepatic code, the observed increases in incidence rates were upheld (4) and have been subsequently corroborated by other independently collected datasets and World Health Organisation data (7, 14, 15). Biliary tract cancers confer a dismal prognosis: less than 5% overall survival at 5 years (16), equating to a median overall survival of 9 to 10 months (17). This is attributable to their late presentation, complexity of diagnosis as well as lack of response to conventional chemotherapy.

The aetiology of biliary tract cancer

Although the majority of biliary tract cancer (BTC) arises spontaneously, a number of pathological conditions increase the risk of developing this malignancy.

Established risk factors	**Probable risk factors**
Primary sclerosing cholangitis (PSC) (18, 19)	Smoking
Hepatolithiasis (20)	
Clonorchis sinensis infection (21)	
Opisthorchis viverrini infection (21)	
Choledochal cyst (congenital biliary cystic disease)(22, 23)	
Cirrhosis (24)	
Hepatitis C virus infection (24, 25)	
Hepatitis B virus infection (24)	
Obesity (24)	
Type II diabetes mellitus (24)	
Alcohol (24)	

Table 1.1 Risk factors for the development of biliary tract cancer

The natural history of primary sclerosing cholangitis is heterogeneous and a variable incidence of cholangiocarcinoma reported (18, 19). The overall lifetime risk of developing cholangiocarcinoma is 10-15% (26). This represents a particularly dismal prognosis for these patients as they will rarely be candidates for resection due to multifocal disease or inadequate residual hepatic function.

The propensity for patients with congenital biliary cystic abnormalities to develop malignancy is thought to be due at least in a proportion of patients to chronic reflux at an abnormal choledochopancreatic junction and similarly patients who have undergone sphincteroplasty or sphincterotomy for benign conditions are at an increased risk of developing malignancy compared to the general population (22, 23).

Infection with the trematode *Opisthorchis viverrini* is endemic in south east Asia particularly Thailand, Vietnam, Loas and Cambodia. *Clonorchis sinensis* is prevalent in Korea and China. Both species are now classified as a type I carcinogen by the International Agency for Research in Cancer of the World Health Organisation and chronic infection is associated with a 27 fold increased risk of developing cholangiocarcinoma (21). Similarly chronic inflammation secondary to intrahepatic pigmented hepatolithiasis, especially common in Japan, is a contributing factor to high incidence rates in these regions (20).

Due to the relatively low incidence of BTC in regions of the world where liver parasite infection is uncommon, meta-analysis of smaller epidemiological studies has been required to determine the true odds ratios for potential aetiological factors previously implicated in this disease (27). These studies have concluded that Hepatitis C Virus (HCV) and Hepatitis B Virus (HBV) infection, cirrhosis, alcohol, type II diabetes mellitus and obesity are all major risk factors for the development of cholangiocarcinoma (24).

Existing treatment strategies

Surgery is the sole cure for biliary tract cancer, however less than 7% of patients present with disease that is amenable to curative resection (28). This procedure usually involves excision of the involved hepatic lobe (partial hepatectomy) and extrahepatic biliary system, regional lymphadenectomy and Roux-en-Y hepaticojejunostomy. For tumours involving the distal ducts, a pancreaticoduodenectomy may be required. Contraindications to surgery include contralateral or bilateral vascular encasement, or tumour extension bilaterally to the level of the secondary biliary branches. Until recently the Bismuth-Corlette classification system has been used to assess suitability for surgical resection (29). This system stratifies patients solely on the extent of ductular involvement of the tumour and therefore has had little predictive value in terms of either resectability or survival. The American Joint Committee on Cancer (AJCC) 6th edition classified tumours based on histopathological criteria and so similarly was not useful for preoperative staging (30). Consequently a modified score, the Blumgart clinical staging system (31) is now used, which takes into account the extent of bile duct and portal vein involvement as well as the presence of hepatic lobar atrophy and is incorporated into the 7th edition of the AJCC staging system. The most important predictor of post-resectional recurrence is a positive resection margin (32). Well-differentiated histology and a papillary phenotype are independent predictors of long-term survival (33). Given the incidence of BTC and the proportion of patients suitable for resectional surgery, the efficacy of adjuvant chemoradiation has been difficult to assess through clinical trials and no data currently support its use (34).

A single centre in the USA has pioneered liver transplantation as a curative option for patients with perihilar cholangiocarcinoma (35). Patients with unresectable disease including patients with PSC who meet a rigorous selection criteria undergo a treatment protocol of neoadjuvant external beam radiotherapy followed by intracavitary brachytherapy with iridium-192 and oral capecitabine up until transplantation. Once prioritised, patients undergo staging laparotomy to exclude

extrahepatic or nodal metastasis previously missed by endoscopic ultrasound-guided biopsy before going on to transplantation. Initial results from this highly-selected cohort appear encouraging. Recurrence-free survival is reported to be 68% at 3 years, plateauing at 60% at 10 years. Predictors of recurrence are a high CA19-9 level, portal vein encasement and residual tumour on explant. Pre-transplantation drop out from the waiting list is predicted by a high CA19-9, mass >3cm in radial diameter or a MELD score of >20 (36). These results have recently been supported by initial results reported by the Irish National Liver Transplantation Programme, who report a similar survival rate of 61% at 4 years (37). In both these uncontrolled studies, patients are stringently selected and indeed, not all patients undergoing neoadjuvant treatment progress to liver transplantation. Indeed it could be argued that patients not progressing to surgery are subjected to a worse end of life experience than those undergoing conventional therapy. In this context it is difficult to directly compare outcome data from those receiving a graft with published survival rates following resection, and therefore transplantation remains an experimental treatment in a limited number of centres.

The majority of patients with BTC are not suitable candidates for any surgical option and for them the goals of treatment are supportive care and maximisation of quality of life. Multiple studies have been performed using chemotherapeutic agents either alone or combination (fluropyrimidines, platinum agents, gemcitabine, taxanes and irinotecan) and demonstrate partial disease response rates of the order of 10-30% but with only modest benefits in overall survival (38-41). One recent phase III randomised clinical trial however has demonstrated a significant improvement in short term survival in response to combined treatment with cisplatin and gemcitabine compared with gemcitabine alone, and this has now been adopted as an accepted standard of care (17). Clinical trials are ongoing to assess the use of neoadjuvant or adjuvant chemotherapy in patients undergoing curative resection for BTC.

Other agents currently undergoing clinical trials for BTC include monoclonal antibodies targeted to receptor tyrosine kinases, particularly against the Epidermal Growth Factor (EGF) and Fibroblast Growth Factor (FGF) pathways. Encouraging initial results have demonstrated an improvement in disease progression-free survival and in a subgroup of patients, complete response or response sufficient to permit surgical resection (42-44). Combination with a VEGFR inhibitor similarly appears to induce partial disease response (45).

The use of palliative radiation or photodynamic therapy have not been widely adopted even for locally advanced disease without distant metastasis due to a lack of survival benefit compared to other palliative measures such as stenting, percutaneous biliary drainage or biliary-enteric bypass (46). These measures form the basis of supportive care and symptomatic relief to improve quality of life for the majority of patients with this disease.

The genomic mutations of biliary tract cancer

Compared to other solid tumours types little is known of the genetic, epigenetic and chromosomal aberrations occurring during the pathogenesis of cholangiocarcinoma. Few studies have used genomic sequencing to analyse somatic changes and hitherto this has not been performed in a large cohort of human specimens. Exome sequencing of eight fluke-associated tumours has been used to validate recurrently mutated genes observed in a larger cohort of 46 cases (47). This study identified abnormalities in a number of known tumour suppressor and oncogenes including *TP53* (44.4%), *KRAS* (16.7%) and *SMAD4* (16.7%) as well as other genes not previously implicated including *MLL3, ROBO2, RNF43, PEG3* and *GNAS*. The same group went on to compare fluke-associated with non-fluke associated tumours using a larger number of cases, identifying a difference in mutational signature. A higher frequency of mutations was observed in *BAP1, IDH1* and *IDH2* in sporadic ICC compared with infection-related tumours where *TP53* was more commonly mutated (48). These findings corroborate a pattern independently identified in which two biological classes of ICC appear to exist; those associated with inflammation, up-regulation of cytokines and inflammatory signalling pathways including STAT3 activation, and those termed 'proliferative', characterised by activation of oncogenic signalling including MAPK and MET, frequent DNA amplifications, copy number alterations and mutations in *KRAS* and *BRAF*. This second group appears to be associated with poorer clinical outcomes (49). Similarly other laboratories have highlighted *KRAS* mutation and HER2/EGFR signalling as poor prognostic indicators, characterised by transcriptional enrichment of genes regulating proteosomal activity (50, 51). In general terms the mutational signature of ICC does appear to be heterogeneous compared with other tumour types (52). Interestingly mutations in *IDH1* and its mitochondrial counterpart *IDH2* are repeatedly identified in ICC (48, 53-55). *IDH1/2* aberrations have been previously identified in a limited but stereotypical group of tumours; gliomas, acute myeloid leukaemia and chondrosarcomas, all of which demonstrate a hypermethylated phenotype and intense research is focussing on these targets for future therapeutic

development. Few studies have assessed the global methylation changes in ICC. Initial reports suggest however that, like most cancers, ICC has non-randomly distributed patterns of promoter methylation that are enriched for in cancer-related pathways including Wnt, TGFβ and PI3K signalling (56).

The tumour-stroma microenvironment

ICC is characterised by an intense desmoplastic reaction in which multiple cell types including myofibroblasts, inflammatory and vascular cells interact with neoplastic epithelia invested by a supporting 3-dimensional extracellular matrix to actively support tumour growth. The extent of desmoplasia and expression of the activated myofibroblast marker α-smooth muscle actin (α-SMA) inversely correlate with patient survival (57, 58) and there is a multitude of evidence in favour of the concept that cancer-associated fibroblasts (CAFs) actively drive tumour cell growth (59, 60). This population of CAFs appears to be phenotypically heterogeneous, for example tumours with a distinct subpopulation expressing the glycoprotein podoplanin have reduced survival and greater lymphatic metastasis (61). Furthermore CAFs secrete growth factors that enhance tumour cell migration and invasiveness including HGF, SDF-1, periostin and tenascin-C (62-64). In particular, secretion of matrix metalloproteases, especially MMP1, 2 and 9 serves to remodel matrix and promote cancer progression and invasiveness (65). The dominant result of CAF growth factor secretion however is a fibrogenic response, whereby myofibroblasts produce a dense stromal scaffold rich in an extensive array of modified extracellular matrix proteins, including fibrillar collagens (I, III, V and XI), laminin and the basement membrane proteins fibronectin and collagen IV (66). In comparison to hepatocellular carcinoma, this microenvironment is relatively hypovascular. Hypoxia and associated hypoxia-inducible factors (HIFs) are likely to play a role in tumour behaviour but again, this is an understudied area of research in ICC. Neoangiogenesis however is intrinsically linked to metastasis and a number of pro and anti-angiogenic factors have been identified to be up-regulated in ICC, including VEGF, the endothelins and thrombospondin-1 (67, 68).

The stromal microenvironment of ICC has an abundant inflammatory infiltrate including neutrophils, monocytes and T cells, although the precise role of these cells in tumour progression has yet to be fully characterised. As in other cancer types, a major subset of these cells is tumour-associated macrophages. Little work has been

done in ICC to assess their contribution to tumour progression, however it is known that they stain positively for CD68 and the 'alternatively' activated or 'M2' marker CD163 and that although macrophage density does not correlate with overall survival, infiltration of $CD163^+$ macrophages does inversely correlate with disease-free survival (69). Furthermore patients with ICC have higher levels of $CD14^+$ $CD16^+$ dual positive circulating monocytes (the precursors of the tissue macrophage), compared with healthy patients or patients with benign disease, and that this is associated with poor clinical outcome and rapid tumour progression (70).

This malignant niche is rich in soluble cytokines and growth factors released by both neoplastic epithelia as well supporting and inflammatory cells. Transforming growth factor beta (TGFβ) secreted by multiple cell types but particularly cancerous epithelia and CAFs, has a dominant role in driving both fibrosis through matrix deposition and in cholangiocarcinoma progression via direct stimulation of cancer cell proliferation. Direct inhibition of tumour development and regression of established fibrosis can be achieved *in vivo* using a neutralising monoclonal antibody targeted against TGFβ or genetic deletion of its receptor TGFbr2 (71, 72). In addition a strong association has been established between the inflammatory cytokine interleukin-6 (IL-6) and ICC progression (73). This is thought to be mediated through the effects of IL-6 on aberrant promoter methylation including that on the EGFR gene. (74)

Figure 1.1 The tumour microenvironment of biliary tract cancer

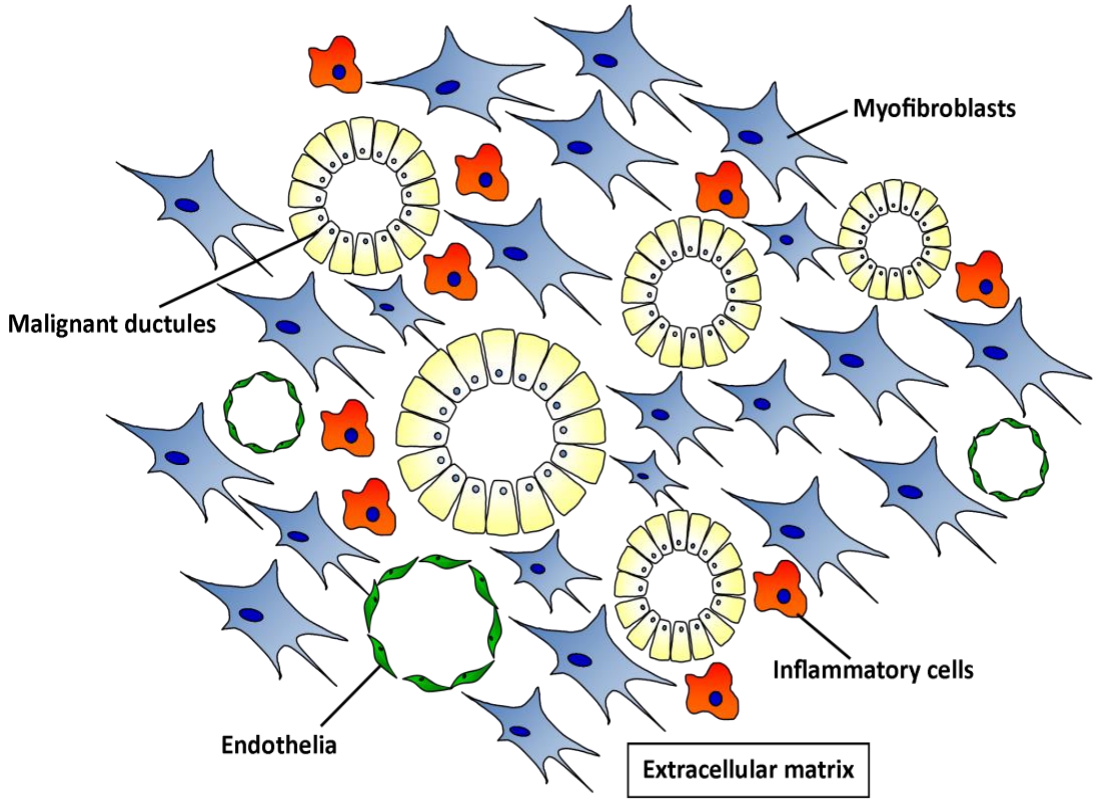

Figure 1.1 *The tumour microenvironment of cholangiocarcinoma.* Malignant biliary ductules are invested by αSMA positive myofibroblasts which secrete soluble factors and extracellular matrix proteins, contributing to the surrounding dense desmoplasia. Inflammatory cells including neutrophils, T cells and tumour-associated macrophages infiltrate tumours, phagocytosing tumour cells and secreting cytokines. Neoangiogenesis promotes tumour growth and endothelia secrete growth factors including VEGF.

Rodent models of ICC

Until recently the number of rodent models of ICC that faithfully recapitulate the inflammatory stromal histology and clinical features of the human cancer have been few. Several rat models using chemical carcinogens have been developed to mimic the stepwise progression of biliary carcinogenesis with good tumour penetrance, the most widely used of which is oral administration of thioacetamide (TAA) (75). Cytochrome P450 (2B and 2E1) and flavin monooxygenase enzymes in zone 3 of the liver metabolise TAA to potently hepatotoxic products which disrupt ribosomal function, alter protein assembly and stimulate DNA synthesis (76, 77). Prolonged administration reproducibly results in bile duct proliferation, dysplasia and ultimately carcinoma, with a 50% penetrance at 16 weeks and 100% at 22 weeks. Histological features closely mimic human disease, with metaplasia foci, a dense desmoplastic stroma and neoplastic ducts displaying CK19, c-Met and c-erb-B2 positivity. Alternative chemical agents inducing biliary carcinogenesis in rat include furan (78) and 3'-methyl 4-dimethylazobenzene (79, 80).

Alternative but less practicable approaches have used orthotopic transplantation of transformed cholangiocytes (81, 82) or have combined administration of dimethylnitrosamine (DEN) with liver fluke *Opisthorchis viverrini* metacercariae in hamster (83).

Transgenic murine models of ICC are now emerging. Currently the only murine model of gallbladder adenocarcinoma employs overexpression of wild type rat ErbB-2 under control of the cytokeratin 5 (CK5) promoter with all homozygous animals developing de novo tumours between 3 and 8 months of age (84). ICC develops with high penetrance (100%) following liver-specific deletion of the tumour suppressors Smad4 and Pten using an embryonic albumin-driven Cre recombinase system (85). Neoplastic foci emerge at 2 months of age in all animals carrying both gene deletions, compared to no tumour formation in Smad4-only deleted mice and only a third of Pten-only deleted animals at one year, suggesting a synergistic relationship between these tumour suppressors. This albumin-specific

Cre recombines loxP sites in both cholangiocytes and hepatocytes, but interestingly hepatocellular tumours only developed in mice carrying Pten deletion.

An constitutive albumin-linked Cre system has also been used to combine tissue-specific p53 deletion with an activating mutation of $Kras^{G12D}$ (86) . Albumin is expressed in all hepatoblasts during embryogenesis and thereby in the adult liver recombination of floxed alleles has occurs in hepatocytes, cholangiocytes and hepatic progenitor cells (HPCs) in this model. Animals carrying activated $Kras^{G12D}$ mutation and homozygous loss of p53 developed tumours by 9 weeks of age (median survival 19 weeks); those heterozygous for p53 deletion developed tumours at 32 weeks (median survival 52 weeks). Animals without Kras mutation but homozygous for p53 deletion were followed to one year of age without abnormality.

The use of an alternative promoter Cyp2A1 (referred to as AhCre) expressed in mature hepatocytes but also in gallbladder epithelium, has similarly been used to conditionally induce Pten deletion and kRas activation in the adult liver (87). Findings from this study mirrored those seen by O'Dell et al. in that mice with Pten deletion or Pten deletion combined with kRas activation displayed reduced survival and histological biliary neoplasia, whereas animals with kRas activation alone were histologically normal.

An alternative strategy of disease modelling is to combine transgenic tumour suppressor deletion or oncogene activation with chronic biliary injury. Administration of the hepatotoxin and pro-fibrotic agent carbon tetrachloride (CCl_4) to p53 null mice over a 16 week period precipitates multifocal ICC in p53-/- and p53+/- mice with an allelic dose dependant reduction in survival. A number of other tumour types also develop in these animals however, including HCC, lymphoma and sarcoma, and the high reported mortality precludes its widespread adoption as useful model of ICC.

In summary, compared to other cancer types, rodent models of ICC are flawed, and consequently one of the principal aims of this study was to develop a more specific murine model in which genetic alterations within the biliary compartment of the liver are permissable, to allow interrogation of epithelial signalling during ICC tumorigenesis.

The cell of origin of ICC

Historically it has been assumed that ICC arises from the oncogenic transformation of mature biliary epithelia in light of its glandular histological morphology, location within and adjacent to the biliary network and expression of cholangiocyte specific proteins including mucin and biliary cytokeratins 7 and 19 (88). Moreover the propensity for patients with chronic biliary inflammation to develop ICC, in particular those with primary sclerosing cholangitis or liver fluke infection, has added further weight to this theory (21, 89). Bipotential hepatic progenitor cells have also been considered a cellular source, especially in tumours classified as combined hepatocellular cholangiocarcinoma (CHC); which display features of both cholangiocarcinoma and hepatocellular carcinoma, as well as cholangiolocellular carcinoma (CLC), where tumours display prominent ductular reaction and cords resembling the canals of Hering (90, 91).

Interestingly however the incidence of ICC is also increased in chronic hepatocellular injury such as HCV and HBV infection indicating a more complex cellular origin of these cancers (24) and indeed recent work has demonstrated mature hepatocytes possess potential for transdifferentiation into ICC (92, 93). In these fate-tracing experiments tumours were established in transgenic mice carrying an inducible heritable label for either hepatocyte (Alb-CreER^{T2}) or biliary (CK19-CreER^{T2}) lineages using the chemical carcinogen thioacetamide (TAA). Labelled neoplastic nodules positive for Epithelial Cell Adhesion Molecule (EpCAM) were observed in tumours arising in Alb-CreER^{T2} but not CK19-CreER^{T2} animals, suggesting that ICC arises from hepatocytes rather than cholangiocytes in this model (93). This transdifferentiation of hepatocytes to a biliary program is shown to be dependent on intracellular Notch signalling through gain and loss of function experiments. Overexpression of the Notch1 intracellular domain in Albumin-expressing cells (Alb-CreER^{T2};R26R$^{Notch/+}$) or conversely deletion of its downstream effector Hes1 (Alb-CreER^{T2};Hes1$^{fl/fl}$) resulted in a respective increase and decrease in the number of primitive CK19-positive ductules formed. Similarly, an independent

group have demonstrated injection of a N1-ICD transposase-mediated plasmid to result in the formation of biliary cystadenomas, which in combination with a myristolated AKT1 plasmid precipitate the formation of ICC displaying biliary lineage markers 1.5 weeks following injection (92). Interestingly these tumours developed around the central lobule of the liver. Tumours were subsequently lineage-traced using an adeno-associated virus to deliver a hepatocyte-specific Cre recombinase (driven by a transthyretin promoter) in R26R-EYFP transgenic mice. N1-ICD/AKT Plasmid injection resulted in eYFP positive tumours staining positive for biliary (Sox9, Ck8) indicating that similarly in this system the cell of origin was the hepatocyte.

The Canonical Notch signalling pathway

Notch signalling is one of the most highly conserved pathways in metazoan evolution. It is one of a tightly restricted number of pathways including Hedgehog, Wingless(Wnt), Transforming growth factor beta, Receptor tyrosine kinase and JAK/STAT that act individually and in combination during development to co-ordinate cellular transcriptional responses and thereby regulate cellular proliferation or death, binary cell fate decisions, specification, tissue patterning and morphogenesis (94). This orchestration allows complex multicellular tissues organs and organisms to develop with fidelity but also means that perturbation in these signals through mutation or dysregulation results in a wide range of developmental syndromes. Moreover these pathways continue to regulate the homeostasis of adult tissues and regeneration following injury, and therefore aberration of these signals also promotes the onset of adult disorders of tissue repair including cancer.

The core canonical Notch pathway is activated through cell to cell communication involving ligand and receptor tethered to the membrane of their respective cells. Notch signal transduction is unusual in that this interaction triggers a series of proteolytic cleavage events which release an active, truncated form of the receptor which translocates to the nucleus to effect transcription of Notch target genes (Figure 1.2).

Figure 1.2 The core pathway of Notch signalling in mammals.

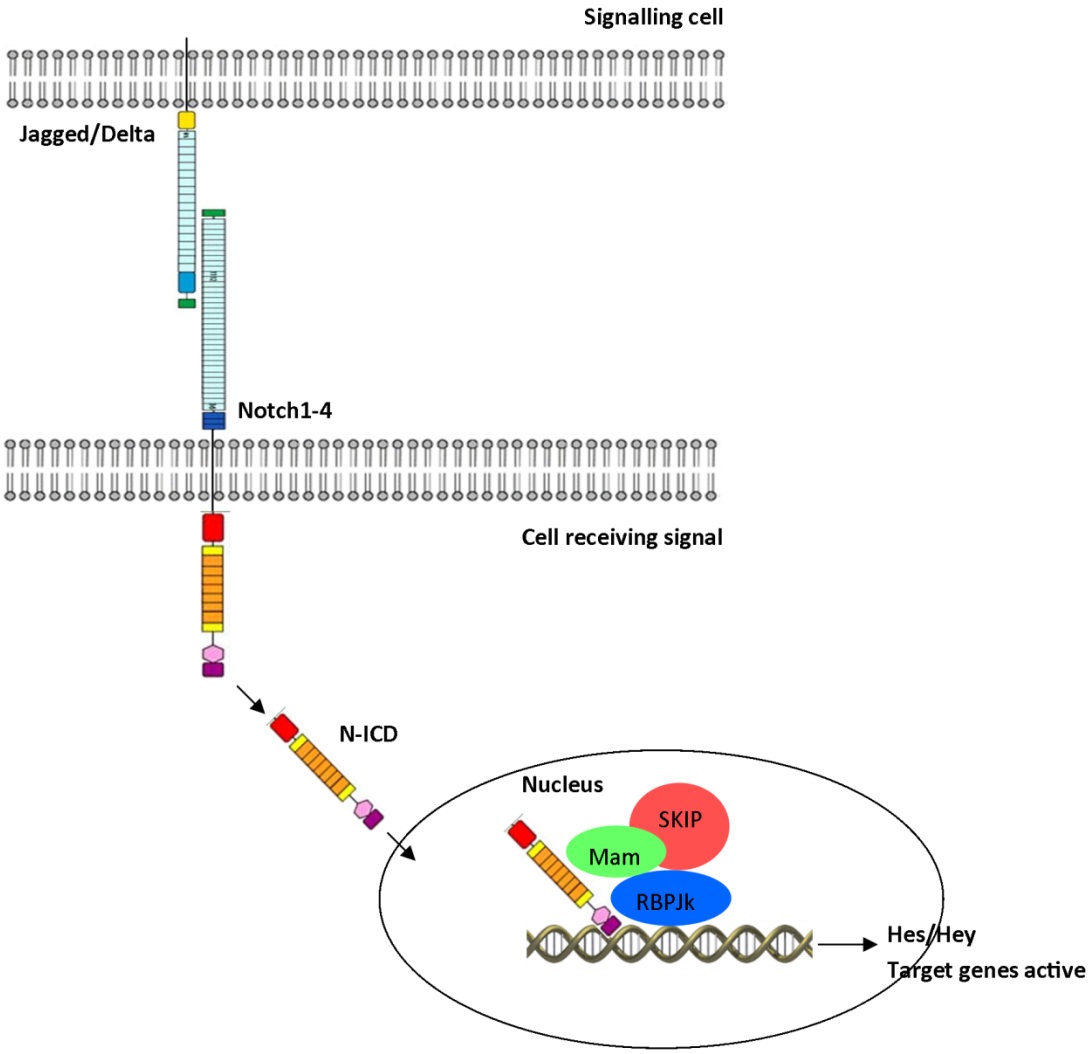

Figure 1.2 *The core pathway of Notch signalling in mammals.* Notch ligand is provided by a neighbouring cell to interact with one of four receptors (Notch 1, 2, 3 or 4). This triggers enzymatic cleavage of receptor into an activated, truncated form (N-ICD) which travels to the nucleus. In the absence of N-ICD, Notch target genes are maintained in an actively repressed state, however when N-ICD forms a complex with the DNA binding protein RBPJκ, co-repressors are displaced by co-activators including MAML and SKIP and transcription of downstream Notch target genes (Hes/Hey) occurs.

The Notch Receptors

The *Notch* gene of *Drosophila melanogaster* codes for a single 300kD type I transmembrane glycoprotein receptor. Two paralogs are found in *Caenorhabditis elegans* (cLIN-12 and c-GLP-1) and four in human: *NOTCH 1, 2, 3* and *4.* Although in *C.elegans* the two Notch paralogs can fully substitute for each other, in mammals the four receptors each have both overlapping and distinct tissue distributions as well as redundant and distinct functions (95). All receptors are constituted by three principal domains: an extracellular region, a transmembrane portion and an intracellular domain (N-ICD) (Figure 1.3).

The extracellular domain comprises at its N terminals between 29 and 36 tandem epidermal growth factor (EGF)-like repeats which mediate ligand interaction and determine ligand selectivity according to context (96, 97). Functionally productive interactions between neighbouring cells known as *trans* interactions are mediated by repeats 11 to 12, whereas repeats 24 to 29 have been implicated in *cis* interactions, i.e. between receptors and ligands expressed on the same cell where no signal is transmitted. These EGF repeats contain motifs for fucosylation (by O-Fut1) and glucosylation (by Rumi) and the ligand-binding regions of the four paralogs differ in these modification patterns. Proximal to the EGF repeats, a negative regulatory region (NRR) is found, composed of three cysteine-rich Lin12-Notch repeats (LNR) and a heterodimerisation domain, which act to prevent signal transduction in the absence of ligand binding (i.e. this region maintains the autoinhibitory resting state of the receptor).

The transmembrane portion of the receptor contains a single domain characterised by a C-terminal sequence of 3 to 4 arginine-lysine residues that acts as a "stop translocation" signal.

Inside the cell an RBPJκ-association molecule (RAM) domain links the single-pass transmembrane region with seven ankyrin repeats, followed by a nuclear localisation sequence and a transactivation domain. At the C-terminal, a degron*-

containing PEST (proline/glutamic acid/serine/threonine-rich motif) sequence regulates the stability of the NICD.

In *Caenorhabditis elegans* the two Notch paralogs can fully substitute for each other in cell fate decisions (98). Of the four mammalian receptors, Notch1 and 2 exhibit the highest structural similarity. Only these two paralogs contain a full transactivation domain (TAD), located C-terminal to the ANK repeats (99). Notch3 displays a particularly short TAD-containing region and this is thought to account for a weaker transcriptional activity of the N3-ICD compared to that of Notch1 and 2. Comparison of amino acid identity between Notch1 and 3 has revealed high similarity in the ankyrin repeat region (72%) compared to the RAM (42%) and C-terminal (21%). Such differences have been proposed to account for the differential ability of Notch paralogs recruit co-activators and repressors as well as a differential capacity to undergo conformational changes (99). Furthermore the extracellular domain of Notch3 lacks certain EGF repeats found in Notch1 and 2 (100).

* Degron A specific sequence of amino acids in a protein that drives the starting place of degradation.

Figure 1.3 The structural organisation of mammalian Notch receptors.

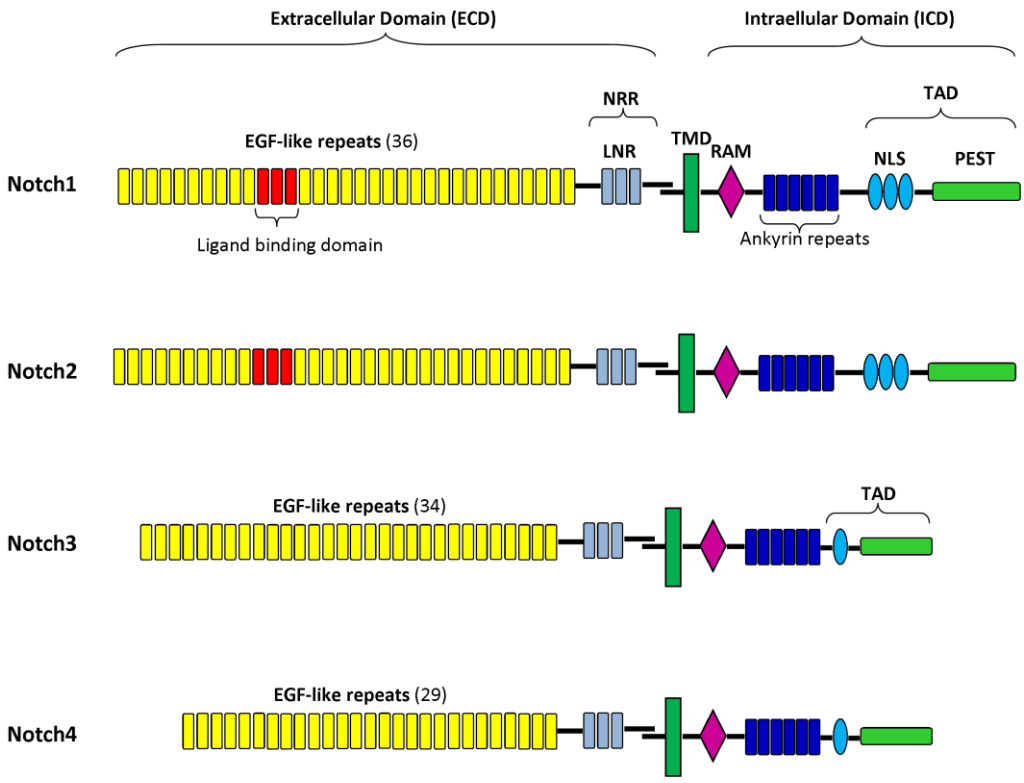

Figure 1.3 *The structural organisation of mammalian Notch receptors.* Notch receptors are membrane-spanning (type I) proteins, each comprising an extracellular domain (ECD), transmembrane domain (TMD) and intracellular domain (ICD). The extracellular region is composed of a sequence of EGF-like repeats, of which some mediate ligand interactions. Furthermore the EGF-like repeats contain motifs for fucosylation (by O-fut) and glycosylation (by Rumi) during translation, and the distribution of these differs between paralogs. Proximal to this, the negative regulatory region (NRR) abuts the transmembrane domain (TMD). The intracellular domain (ICD) contains an RBPJκ-association molecule (RAM) for partner binding, a nuclear localisation sequence (NLS), seven ankyrin repeats, a transactivation domain (TAD) and a conserved PEST motif.

Receptor-ligand interactions

Activation of Notch signalling in mammals is initiated through a short-range 'juxtacellular' interaction between receptor and one of five ligands tethered within the membrane of a neighbouring cell. Although it is believed that in mammals any one of the five ligands (Delta-like1,2,3 or Jagged1,2) are able to interact and stimulate any of the four Notch receptors (Notch1,2,3,4), genetic screens in *drosophila* have revealed that it is the EGF-8 repeat in the receptor's extracellular domain which discriminates between Delta or Serrate binding and this has been evolutionarily conserved to the mammalian homologs Delta-like and Jagged (97). Screening of *drosophila* mutants has also elucidated that missense mutations in the ligand *Delta* that cause defective ubiquitylation of the ligand's intracellular portion or those causing dysfunction of endocytosis and intracellular receptor trafficking result in disruption of functional signalling following receptor-ligand interaction (101). It is important to note there is no signal amplification in the Notch pathway – one ligand binds to one receptor, whose intracellular domain translocates to the nucleus to drive target gene transcription. As a consequence, ligand and receptor availability at the cell surface is the sole determinant of signal strength and effector transcription. Therefore spatial and temporal expression of Notch ligand is tightly regulated during development and injury to ensure the effects of Notch are co-ordinated in a context-dependent manner. Post-translational ligand modifications such as ubiquitylation by the E3 ubiquitin ligases *Mindbomb* and *Neuralized* are consequently important regulators of ligand presentation and thereby pathway activity (102). A novel gene complex known as *Bearded* in *drosophila* code for a family of proteins that are able to negatively regulate *Neuralized* activity and therefore reduce efficiency of Notch activation, but are themselves Notch target genes, thereby providing a negative feedback loop to control signal strength (103).

Much still remains to be ascertained about the functional consequences of different combinations of receptor-ligand interaction, although there is consensus that

binding with Dll3 ligand in *xenopus* and mammals is actually suppressive to Notch signalling (104).

Intra-membrane Proteolysis

The Notch pathway is set apart from other conserved signalling cascades by a series of proteolytic cleavage events that occur within the membrane of the signal-receiving-cell following ligand binding. The initial interaction triggers cleavage of Notch at its negative regulatory region (NNR) by ADAM, a disintegrin and metalloproteases, an event known as S2 cleavage (Figure 1.4). This releases an 'ectodomain', leaving behind an intermediate fragment known as Notch extracellular truncation (NEXT), which becomes the substrate for the gamma-secretase complex. This multi-protease complex cleaves the receptor sequentially, starting at the inner plasma membrane (S3) and ending within the transmembrane domain (S4), causing release of the intracellular domain of the receptor (N-ICD) which is then free to translocate to the nucleus. Γ-secretase cleavage can occur both at the membrane and in the endosome, however cleavage in the membrane produces a more stable N-ICD.

Point mutations or viral integration in the S2 cleavage site in the negative regulatory region (NRR) result in Notch signalling in the absence of ligand, such as is seen in acute T lymphoblastic leukaemia in humans or lymphoma in mice (105, 106). It is the steric structure of this NRR which defines the Notch receptor to be 'OFF' in its resting state. Gamma-secretase itself is made up of four membrane proteins: the catalytic unit presenilin and three co-factors: Nicastrin (NCT), Pen2 and Aph1. Two different isoforms of both presenilin and Aph1 exist in mammals, meaning that at least four gamma-secretase complexes can exist, each resulting in differing protein interactions, although the precise functions of the various complexes is as yet unknown.

Figure 1.4 Regulated proteolysis mediates Notch receptor maturation and activation.

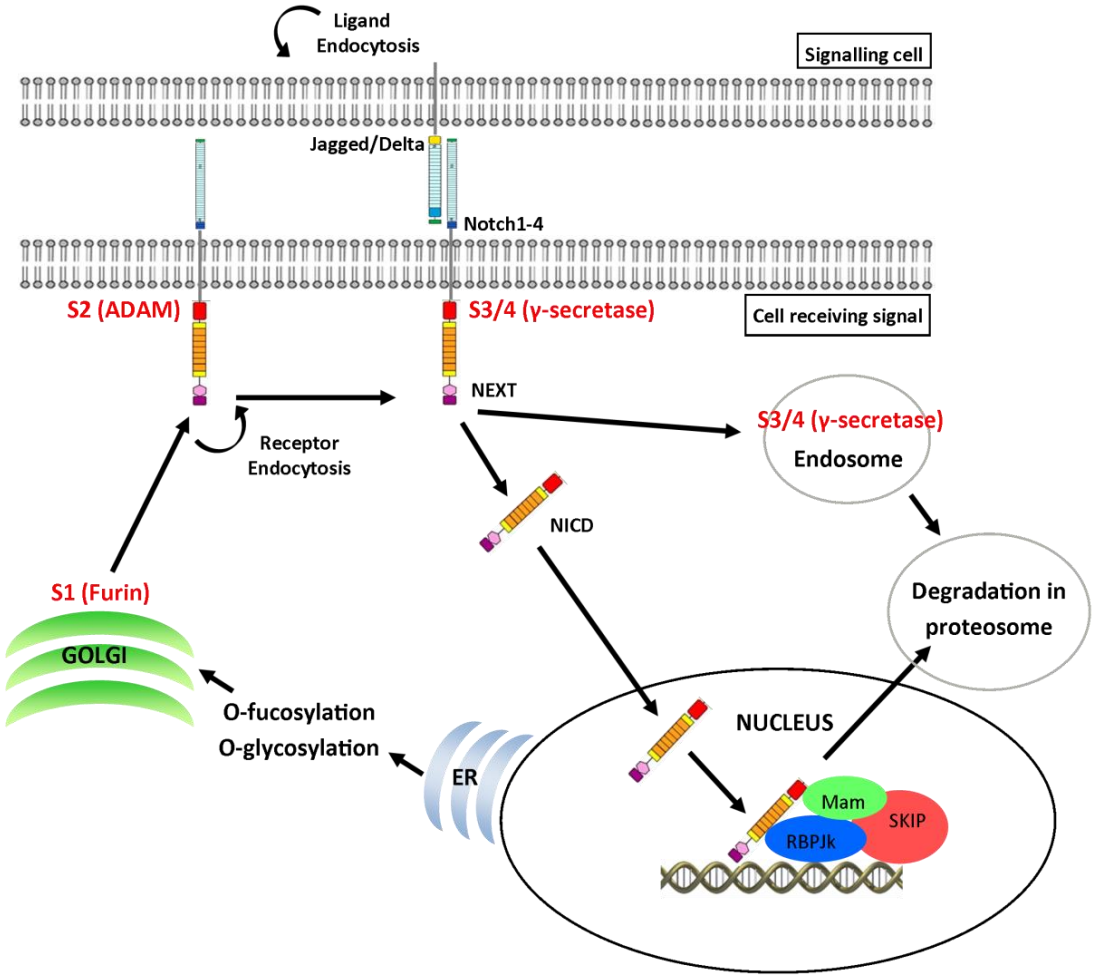

Figure 1.4 *Regulated proteolysis mediates Notch receptor maturation and activation.* Following translation the Notch receptor undergoes a maturation process involving fucosylation and glycosylation by the enzymes O-fut and Rumi before its first proteolytic cleavage event in the golgi at site 1 (**S1**) by furin. The receptor can then be targeted to the membrane as a heterodimer. Following ligand-receptor interaction ligand endocytosis begins to occur exerting a mechanical force upon the receptor and inducing a conformational change which exposes the **S2** site for cleavage by ADAM metalloproteases. This generates the Notch extracellular fragment (NEXT), a γ-secretase substrate. Progressive cleavage by γ-secretase at **S3** and **S4** releases the N-ICD for nuclear translocation.

The Canonical pathway: ICD translocation and target transcription

It remains unknown how the translocation of the intracellular domain (N-ICD) is regulated. DNA binding requires the presence of CSL (RBPJκ in mammals) which, in the absence of N-ICD acts to repress transcription of Notch target genes through recruitment of co-repressor proteins including SKIP, hairless, CtBP or Groucho (TLE). Such repression however is complex and thought to be of variable significance in different tissue contexts. In skin for example, RBPJκ mutants do not display as severe a phenotype seen in animals that have lost either multiple Notch receptors or gamma-secretase, indicating that there may be de-repression of Notch targets in these animals, however in contrast, loss of RBPJκ in Notch mutants does not alleviate their phenotype (107). Adding further to the complexity, occupancy of RBPJκ on Notch target gene promoters can also be transient, and further work is required to better understand the mechanisms of this crucial step in the pathway.

N-ICD contains a RAM domain (RBPJκ Associated Molecule) which mediates binding to RBPJκ and induces dissociation of transcriptional repressors. The co-activator Mastermind-like (MAML) as well as other co-activators including SKIP are then recruited and this complex can recruit histone acetylases (including p300) and chromatin remodelling factors to assemble a transcriptional activator complex on target promoters. Notch target genes are numerous; however in mammals the archetypal family is the Hairy/Enhancer of Split genes (Hes) which encode a series of basic Helix Loop Helix (bHLH) proteins which are often functionally redundant and which certainly exert different actions in different cell types. The determination of such differing responses is thought to be a result of crosstalk from other pathways but might also be a result of the action of Notch-responsive enhancer elements. Much has yet to be learnt about the factors governing transcription of target promoters, which are not stereotypical; for example even Hes1 is not always activated by Notch1 (108).

Termination of Notch signalling

The cellular processes regulated by Notch activity require that its effectors have a short nuclear half-life. In this way, assembly of the transcriptional activating complex RBPJκ-NICD-MAML also results in N-ICD dissociation. This is achieved in part, by recruitment of factors including Cyclin dependent kinase 8 (CDK8) which phosphorylates N-ICD, thereby converting it into a substrate for the ubiquitin E3 ligase SEL10 and targeting it for degradation by the proteosome (109). In the absence of N-ICD, RBPJκ will again recruit its co-repressors (in *drosophila*, Hairless and Groucho. No mammalian homolog for Hairless has been identified, but SMRT and SHARP are proteins which can recruit the co-repressor CtBP. SKIP may also form part of this repressor complex). It is likely that other kinases and other E3 ligases are also involved and that these vary according to context.

Notch signalling and cell fate

The Notch pathway functions at many different stages of development and adult tissue homeostasis to regulate cell number and determine cell fate. The unusual property of Notch is the transmembrane nature of both ligand and receptor, meaning that signalling is restricted to only occurring between neighbouring cells. The consequence is that Notch functions via three general modes of action:

Lateral Inhibition

During development there is frequently a requirement for amplification of small (and often random) differences between equivalent cells in order to generate different cell types from a seemingly homogenous population. For example in the developing hermaphrodite gonad of *C.elegans,* Notch signals between two neighbouring cells so that one specifies to become an anchor cell and one a uterine precursor cell. Initially both the receptor *lin-12* and the ligand *lag-2* are expressed equally in both cells, however autoregulation of *lin-12* transcription amplifies stochastic fluctuations in expression so that *lin-12* gets restricted to the presumptive uterine precursor cell and *lag-2* to the anchor cell (110).

Lineage Commitment

Asymmetric cell division is a faithful and efficient way of producing cell fate diversity during development. In the developing peripheral nervous system of *drosophila melanogaster,* asymmetric inheritance of the Notch antagonist Numb results in the specification of sensory organ precursor (SOP) cells into either a neuronal or supporting cell type (111). Asymmetric distribution of other Notch regulators including *Neuralized* mediates cell fate commitment in multiple developmental and adult regenerative contexts (112-114).

Inductive signalling & formation of boundaries

Despite being a juxtacellular signal, Notch can in fact co-ordinate the generation of developmental signalling boundaries through restriction of expression of Notch

components including ligands, target genes and the Notch modulator Fringe (114, 115). For example restriction of *Esl* target genes across the dorso-ventral boundary of the wing imaginal disc in *drosophila* forms a boundary across which sensory organ cells and trichomes (hair cells) are specified in a distinctive pattern (116).

Notch signalling in liver development

Notch activity is critical for the faithful embryological development of multiple tissues in diverse organisms through regulation of cell fate decisions. The extent of this influence is evident following mutation or transgenesis resulting in loss of Notch function as in the inherited disorder Alagille syndrome (117-119). This autosomal dominant congenital syndrome is a heterogeneous disorder characterised by cholestasis and jaundice as a result of failure of development of the intrahepatic bile ducts. This disorder occurs in approximately 1 in 70,000 births and is the second most common cause of intrahepatic cholestasis in infancy. Despite its autosomal dominant inheritance, expressivity is variable and the phenotype can range from an apparently normal phenotype through to severe liver failure requiring transplantation. Life expectancy is dependent on the degree of liver failure present.

Hepatobiliary anomalies are typically accompanied by congenital heart defects particularly pulmonary valve hypoplasia and peripheral pulmonary artery stenosis. Musculoskeletal abnormalities are also present, including 'butterfly' vertebrae, where there is a reduced interpedunculate distance in the lumbar spine, and stereotypical craniofacial malformations including a broad forehead, deep set eyes, a pointed mandible and bulbous tip of the nose (119, 120). Less frequently renal and vascular abnormalities occur. Most patients are of normal intelligence, although learning disabilities and mental retardation have been reported (117).

In 94% of individuals with a clinically confirmed diagnosis Alagille syndrome is the result of mutation of the *JAG1* gene (121). A minority of patients carry mutations in the *NOTCH2* receptor (117, 122). *JAG1* mutations are a result of premature termination codons in 72%, splice site mutations in 15% and missense mutations in 13% of cases. Between 3 and 7% have deletions encompassing the entire gene (123). Furthermore the resulting phenotypes are indistinguishable between patients with full gene deletions and those with intragenic mutations; indicating *JAG1* haploinsufficiency is sufficient for Alagille syndrome (123). In addition non-genetic

gene modifications are likely to also be important in accounting for the variable expressivity of the disease. For example it is known that monozygotic twins can exhibit differing phenotypes. One case report describes one twin with severe pulmonary atresia and mild liver disease; the other with Tetralogy of Fallot and severe liver failure requiring transplantation (124).

The molecular result of such mutations in Notch is that hepatoblasts in the embryonic liver fail to express hepatic nuclear factor (HNF) 1 beta; a key biliary specific transcription factor, and hence embryonic biliary precursors are unable to differentiate down the biliary fate route (125).

Congenital intrahepatic dilatation of the bile ducts (Caroli disease and syndrome) is a rare developmental malformation corresponding to type V in the Todani classification of congenital bile duct cysts (126). It is commonly associated with congenital hepatic fibrosis which is thought to arise as a result of remodelling of the ductal plate in response to cystic dilatation of the intrahepatic bile ducts (127). Patients with Caroli disease are at 100 times greater risk of developing BTC than the general population (128). Immunohistochemical studies have demonstrated that in a rat model of Caroli disease, myofibroblasts were abundantly present in the portal tracts of embryonic (E20), one day old and one week old animals, and that these mesenchymal cells express Jagged1. Furthermore Notch2 appears to be up-regulated by cholangiocytes in this model (129). More studies are required to assess the full contribution of Notch to the pathogenesis of this developmental anomaly.

It is surprising and unexplained why mice with the genotype of Alagille syndrome do not recapitulate the clinical phenotype seen in man. Gene targeting has permitted detailed characterisation of Notch pathway mutations in the mouse embryo. Heterozygous mutation of *Jag1* alone results in defects in the anterior chamber of the eye but not the full suite of phenotypic characteristics. *Jag1* null mutants die before birth due to vascular defects in the yolk sack (130). The human phenotype is observed in mice heterozygous for *Jag1* in addition to mutation in

either *Notch2* or any one of the Fringe glycosyltransferase genes which modify receptor-ligand affinity: Lunatic (*Lfng*), Radical (*Rfng*) or Manic (*Mfng*) Fringe (131, 132). These mice exhibit growth retardation, jaundice and bile duct paucity in addition to cardiac, ocular and renal abnormalities as seen in Alagille patients. Gene targeting of the Hes/Hey family of Notch effectors results in a spectrum of phenotypic characteristics. *Hey2* mutants demonstrate similar cardiac abnormalities seen in human patients (133, 134).

Table 1.2 Phenotypes associated with mutations in murine Notch

Mutation (mouse)	Phenotype
Jag1	Embryonically lethal (hom); eye defects (het) (130)
Jag1; Notch2	Alagille syndrome (132)
Jag1; Lfng/Rfng/Mfng	Alagille syndrome (131)
Notch1 (AlbCre;Notch1$^{flox/flox}$)*	No abnormality in bile duct architecture (135)
Notch2 (Alb1Cre;Notch2$^{flox/flox}$)*	Alagille syndrome (136)
Notch1;Notch2 (AlbCre;Notch1$^{flox/flox}$Notch2$^{flox/flox}$)**	Disorganised biliary architecture with multiple immature, dilated ducts extending into the hepatic lobe (135)
Hes1	Normal ductal plate; No tubular morphogenesis at birth (die perinatally due to CNS defects) (137, 138)

* (N.B: Constitutive knockout mice for *Notch1* or *Notch2* display embryonic lethality before day 11.5)

** (N.B: Phenotype rescued by addition of a single copy of Notch2 (but not Notch1))

Conditional ablation of Notch2 in hepatoblasts (AlbCre-Notch2$^{flox/flox}$) decreases the density of intrahepatic bile ducts in a dose-dependent fashion, whilst activation of Notch (AlbCre-ROSA^{Notch1}) has the opposite effect. It is also clear that there is redundancy between Notch receptors as Cre-mediated deletion of RBPJκ results in a more severe phenotype with associated parenchymal injury, and that this process may act independently of the downstream Notch effector Hes1 (139). Interestingly such regulation of the 3-dimensional ductal architecture is not mediated through a

change in proliferation of bile duct progenitor cells, suggesting that Notch is playing a permissive role for other signalling networks to drive cholangiocyte specification (140). Indeed, combining deletion of Notch (Rbpjκ) with deletion of the biliary transcription factor HNF-6 results in a more severe phenotype than Notch deletion alone (141). Furthermore the source of Jagged1 ligand driving Notch activity during this phase of duct formation has been identified as the portal vein mesenchyme (SM-22Cre) rather than the endothelia of the portal vein (V-CadherinCre) (142). This role for Notch in the development of the intrahepatic bile ducts is evolutionarily conserved across species; deletions of *Notch* and *Jagged* in zebrafish cause an Alagille's phenocopy and staged administration of pharmacological Notch inhibitors during development causes retardation of growth and expansion of the ductal network (143, 144).

Such mutant phenotypes provide evidence that Notch is required for tubular morphogenesis and arborisation of the intrahepatic bile ducts in the developing liver. The transgenic systems used here fail however to define its role in the earlier developmental stage of specification and differentiation of bipotential hepatoblasts into biliary progenitors and later biliary epithelial cells. Albumin transcription begins at approximately embryonic day 9.5, concomitant with the commencement of ductal plate specification and is likely a consequence of hepatoblast fate commitment itself, making these conditional knockout mice a flawed model in which to study the mechanisms of fate determination in the developing liver bud. Consequently mouse transgenics have been engineered in which Cre recombinase could be driven by one of the transcriptional activators of the liver-specific programme, Foxa3 (HNF-3G), in order to interrogate the requirement of Notch during these earlier events of hepatoblast specification (145). Hepatic Nuclear Factors (HNFs) are members of the Forkhead class of DNA binding proteins and drive transcription of liver-specific transcripts including albumin and transthyretin (146). This Cre-based construct was used to induce deletion of Rbpjκ , the downstream nuclear binding partner of all four Notch paralogs to bypass potential

redundancy between receptors. This resulted in a reduced number of ductal plate cells at E16.5 and bile ducts later at P0, indicating a requirement for Notch in both the generation of the ductal plate as well as duct formation. In contrast over-expression of N1-ICD using Foxa3-Cre resulted in the ectopic appearance of biliary cells which displayed features of mature epithelia as early as E16.5, suggesting Notch drives biliary differentiation of hepatoblasts (145). In support of this, transfection of cultured fetal hepatoblasts with a N1-ICD plasmid significantly reduces the expression of hepatocyte (and hepatoblast) markers including albumin, whilst inhibition of Notch2 with siRNA or gamma-secretase inhibitors promoted hepatocyte differentiation (147).

Finally, Notch also plays a role in the ontogeny of the extrahepatic biliary system. Hes1 is expressed in the extrahepatic bile ducts throughout development and acts to repress differentiation of these cells to a pancreatic programme by directly inhibiting transcription of the proendocrine gene Neurogen3. Hes1 deficient mice fail to develop a gallbladder and exhibit hypoplasia of the extrahepatic bile ducts (148).

Notch signalling during adult tissue homeostasis

In line with its prevailing role for maintaining 'stemness' and inhibiting differentiation, Notch acts to sustain normal homeostasis in a variety of adult tissues through regulation of stem cell pools and control of cell fate. This has been best characterised in the most actively self-renewing of endodermal organs, the intestinal epithelium. The crypt-villus axis is maintained by canonical Wnt signalling. When Apc, a key negative regulator of Wnt is deleted transgenically, or mutated in colorectal cancer, intestinal cells remain highly proliferative and fail to differentiate into enterocytes or migrate up the villus (149). It is now known however that Notch ligand (Dll1, Dll4) supplied by Paneth cells within the crypt acts to maintain the Lgr5 stem cell population; an example of how stem cells can receive niche support from their own specialised differentiated progeny (150). Genetic deletion or pharmacological inhibition of this Notch activity induces transdifferentiation of proliferating progenitor cells into a post-mitotic secretory, goblet cell phenotype (151, 152).

The role of Notch in liver homeostasis is less defined. Very few studies have been performed to genetically delete Notch components in the adult liver in the absence of injury. One study has used a Cre-loxP system under the control of an Mx1 promoter to delete Notch1 (Mx1Cre-Notch1$^{flox/flox}$) (153). Mx1 protein is an interferon-induced binding protein that forms part of the innate immune response against viral infection (154). In response to interferon (IFN), expression of this protein is induced in the liver (hepatocytes and biliary epithelial cells) and bone marrow. Without additional injury, the resultant phenotype following IFN administration and Notch1 deletion was nodular regenerative hyperplasia (NRH) of the liver; an increase in liver weight and parenchymal nodulation without associated inflammation, fibrosis or venous congestion. Notch1 knockout animals displayed a dramatic increase however in the number of BrdU positive hepatocytes and the authors suggest that mutual inhibitory signalling between Jagged1 and Notch1 positive hepatocytes might account for the majority of hepatocytes

remaining in an extended period of G_0 quiescence. It should be noted however that the observation of Jagged1 expression on hepatocytes has not been widely replicated (155).

Although embryonic deletion of Notch2 is known to result in ongoing dysfunction of intrahepatic bile duct organisation long into the post-natal period, adult biliary deletions of Notch once normal ductal development has been completed have not been performed. Consequently true assessment of the ongoing requirement for Notch activity in biliary maintenance cannot as yet be made.

In spite of this, descriptive studies have been performed to define the expression of Notch pathway components in human adult and fetal liver. Flynn and colleagues for example have detected mRNA transcript for all four Notch receptors in fetal, paediatric normal and diseased liver. In the developing liver they found Notch3 detectable on mesenchymal cells adjacent to ductal plate cells expressing Jagged1 ligand (156). This is consistent with the findings of Zong et al. who found Jag1 to be expressed in portal vein endothelium from E12.5 onwards and on the portal side of ductal structures by E16.5 where it co-localised with CK19 and Sox9. No Jag1 was detectable on the parenchymal side of the ductal plate at any stage of development. Similarly, they observed Hes1 on peri-portal and endothelial cells at the early stage of ductal plate development (E12.5), and by E18.5 this was also on mature ductal structures, co-localising with HNF4α (145).

Further than this, the results of immunohistochemical analyses of Notch proteins in healthy liver have frequently produced inconsistent results. In healthy paediatric liver Flynn et al found Notch1 and Notch2 detectable on bile ducts but also reported expression on hepatic arteries and hepatocytes. In contrast they observe Notch3 on hepatocytes, portal veins and hepatic arteries, with Notch4 only detectable on arteries (156). Nijjar et al. report expression of Notch1 and 2 on the sinusoidal endothelium as well as the bile ducts, and Notch2 in hepatocytes. Notch3 is reported to be found on bile ducts, hepatocytes and the vasculature (157). Both

studies find very little Notch4 expression. All studies concur that the Notch ligand Jagged1 appears to be the dominant ligand in healthy liver and is up-regulated during disease, however there still remains some debate as to which cell types represent its source (155, 158).

Notch signalling in adult liver disease & regeneration

The adult liver has a remarkable capacity for regeneration following injury. After 2/3 partial hepatectomy in the rat, the residual liver lobes enlarge to restore liver mass within 5 to 7 days, and up to 90% of the parenchyma can be removed whilst still achieving eventual restoration of original size (159). In the healthy liver this process is achieved through hepatocyte division; the potential for which appears almost unlimited. As many as 12 sequential hepatectomies have been performed in rat without apparent impairment of regenerative capacity (160). In chronically diseased liver for example cirrhosis however, proliferation of hepatocytes can fail and the liver becomes reliant on activation of a population of bipotential hepatic progenitor cells (HPCs) with the ability to differentiate into either hepatocytes or biliary epithelia (161, 162). These activated cells thought to arise from the terminal ductules of 'Canals of Hering' and their accompanying inflammatory reaction have been described as 'Ductular Reactions' (163) and are found in all forms of chronic and severe acute liver diseases in man both biliary and hepatocellular, with numbers correlating with disease severity (164-166).

Biliary atresia is a paradigm cholangiopathy in which ductular reaction, inflammation and portal fibrosis occur in response to destruction or failure of development of the major extrahepatic bile ducts. This contrasts with Alagille syndrome, where there is a lack of ductular reaction and progenitor cells with accompanying loss of the biliary transcription factor HNF1β, implying that Notch signalling may indeed play a role in progenitor-mediated parenchymal repair (125). A deficiency of Notch signal in the embryo resulting in biliary malformation implies that Notch is required for faithful development and maintenance of the biliary system. Notch pathway components are up-regulated in response to chronic biliary diseases in man including primary biliary cirrhosis (PBC) and primary sclerosing cholangitis (PSC). This contrasts to hepatocellular insults such as Hepatitis C Virus (HCV) infection and is evident both in terms of gene transcription and protein expression (155, 157, 158, 167, 168). Importantly such up-regulation includes the

downstream target effectors of Notch, in particular Hes1 and Hey1 (158). For instance isolated CK7 positive ductular reactions laser microdissected from human PSC and PBC livers exhibited high expression of NOTCH1 and NOTCH2 compared to those from livers infected with Hepatitis C Virus (169). Jagged1 and Dll4 are the only Notch ligands expressed by the human liver. Jagged1 is strongly up-regulated during chronic biliary disease, and has been described on HPCs, hepatocytes and hepatic stellate cells (155, 170, 171). Little is known about Notch activity in liver fluke cholangiopathies. Exome sequencing studies have identified a number of genetic alterations that appear to discriminate fluke-associated and sporadic BTC, however in these series Notch does not appear to be a target of mutagenesis. Further work is required to determine whether wild type Notch plays a role in these conditions.

During chronic liver disease the local microenvironment changes in response to damage; myofibroblasts and inflammatory cells infiltrate regions of local necrosis and produce growth factors and matrix proteins including laminin to form a stereotypical niche that will promote expansion of the HPC pool and re-epithelialisation of the liver parenchyma (172). In biliary disease this niche is characterised by a close spatial relationship between αSMA positive myofibroblasts and the emerging HPCs, resemblant of the portal mesenchyme in the embryo, forming a potential juxtacellular communication through which mesenchymal Jagged1 can activate epithelial Notch activity (158).

Chronic biliary disease can be modelled in the mouse using 3,5-diethoxycarbonyl-1,4-dihydrocollidine (DDC) dietary induced injury (173). Notch inhibition through genetic deletion (AlbCre-Rbpj$\kappa^{flox/flox}$) or gamma-secretase inhibitors results in a decreased number of HPCs and ductular reaction in mice fed with DDC, with an accompanying reduction transcription of Hes/Hey Notch targets and genes involved in biliary differentiation (HNF6; HNF1β; γGT) (158, 174). In Notch2

knockout mice (AlbCre-Notch2$^{flox/flox}$) fed with DDC, clusters of CK19 positive cells are unable to form ductular reactions with a normal tubular structure; RBPJκ knockouts suffer a more severe injury with an almost absence of ductular reaction and accompanying parenchymal necrosis (174).

The bipotential switch in cell fate of HPCs towards cholangiocyte or hepatocyte is mediated by the Notch antagonist Numb. During hepatocyte injury inflammatory macrophages phagocytose hepatocyte and matrix debris, triggering secretion of Wnt3a into the niche. This activates β-catenin-mediated Wnt signalling within HPCs, transcription of Wnt downstream targets TCF-LEF, and stimulates expression of hepatocyte genes including HNF4α and the ubiquitin ligase and Notch antagonist Numb. Inhibition of Numb with siRNA causes in reactivation of the Notch pathway and up-regulation of the biliary gene programme (Hes1; HNF1β; HNF6) (158). Transgenic overexpression of Notch in hepatocytes using adeno-associated viral delivery of hepatocyte-specific Cre reprograms hepatocytes to the biliary lineage (175).

Notch therefore appears necessary and sufficient for embryological development of the biliary tree in terms of both cholangiocyte specification of hepatoblasts and tubular morphogenesis of the branching ductular network. It would appear likely that this role extends to maintenance of this system in the homeostatic adult liver and has certainly been shown to be a required signal during progenitor-mediated regeneration following biliary injury in disease.

Notch signalling in cancer

The implication of Notch in the aetiology of cancer arose from the discovery that a proportion of patients with T cell acute lymphoblastic leukaemia (T-ALL) carry a (7;9) translocation of the β T cell receptor (*TCRβ*) gene to a locus within the coding region for Notch1. The result is expression of a truncated and constitutively active Notch1 protein (also known as translocation-associated Notch1 (TAN-1)) (176). Functional characterisation of Notch1 led to the discovery that the receptor is needed for the commitment of pluripotent progenitors to a T cell fate (177) and later the assembly of the pre-T cell receptor complex in immature thymocytes (178). Such a role would explain the later discovery that more than 50% of human T-ALLs carry activating mutations involving the extracellular heterodimerisation and PEST domains of Notch1 (105). T-ALL can therefore be modelled very effectively in the mouse through transplantation of N1-ICD over-expressing bone marrow into irradiated mice (100% disease penetrance) (179). Notch2 and Notch3 have also been implicated in the pathogenesis of T cell leukaemia (180-182).

Mutations of Notch leading to oncogenesis are much rarer in non-haemopoietic systems; rather it is dysregulation of wild type Notch activity that appears to promote tumorigenesis in solid organs. In non-small cell lung cancer (NSCLC) gain-of-function mutations in Notch1 have been reported in up to 10% of cases (183), however more frequently there appears to be loss of the Notch antagonist Numb (183) or over-expression of activity through the Notch3 receptor paralog (184). Furthermore it has been demonstrated through genetic deletion experiments that the canonical Notch components RBPJκ and the gamma-secretase complex are both necessary for the formation of $Kras^{G12D}$–driven NSCLCs in mouse (185). In human disease expression of Notch1 and its ligand Dll4 are prognostic of poor outcome (183, 186). Tumour progression in many cancer types is thought to be driven by self-renewal of a distinct population of tumour propagating cells which also are likely to mediate drug resistance (187-190). In NSCLC it appears that Notch, and in particular the Notch3 enriches with the markers CD24 and ITGB4,

with tumour-propagating ability and that the gene signature of this population is predictive of poor prognosis in human disease. These markers appear to represent a stable population following serial transplantation and which enriches after treatment with chemotherapy. ShRNA experiments demonstrate the Notch3 receptor plays a non-redundant role in driving self-renewal of these cells *in vivo* (191).

Activation of different Notch receptor paralogs appear to action different effects according to context. Notch1 and Notch2 are expressed in different compartments in pancreas; Notch1 is expressed by acinar cells whereas Notch2 appears in the ductal epithelium and becomes up-regulated in the PanIN lesions of pre-malignancy and in invasive tumours (192). Genetic deletion of Notch2 but not Notch1, results in a significant improvement in survival in a $kRas^{G12D}$-driven model of pancreatic ductal adenocarcinoma (PDA) and a reduction in tumour progression (193). As in lung cancer, blockade of Notch using gamma-secretase inhibitors inhibited the growth of human PDA cell lines as well as the *in vivo* formation of tumours in a Notch-dependent fashion (192).

The role of Notch in mammary stem cells has been well characterised and acts to commit cells exclusively along a luminal lineage whilst promoting self-renewal. Transgenic activation of Notch in differentiated luminal cells promotes tumorigenesis, triggering the development of hyperplastic nodules and re-activating clonogenic capacity (194). It has been suggested that one mechanism by which the stroma may be supporting tumour cell growth is through provision of Notch ligand although this evidence is not well developed. Inflammatory stromal cytokines and epigenetic dysregulation of NIK expression leads to over-activation of NFκ-B signalling in triple negative breast cancer and up-regulated Jagged1 expression (195). Furthermore Jagged2 expression is negatively correlated with both overall and metastasis-free survival in breast cancer patients (196). In breast cancer metastases it has been shown that stromal hypoxia leads to up-regulation of Jagged2 expression, particularly at the invasive fronts of tumours. Furthermore up-

regulation of Jagged1 by breast ductal carcinoma cells themselves can activate Notch signalling in osteoblasts and promote osteolytic bone metastasis (197). It is thought that *Aes* (*Amino-terminal Enhancer of Split*) (a member of the Groucho/Transducin-like Enhancer of Split (TLE) family) acts as an endogenous inhibitor of metastasis through repression of Notch transcription and indeed hepatic metastases of primary colorectal tumours can be suppressed using gamma secretase inhibition (198). In pancreas direct co-culture of stellate cells with cancer cells leads to activation of epithelial Notch and enhancement of proliferation compared to indirect co-culture (and stimulation via non-juxtacellular signalling pathways)(199). Furthermore in PDA it is thought that mesenchymal stem cell-derived myofibroblasts are able to maintain stemness in tumour-initiating epithelial cells through Notch provision (200). Perhaps the strongest data comes from B-lineage ALL, where clonal expansion of B cells is highly dependent on signals from the surrounding microenvironment of the bone marrow. Bone marrow mesenchymal cells express Notch ligands, in particular Jagged1,2 and Dll1 (201). Specific neutralising antibodies targeted against Jagged1,2 and Dll1 results in an increase in stromal-mediated apoptosis of B-ALL cells via up-regulation of Blc2 and down-regulation of Caspase3 (202).

Notch signalling in primary liver malignancies

In comparison to other tumours types, the role for Notch in primary hepatic tumorigenesis is less well defined. Constitutive expression of N2-ICD in albumin expressing cells is sufficient to induce HCC and biliary hyperplasia with associated up-regulation of pro-proliferative genes in both hepatocytes and biliary epithelia (203). Furthermore N2-ICD overexpression accelerate DEN-induced hepatic tumorigenesis with resulting tumours exhibiting less differentiation than DEN alone controls. In addition to this reduction in HCC latency, Alb-Cre;N2-ICD mice treated with DEN concomitantly develop ICC. Immunohistochemical analysis of Notch1, Notch2 and Hes1 has been performed in BTC, and whereas expression of these was

reported to be absent in homeostatic biliary epithelia, tumours appeared strongly positive, in particular for Notch1 (204). The full role of endogenous, wild-type Notch in ICC has yet to be fully characterised.

The mechanisms by which Notch promotes malignancy

To fulfil its role in self-renewal and maintenance of stem cell pools, it is likely that wild type Notch interacts with molecular pathways controlling proliferation, regulation of the cell cycle or apoptosis. The frequency with which dysregulation of the Ras cascade occurs in human tumours has prompted enquiry as to whether there is communication between oncogenically activated Ras and Notch signalling, however this relationship appears complex (205). These authors have used two *in vitro* systems to address this question: human foreskin fibroblasts and human embryonic kidney epithelial cells (HEK), both expressing the telomerase reverse transcriptase subunit (hTERT), SV40 oncoproteins and oncogenic H-RasV12. They demonstrated Ras to be upstream of Notch1, with Ras activation inducing CBF-1 reporter activity, up-regulation of the active subunit of Notch 1 (N1-ICD), and its translocation to the nucleus. Similarly introduction of a dominant negative form of H-Ras led to down-regulation of Notch activity. Transfection of Ras-transformed cells with an antisense Notch construct, but not cells expressing SV40 alone resulted in a significant reduction in proliferation. The same was seen following treatment with gamma-secretase inhibitors. To test this interaction *in vivo*, transformed fibroblasts were injected into NOD/SCID mice and tumour burden assessed. Tumour growth was exponential in all animals that received vector-transfected cells, whereas no tumours were observed in any animals that received cells transfected with antisense Notch until as late as day 35.

The authors of this study observed that Notch1 transcription was only modestly increased by H-RasV12, suggesting that Notch1 protein is modified by Ras at a post-transcriptional level. Immunoprecipitation confirmed that Notch1 protein was much more dramatically affected by Ras transformation, and in particular Pre-Senilin1 (PS1), a component of the gamma-secretase complex appeared to be significantly induced by H-RasV12 activation and decreased following transfection with dominant negative Ras. Q-rtPCR confirmed these effects to be post-transcriptional. To test which level of the Ras cascade was acting to regulate Notch,

pharmacological inhibitors of the pathway (MEKK, MEK1/2, PI3k, p38 and PKC) were tested; only cells treated with a p38 inhibitor demonstrated any reduction in Notch1 and PS1 proteins and proliferation. Furthermore this effect could be abolished with introduction of N1-ICD. These findings together indicate that in these contexts Notch1 was acting as a key downstream mediator of oncogenic Ras and in fact was necessary to maintain the neoplastic phenotype in Ras transformed cells.

Such an interaction between Notch and Ras has been described in other systems and in other species (206-208). It has been suggested downstream activation of Notch by oncogenic Ras represents the pathological aberration of a physiological feedback mechanism in which Ras uses Notch to regulate its own signalling. Thus a mechanism is presented by which Notch can exert completely different effects in transformed cells from its physiological role in healthy tissues.

Collaboration between Notch and other oncogenic pathways have also been described: *c-myc* in a mouse model of thymoma driven by truncated Notch (106); oncogenic products E6 and E7 of papillomavirus 16 driving downstream activation of AKT in invasive cervical tumours (209); TGFα during acinar to ductal metaplasia in exocrine pancreas and consequently adenocarcinoma (210).

It therefore seems clear that the cell survival signals potentiated by Notch vary according to both cellular context and the genetic alterations that have occurred within the cell.

Chapter 2: HYPOTHESES & AIMS

Hypotheses

(i) The tumour-stroma microenvironment in ICC represents an aberrant pathological extension of the regenerative hepatic progenitor cell niche of chronic liver disease

(ii) Notch activity within cancerous biliary epithelia is driving tumour progression

(iii) Ablation of Notch signalling will attenuate tumour expansion

(iv) Pharmacological Notch inhibitors represent a potential therapeutic strategy in ICC

Aims

(i) To generate a conditional transgenic model of ICC in mouse to enable inducible and specific deletion of Notch within the biliary compartment

(ii) To characterise endogenous Notch pathway expression in human ICC and rodent models

(iii) To elucidate Notch function in disease progression of ICC

(iv) To assess the potential of targeting Notch as a future therapeutic strategy in ICC

Chapter 3: MATERIALS & METHODS

Human Tissue Collection & Ethical approval

Freshly frozen human tissue was obtained prospectively from patients undergoing hepatic resection of ICC at the Royal Infirmary of Edinburgh with written informed consent and local ethical approval from the NHS Lothian Tissue Governance ethics committee (10/S1402/33). In addition archival formalin-fixed paraffin embedded human tissue was also obtained from the South East Scotland SAHSC Bioresource and MRC Sudden Death Brain and Tissue Bank (10/H0716/3) Healthy liver tissue was collected and fixed following a standardised operating procedure, however BTC samples were obtained over a 20 year period without standardisation.(211).

In vivo models of ICC

All animal experiments were performed according to UK Home Office regulations and with local veterinary approval (PIL 60/12907). All animals were housed in rooms with a 12:12 hour light:dark cycle at an ambient temperature of 22 ± 1°C and given chow and water *ad libitum*. Culling was performed using a Schedule 1 procedure (either CO_2 asphyxiation or cervical dislocation).

Chemically induced models of ICC

Eight week old male Sprague-Dawley rats ≥350g were administered 0.06% thioacetamide (TAA) in drinking water sweetened with orange squash (5:1) for 26 weeks. Rats were monitored with daily weights and observation of clinical condition and supplemented with mashed diet made with TAA water. If rats lost ≥20% body weight or displayed clinical signs of dehydration, animals were temporarily administered normal drinking water without TAA. This period did not exceed 72 hours in any given rat. Tissue from a timecourse of rats on the TAA regimen was also used in this study, kindly donated by Andrew Robson (previous MRC Clinical Research Fellow Forbes Lab). In this case rats were sacrificed at the

following timepoints: 10, 12, 14, 16, 20, 22, 24 and 26 weeks (n=3 at each timepoint). Control animals received 26 weeks of normal drinking water (n=6).

Xenograft model of ICC

Six week old male immunocompromised mice (CD1-Nude) received bilateral subcutaneous flank injections of the human ICC cell line CC-LP-1 (5×10^5 cells/injection (100μl))(212). Tumours were allowed to establish over a 28 day period before mice were exposed to treatment regimens. Tumour burden was assessed following harvesting and tumour dissection using a fine balance to measure tumour mass and digital calipers to measure maximal tumour length and width. Tumour volume was then calculated using the modified ellipsoid formula: $\frac{1}{2}(\text{length} \times \text{width}^2)$. I found this to be a more accurate assessment than serial external measurement of tumours through the skin using digital calipers which did not produce reproducible measurements.

Transgenic models of ICC

$CK19CreER^T$ mice on a mixed genetic background were obtained as a kind gift from Guoquaing Gu, Vanderbilt Medical Centre, Tennessee, USA. $R26ReYFP^{f/f}$ mice on a C57/Bl6 background were obtained as a kind gift from Owen Sansom, Beatson Institute for Cancer Research, Glasgow, UK. $Trp53_{tm1Brn}$ ($p53^{f/f}$) and B6.129S4-$kras^{tm4tyj}$/J ($kRas^{G12D}lsl$) mice were purchased from Jackson Laboratories. Mice were cross-bred to produce the following lines:

$CK19CreER^T;R26ReYFP^{f/f}$

$CK19CreER^T;R26ReYFP^{f/f}p53^{f/f}$

$CK19CreER^T;R26ReYFP^{f/f}p53^{f/f}kRas^{lsl}$

Cre Induction

Recombination of loxP sites by Cre was induced using i.p. injection of 30mg/ml tamoxifen (TM) (Sigma) in corn oil. Two regimes were used to assess efficiency of Cre:

- One injection of 80mg/kg TM (n=25)
- Three injections of 4mg TM on alternate days (n=19)

The following experimental groups were used in both regimes:

Cre – $YFP^{+/+}$ TM +

Cre + $YFP^{+/+}$ TM –

Cre + $YFP^{+/-}$ TM +

Cre + $YFP^{+/+}$ TM +

Mice were sacrificed 5 days post-injection. Cre efficiency was assessed by performing immunohistochemistry staining for YFP. The number of YFP +ve and total number of bile duct cells were counted on 50 consecutive fields at a magnification of x400 to quantify both the total number of YFP+ve cells as well as the proportion of bile ductal cells +ve for YFP. One section per mouse was used in this analysis.

Genotyping

A commercial service (Transnetyx©) was used to undertake all genotyping for this project. Ear notches were taken at the time of weaning at 4 weeks of age.

Pilot Model 1: $CKCreER^{T}$;$R26ReYFP^{f/f}p53^{f/f}$ + CCl_4

$CK19CreER^{T}$;$R26ReYFP^{f/f}p53^{f/f}$ mice underwent induction of Cre at 6 weeks of age with 3 x 4mg i.p. injections of TM. At 8 weeks of age mice then underwent 3 x weekly i.p. administration of 1µl/g carbon tetrachloride (CCL4) in olive oil or olive oil control for 16 weeks. $CK19CreER^{T}$;$R26ReYFPp53^{+/+}$ n=21; $CK19CreER^{T}$;$R26ReYFPp53^{+/-}$ n=21. Mice were culled at 24 weeks of age.

Pilot Model 2: CKCreER^{T};R26ReYFP$^{f/f}$p53$^{f/f}$ + TAA

CK19CreER^{T};R26ReYFP$^{f/f}$p53$^{f/f}$ mice underwent induction of Cre at 6 weeks of age with 3 x 4mg i.p. injections of TM. At 6 weeks of age mice were administered 600mg/l oral TAA for 26 weeks. CK19CreER^{T};R26ReYFPp53$^{+/+}$ n=4; CK19CreER^{T};R26ReYFPp53$^{+/-}$ n=14 CK19CreER^{T};R26ReYFPp53$^{-/-}$ n=7. Mice were culled at 32 weeks of age.

Pilot Model 3: CKCreER^{T};R26ReYFP$^{f/f}$p53$^{f/f}$ kRas

CK19CreER^{T};R26ReYFP$^{f/f}$p53$^{f/f}$kRas mice underwent induction of Cre at 6 weeks of age with 3 x 4mg i.p. injections of TM. Mice were observed daily for clinical signs of tumour formation for a period of up to 9 months.

Quantification of tumour burden *in vivo*

Presence or absence of malignancy was confirmed by a specialist liver histopathologist in each model (Dr Timothy Kendall). Rat livers were manually cut into 3mm sections before being aligned and paraffin embedded to ensure a maximal surface area of liver was available on each 4μm section. 4 to 5 blocks were generated per animal. H&E staining was performed on one section from every block for each animal. A blinded liver histopathologist manually demarcated tumour boundaries for each section and assessed tumour area using Image J software, as well as counting the total number of tumours.

Inhibition of Notch signalling *in vivo*

Gamma-secretase inhibition of ICC in rat

The gamma-secretase inhibitor N-[N-(3,5-Difluorophenacetyl)-L-alanyl]-S-phenylglycine t-butyl ester (DAPT) was administered to male Sprague-Dawley rats undergoing the TAA regime of tumour induction as previously described. 10mg/kg DAPT or equivalent volume of olive oil control was administered by i.p. injection on

3 consecutive days followed by 4 rest days for 5 weeks between weeks 21 and 26 of TAA administration (DAPT n=8; Control n=12). Rats were culled at 27 weeks.

Gamma-secretase inhibition of ICC xenografts

Xenografted tumours were established as previously described. After 28 days of engraftment, mice were administered 40mg/kg DAPT in olive oil i.p. or equivalent volume of olive oil control on 3 consecutive days followed by 4 rest days for 2 weeks (n=4).

Tissue and Cellular analysis

Tissue preparation

At the time of sacrifice murine and rat livers were flushed using 5 or 10mls sterile PBS via the IVC and liver, kidney, spleen, intestine and lung harvested. All tissues were fixed overnight in 4% buffered formalin or methacarn (60% methanol; 30% chloroform; 10% acetic acid) before being transferred to 70% ethanol. Following fixation tissue was embedded in paraffin and cut into 4μm sections.

Immunostaining of paraffin embedded sections

Immunostaining was performed according to protocols previously described by our laboratory (172). De-waxing was performed using 10 minutes of immersion in xylene before re-hydration with serially dilute ethanol solutions before transfer to PBS. Sections were mounted in sequenza racks with PBS.

Blockade of endogenous peroxidase activity was performed as part of all protocols using 3% hydrogen peroxide (Sigma) for 10 minutes before washing with PBS containing 0.01% Tween20 (Sigma) for permeabilisation. For peroxidase detection endogenous avidin and biotin were blocked at this point using an avidin-biotin blocking kit (Dako); 15 minutes incubation with avidin followed by 3 PBS washes and 15 minutes incubation with biotin followed by 3 PBS washes. Antigen retrieval was performed using microwave based heat or enzymatic digestion (see Table 2.1

for antigen-specific protocols). Sections were washed a further 3 times in PBS before incubating for one hour with a universal protein block (Spring Bioscience). Sections were then incubated with the appropriate primary antibody (in antibody diluent (Invitrogen)).

Table 2.1 Table of primary antibodies

Primary Ab	Clone/Cat. no.	Species	Fixation	Ag Retrieval	Incubation
Notch1	Abcam ab8925	Goat	Formalin	10 mins HP M/W Sodium citrate	1 in 50 O/N 4°C
Notch2	Santa Cruz sc-7423	Goat	Cells only	10mins 0.01% Triton X	1 in 50 O/N 4°C
Notch3	Abcam ab23426	Rabbit	Formalin/ Methacarn	2 x 5mins HP M/W Tris EDTA	1 in 100 O/N 4°C
Notch4	Santa cruz sc-32613	Goat	Cells only	10mins 0.01% Triton X	1 in 50 O/N 4°C
Jagged1	Santa cruz Sc-8303	Rabbit	Methacarn	10mins 0.01% Triton X	1 in 100 O/N 4°C
CK19	Troma III	Rat	Formalin	10 mins HP M/W Sodium citrate	1 in 200 O/N 4°C
CK19	Novocastra NCL-CK19	Mouse	Methacarn	0.01% Trypsin in 0.1% CaCl 8mins 37°C	1 in 100 O/N 4°C
mAChR3	Abd Serotec AHP1355	Rabbit	Formalin	2 x 5mins HP M/W Tris EDTA	1 in 100 O/N 4°C
Epcam	Abcam Ab3392	Rabbit	Formalin	2 x 5mins HP M/W Sodium citrate	1 in 100 O/N 4°C
Sox9	Millipore AB5535	Rabbit	Formalin	2 x 5mins HP M/W Sodium citrate	1 in 500 1hr RT
Pan Cytokeratin	Dako Z0622	Rabbit	Formalin	5mins HP M/W Sodium citrate + 5 mins Proteinase K 37°C	1 in 200 1hr RT
MRP5	GeneTex GTX23377	Rat	Formalin	5mins LP M/W Tris EDTA	1 in 100 O/N 4°C
CD44	Biolegend 103005	Rat	Formalin	2 x 5mins HP M/W Tris EDTA	1 in 100 O/N 4°C
αSMA	Sigma A5228	Mouse	Formalin	3 x 5mins HP M/W Sodium citrate	1 in 1000 2hrs RT
pAKT (Thr308)	Cell Signalling #4056	Rabbit	Formalin	2 x 5mins HP M/W Sodium citrate	1 in 100 O/N 4°C
pAKT (Ser473)	Cell Signalling #4060	Rabbit	Formalin	3 x 5mins HP M/W Sodium citrate	1 in 25 O/N 4°C
pS6 Ribosomal protein	Cell Signalling #4858	Rabbit	Formalin	2 x 5mins HP M/W Sodium citrate	1 in 500 O/N 4°C
pmTor (Ser2448)	Cell signalling #2976	Rabbit	Formalin	2 x 5mins HP M/W Sodium citrate	1 in 1000 O/N 4°C
c-Met	Abcam ab5662	Rabbit	Formalin	2 x 5mins HP M/W Tris EDTA	1 in 100 O/N 4°C
TGFβRII	Santa cruz Sc-220	Rabbit	Formalin	2 x 5mins HP M/W Tris EDTA	1 in 100 O/N 4°C
CYP2D6	Prof Roland Wolf	Sheep	Formalin	2 x 5mins HP M/W	1 in 200

	Uni of Dundee			Sodium citrate	O/N 4°C
CD31	Abcam Ab28364	Rabbit	Formalin	2 x 5mins HP M/W Tris EDTA	1 in 100 O/N 4°C
GFP	Abcam ab13970	Chicken	Formalin	2 x 5mins LP M/W Tris EDTA	1 in 500 1hr RT
GFP	Abcam ab	Goat	Formalin	3 x 10mins HP M/W Sodium citrate	1 in 400 1hr RT
p53	Abcam Ab26	Mouse	Formalin	2 x 5mins HP M/W Sodium citrate	1 in 200 O/N 4°C
BrdU	Abcam Ab6326	Rat	Formalin	2 x 5mins HP M/W Sodium citrate	1 in 100 O/N 4°C
Nanog		Rat	Frozen	10mins 0.01% Triton X	1 in 100 O/N 4°C
Oct4	Santa cruz Sc-8629	Goat	Frozen	10mins 0.01% Triton X	1 in 100 O/N 4°C

Table 2.1 *Table of primary antibodies*

M/W Microwave based heat for antigen retrieval (HP High power; LP Low power). Sections were incubated with primary antibody either overnight at 4°C (O/N) or for an hour at room temperature (RT).

Following incubation, sections were washed three times in PBS before incubation for 30 minutes with the appropriate secondary antibody.

Table 2.2 Table of secondary antibodies

Species	Conjugation	Source	Dilution
Anti-Goat	Alexa 555	Invitrogen	1 in 200
Anti-Rabbit	Alexa 555	Invitrogen	1 in 200
Anti-Mouse	Alexa 555	Invitrogen	1 in 200
Anti-Sheep	Alexa 555	Invitrogen	1 in 200
Anti-Rabbit	488	Invitrogen	1 in 200
Anti-Rat	488	Invitrogen	1 in 200
Anti-Chicken	488	Invitrogen	1 in 200
Anti-Rabbit	Biotinylated	Dako	1 in 200
Anti-Goat	Biotinylated	Dako	1 in 200
Anti-Mouse	Biotinylated	Dako	1 in 200
Anti-Rabbit	HRP	Dako	1 in 200 (1 in 500 Tyramide)
Anti-Goat	HRP	Dako	1 in 200 (1 in 500 Tyramide)
Anti-Mouse	HRP	Dako	1 in 200 (1 in 500 Tyramide)
Anti-Chicken	HRP	Dako	1 in 200 (1 in 500 Tyramide)

Table 2.2 *Table of secondary antibodies*

After 3 PBS washes, sections for peroxidase detection were incubated for 30 minutes with RTU Avidin-Biotin complex kit (Vector). A further 3 PBS washes were performed before application of DAB (3,3'-Diaminodenzidine) chromogen substrate (Dako). Length of incubation was visually judged according to colour before 3 final PBS washes. Sections were counterstained with Harris Haematoxylin for 10 seconds and washed in tap water before immersion in Scott's tap water for 5 seconds followed by further washing. De-hydration was achieved with serially more concentrated ethanol solutions and xylene (2 x 5 minutes). Coverslips were mounted with Pertex.

For fluorescent detection, sections were washed 3 times with PBS following secondary antibody incubation. In most cases antibodies with directly conjugated fluorophores were used, in which case at this point coverslips were mounted using

DAPI-containing fluoromount (Southern Biotech). In the case of dual immunofluorescence where the two primary antibodies were raised in the same host species, a tyramide amplification kit was used (PerkinElmer). Here primary antibodies were diluted 50 times their standard concentration and a peroxidase-conjugated secondary antibody used before application of Tyramide amplification reagent (1 in 50 in amplification diluent). Sections were immersed in hot sodium citrate buffer for 2 minutes following application of the first secondary antibody and retrieval of the second antigen. Coverslips were mounted using DAPI-containing fluoromount as before.

Immunocytochemistry

Cells for immunocytochemistry were cultured on chamber slides before PBS washing and fixation with cold 1:1 methanol/acetone at room temperature for 10 minutes. Protein blocking was performed as before with for 1 hour before application of primary antibody (see table). 3 PBS washes were performed before incubation with the appropriate secondary antibody for 30 minutes at room temperature. DAPI-containing fluoromount was used to mount coverslips.

TUNEL

For detection of apoptosis by TUNEL, an *in situ* cell death detection fluorescein kit (Roche) was used according to manufacturer's instructions. Frozen sections were pre-treated with 10μg/ml proteinase K and permeabilisation with 0.1% Triton X.

Microscopy

A Nikon Eclipse E600 microscope was used for all bright field and fluorescent microscopy in conjunction with Axiovision Elements software v3.0.

Cell counting and image analysis

For cell counting and pixel analysis up to 50 photomicrographs were taken under standardised conditions at a magnification of at least x200. In xenograft experiments where the total area of tissue was more limited, the entire field was photographed and analysed. Image J software was used for cell counting. Adobe

Photoshop was used for pixel analysis. The 'fuzziness' function was used to select single colour intensity and standardised to Dapi to control for cell number. Results are expressed as the mean percentage of positive pixels per field.

Flow cytometry, cell sorting & cell cycle analysis

CC-LP-1 cells grown in monolayer on plastic were prepared using the following method for flow cytometric analysis: Cells were washed x 3 in PBS and incubated for 20 minutes in cell dissociation buffer (Invitrogen). Cells were spun at 1000rpm for 5 minutes; the pellet re-suspended in 100μl 10% human serum in PBS and incubated on ice for 15 minutes for blocking. Cells were washed x 3 with FACS buffer (2% human serum in PBS) and spun again at 500g for 5 minutes. Serial dilutions were performed to determine the optimal concentration of antibody for analysis. Cells were incubated in 100μl 1:100 Notch3 PE-conjugated antibody or isotype control in FACS buffer for 30 minutes or taken for unstained controls. Cells were then washed with FACS buffer x 3 and spun at 1000rpm for 5 minutes before being re-suspended in 400μ FACS buffer. 7-AAD was added at a 1:50 concentration before analysis as a live/dead marker. 1μl of Notch3 antibody was added to 1 drop of positive IgG beads as a positive control. Cells were sorted according to forward and side scatter to exclude debris before being gated at the top and bottom 5% of Notch3 expression. Cells were sorted directly into culture medium using a BD FACS Aria II. For cell cycle profiling, DNA staining solution (Sony Biotechnology) was added to samples immediately before analysis.

Western Blotting

Lysates were prepared using the following lysis buffer: 25mM NaHepes, 0.3M NaCl, 1.5mM $MgCl_2$, 0.2mM EDTA, 0.5% Triton X-100, complete protease inhibitor (Roche), 0.5mM dithiothreitol, 1mM sodium orthovanadate, pH 7.4. 30mg fresh whole liver was homogenised directly into 500μl buffer; 150μl buffer was used to lyse one well of cells growing in monolayer on plastic in a 6 well plate. Lysates were sonicated x 3 to minimise nucleotide contamination.

Protein content of samples was quantified using a BSA standard and BCA reaction with Pierce reagent. Protein quantity was standardised using lysis buffer before samples were reduced and denatured by heating to 70°C for 10 minutes in NuPAGE sample buffer and 10% β-mercaptoethanol. 4-12% Bis-Tris NuPAGE or 3-8% Tris-Acetate NuPAGE mini gels were used to run samples, using 1x Tris Acetate or 1x MOPS running buffer respectively. Bis-Tris gels were run at 200V for 35 minutes; Tris-Acetate gels at 150V for 60 minutes. Precision Plus Dual Colour or Precision Plus Kaleidoscope ladders (BioRad) were used to asses molecular weight.

Blotting was performed for 1 hour at 350mA onto nitrocellulose membrane using Toubin's transfer buffer (192mM Glycine, 25mM Tris, 200ml methanol, 800ml dH_20). Protein transfer was confirmed using Ponceau red solution. Blots were washed x3 in TBS-Tween (TBST) (2.42g Tris, 18g NaCl pH 7.4) with 0.1% Tween20 before blocking with 5% powdered fat-free milk (Marvel) or Odyssey blocking buffer (Licor) for 2 hours. Blots were washed again x 3 with TBST before incubation with primary antibody in 5% milk or blocking buffer for either 3 hours at room temperature or overnight at 4°C. Blots were washed again x 3 with TBST before incubation with species-appropriate HRP-conjugated secondary antibodies in TBST (1 in 2000) for one hour at room temperature. Blots were washed x 3 in TBST and exposed with chemiluminescent horseradish peroxidase substrate (1:1) (Amersham) using x-ray film or the Odyssey digital system (Licor). To strip blots for re-probing the following stripping buffer was used: 15g glycine, 1g SDS, 1% Tween 20 1L dH_20, pH2.2. Blots were incubated in stripping buffer for 10 minutes before being washed x 3 PBS 10 minutes and x 3 TBST 5 minutes and re-blocking with 5% milk. Loading controls were performed for all blots using antibodies against β-actin or GAPDH depending on the molecular weight of the protein of interest.

The following antibodies were used for western blotting in this study:

Primary Ab	Clone/Cat. no.	Species	Dilution	Incubation
Notch3	ab23426/Abcam	Rabbit	1 in 1000	Overnight 4°C
RBP 1F1 (RBPJκ)	IgG2b/Ascension	Rat	1 in 1000	Overnight 4°C
Beta-actin	AC-74/Sigma	Mouse	1 in 5000	3 hours RT

GAPDH	ab9483/Abcam	Goat	1 in 5000	3 hours RT
Secondary Ab	**Clone/Cat. no.**	**Species**	**Dilution**	**Incubation**
HRP	Dako	Rabbit	1 in 2000	2 hours RT
HRP	Dako	Goat	1 in 2000	2 hours RT
HRP	Dako	Rat	1 in 2000	2 hours RT
HRP	Dako	Mouse	1 in 2000	2 hours RT

Table 2.3 *Table of antibodies used in western blotting*

In vitro work

Culture of immortalised cell lines

The following immortalised cell lines were used in this study:

Name	**Origin**	**Reference**
CC-LP-1	Intrahepatic cholangiocarcinoma (human)	Shimizu *Int. J. Cancer* 2006
CC-SW-1	Intrahepatic cholangiocarcinoma (human)	Shimizu *Int. J. Cancer* 2006
SNU-1079	Intrahepatic cholangiocarcinoma (human)	Ku *Br.J. Cancer* 2002
SNU-1196	Extrahepatic cholangiocarcinoma (human)	Ku *Br.J. Cancer* 2002

Table 2.4 *Table of immortalised cell lines*

All lines were grown in 4% CO_2 at 37°C in Dulbecco's Modified Eagle Medium (Gibco) with 4.5g/l glucose, 2.5% fetal calf serum, 2mM L-glutamine, 10U/ml penicillin and 100μg/ml streptomycin. Cells were allowed to reach an 80% confluence level before they were trypsinised for re-plating. Cell counting was performed manually using a haemocytometer.

Assays of cell viability

For cell counting trypan blue was used as a live/dead stain. MTT (3-(4,5-dimethylthiazol-2-yl)-2,5-diphenyltetrazolium bromide) assay was used for formal assessment of cell viability. Cells were plated at a density of 1 x 10^5/ml in 96 well plates in the presence of appropriate experimental conditions or control in triplicate. Cells were cultured for 48 hours before 20μl 5mg/ml MTT was added and incubated

at 37°C for 4 hours. Media was then aspirated and 150μl of DMSO added per well. Plates were agitated on a shaker for 15 minutes before being read by a spectrophotometer at a wavelength of 570nm with a reference wavelength of 630nm. All viability experiments were repeated three times.

Tumour Spheroid culture

Multicellular sphere culture has been widely adopted as a model to study cancer cell behaviour, in particular that of cancer stem cells (CSCs); serial sphere formation and serial tumour engraftment are proposed as a functional surrogates of self-renewal capacity (213). In neuroblastoma for example, cells with serial sphere forming capacity are known to be enriched for the stem cell markers CD133, ABC transporter proteins, Wnt and Notch (213). Furthermore hypoxia arising within the centres of tumour sphere is thought to model necrosis occurring within the centres of solid tumours (214-216). The human cholangiocarcinoma lines CC-LP-1, SNU-1079 and CC-SW-1 were plated at a density of 1 x 10^5 cells/ml onto low adhesion culture plates (Corning). Aggregations of cells could be observed within 4 hours of plating and full tumour spheroids by 24 hours. This process was captured using a Zeiss (Observer) timelapse microscope.

Assays of clonogenicity

Cells were plated at clonal density (500cells/cm^2) and kept in culture for up to 4 weeks. The number of colonies formed per well was then counted.

Chemotherapy studies

ICC cells were plated at a density of 1 x 10^5 cells/ml in 96 well plates using standard medium. Chemotherapeutic agents were added to the culture medium at the following concentration ranges: 5-fluorouracil 0 to 100mM; gemcitabine 0 to 200μM; cisplatin 0 to 200μM. Cells were cultured with and without the addition of 50μM of the γsecretase inhibitor DAPT. Cell viability was assessed using MTT assay after 72 hours of culture and experiments were performed in triplicate.

Notch inhibition *in vitro*

The gamma-secretase inhibitor N-[N-(3,5-Difluorophenacetyl)-L-alanyl]-S-phenylglycine t-butyl ester (DAPT) (Tocris) and the HDAC1 inhibitor Trichostatin A (Sigma) were used to investigate the effects of Notch inhibition *in vitro.* The cancer lines CC-LP-1, CC-SW-1, SNU-1079 and SNU-1196 were plated in 96 well plates at a density of 1 x 10^4 cells per well or on low-adherence 6 well plates at a density of a 1.6 x 10^6 per well. Both agents were solubilised in DMSO. Drug or equivalent volume of DMSO was added to the media in increasing concentrations across the following range: 0 - 100μM. Cell viability was assessed using MTT assay. Cells were cultured for 48 hours before 20μl tetrazolium was added to each well, shaken on a rocker for 15 minutes in the dark and 150μl DMSO added before reading the absorbance on a spectrophotometer (BMG Labtech). A wavelength of 570nm was read with a reference wavelength of 630nm. For assessment of tumour spheroid formation, photomicrographs of each well were taken and the diameter of tumour spheres measured digitally. Spheres ≥50μm in maximal diameter were counted.

Luciferase reporter assays

To assay activity via the PI3K/AKT pathway *in vitro*, a Cignal FOXO luciferase assay was purchased (SA Biosciences). This commercial lentiviral reporter construct contains a mixture of an inducible FOXO-responsive firefly luciferase and constitutively (CMV) expressing *Renilla* luciferase (40:1) (Figure 2.1).

Human cholangiocarcinoma cells (CC-LP-1) previously transfected with shRNA targeted against NOTCH3 or scrambled sequence control were plated into 96 well white-bottomed plates in high glucose DMEM medium without serum and antibiotics at a density of 1 x 10^4 cells/well and left to adhere overnight. The following day cells were transfected with lentiviral particles using a multiplicity of infection (MOI) of 50 (total of 2.5 x 10^5 transducing units (TU) per well). Negative (a mixture of non-inducible firefly and *Renilla* luciferase (40:1)) and positive (constitutively expressing firefly luciferase and *Renilla* (40:1)) controls (also purchased from SABiosciences) were included. All transfections were performed in

triplicate. Viral particles were incubated at room temperature with 0.6µl/well of SureENTRY™ transduction reagent (Qiagen) in 25µl/well culture medium for 20 minutes before being added dropwise onto cells. The following day, cells were washed with PBS and replaced with medium supplemented with antibiotics and 2.5% FCS. To quantify the luminescence of the FOXO and *Renilla* driven luciferase activity on day 4, a Dual-Luciferase Reporter Assay (Promega) was used according to manufacturer's instructions. Luminescence was read using a Promega Glomax luminometer.

Figure 2.1 Lentiviral FOXO luciferase reporter construct (Qiagen Cignal Lenti FOXO Reporter

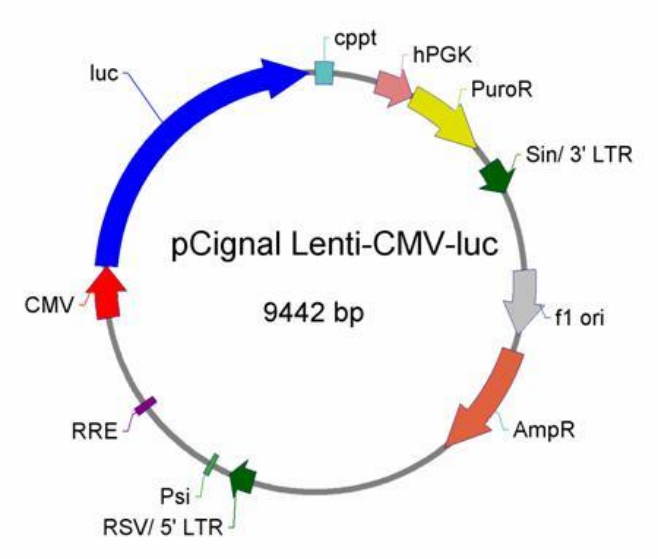

http://www.sabiosciences.com/reporter_assay_product/HTML/CLS-PCL.html

Figure 2.1 *Lentiviral FOXO luciferase reporter construct (Qiagen Cignal Lenti FOXO Reporter Assay).* A FOXO-responsive luciferase vector encoding firefly luciferase under the control of a minimal (m)CMV promoter and tandem repeats of the FOXO binding site.

RNA interference studies

siRNA *in vitro*

Commercial pre-designed short interfering RNA species targeted against the NOTCH3 or RBPJκ genes were purchased (SABiosciences). Four independent sequences were obtained for each gene of interest as well as a scrambled sequence control (Qiagen negative Allstars siRNA control). Human ICC cell lines were transfected using a lipofectamine 'fast forward' transfection protocol using HiPerfect reagent (Qiagen) according to manufacturer's instructions. Briefly, cells were plated in 24 well plates at the following densities: SNU-1079 1.8 x 10^4/well; CC-LP-1 5.6 x 10^4/well; CC-SW-1 7.0 x 10^4/well and allowed to adhere at 37°C for one hour. siRNA complexes were made up in the following ratio: 5nM siRNA (37.5ng); 3µl HiPerfect reagent; 96.7µl serum-free media. Complexes were incubated at room temperature for 10 minutes and added drop wise onto cells, swirling the plate for even distribution. Scrambled sequence and untransfected controls were prepared in the same way. The following day, cells were washed in PBS and media replaced. 48 hours post-transfection three wells were lysed for RNA and protein extraction to check gene knockdown efficiency.

The following siRNA duplexes were used in this study:

Gene Name	siRNA name	Gene Accession No.	Target Sequence
NOTCH3	Hs_Notch3_1	NM_000435	5'-CAGCGTGACCGAGATAGGTCA-3'
NOTCH3	Hs_Notch3_2	NM_000435	5'-ATGCCTAGACCTGGTGGACAA-3'
NOTCH3	Hs_Notch3_3	NM_000435	5'-AAGAATAGTTAACACTCAAA-3'
NOTCH3	Hs_Notch3_5	NM_000435	5'-CTGCGATTAATGAGGATGA-3'
RBPJκ	Hs_RBPJ_1	NM_005349	5'-TAGGGAAGCTATGCGAAATTA-3'
RBPJκ	Hs_RBPJ_2	NM_005349	5'-GTGGCTGGAATACAAGTTGAA-3'
RBPJκ	Hs_RBPJ_3	NM_005349	5'-TCCAGTAACTTTGGTCCGAAA-3'
RBPJκ	Hs_RBPJ_SUH_7	NM_005349	5'-CACGCTATTATAGTACACCTT-3'

Table 2.5 *Table of siRNA duplexes*

Growth of shRNA plasmids

For permanent silencing of gene expression, knockdown human cell lines were generated using delivery of plasmids containing shRNA sequences targeted against NOTCH3. Four commercial SureSilencing NOTCH3 shRNA plasmids (pGeneClip™) were purchased with scrambled sequence controls (SABiosciences).

Figure 2.2 NOTCH3 shRNA plasmid

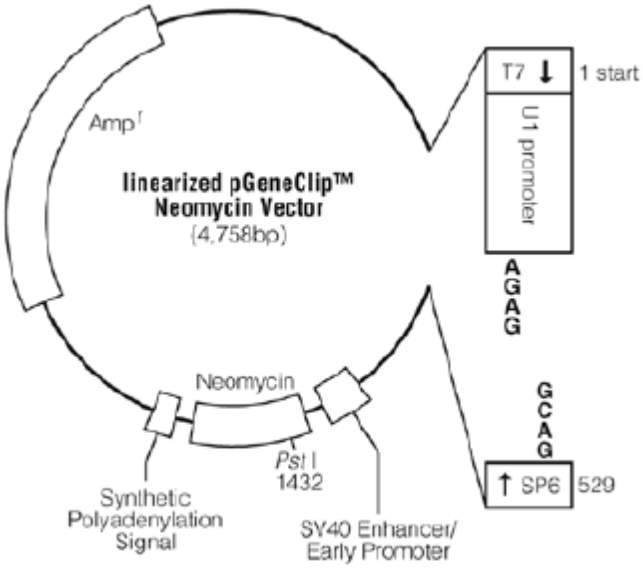

Figure 2.2 *NOTCH3 shRNA plasmid*

These vectors were driven by U1 promoters and contained ampicillin and puromycin resistance cassettes for selection. The full sequence of the vector is available at: http://www.sabiosciences.com/RNAiResource.php.

1µg pDNA was used to transform 50µl DH5α E.coli (Invitrogen). Bacteria were incubated on ice for 30 minutes before being subject to heat shock in the waterbath at 42°C for 30 seconds. 250µl lysogeny broth (LB) was added to each culture and incubated at 37°C for 60 minutes in a shaker before 20µl was taken for culture on LB agar containing ampicillin (1 in 1000) at 37°C overnight. Two independent colonies were picked from each plate and dispensed into 3mls LB containing ampicillin (1 in 1000). Cultures were incubated at 37°C in a shaker for 12 hours. When cloudy, 200µl of culture was added to 250mls LB (1 in 1000 ampicillin) and again incubated at 37°C overnight. DNA was purified and eluted from cultures using a plasmid maxi prep kit (Qiagen) according to manufacturer's instructions.

DNA quality and quantity was assessed using Nanodrop spectrophotometry (ThermoFisher). A Pst-1 restriction digest and gel electrophoresis was performed to ensure construct insertion had taken place.

DNA transfection of all four NOTCH3 shRNA sequences and scrambled control were performed in the human ICC cell line CC-LP-1. Cells were plated into 6 well plastic culture dishes at a density of 1.6 x 10^5 cells/well and transfected with 0.5µg pDNA the day after seeding using Effectene transfection reagent (a nonliposomal lipid reagent) in conjunction with Buffer EC and Enhancer (Qiagen). After 48hours cells were washed with PBS and media replaced with media containing 5µg/ml puromycin. Cells were cultured in puromycin-containing media and observed daily for the appearance of colonies. Once formed, colonies were individually picked with a pipette tip and transferred to a new culture plate and expanded. Three colonies per shRNA sequence were cultured in this way. Rt-qPCR and western blotting were performed for Notch3 to assess knockdown efficiency.

DNA and RNA analysis

RNA extraction, purification and specification

In preparation for RNA extraction, whole livers were snap frozen on dry ice at the time of harvest and stored at -80°C. 50mg of tissue per preparation was defrosted and dissociated with an electric homogeniser in 500µl Trizol Reagent (Amersham). 100µl chloroform was added, vortexed thoroughly and spun at 12000g for 15 minutes at 4°C. The aqueous phase was transferred to a clean Eppendorf before adding 100µl of molecular grade 70% ethanol. For cells, 1 x 10^6 cells were lysed in 350µl RLT buffer (Qiagen) before the addition of ethanol.

A Qiagen RNEasy Mini kit was used for RNA purification. 700µl of each sample was transferred to the columns provided and spun at 8000g for 15 seconds. 500µl RW1 buffer was added to wash the membrane and samples spun again at 8000g (15s). Two washes with RPE buffer (500µl; 700µl) were performed and each time

spun at 8000g. Columns were dried by spinning at 16000g for 1 minute before elution in 30µl RNase-free water.

RNA concentration and purity was determined using a Nanodrop spectrophotometer (ThermoScientific). The following parameters were used as an acceptable standard.

RNA concentration	>50ng/µl
RNA purity 260/280 ratio	>2
RNA purity 260/230 ratio	>1.8

Table 2.6 *Standards of RNA quality and purity*

For extraction of RNA from formalin fixed, paraffin embedded archival samples a Qiagen RNEasy FFPE extraction kit was used. 20µm sections were cut and placed into RNase-free tubes. 160µl of deparaffinisation solution was added to each sample and vortexed vigorously. Samples were incubated at 56°C for 3 minutes using a heat block and allowed to cool to room temperature. 150µl of proteinase K lysis buffer was added, vortexed and then centrifuged at 11000g for 1 minute. 10µl proteinase K was added to the lower, aqueous phase and mixed by pipetting to release RNA. Samples were then incubated at 56°C for 15 minutes and then 80°C for 15 minutes to reverse formalin cross-linking. The lower, uncoloured phase was then transferred into a new tube and incubated on ice for 3 minutes before centrifuging at 20000g for 15 minutes. The supernatant was transferred to a new tube and 16µl DNase boosting buffer and 10µl DNase added and incubated at room temperature for 15 minutes. 320µl RBC buffer was added to each sample and mixed followed by 720µl ethanol. 700µl of sample was transferred to an RNeasy MinElute column and spun for 15 seconds at 8000g. This step was repeated until all the sample had passed through the column. RNA was then purified using the same steps as described above for freshly extracted RNA, but eluted into 14µl RNase free water.

Reverse Transcription

100ng to 1µg RNA was reverse transcribed using a Qiagen Quantitect Reverse Transcription kit. Samples were standardised to the appropriate concentration by dilution in RNase free water. Elimination of genomic DNA was performed by incubating with gDNase at 42°C for 10 minutes. Template was then incubated with 1µl reverse transcriptase and random hexamers at 42°C for 30 minutes and the reaction quenched by heating to 90°C for 3 minutes.

rt-qPCR & PCR Arrays

Real time qPCR was performed using SYBR Fast reagent (Qiagen) in 384 well plates with a Roche 480 Lightcycler. 5µl cDNA was used per reaction. cDNA was diluted 1 in 200 with RNase free water unless the gene of interest was known to be lowly expressed e.g. Notch target genes where cDNA was diluted 1 in 10. Commercial quantitect primers (Qiagen) were used in all cases (see table). 5µl cDNA, 6.25µl SYBR and 1.25µl primer were used in each reaction. 18S was used as a standard reference gene with Taqman ROX master mix (Applied Biosystems). Cycling conditions were as follows:

Cycles	Temperature (°C)	Duration (s)
Activation	95	20
40 Cycles: Denaturation	95	10
Anneal/Extend	60	30
Melt Curve	95	15
	60	15
Cooling	40	30

Table 2.7 *Table of cycling conditions for rt-qPCR (Roche Lightcycler 480)*

The standard curve method was used to estimate amplification efficiency for each quantitect primer. cDNA template from each sample was combined and serially diluted 1:1 with RNase free water to produce a range of concentrations. Target gene expression was normalised to that of 18S rRNA. Specificity of PCR products was

confirmed by melting curve analysis. The following commercial pre-designed primers were used in this study (Qiagen):

Table 2.8 Table of primers

Species	Gene Symbol	Assay name	Accession Number
Human	NOTCH1	Hs_NOTCH1_1_SG	NM_017617
	NOTCH2	Hs_NOTCH2_1_SG	NM_024408
	NOTCH3	Hs_NOTCH3_1_SG	NM_024408
	NOTCH4	Hs_NOTCH4_1_SG	NM_004557
	JAG1	Hs-JAG1_1_SG	NM_000214
	JAG2	Hs-JAG2_1_SG	NM_002226
	DLL1	Hs_DLL1_1_SG	NM_005618
	DLL3	Hs_DLL3_1_SG	NM_016941
	DLL4	Hs_DLL4_1_SG	NM_019074
	HES1	Hs_HES1_1_SG	NM_005524
	HES4	Hs_HES4_1_SG	NM_001142467
	HEY1	Hs_HEY1_1_SG	NM_001040708
	HEY2	Hs_HEY2_3_SG	NM_012259
	HEYL	Hs_HEYL_1_SG	NM_014571
	NUMB	Hs_NUMB_1_SG	NM_001005743
	RBPJκ	Hs_RBPJ_1_SG	NM_005349
	CCND1	Hs_CCND1_SG	NM_053059
	CCND2	Hs_CCND2_SG	NM_001759
	CCNE1	Hs_CCNE1_SG	NM_001238
	MET	Hs_MET_1_SG	NM_000245
	IRS1	Hs_IRS1_1_SG	NM_005544
	FAS	Hs_FAS_1_SG	NM_000043
	FADD	Hs_FADD_1_SG	NM_003824
	XIAP	Hs_XIAP_1_SG	NM_001167
	RAC1	Hs_RAC1_1_SG	NM_006908
	PTEN	Hs_PTEN_5_SG	NM_000314
Mouse	Notch1	Mm_Notch1_1_SG	NM_008714
	Notch2	Mm_Notch2_1_SG	NM_010928
	Notch3	Mm_Notch3_1_SG	NM_008716
	Notch4	Mm_Notch4_1_SG	NM_010929
	Jag1	Mm_Jag1_1_SG	NM_013822
	Jag2	Mm_Jag2_1_SG	NM_010588
	Hes1	Mm_Hes1_1_SG	NM_008235
	Hey1	Mm_Hey1_2_SG	NM_010423
	Hey2	Mm_Hey2_1_SG	NM_013904
	HeyL	Mm_Heyl_1_SG	NM_013905

Rat	Notch1	Rn_Notch1_1_SG	NM_001105721
	Notch2	Rn_Notch2_1	NM_024358
	Notch3	Rn_RGD:620761_1_SG	NM_020087
	Notch4	Rn_Notch4_1_SG	NM_001002827
	Jag1	Rn_Jag1_1_SG	NM_019147
	Jag2	Rn_Jag2_1_SG	XM_001073124
	Hes1	Rn_Hes1_2_SG	NM_024360
	Hes5	Rn_Hes5_1_SG	NM_024383
	Hey1	Rn_Hey1_1_SG	NM_001191845
	Hey2	Rn_Hey2_1_SG	NM_130417
	HeyL	Rn_Heyl_2_SG	NM_001107977
	Irs1	Rn_Irs1_1_SG	NM_000314
	Pten	Rn_Pten_1_SG	NM_031606
	Fadd	Rn_Fadd_2_SG	NM_152937

Table 2.8 *Table of primers*

Notch pathway gene expression and proto-oncogene profiling was performed using the following RT2 Profiler PCR arrays (SA Biosciences):

Product No.	Target	Species
PAHS-059Y	Notch pathway	Human
PARN-059Z	Notch pathway	Rat
PAHS-133Z	Liver cancer	Human

Table 2.9 *Table of PCR arrays used in this study*

Plates were prepared according to manufacturer's instructions and the following Lightcycler conditions used:

Cycles	Temperature (°C)	Duration
1	95 95	10 min 15s
45	60	1 min

Table 2.10 *Table of cycling conditions for RT^2 profiler arrays (Roche Lightcycler 480)*

Data was analysed using online software provided by SA Biosciences at http://pcrdataanalysis.sabiosciences.com/pcr/arrayanalysis.php.

Statistical analyses

Statistical analyses were performed using Prism software (Graphpad Inc). All data were assessed for normal distribution using a D'Agostino and Pearson omnibus normality test ($p<0.05$). Data are expressed as means ± standard error unless otherwise stated. For comparison between two groups, parametric data were analysed using an unpaired two-tailed Student's t test. For non-parametric data and where n was too small to determine distribution a Mann-Whitney U test was used. Comparisons between two or more groups were made using a one-way ANOVA (Kruskall-Wallis) and where multiple variables were compared between two or more groups a two-way ANOVA was used. Survival analyses have been performed using the Kaplan-Meier method with comparisons between groups determined with the Log-rank test. Levels of significance have been denoted using the following notation: * $p\leq0.05$; ** $p\leq0.01$; ***$p\leq0.001$.

Non-linear regression analyses were performed using Prism software for dose response curves generated from ICC cells treated with chemotherapy with and without γ-secretase inhibition. Log[inhibitor} vs. response curves with three parameters were used to generate each fit, constraining the top to 1.0 (data normalised to no drug controls). The mean IC_{50}s of treatment groups were compared using the Mann-Whitney U test and significance set at $p=\leq0.05$.

Chapter 4: Establishing a murine model of ICC

Introduction

Transgenic murine technology such as the Cre-loxP system allowing temporal and cell-specific gene deletion or expression offers an unprecedented opportunity to better understand the cellular biology underpinning disease, particularly in adulthood. Few murine models of ICC exist and therefore one of the principal aims of this project was the development of a novel conditional transgenic murine model of ICC to permit targeted genetic manipulation and characterisation of the signalling pathways underpinning its pathogenesis. In this way, I aimed to improve the specificity of previously published models which have generated both HCC and ICC in the liver, by using transgenic alterations frequently observed in human disease (85, 87, 217). I hypothesised that by inducing mutations known to occur in ICC in man, a model could be generated that would more faithfully recapitulate tumour behaviour and response to therapy. As such, I chose an approach that combined targeted genetic deletion of tumour suppressors in biliary cells with delivery of chronic injury using toxins. As chronic inflammation is an established risk factor for the development of malignancy, I hypothesised that the combination of chemically induced injury and tumour suppressor deletion would establish cycles of cholangiocyte death and proliferation and create a pro-carcinogenic microenvironment to promote cancer development.

To this end, I used mice carrying a tamoxifen-inducible Cre recombinase ($CreER^T$) transgene linked to a cytokeratin 19 promoter (218). Cytokeratin 19 (CK19) is an intermediate filament protein (type I cytokeratin) located in the skin epidermis and multiple epithelial beds including oesophagus, intestine, pancreas, thymus and bile ducts. Importantly in the liver CK19 is expressed both in HPCs and mature cholangiocytes, but importantly not hepatocytes, so that recombination specifically

occurs within the biliary compartment. Furthermore 92% of intrahepatic cholangiocarcinomas exhibit positivity for CK19 (219).

I have used two alternative fluorescent reporter systems in the generation of this model. The first contains a lox-stop-lox eYFP sequence knocked into the Rosa26 locus ($R26^{eYFP/eYFP}$), so that in the presence of tamoxifen the stop codon is excised by Cre, permitting transcription of eYFP. This is the original reporting system for the $CK19CreER^T$ mouse as described by Means et al. (218). In addition I also utilised a second system in which $CK19CreER^T$ mice were cross-bred with an Ai14 tdTomato reporter mouse purchased from Jackson laboratories. This mouse carries a Rosa-CAG-LSL-tdTomato-WPRE::deltaNeo insert; i.e. a CAG promoter driven tdTomato reporter inserted into the Rosa locus with a STOP codon flanked by loxP sites. In this way STOP is excised in the presence of Cre, permitting transcription of tdTomato and hence tracking of recombined cells.

Deletions of the tumour suppressor *TRP53* are common in human ICC (220). Both $CK19CreER^T$eYFP and $CK19CreER^T$tdTom mice were therefore cross-bred with mice carrying loxP sites flanking *TRP53* to generate the transgenic lines $CK19CreER^T;R26^{eYFP};p53^{flox/flox}$ (herein referred to as $CK19CreYFPp53^{f/f}$) or $CK19CreER^T;R26tdTom;p53^{flox/flox}$ (herein referred to as $CK19CreTomp53^{f/f}$).

Cre recombination efficiency

I first sought to establish the efficiency with which Cre recombines loxP sites in this model. Two dosing regimens of tamoxifen were tested that had been previously published: a single dose of 80mg/kg i.p. or three doses of 4mg i.p. on alternate days, both when mice reached 6 weeks of age (218). eYFP expression was assessed 7 days following the last tamoxifen injection. eYFP positive cells were manually counted from 50 consecutive fields on one section per animal. The proportion of eYFP positive cells as a percentage of the total number of bile duct cells was determined (as assessed by morphology on DAB immunohistochemistry). Only cells that

formed part of a ductal structure (i.e. those surrounding a lumen) were included. For both dosing schedules, no eYFP expression was observed in the absence of Cre (n=14) or absence of tamoxifen (n=3). In the presence of Cre the proportion of recombined cholangiocytes in response to 80mg/kg tamoxifen was 15.4% ±1.19 (n=6) compared to 13.71% ±2.32 (n=9) in response to three 4mg doses on alternate days (Figure 4.1B).

As recombination efficiency was not statistically different between the two doses, it was decided to use the dose published by Means et al. in the original description of the CK19CreERT mouse (218). Three doses of 4mg of tamoxifen were used for all subsequent experiments in this study.

Figure 4.1 Cre recombination efficiency of the CK19CreER^{T}eYFP mouse.

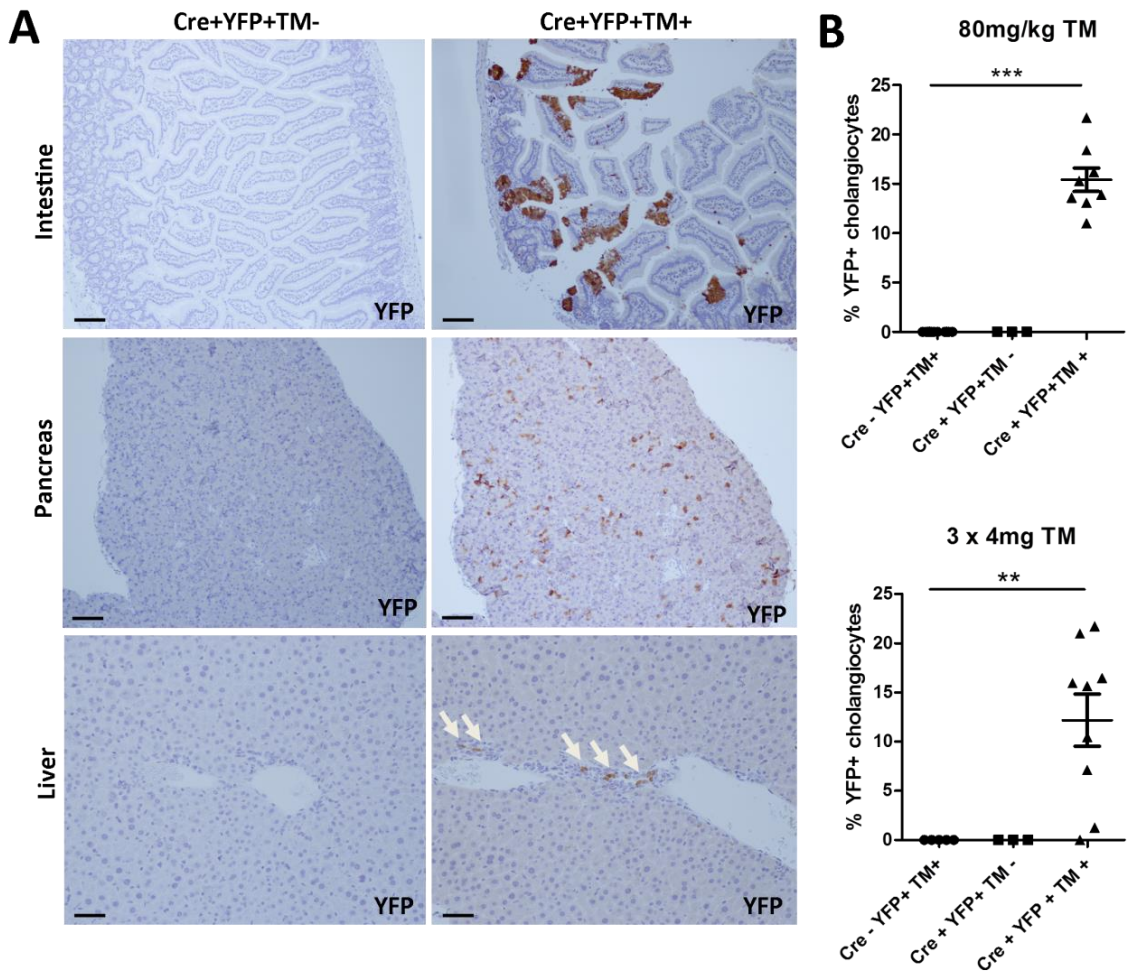

Figure 4.1 *Cre recombination efficiency of the CK19CreER^{T}eYFP mouse.* (**A**) Immunohistochemical staining for eYFP in endodermal tissues 7 days after 3 doses of 4mg tamoxifen i.p. (Antibody targeted to GFP). eYFP positivity was observed in enterocytes in intestine and ductular epithelia in pancreas and liver. In liver eYFP positivity was observed only in the presence of Cre and tamoxifen and only in ductular cells (white arrows). No expression was observed in hepatocytes. Scalebars represent 100μm. (**B**) The number of eYFP positive cholangiocytes as a proportion of the total number of ductal cells per mouse is represented in the absence of Cre and presence of tamoxifen (Cre-TM+); presence of Cre but absence of tamoxifen (Cre+TM-) and presence of Cre and tamoxifen (Cre+TM+). In response to

80mg/kg tamoxifen, 15.41% ±1.19 cholangiocytes were eYFP positive compared to 13.71% ±2.32 following 3 doses of 4mg tamoxifen. Statistical differences between groups represented on the graphs are calculated using the one way analysis of variance test (80mg/kg regime p=<0.0001; 3 x 4mg regime p=0.0039). * p≤0.05; ** p≤0.01; ***p≤0.001.

To ensure eYFP positive cells were exclusively labelling cells within the biliary and progenitor compartments within the liver and not hepatocytes, I performed co-immunofluorescent staining for YFP and the biliary markers pan-cytokeratin and Sox9, as well as the mature hepatocyte marker Cyp2D6 (Figure 4.2).

Figure 4.2 eYFP is expressed by biliary and progenitor cells but not hepatocytes in CK19CreYFP mice.

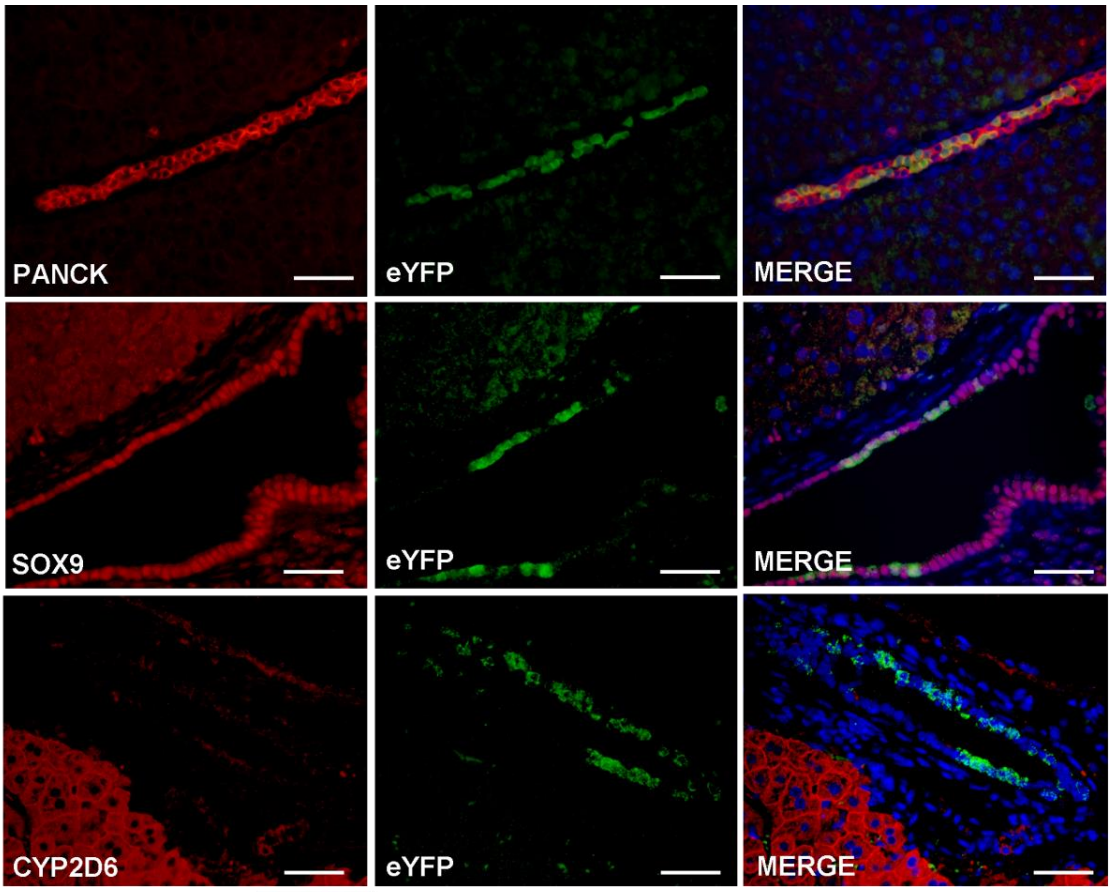

Figure 4.2 *eYFP is expressed by biliary and progenitor cells but not hepatocytes in CK19CreYFP mice.* Representative photomicrographs from CK19YFPp53 mice following tamoxifen administration demonstrating eYFP positivity (green) co-localising with the biliary markers pan-cytokeratin and Sox9 but not the mature hepatocyte marker CYP2D6 (red). Scalebars represent 100μm.

Pilot ICC Model 1: CK19CreYFPp53$^{f/f}$ + CCl_4

Carbon tetrachloride (CCl_4) is a potent hepatotoxin and the most extensively characterised inducer of liver fibrosis. Following a single dose, centrizonal necrosis and steatosis occur; however after prolonged administration fibrosis, cirrhosis and hepatocellular carcinoma are induced (221, 222). In light of previous reports of concomitant ICC and HCC formation in p53 null mice in response to chronic intermittent toxin exposure with CCl_4 (217), this experiment was designed to determine whether CCl_4 induced injury in combination with inducible, targeted deletion of p53 in biliary cells could result in a more specific model of ICC.

Clinical Course:

CK19CreYFPp53$^{wt/wt}$ and CK19CreYFPp53$^{wt/flox}$ mice were induced with 3 injections of 4mg tamoxifen i.p. and allow to recover before undergoing chronic intermittent injury with 1ul/g CCl_4 or olive oil i.p 3 times a week for 16 weeks. This model was associated with an unacceptably high mortality rate (combined mean survival 84.89 ±13.77 days) and therefore CK19YFPp53$^{flox/flox}$ mice were not commenced on the protocol. Death did not correlate to weight loss and clinical deterioration of mice was rapid and unpredictable. No clinical signs of liver failure such as jaundice were evident and no tumour formation was observed on post-mortem examination.

Figure 4.3 Pilot model 1: CK19CreYFPp53$^{f/f}$ + 16 weeks CCl_4

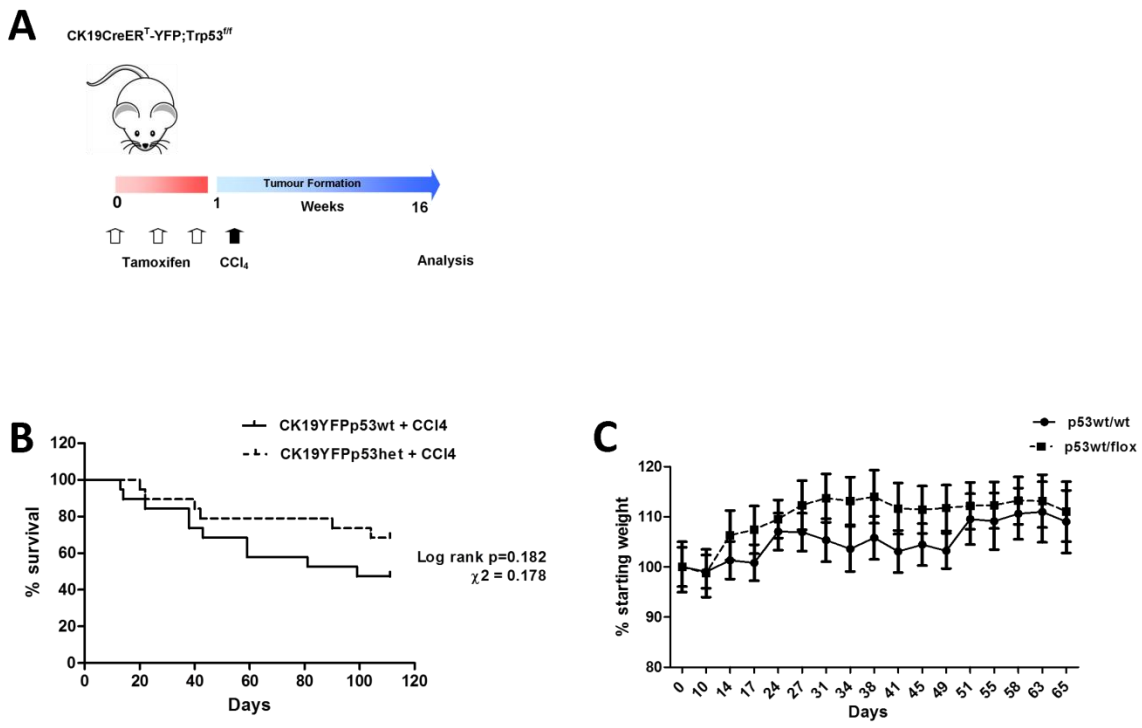

Figure 4.3 *Pilot model 1: CK19CreYFPp53$^{f/f}$ + 16weeks CCl_4* (A) Experimental schematic: Cre was induced with 3 x 4mg tamoxifen i.p. followed by damage with chronic, intermittent 1µl/g CCl_4 i.p 3 times a week for 16 weeks. (B) Kaplan-Meier survival curve for CK19YFPp53$^{wt/wt}$ (n=19) and CK19YFPp53$^{wt/flox}$ (n=20) mice undergoing chronic injury with CCl_4 for 16 weeks. (C) Daily weights of CK19YFPp53$^{wt/wt}$ and CK19YFPp53$^{wt/flox}$ mice undergoing chronic injury with CCl_4 for 16 weeks.

Histological Appearance:

All mice receiving vehicle displayed normal liver architecture. Following 16 weeks of intermittent CCl_4 administration, livers from mice of all genotypes exhibited severe centrilobular necrosis, intense inflammatory infiltrates and extensive steatotis (Figure 4.4). As anticipated, picro-sirius staining demonstrated extensive collagen deposition with bridging fibrosis in both p53 wild type and p53 heterozygous floxed animals, with associated infiltration by αSMA positive myofibroblasts. H&E and pan-cytokeratin staining revealed no biliary hyperplasia or invasive adenocarcinoma (and no hepatocellular carcinoma), as assessed by a liver histopathologist. Furthermore no significant ductular reaction or parenchymal migration of progenitor cells were observed in this model (Figure 4.4).

Figure 4.4 Histology Pilot model 1: CK19CreYFPp53$^{f/f}$ + 16weeks CCl_4

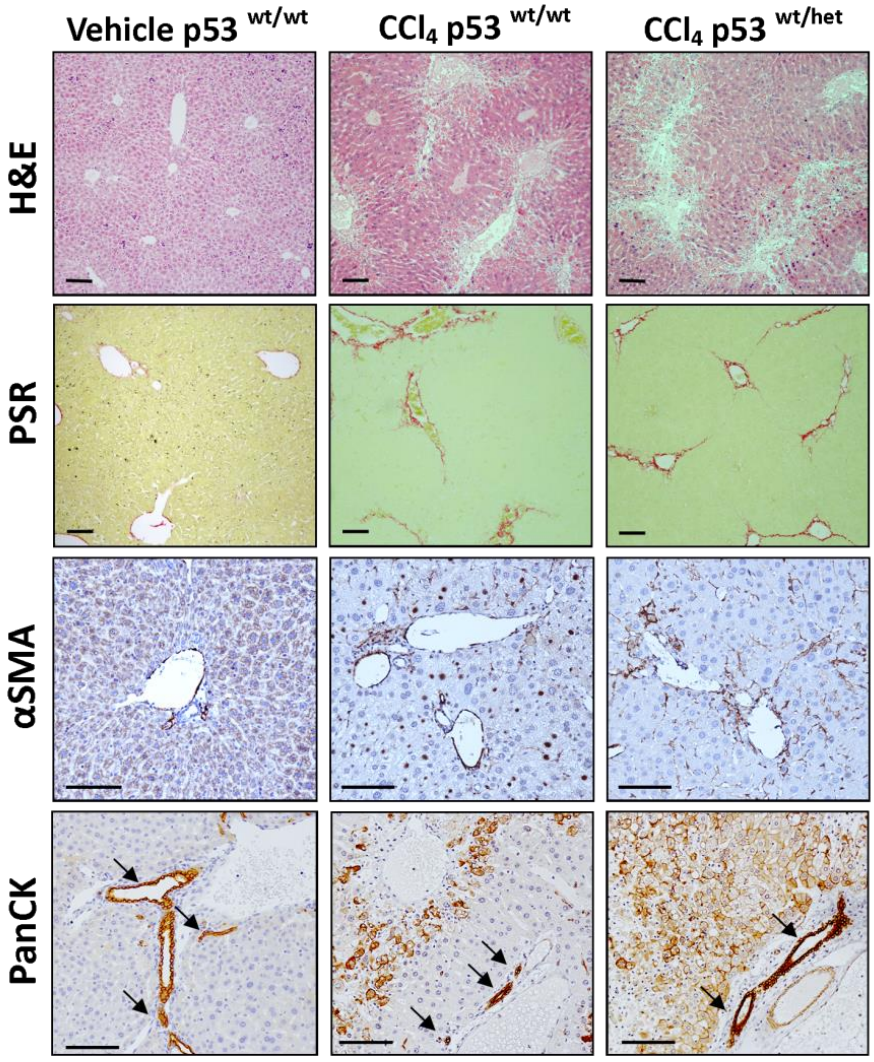

Figure 4.4 *Histology Pilot model 1: CK19CreYFPp53$^{f/f}$ + 16weeks CCl_4* In comparison to mice receiving vehicle, CK19YFPp53$^{wt/wt}$ and CK19YFPp53$^{wt/flox}$ mice undergoing chronic injury with CCl_4 demonstrated severe centrilobular necrosis with associated inflammatory infiltrate on H&E staining (top panel). Extensive collagen deposition with bridging fibrosis was observed in all animals receiving CCl_4 and this was associated with infiltration of αSMA positive myofibroblasts (middle panels). No significant ductular reaction or progenitor cell activation was observed in this model; PanCK staining showed ductular positivity (black arrows) but no

hyperplasia or parenchymal migration of progenitor cells (lower panel). Scalebars represent 100μm.

Pilot ICC Model 2: CK19CreYFPp53 + TAA

Thioacetamide (TAA) is an organosulphur which is metabolised to carcinogenic products in zone 3 hepatocytes, triggering the development of multifocal invasive biliary adenocarcinoma in rats (75). Following Cre induction with tamoxifen, TAA was orally administered to CK19CreYFPp53$^{wt/wt}$, CK19CreYFPp53^{wtflox} and CK19CreYFPp53$^{flox/flox}$ mice for 26 weeks (Figure 4.5A).

Clinical Course:

Mortality was unacceptably high in female mice commenced on this protocol (4 out of 7 female mice within the first 17 days of the protocol) and accordingly in females the experiment was terminated and mice culled via a Schedule 1 method. A lower body weight at the start of the experiment in female mice meant that animals were less able to tolerate the initial dehydration and weight loss occurring on commencement of TAA (TAA is a sulphurous, unpalatable compound).

All male mice weighing ≥25g at the time of Cre induction survived irrespective of genotype, although weight gain was slower than would be expected in transgenically matched mice receiving drinking water alone (Figure 4.5B). No animals died from tumour-related causes before the experimental end-point at 26 weeks. No clinical signs of liver failure including jaundice, bleeding or ascites were evident even at 26 weeks. Liver injury as assessed by serum biochemical markers of liver function (ALT, AST, ALP, bilirubin and albumin) were equivalent between mice carrying one or two floxed alleles for p53 (haemolysis of samples from wild type mice left n=1 for analysis) (Figure 4.5C).

Figure 4.5 Pilot model 2: CK19CreYFPp53$^{f/f}$ + 26weeks TAA

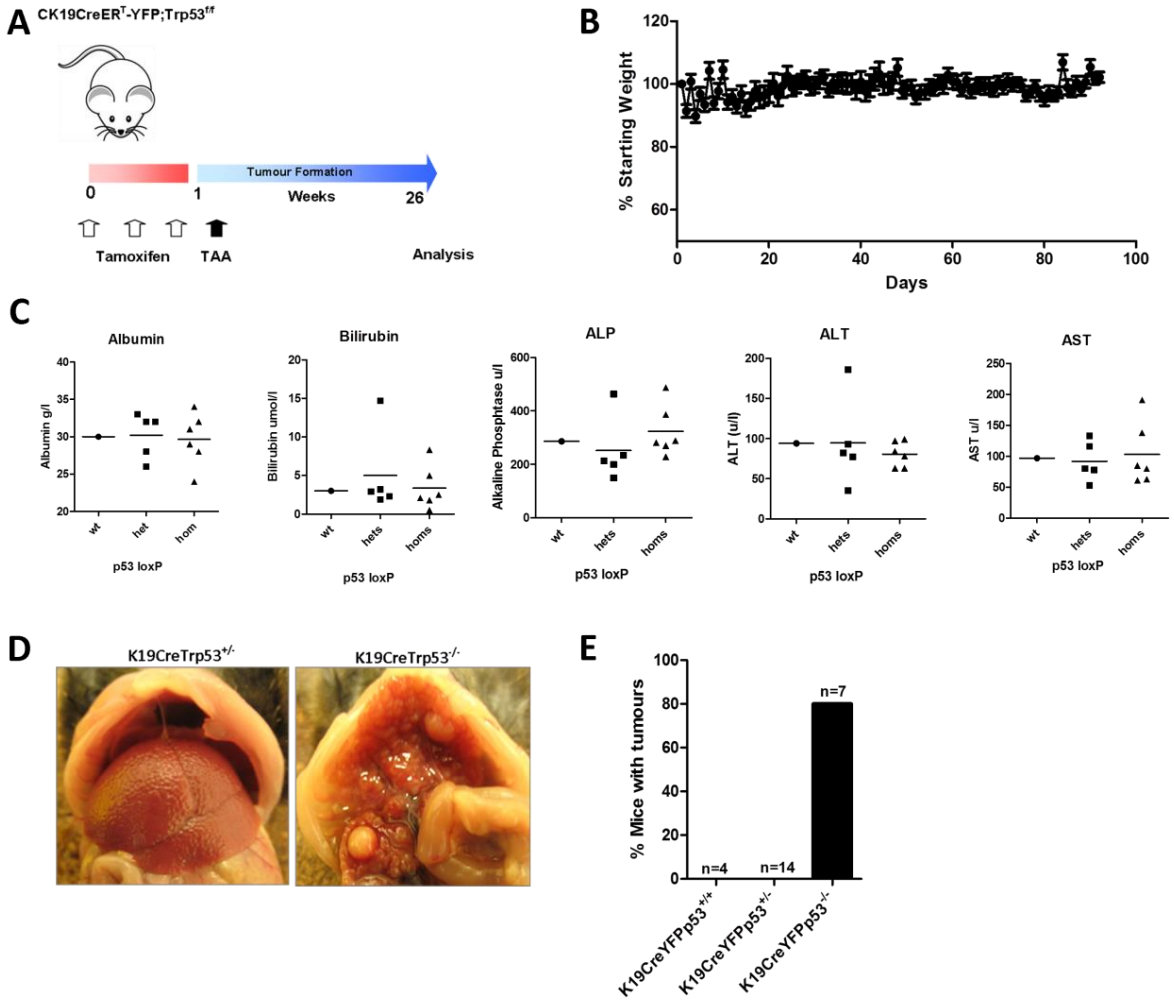

Figure 4.5 *Pilot model 2: CK19CreYFPp53$^{f/f}$ + 26weeks TAA* (A) Experimental schematic of Cre induction with 3 x 4mg tamoxifen i.p. followed by administration of 600mg/ml TAA in the drinking water for 26 weeks. (B) Weights of male CK19YFPp53$^{wt/wt}$, CK19YFPp53$^{wt/flox}$ and CK19YFPp53$^{flox/flox}$ mice undergoing chronic injury with TAA for 26 weeks. (C) Liver function tests in CK19YFPp53$^{wt/wt}$, CK19YFPp53$^{wt/flox}$ and CK19YFPp53$^{flox/flox}$ mice undergoing chronic injury with TAA for 26 weeks (Note n=1 for CK19CreYFPp53$^{wt/wt}$ mice due to haemolysis of samples). No significant difference in serum markers of liver function was observed between

CK19YFPp53$^{wt/flox}$ and CK19YFPp53$^{flox/flox}$ mice (Mann-Whitney U Test). Data are represented as mean ± S.E.M. (D) Macroscopic appearance of tumours arising in CK19YFPp53$^{flox/flox}$ mice following 26 weeks of TAA. (E) Frequency of tumour occurrence in CK19CreYFPp53$^{wt/wt}$, CK19YFPp53$^{wt/flox}$ and CK19YFPp53$^{flox/flox}$ mice following 26 weeks of TAA. 5 out of 7 CK19CreYFPp53$^{flox/flox}$ mice exhibited tumours.

Histological appearance:

All mice receiving vehicle exhibited preserved liver architecture. No tumours were observed in CK19CreYFPp53$^{wt/wt}$ or CK19CreYFPp53$^{wt/flox}$ mice following tamoxifen induction and 26 weeks of treatment with TAA. Both these groups of animals did however demonstrate extensive periportal inflammation, centrilobular necrosis and pseudo lobule formation, as observed on H&E staining. Ductular reactions were frequent; however there was no evidence of dysplasia or cellular atypia (Figure 4.6).

Multifocal tumours were observed in 5 out of 7 mice carrying homozygous floxed alleles for p53 (Figure 4.5 D-E). These areas were well to moderately differentiated adenocarcinoma with associated mucin production and desmoplasia. Areas of dysplasia not amounting to full adenocarcinoma were also present. No hepatocellular carcinoma was observed in any animals (Figure 4.6). Staining with picrosirius red revealed extensive collagen deposition with bridging fibrosis in all genotypes receiving TAA. Staining was particularly dense around and within tumours in CK19CreYFPp53$^{flox/flox}$ mice. αSMA positivity was limited to blood vessels in mice receiving vehicle. Periportal infiltration of αSMA positive myofibroblasts was observed in mice of all genotypes receiving TAA and in mice that developed tumours, staining was intense in areas of tumour-associated desmoplasia (Figure 4.6).

Figure 4.6 Histology Pilot model 2: CK19CreYFPp53$^{f/f}$ + 26weeks TAA

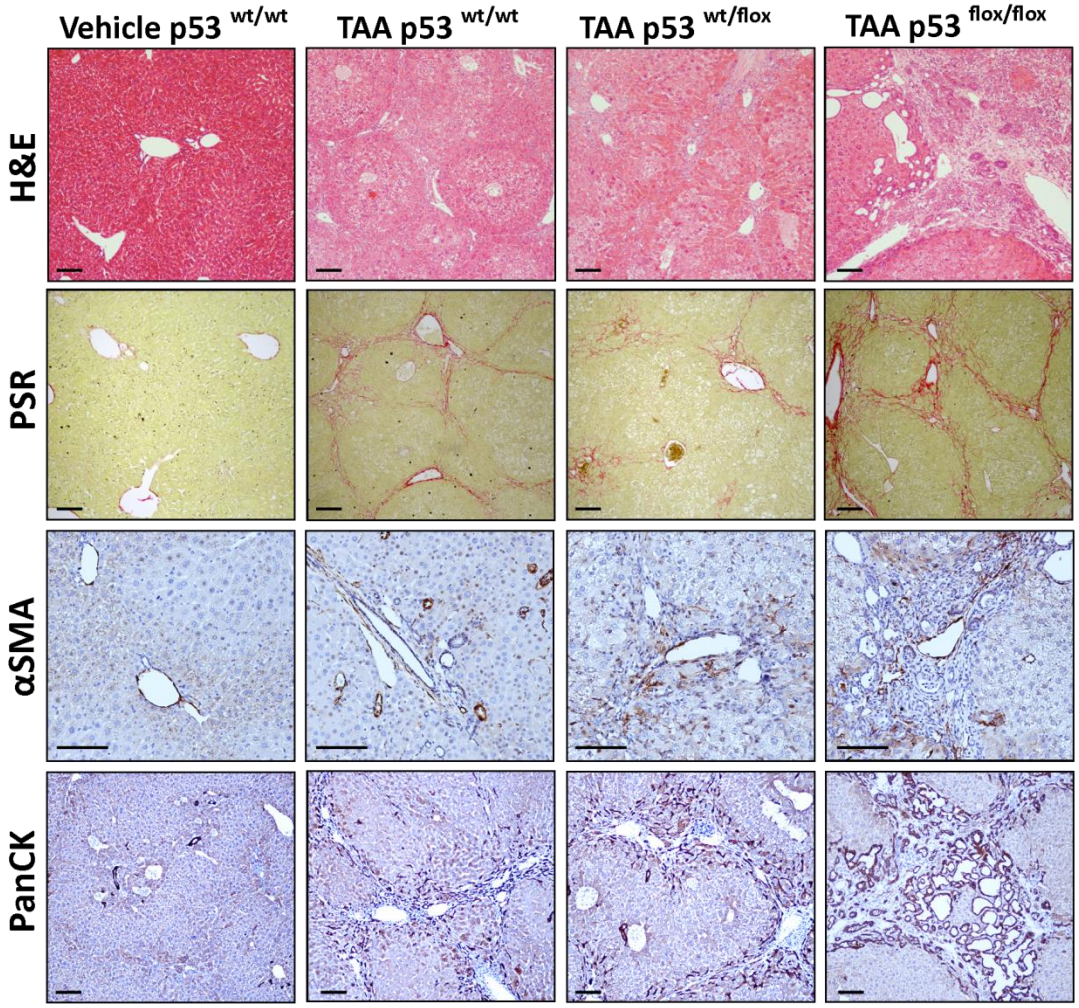

Figure 4.6 *Histology Pilot model 2: CK19CreYFPp53$^{f/f}$ + 26weeks TAA* H&E staining upper panel: Mice receiving treatment with vehicle display normal liver architecture. CK19YFPp53$^{wt/wt}$ and CK19YFPp53$^{wt/flox}$ mice exhibit extensive periportal inflammation, steatosis and pseudo lobule formation but no biliary dysplasia or malignancy. CK19YFPp53$^{flox/flox}$ mice display multifocal areas of well to moderately differentiated adenocarcinoma with mucin production and dense desmoplasia. Areas of dysplasia not amounting to adenocarcinoma are also present. Picrosirius red and αSMA staining reveal extensive collagen deposition with bridging fibrosis and periportal and peritumoral infiltration of myofibroblasts (centre two panels). Pan-cytokeratin staining reveals extensive HPC activation with portal-portal

bridging in TAA treated CK19YFPp53$^{wt/wt}$ and CK19YFPp53$^{wt/flox}$, extending between foci of invasive adenocarcinoma in CK19YFPp53$^{flox/flox}$ mice (lower panels). Scalebars represent 100μm.

Figure 4.7 Tumours arising in CK19CreYFPp53$^{f/f}$ mice after 26 weeks TAA express biliary epithelial markers

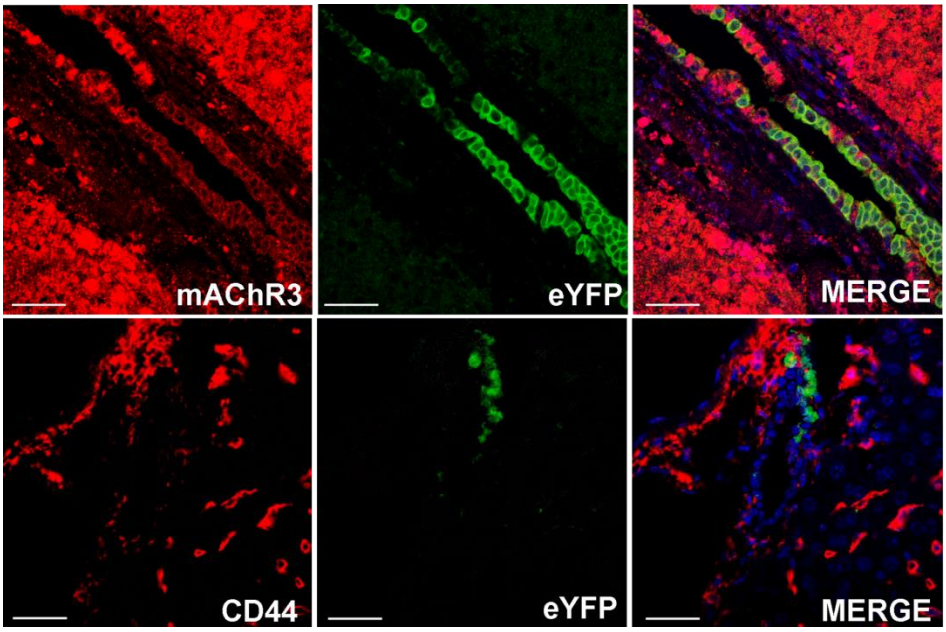

Figure 4.7 *Tumours arising in CK19CreYFPp53$^{f/f}$ mice after 26 weeks TAA express biliary epithelial markers.* Tumours found in CK19CreYFPp53$^{f/f}$ mice express markers of cholangiocyte differentiation including pan-cytokeratin (Figure 4.6), mAChR3 (red) and CD44 (red). Scalebars represent 100μm.

Pilot ICC Model 3: CK19CreYFPp53kRas

The KRAS oncogene is activated in 20 to 50% of biliary tract cancers in man (223-225). Non-inducible somatic activation of kRas and deletion of p53 in Albumin-expressing cells (Alb-Cre;$kRas^{G12D}$;$p53^{flox/flox}$) has been previously described in mice to induce ICC, HCC and tumours with a mixed morphology that recapitulate the histology of human disease (86). I hypothesised that targeting these mutations to the $CK19^{+}$ population in the adult mouse liver would improve the specificity of this mode; inducing the formation of biliary and not hepatocellular tumours. Six week old CK19CreYFP$p53^{f/f}$;$kRas^{G12D}$ mice underwent induction of Cre with tamoxifen (3 injections of 4mg i.p on alternate days) and were observed for a period of up to 26 weeks (Figure 4.7A).

Clinical Course:

Following Cre induction, mice were monitored for body weight and signs of illness. Animals displaying signs of clinical deterioration were culled and included as events for survival analysis. The most common clinical abnormalities observed were abdominal swelling, high respiratory rate and non-specific signs of poor condition such as hunched posture, ruffled coat and reduced movement (Table 4.1). CK19CreYFP$p53^{flox/flox}$f$kRas^{G12D}$ mice exhibited significantly shorter survival than CK19CreYFP$p53^{flox/wt}$f$kRas^{G12D}$ mice: 41 ±2.7 days vs. 91.9 ± 11.9 days (Log rank p-0.019) (Figure 4.7B), suggesting the combination of total loss of p53 and kRas activation might be additive in their tumour promoting effects. In light of this unacceptable mortality the experiment was terminated early in the CK19CreYFP$p53^{flox/flox}$f$kRas^{G12D}$ cohort, hence the small n (n=3).

Figure 4.8 Pilot model 3: CK19CreYFPp53$^{f/}$fkRasG12D.

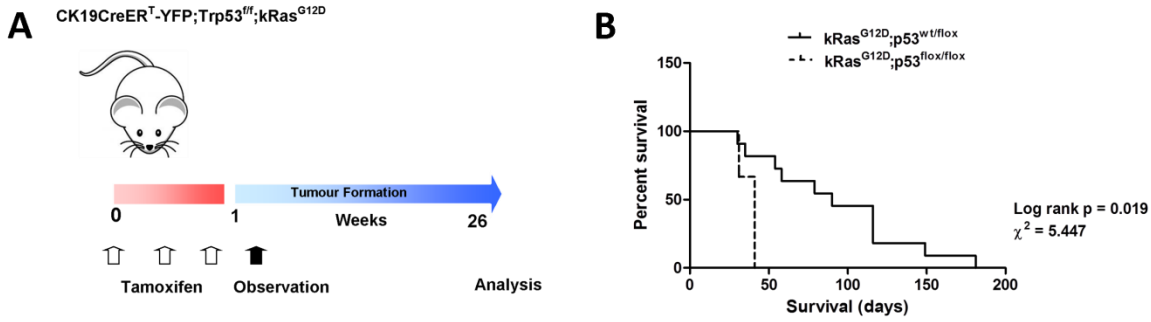

Figure 4.8 *Pilot model 3: CK19CreYFPp53$^{f/}$fkRasG12D.* (**A**) Experimental schematic: CK19CreYFPp53$^{f/f}$kRasG12D mice were induced with 3 injections of 4mg tamoxifen i.p. and observed for up to 26 weeks. (**B**) Kaplan-Meier survival analysis showing of CK19CreYFPp53$^{flox/wt}$fkRas^{G12D} (n=14) and CK19CreYFPp53$^{flox/flox}$fkRas^{G12D} mice (n=3) following induction of Cre with tamoxifen. The mean survival of CK19CreYFPp53$^{flox/wt}$fkRas^{G12D} mice was 91.9 ± 11.9 days compared to 41 ± 2.7 days in CK19CreYFPp53$^{flox/flox}$fkRas^{G12D} mice (Log rank p=0.019).

Table 4.1 Table of survival, clinical signs and tumour type for CK19CreYFPp53$^{f/f}$kRas^{G12D} mice.

Mouse ID	Cre	p53flox	kRas^{G12D}	Survival (days)	Clinical signs/Findings at necropsy	Histopathology
HO5	+	het	+	58	High respiratory rate, hunched posture	N.A.D
HO6	+	het	+	35	Weight loss. No macroscopic abnormality at necropsy.	N.A.D
HR11	+	het	+	54	Abdominal swelling; Large paracolic mass	Submucosal GI tract spindle cell tumour
IU3	+	het	+	149	Quick respiratory rate, abdominal swelling, weight loss	
KF4	+	het	+	116	Lip papilloma Abdominal swelling; large pelvic tumour	Spindle cell carcinoma attached to spermatic cord (pleiomorphism andmitotic activity); squamous papilloma
JG3	+	het	+	79	Weight loss, hunched posture, ruffled coat	N.A.D
JG4	+	het	+	181	Lip papilloma	Squamous papilloma
JG6	+	het	+	116	Weight loss, reduced movement No abnormality at necropsy	No tissue (FD in cage)
JG10	+	het	+	116	Abdominal swelling, ruffled coat, hunched posture	N.A.D
JG11	+	het	+	116	Abdominal swelling, ruffled coat, hunched posture	N.A.D
JG12	+	het	+	116	Abdominal swelling, ruffled coat, hunched posture	N.A.D
JG14	+	het	+	31	Found dead in cage	N.A.D
JG40	+	het	+	30	Abdominal swelling	No tissue (FD in cage)
JG41	+	het	+	90	Abdominal swelling; weight loss, hunched posture	No tissue (FD in cage)
LX4	+	hom	+	41	Weight loss, hunched posture, slow movement	N.A.D
LX5	+	hom	+	41	Weight loss, hunched posture, slow movement	N.A.D
KF2	+	hom	+	31	Weight loss, hunched posture, slow movement	N.A.D

Table 4.1 *Table of survival, clinical signs and tumour type for CK19CreYFPp53$^{f/f}$kRas^{G12D} mice.*

Histological appearance:

To maximise the surface area of tissue available for histological examination, tissues were manually cut into 3mm portions before embedding and sectioning, three of which were stained with H&E for analysis. At the time of necropsy, no mice demonstrated macroscopic tumours of the liver and histological analysis revealed a normal liver architecture in all animals. Tissues from all animals were examined by a specialist histopathologist and four out of the fifteen animals exhibited tumours. Two displayed benign squamous papillomas of the lip and two malignant spindle cell carcinomas. These exhibited pleiomorphism and frequent mitotic activity and arose from the spermatic cord and invaded the adjacent skeletal muscle in one case and arose from the GI tract submucosa in another (Figure 4.8).

Figure 4.9 kRas activation and p53 deletion in CK19^{+} cells does not result in ICC.

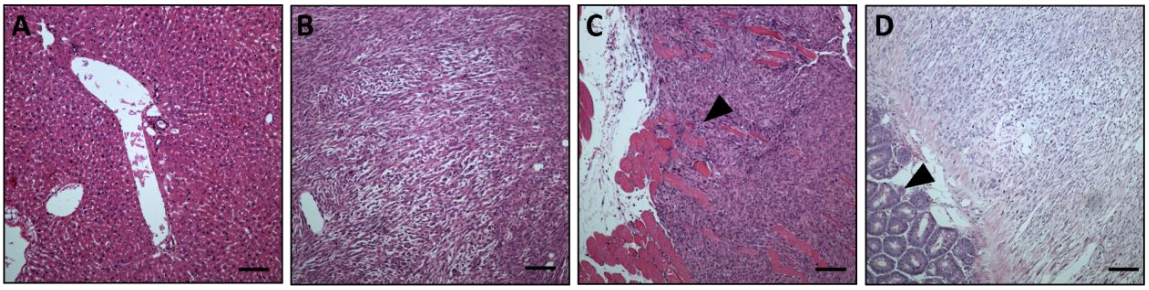

Figure 4.9 *kRas activation and p53 deletion in CK19^{+} cells does not result in ICC.*

(**A**) H&E staining showed liver histology to be normal in all animals. (**B-C**) One animal (KF4) exhibited a spindle cell tumour arising from the spermatic cord and invading adjacent skeletal muscle (filled arrowhead in C indicates skeletal muscle). (**D**) One animal (HR11) exhibited a spindle cell tumour arising from the submucosa of the GI tract (filled arrowhead in D indicates adjacent normal crypt architecture). Scalebars represent 100μm.

Despite a broad range of epithelial tissues being examined for tumour occurrence (lung, intestine, pancreas, oesophagus, thymus), a proportion of animals in this protocol exhibited clinical signs warranting Schedule 1 cull, and yet no abnormality was detected histologically. In addition to the solid organs examined, cytokeratin 19 is expressed in skin, prostate, ovary and mesothelia, making it possible that these animals carried tumours that were not detected. At this point however, in light of the absence of biliary tumours, hyperplasia or other liver pathology, and given the high mortality associated with this model, I decided to terminate the trial of this model and focus attention on the CK19YFPp53$^{flox/flox}$ +TAA model (pilot model 2) for further studies.

Discussion

Rapidity of breeding and the ability to target genetic mutagenesis to produce specific phenotypes have made the mouse (*mus musculus*) the preferred rodent system for modelling human disease (226). At the onset of this project few mouse models of ICC had been described, and none that specifically target genetic mutation to the biliary compartment of the liver (85, 86, 217). Here I aimed to generate a novel model that would not only closely mimic human disease but enable future interrogation of the influence of other epithelial genes during the pathogenesis of ICC.

Two of the three tested models (Pilot model 1 (CK19CreYFPp53$^{f/f}$ + CCl_4) and Pilot model 3 (CK19CreYFPp53$^{f/f}$kRas)) conferred unacceptably high mortality rates and neither resulted in the formation of ICC. Neither of these models has been pursued any further for those reasons. On the other hand, Cre-mediated deletion of p53 in CK19 positive cells followed by chronic intermittent injury with TAA (Pilot model 2) reproducibly induced multifocal invasive biliary adenocarcinoma (tumour penetrance of 71% at 26 weeks). Both loss of p53 and chronic biliary inflammation are frequent occurrences in human ICC. Histologically these tumours exhibited many similarities to disease in man, including a dense desmoplastic inflammatory stromal reaction, intraneural invasion, atypical ductular proliferation with associated progenitor activation, mucin production, and positivity for cholangiocyte and biliary markers, including the muscarinic acetyl choline receptor 3 (mAChR3), cytokeratins and CD44. No regions of HCC were observed in any animals; distinguishing this model in its specificity from other previously described approaches, particularly those relying on Albumin driven Cre systems (86, 217).

It is important to note however that the pattern of disease observed in this model does differ from that typically seen in ICC in man; fewer than 10% of patients with biliary tract cancer (including extrahepatic tumours) exhibit multifocal disease or

diffuse involvement of the biliary tree (227). Although recombination efficiency of this CK19Cre system was only 13.7%, it is likely that diffuse p53 deletion throughout the biliary network is permissive to the concomitant development of multiple tumours at different sites. It might be argued that the multifocal nature of ICC may make this a problematic model in which to study prognosis or response to therapy, as disease is likely to progress much more rapidly or behave differently to solitary tumours as is more commonly observed in man. In terms of studying the molecular drivers of tumorigenesis however, this characteristic might be an advantage, allowing comparison between multiple tumours arising from a syngeneic organ. This might be particularly useful if wishing to study the clonal evolution or heterogeneity of tumours, or for example how chemically-induced mutagenesis arises.

In summary I can conclude that this protocol has produced a novel pre-clinical model of ICC with an acceptable tumour latency and penetrance and with excellent specificity. Histologically tumours closely resemble ICC in man and exhibit biliary-specific proteins, although the pattern of disease is multifocal. Most importantly however, this model will provide a platform from which specific genetic alteration of the biliary compartment can be performed in future studies of ICC pathogenesis, including the studies of this project.

Chapter 5: Lineage Tracing the Cell of Origin of ICC

Introduction

Historically it has been assumed that ICCs arise following oncogenic transformation of mature biliary epithelia. A glandular histological morphology, location within and adjacent to the biliary network and expression of cholangiocyte specific proteins such as mucin and cytokeratins 7 and 19 have all served to perpetuate this theory (88). Furthermore, patients with chronic biliary inflammation such as primary sclerosing cholangitis or liver fluke infection are 161 and 27 times more likely to develop biliary tract cancer compared to the general population (89, 228). The hepatic progenitor cell has also been put forward as a potential candidate for the cell of origin of these tumours, in light of the existence of combined hepatocellular cholangiocarcinoma (CHC); tumours containing features of both cholangiocarcinoma and hepatocellular carcinoma, and cholangiolocellular carcinoma (CLC); tumours characterised by ductular reaction and cords resembling the Canals of Hering (91).

Interestingly however, there is also an increased incidence of ICC in a subgroup of patients with chronic hepatocellular injury, in particular those with long-standing HBV and HCV infection (24). In this context ICC can appear to form as mass lesions within the hepatocyte parenchyma, suggesting the cell of origin may be more complex than originally thought. Indeed recent published data has confirmed that ICC can arise from fully differentiated hepatocytes. In the first of these reports Fan and colleagues used hydrodynamic tail vein injection to deliver a Notch intracellular domain plasmid to overexpress Notch in the liver (92). This consistently resulted in biliary tumour formation by 20 weeks and could be accelerated to 5 weeks when combined with delivery of an AKT overexpressing plasmid. This model was then performed in R26-EYFP mice concomitantly with delivery of an adenoassociated viral vector expressing Cre recombinase from the hepatocyte-specific promoter transthyretin (AAV8-Ttr-Cre). In the presence of Cre,

a stop codon would be excised to permit eYFP transcription. The authors demonstrate that eYFP positivity within tumours co-localised with the biliary markers Sox9 and CK8 but not with the hepatocyte marker Mup, suggesting that Notch and AKT drive transdifferentiation and transformation of hepatocytes into ICC.

In the second study Sekiya and colleagues adopted a transgenic labelling approach using inducible albumin and cytokeratin 19 driven Cre systems to independently label the two cell types in the liver with lacZ or eYFP (93). Cre was induced with tamoxifen and mice administered thioacetamide for 30 weeks, after which time tumours demonstrating typical histology of ICC had formed in all animals. The authors found that tumours in all Alb-CreER^{T2};R26^{lacZ} mice but none from CK19-CreER^{T2};R26^{lacZ} mice demonstrated β-gal positivity co-localising with Epcam expression. They conclude that this strongly suggests ICC arises from hepatocytes and not cholangiocytes. They go on to show that tumour formation can be accelerated by overexpressing Notch intracellular domain in albumin expressing cells (Alb-CreER^{T2};R26R$^{Notch/+}$), and conversely impeded through deletion of the Notch target gene Hes1 (Alb-CreER^{T2}; R26RHes1$^{f/f}$).

CK19^{+} expressing biliary epithelia can give rise to ICC

In this study I use a similar cytokeratin 19 driven Cre-loxP system (CK19-CreER^{T}) to label cells with an eYFP fluorophore, but in addition I have targeted deletion of the tumour suppressor p53 (a common occurrence in ICC in man), to the CK19 expressing population (CK19-CreER^{T};R26eYFP;p53$^{f/f}$). Mice were administered TAA for 26 weeks. As described in the preceding chapter, tumours developed in 5 out of 7 mice carrying homozygous floxed p53 alleles.

Immunostaining for eYFP revealed positivity in all histologically identified neoplastic nodules, although interestingly not all cells within tumours staining positively for pan-cytokeratin were also YFP positive, suggesting that in this model

tumours are not necessarily arising from proliferation of a single YFP positive, p53 null clone (Figure 5.1).

Figure 5.1 Biliary tumours arise from CK19 positive cells in a TAA model of ICC.

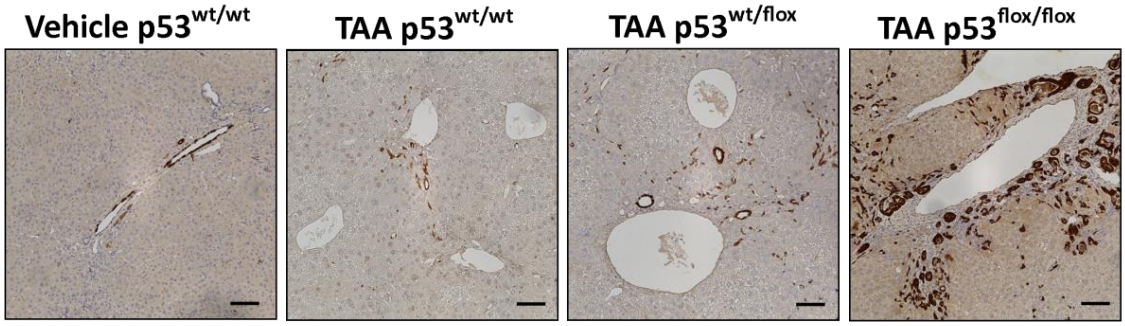

Figure 5.1 *Biliary tumours arise from CK19 positive cells in a TAA model of ICC.* eYFP immunostaining in CK19YFPp53$^{f/f}$ mice following 26 weeks of TAA. Scalebars represent 100μm.

To confirm the identity of eYFP positive cells in this model I performed co-fluorescent immunohistochemistry for eYFP and the biliary markers CK19 and Sox9 as well as the mature hepatocyte marker Cyp2D6. The majority of eYFP positive cells co-localised with CK19 and Sox9, whereas no co-localisation of eYFP with Cyp2D6 was observed.

Figure 5.2 Lineage traced eYFP^{+} cells co-localise with biliary markers in a TAA model of ICC.

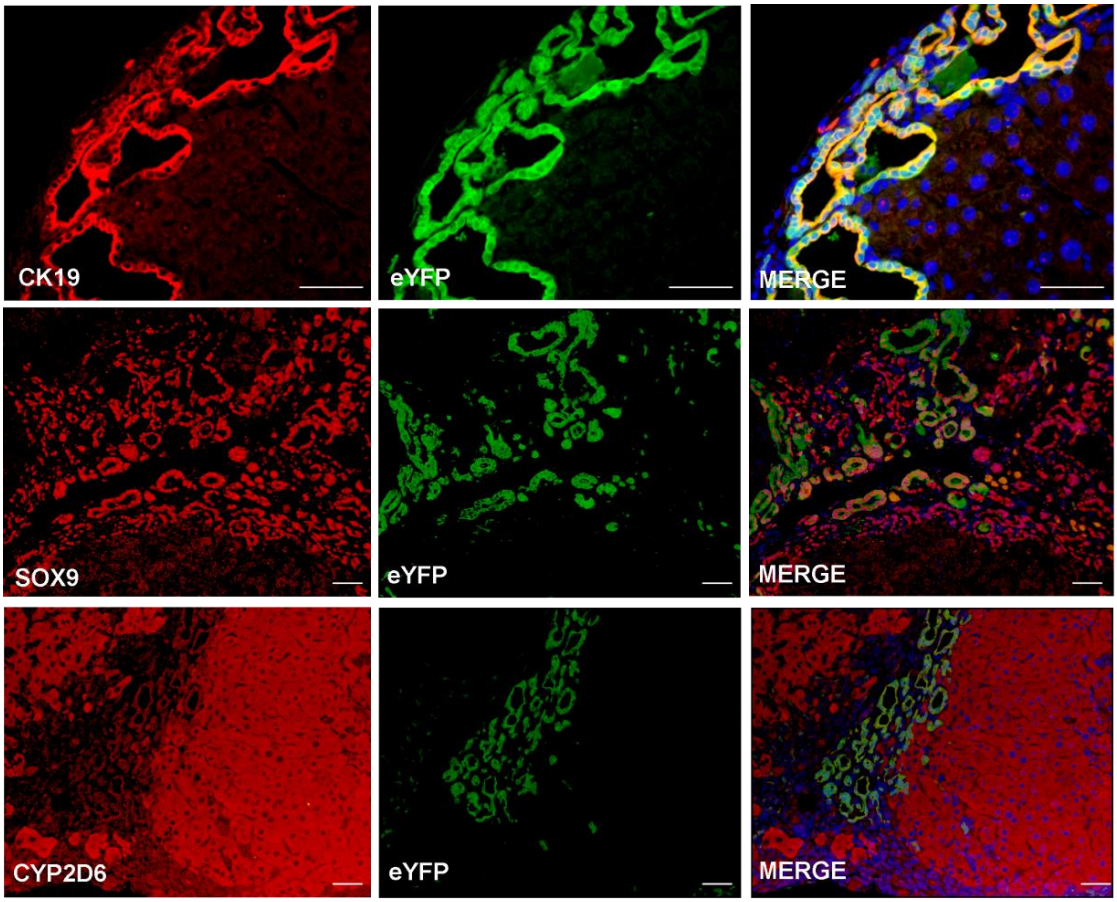

Figure 5.2 *Lineage traced eYFP^{+} cells co-localise with biliary markers in a TAA model of ICC.* Representative photomicrographs of ICC arising after 26 weeks of TAA in CK19YFPp53$^{flox/flox}$ mice. eYFP positivity co-localised with the biliary markers cytokeratin 19 and sox9, but not the mature hepatocyte marker CYP2D6. Scalebars represent 100μm.

Discussion

A principal advantage of the experiments in this study and those published by Sekiya et al. is that they do not rely either on viral delivery of a transgene, nor on overexpression of an oncogenic driver (Notch/AKT) to induce liver tumorigenesis. It can be assumed that chronic injury with the toxin TAA is a more representative model of the *in vivo* situation in ICC in man. *Trp53* deletion at the point of tamoxifen administration as described here does not increase labelling efficiency, but is likely to cause a preferential expansion of the eYFP labelled population in response to TAA induced injury, making it more probable that a transforming event will occur in this population compared with labelled cells in a similar fate tracing experiment without p53 deletion. So although this may explain why labelled tumours were observed in this model and not the experiments described by Sekiya et al. (93), the frequency of p53 loss and chronic biliary inflammation in human ICC would suggest this to be a representative model of biliary carcinogenesis in man. Furthermore the CK19CreYFP mouse has proved to be a poor tool for lineage tracing progenitor-derived hepatocytes during regeneration in the adult mouse liver. The failure to observe eYFP-labelled hepatocytes in dietary models of chronic hepatocellular damage has been attributed to a low recombination and hence labelling efficiency (unpublished data from Forbes lab, Lemaigre lab et al.). In light of this it would therefore appear unlikely that eYFP labelled tumour cells are arising from hepatocytes in this TAA model.

Interestingly not all CK19 positive cells observed within areas of tumour were eYFP positive. One explanation for this might be that eYFP expression is being genetically silenced during the process of ongoing injury and mutagenesis. eYFP negative cells were observed in almost all areas of tumour across different animals and indeed, even within the same ductal structure, sitting alongside eYFP positive cells. It seems statistically improbable although possible, that mutation resulting in eYFP silencing would be occurring at this frequency. An alternative explanation is that non-recombined cells are contributing to tumour formation. Such cells may

either be carrying their own TAA-induced genetic alterations, or be non-transformed cells that have been 'recruited' into the tumour mass e.g. by secreted or induced factors. Whichever of these is the case, it remains interesting that p53 null cells do not entirely take over as the dominant clone within tumours and is consistent with the school of thought that p53 loss acts as a tumour-permissive event rather than a tumour driver. Fluorescently activated cell sorting or laser-capture microdissection of individual tumours from the same liver (to control for recombination efficiency) could be used to separate eYFP positive from eYFP negative cells, followed by sequencing to determine the spectrum of genetic events that have occurred. *In vitro* assays of clonogenicity could then be used to determine the hierarchy of clonal evolution occurring within a single tumour and between tumours. This model would therefore appear to offer an interesting platform from which to study tumour evolution and intra-tumour heterogeneity.

In contrast to the findings of Sekiya et al. and Fan et al., my experiments conclude that cholangiocytes have capacity to give rise to ICC. Currently the limitations of transgenic technologies make it difficult to concomitantly label both cholangiocytes and hepatocytes *in vivo* to assess their contribution to tumorigenesis during different protocols of cancer induction. Furthermore different models may target different cell types for transformation and experiments using indiscriminate delivery of transgenic or viral oncogenic drivers would bias towards a hepatocyte origin simply due to their vast outnumbering of cholangiocytes within the liver. It could be postulated that the probable situation in ICC in man is that different cells of origin may occur according to disease context and factors supplied by the local tumour microenvironment, suggesting that the niche may play a key role in driving tumorigenesis in ICC. What my data have demonstrated however is that the CK19 expressing cholangiocytes or progenitor cells should not be discounted as a target for future therapeutic targeting in ICC.

Chapter 6: The Notch pathway in healthy liver and ICC

Introduction

Notch signalling is a key determinant of biliary development in the embryo where it is activated early on to specify hepatoblasts on the portal side of the ductal plate towards a cholangiocyte fate, but also later during liver patterning to regulate tubular morphogenesis (the appearance of lumina and duct formation) and arborisation (145, 169, 229). Work from our laboratory and others has demonstrated this paradigm extends to the regenerating biliary system following injury in the adult liver (169, 174). Following biliary damage there is a compositional change in the regenerative niche, whereby infiltrating myofibroblasts are able to form close spatial relationships with HPCs and supply Jagged1 ligand to activate Notch. In this context Notch acts both to control HPC number as well as activating a transcriptional programme to specify cells to the biliary lineage (Hes1, Hes5, HNF1β) (104, 169).

Dysregulation of wild type Notch signalling has now been identified as a driver of carcinogenesis in a number of solid organs. Since the commencement of this study, work has been published demonstrating that transgenic overexpression of Notch1 in Albumin expressing cells in the embryo (Alb-Cre;NotchIC) leads to the formation of biliary lineage tumours in the adult mouse liver (230). This transgenic construct drives expression of N1-ICD in virtually all hepatocytes and biliary epithelial cells during the formation of the ductal plate (145). As early as 8 months after birth morphological changes are observed in the livers of these mice and when liver tissue from the Alb-Cre;NotchIC mice is transplanted subcutaneously into the flanks of immunocompromised mice, tumours form which stain positively for the biliary lineage markers CK7 and CK17 (No tumours form from Alb-Cre controls).

Exogenous activation of oncogenes through transgenesis can initiate carcinogenesis in many different tissues and indeed often in tissues where these oncogenes are not

overexpressed or mutated in human cancers. Studies examining KRAS and MYC oncogenes for example have shown that the precise levels of overexpression are absolutely critical to the biological outcome (231). Published data on the role of Notch in ICC have relied on transgenic over-expression of Notch to induce tumorigenesis. The true role of endogenous wild type Notch in the pathogenesis of ICC in man remains unclear. In this study I therefore aimed to undertake a full characterisation of Notch pathway activity in human ICC as well as in rodent models in which Notch has not been transgenically altered. Given the toxicity that has impeded the success of γ-secretase inhibitors (GSIs) in clinical trials for other solid organ tumours; I hoped this approach might identify Notch pathway components that might represent novel targets for therapeutic development.

The Notch pathway is up-regulated in human ICC and rodent models

Notch pathway transcription is up-regulated in human ICC

I began by looking broadly at transcription of the entire Notch pathway using a commercially available targeted Notch PCR array on 5 resected, treatment-naive human ICC cases which were paired with patient-matched non-cancerous liver controls. This RT² Profiler™ PCR Array (SABiosciences) profiles the expression of 84 genes implicated in Notch signalling, including components of the core pathway as well as those involved in receptor binding and processing and putative targets (http://www.sabiosciences.com/rt_pcr_product/HTML/PAHS-059A.html). The technical challenge of macroscopically dissecting a pure sample of intrahepatic bile duct from these samples meant that it was necessary to use whole liver as a non-cancerous control to areas of tumour.

I found components from each stage of the canonical Notch pathway to be up-regulated including ligands, receptors and target effector genes. Interestingly NOTCH3 is the only receptor to be significantly up-regulated (18.202 fold, p=0.000025), NOTCH 1 is transcribed 1.933 fold (p=0.105153), NOTCH2 1.842 fold (p=0.136808) and NOTCH4 1.576 fold (p=0.076371) (Table 6.1 and Figure 6.1). JAG2 is the most highly up-regulated ligand (12.58 fold p=0.003088), followed by JAG1 (8.43 fold p=0.000426). Delta like ligands 1, 3 and 4 are not up-regulated. HEY1 10.25 fold (p=0.016558) and HEYL 6.02 fold (p=0.000829) are the most highly up-regulated target effector genes (Table 6.1 and Figure 6.1).

Table 6.1 Notch pathway PCR Array of human ICC and patient-matched distal non-cancerous liver.

Unigene	Refseq	Symbol	Fold Change	p Value
Hs.8546	NM_000435	**NOTCH3**	18.202	0.000025
Hs.433445	NM_002226	**JAG2**	12.5846	0.003088
Hs.653700	NM_007129	**ZIC2**	12.2213	0.014216
Hs.234434	NM_012258	**HEY1**	10.2518	0.016558
Hs.244723	NM_001238	**CCNE1**	9.1662	0.08289
Hs.728907	NM_000214	**JAG1**	8.4314	0.000426
Hs.173859	NM_003507	**FZD7**	7.5751	0.01193
Hs.472566	NM_014571	**HEYL**	6.0241	0.000829
Hs.525198	NM_003035	**STIL**	5.9598	0.005442
Hs.563344	NM_006186	**NR4A2**	5.0864	0.178302
Hs.159142	NM_001040167	**LFNG**	4.5722	0.172785
Hs.142912	NM_001466	**FZD2**	4.5159	0.125445
Hs.502328	NM_000610	**CD44**	3.3175	0.058305
Hs.386567	NM_004120	**GBP2**	3.1529	0.020033
Hs.492974	NM_003882	**WISP1**	2.8781	0.669151
Hs.137510	NM_006312	**NCOR2**	2.8553	0.078323
Hs.94234	NM_003505	**FZD1**	2.5179	0.251392
Hs.517603	NM_002405	**MFNG**	2.4929	0.086738
Hs.591863	NM_003506	**FZD6**	2.3132	0.155446
Hs.664706	NM_024015	**HOXB4**	2.264	0.078899
Hs.149261	NM_001754	**RUNX1**	2.1419	0.279567
Hs.446352	NM_004448	**ERBB2**	1.9708	0.099765
Hs.495473	NM_017617	**NOTCH1**	1.9332	0.105153
Hs.504096	NM_005188	**CBL**	1.8568	0.068651
Hs.487360	NM_024408	**NOTCH2**	1.8422	0.136808
Hs.2256	NM_002423	**MMP7**	1.8389	0.318428
Hs.728902	NM_203458	**NOTCH2NL**	1.838	0.076917
Hs.437922	NM_005376	**MYCL1**	1.7638	0.372321
Hs.390736	NM_003879	**CFLAR**	1.7396	0.122128
Hs.728776	NM_012423	**RPL13A**	1.6804	0.123115
Hs.716382	NM_004210	**NEURL**	1.6387	0.309506
Hs.404914	NM_003183	**ADAM17**	1.6198	0.142189
Hs.436100	NM_004557	**NOTCH4**	1.5761	0.076371
Hs.73090	NM_002502	**NFKB2**	1.546	0.503839
Hs.404089	NM_016169	**SUFU**	1.5366	0.575025
Hs.349094	NM_002351	**SH2D1A**	1.4657	0.332305
Hs.517517	NM_001429	**EP300**	1.3542	0.953128
Hs.592082	NM_003502	**AXIN1**	1.329	0.521975
Hs.251680	NM_000427	**LOR**	1.2918	0.284098

Table 6.1 *Notch pathway PCR Array of human ICC and patient-matched non-cancerous liver.* Table of top 40 differentially up-regulated genes in human ICC vs. patient-

matched non-cancerous liver (n=5). See appendix table 1 for full table of 84 genes profiled.

Figure 6.1 Heat map and volcano plot from Notch pathway PCR Array of human ICC and patient-matched liver.

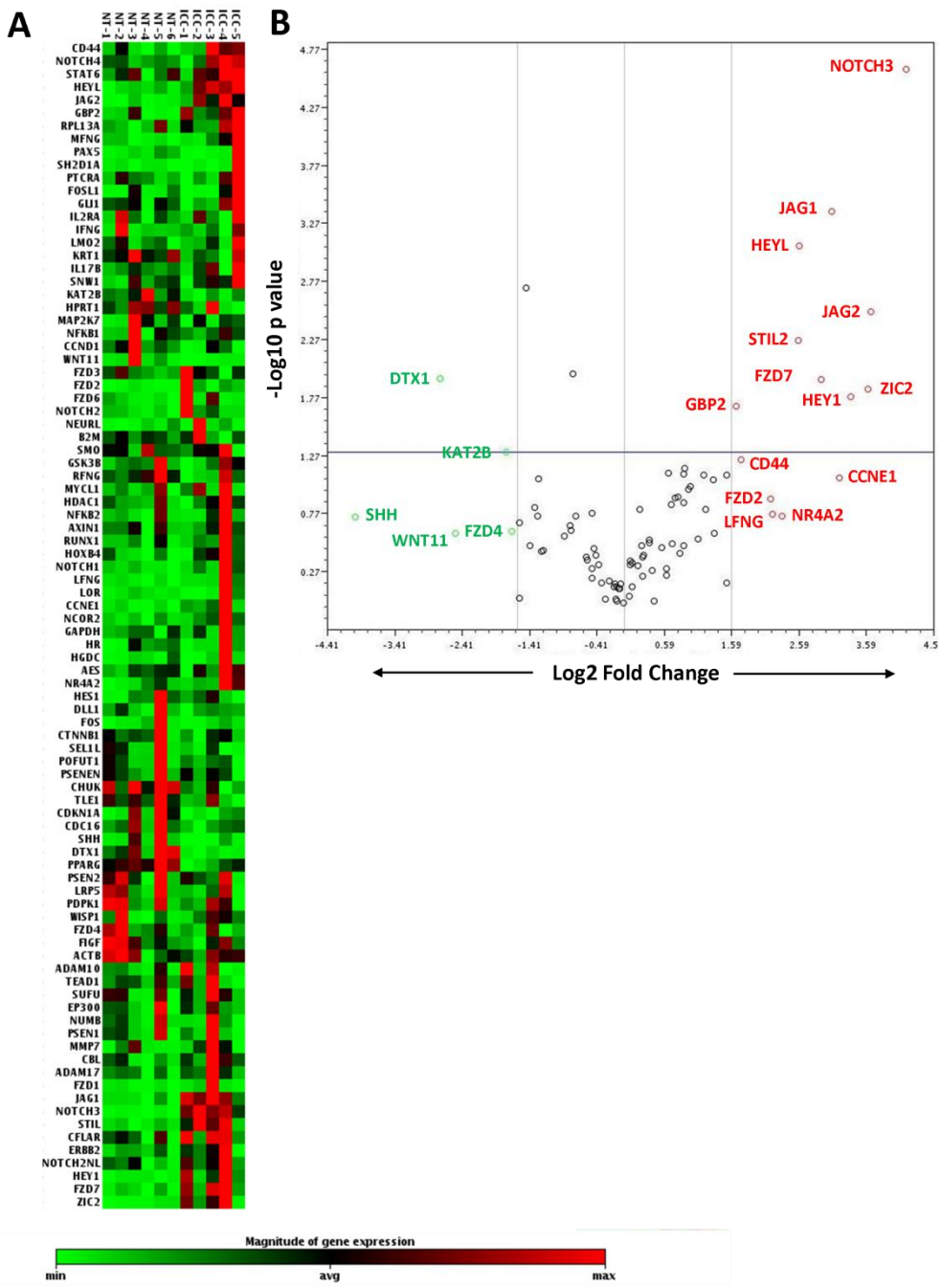

Figure 6.1 *Heat map and volcano plot from Notch pathway PCR Array of human ICC and patient-matched distal liver.* (**A**) Heat map and (**B**) Volcano plot comparing Notch transcription in human ICC vs. patient-matched non-cancerous liver (n=5). Horizontal Grey line represents a p value of 0.05. Vertical grey lines represent

boundary of ≥3 fold down-regulation and ≥3 fold up-regulation respectively. Up-regulated genes are represented in red; down-regulated genes are represented in green.

To corroborate these results with an independent technique, I performed rt-qPCR on the same cohort of tumours and non-cancerous liver controls that had been prospectively collected from patients undergoing resectional surgery at the Royal Infirmary of Edinburgh (Tumours n= 5; Non-cancerous liver n=6) (Figure 6.2). Again I observed the same profile of transcriptional up-regulation; with NOTCH1 up-regulated 3.08 fold ±0.89 (p=0.052); NOTCH2 6.23 fold ±2.85 (p=0.126); NOTCH3 96.85 fold ±59.53 (p=0.043) and NOTCH4 3.03 fold ±1.37 (p=0.082). The Hes/Hey target effectors that were significantly up-regulated on qPCR were Hes4 (9.09 fold ±3.34 p=0.065) and HeyL (4.53 fold ±1.38 p=0.0427).

Figure 6.2 Transcription of the Notch pathway is up-regulated in a prospectively collected cohort of human ICC.

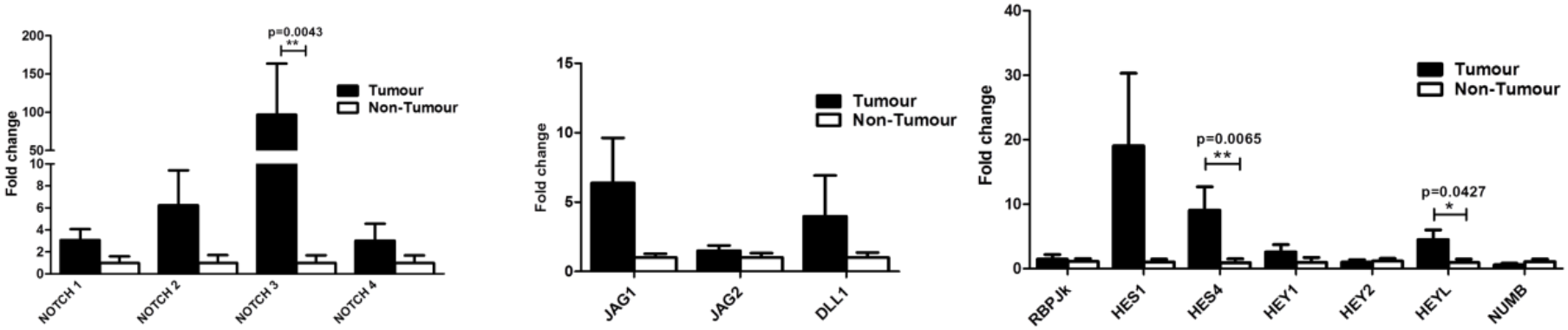

Figure 6.2 *Transcription of the Notch pathway is up-regulated in a prospectively collected cohort of human ICC.* rt-qPCR data of the Notch pathway from a prospectively collected cohort of resected ICC at the Royal Infirmary of Edinburgh (Tumour n=5; Non-cancerous liver n=6). NOTCH1 was up-regulated 3.08 fold (p=0.052); NOTCH2 6.23 fold (p=0.126); NOTCH3 96.85 fold ±59.53 (p=0.043) and NOTCH4 3.03 fold (p=0.082). The Hes/Hey target effectors that were significantly up-regulated on qPCR were Hes4 (9.09 fold p=0.065) and HeyL (4.53 fold p=0.0427). Data are represented as means ±S.E.M. and differences calculated using the Mann-Whitney U test. * p≤0.05; ** p≤0.01; ***p≤0.001.

In addition I used rt-qPCR to analyse Notch activity in a retrospective cohort of archival samples of formalin fixed, paraffin embedded biliary tumours (n=31) and healthy control livers (n=30) collected by the NHS Lothian SAHSC BioResource and Edinburgh MRC Sudden Death Brain and Tissue Bank. RNA was extracted using an FFPE RNEasy kit (Qiagen) and subject to the same quality control as freshly frozen tissue. I observed the same pattern of transcriptional up-regulation as had been seen in the prospectively collected cohort: NOTCH1 was actually down-regulated 0.56 fold ±0.14 (p=<0.0001), NOTCH2 up-regulated 9.38 fold ±3.42 (p=<0.0001), NOTCH3 38.30 fold ±11.46 (p=<0.0001) and NOTCH4 2.26 fold ±0.67 (p=<0.0001). The Notch ligand JAG1 was up-regulated 608.99 fold ±466.51 (p p=<0.0001), JAG2 1578.25 ±662.25 (p=<0.0001) and DLL1 133.14 ±123.90 (p=<0.0001). The target gene Hes1 was up-regulated 861.45 fold ±700.20 (p=<0.0001), Hes4 537.87 ±39.75 (p=<0.0001), Hey1 79.85 39.75 (p=<0.0001), Hey2 685.63 fold ±604.10 (p=<0.0001) and HeyL 289.33 fold 114.37 ±114.37 (p=<0.0001).

Figure 6.3 Transcription of the Notch pathway is up-regulated in a retrospective cohort of paraffin-embedded, formalin-fixed human ICC.

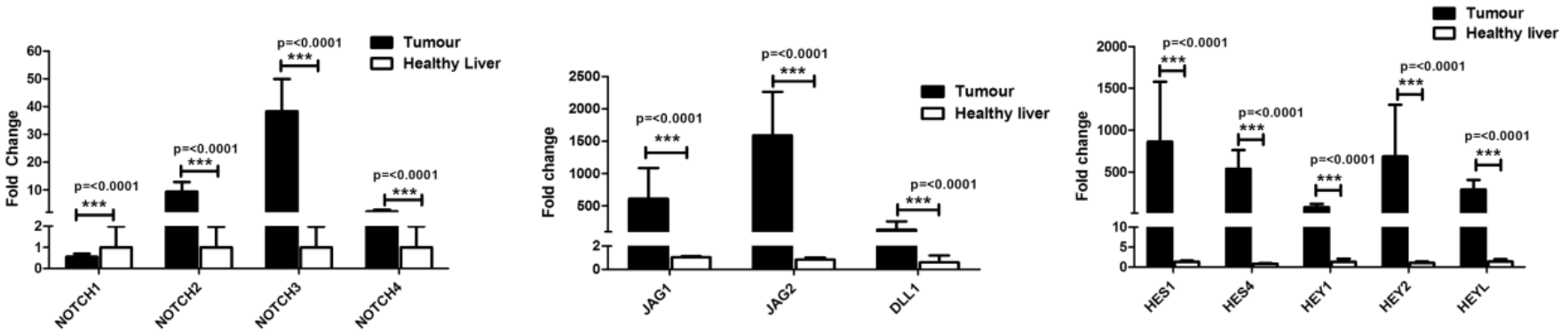

Figure 6.3 *Transcription of the Notch pathway is up-regulated in a retrospective cohort of paraffin-embedded, formalin-fixed human ICC.* rt-qPCR data of the Notch pathway from a retrospective cohort of archival ICC from the NHS Lothian Tissue Bioresource (n=31) and healthy liver controls (n=30). As observed in the prospectively collected samples, NOTCH3 was the most highly up-regulated receptor (38.30fold p=<0.0001). Data are represented as means ±S.E.M. * p≤0.05; ** p≤0.01; ***p≤0.001.

Finally to validate these results from an independently collected and analysed cohort, a collaborator, Dr Mina Komuta, a post-doctoral fellow at Professor Tania Roskams' laboratory, KU Leuven, Belgium analysed a cohort of tumours (n=11) and non-cancerous liver controls (n=6) using the same primers and methods as had been performed on the previous two cohorts. In this group NOTCH3 was again the most highly up-regulated receptor 11.62 fold ±1.34 (p=0.0011) compared to NOTCH1 1.90 fold ±0.40 (p=0.29), NOTCH2 4.13 fold ±0.62 (p=0.0011) and NOTCH4 1.03 fold ±0.18 (p=0.58). Both ligands were up-regulated: JAG1 11.93 fold ±2.67 (p=0.0011) and JAG2 8.12 ±1.60 (p=0.0011). Target genes were transcribed as follows: HES1 1.61 fold ±0.34 (p=0.25), HES4 9.17 ±1.51 fold (p=0.0011), HEY1 3.28 fold ±0.85(p=0.138), HEY2 0.79 fold ±0.22 (p=0.145) and HEYL 4.47 fold ±1.19 (p=0.003).

Figure 6.4 Transcription of the Notch pathway is up-regulated in an independently collected and analysed cohort of human ICC (Roskams Lab, KU Leuven, Belgium).

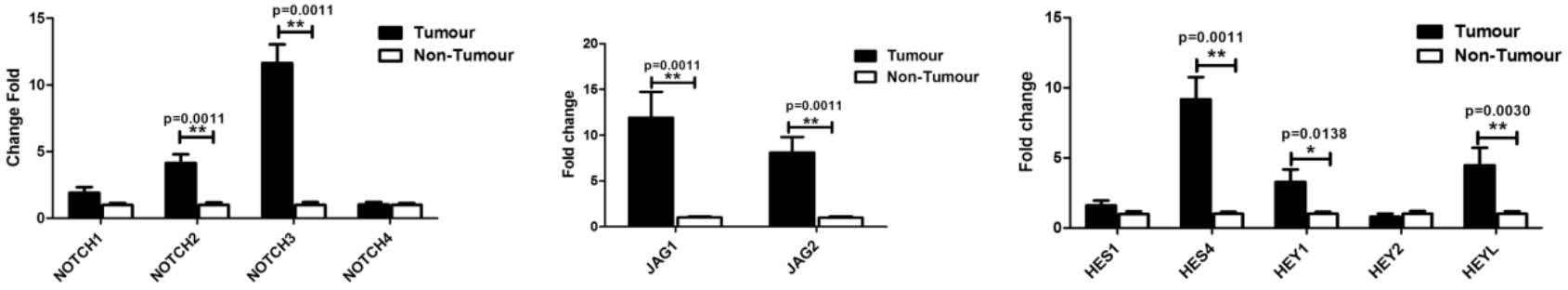

Figure 6.4 *Transcription of the Notch pathway is up-regulated in an independently collected and analysed cohort of human ICC (Roskams Lab, KU Leuven, Belgium).* rt-qPCR analysis of the Notch pathway from a cohort of ICC (n=11) and patient-matched controls (n=6) collected and analysed by Nina Komuta at KU Leuven, Belgium. NOTCH3 was the most highly up-regulated receptor (11.62 fold ±1.34 p=0.0011), JAG1 the most highly expressed ligand (11.93 ±2.67 p=0.0011) and HES4 the most highly up-regulated target gene (9.17 fold ±1.51 p=0.0011). Data are represented as means ±S.E.M. * p≤0.05; ** p≤0.01; ***p≤0.001.

In all the above datasets only intrahepatic and perihilar tumours were analysed; no extrahepatic tumours were included. The same primers and methods were used in the analyses of each cohort, including cDNA dilutions, and therefore I have combined the results to give an overall picture of Notch transcriptional activity in ICC vs. healthy liver. Overall when normalised to non-tumour, NOTCH1 was down-regulated 1.13 fold ±0.20 (p=0.0001), NOTCH2 up-regulated 7.49 fold ±1.88 (p=0.0001), NOTCH3 38.28 fold ±10.30 (p=0.0001) and NOTCH4 2.01 fold ±0.40 (p=0.0001). The Notch ligand JAG1 was up-regulated 363.33 fold ±251.61 (p=0.0001) and JAG2 938.55 fold ±369.51 (p=0.0001). Transcription of target genes was as follows: HES1 483.69 ±368.22 (p=0.0001), HES4 304.19 ±119.83 (p=0.0001), HEY2 384.84 ±317.02 (p=0.0005) and HEYL 160.56 fold ±60.06 (p=0.0001).

Figure 6.5 Transcription of the Notch pathway is up-regulated in ICC.

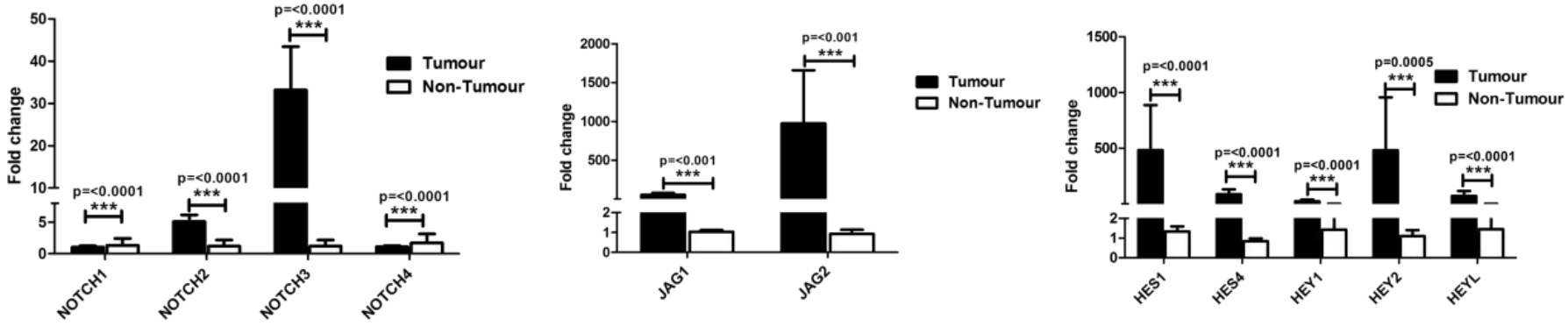

Figure 6.5 *Transcription of the Notch pathway is up-regulated in ICC.* Combined rt-qPCR data of Notch pathway transcription from the above three datasets (Tumour n= 47; Non-cancerous liver=42). NOTCH1 was down-regulated 1.13 fold ±0.20 (p=0.0001), NOTCH2 7.49 fold ±1.88 (p=0.0001), NOTCH3 38.28 fold ±10.30 (p=0.0001) and NOTCH4 2.01 fold ±0.40 (p=0.0001). The Notch ligand JAG1 was up-regulated 363.33 fold ±251.61 (p=0.0001) and JAG2 938.55 fold ±369.51 (p=0.0001). Transcription of target genes was as follows: HES1 483.69 ±368.22 (p=0.0001), HES4 304.19 ±119.83 (p=0.0001), HEY2 384.84 ±21.59 (p=0.0005) and HEYL 160.56 fold ±317.02 (p=0.0001).Data are represented as means ±S.E.M. * p≤0.05; ** p≤0.01; ***p≤0.001.

These data demonstrate across independently collected and analysed cohorts of tumours, that transcription of the receptors Notch2 bit more significantly Notch3 is up-regulated in human ICC. This compares to that of Notch1 and Notch4 which are modestly down-regulated. Ligands Jagged 1 and 2 are over-expressed in ICC, as are all the Hes/Hey target effectors measured, indicating functional activity through the pathway. The differences in quantitation of Jagged ligand expression observed between the cohorts here may be a result of sample size, however it would be interesting to perform a subgroup analysis to control for any background of chronic liver disease that might be present to assess whether different aetiologies of hepatic pathology can differentially activate Notch ligands as a precursor to cancer.

Expression of Notch proteins is up-regulated in human ICC

To compare the expression of Notch proteins in human ICC compared to distal non-cancerous liver, I performed immunohistochemistry in formalin fixed tissue on samples collected locally as well as a tissue microarray containing 42 ICC cores and 42 patient-matched liver controls (Figure 6.7). I found that expression of Notch3 appeared to be much greater within regions of ICC compared to healthy liver, where expression was strongest on the smooth muscle of the hepatic vasculature (Figure 6.6). Positivity was greatest on malignant epithelia, where it was frequently widespread (Figure 6.7), however I also observed regions of ICC exhibiting clusters of Notch3 positive epithelial cells with clear nuclear positivity, suggesting functional pathway activity in these cells (Figure 6.6). Unexpectedly the cancerous stroma was also frequently positive for Notch3 although this was quite variable between patients (Figure 6.6 and 6.8). Furthermore epithelial Notch3 immunopositivity appeared much stronger than that of Notch1 which was only modestly up-regulated compared to healthy ductules. (Figure 6.7).

In contrast Jagged 1 immunoreactivity was principally restricted to the stromal compartment of tumours (Figure 6.6) and co-localised with αSMA (Figure 6.8)

Figure 6.6 Notch3 protein is observed on the hepatic vasculature in healthy liver but appears on malignant ductules and stroma in ICC

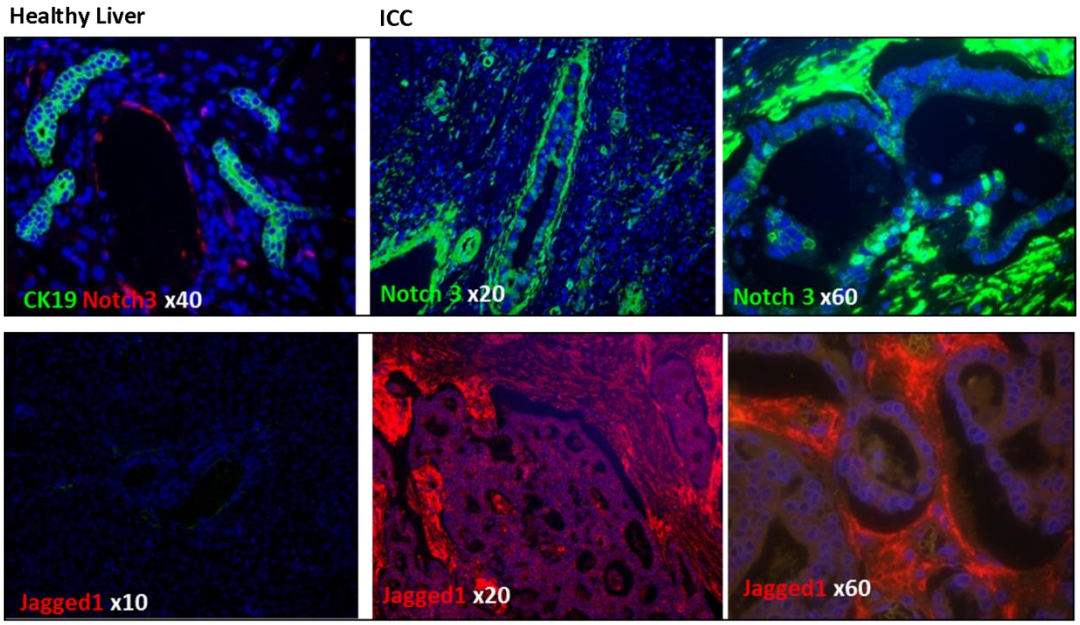

Figure 6.6 Notch3 protein is observed on the hepatic vasculature in healthy liver but appears on malignant ductules and stroma in ICC

In the healthy human liver Notch3 immunoreactivity is confined to the smooth muscle surrounding the hepatic vasculature. In ICC however Notch3 is also expression on malignant ductules and the fibroblastic stroma (upper panel and Figure 6.7). Clusters of positive epithelia can be observed exhibiting nuclear positivity for Notch3-ICD (upper panel, far right). Jagged 1 in contrast is absent in the homeostatic adult liver, but becomes up-regulated in ICC, principally by the cancerous stroma (lower panel).

Figure 6.7 Notch3 protein is up-regulated in human ICC compared to distal non-cancerous liver.

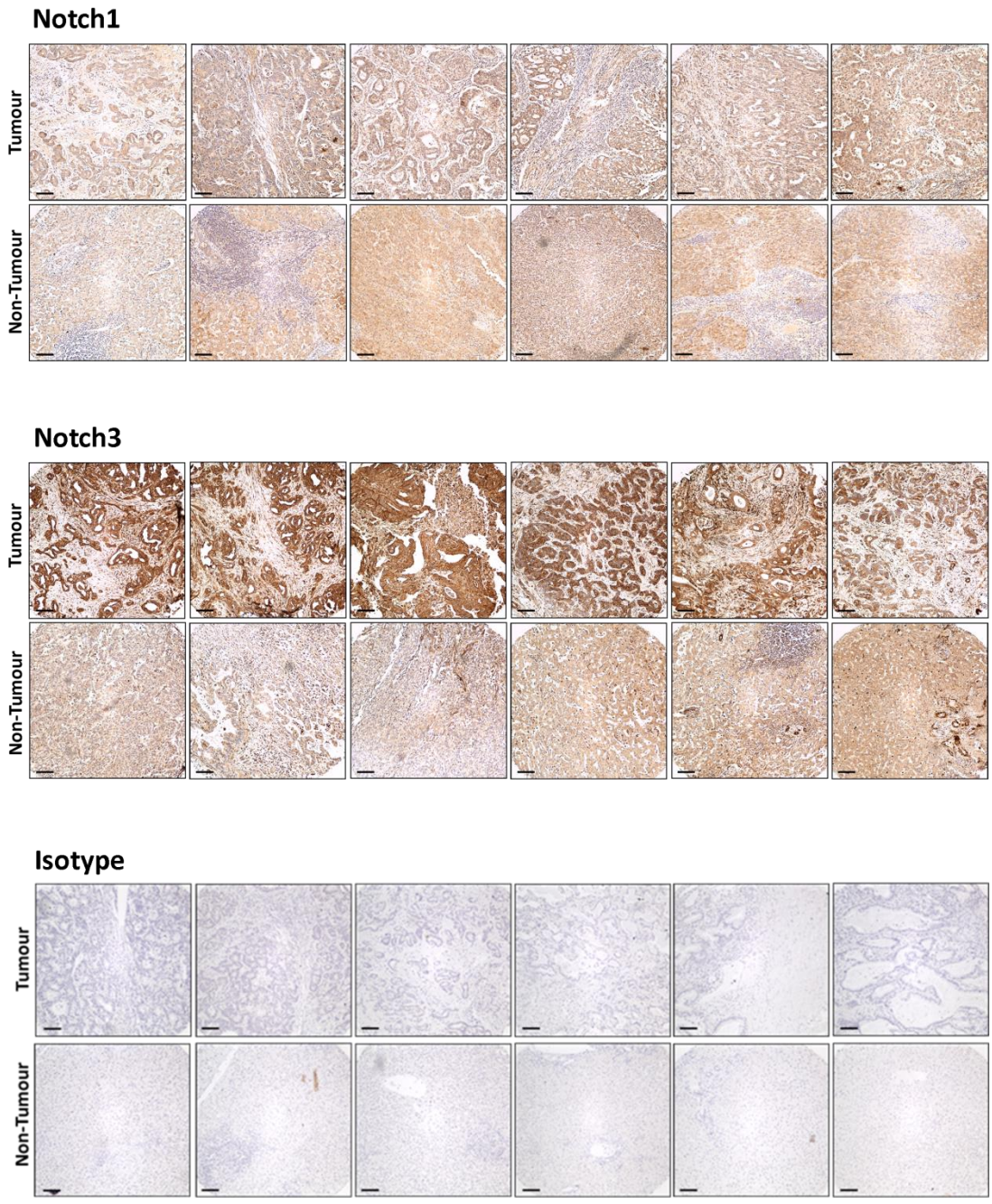

Figure 6.7 *Notch3 protein is up-regulated in human ICC compared to distal non-cancerous liver.* Representative photomicrographs of DAB immunostaining for Notch1 (top panels), Notch3 (middle panels) and rabbit isotype control (lower panels) in tissue microarrays of human ICC and distal non-cancerous liver. Tissue microarrays were

stained with equivalent concentrations of antibody and photomicrographs taken at the same exposure. Scalebars represent 100μm.

Given the apparent up-regulation of the Notch3 receptor in particular, I next co-stained Notch3 with a range of markers of different liver cell types to confirm which cells were expressing Notch3 in tumour and healthy liver (Figure 6.8) . I found some overlap of expression with the Notch ligand Jagged1, which was observed primarily on stromal fibroblasts (upper panel). However I found that Notch3 was expressed by both $CK19^+$ epithelial cells as well as αSMA^+ myofibroblasts in the surrounding stroma (2^{nd} and 3^{rd} panels), and that within the epithelial compartment, nuclear Notch3 positivity could be observed; indicating nuclear localisation of N3-ICD and pathway activity (filled arrowheads in upper panel). Notch3 was not expressed by $CD68^+$ inflammatory cells or $CD31^+$ endothelial cells (lower two panels).

Figure 6.8 Notch3 is expressed by malignant ductules and stromal myofibroblasts in human ICC but not other stromal cell types

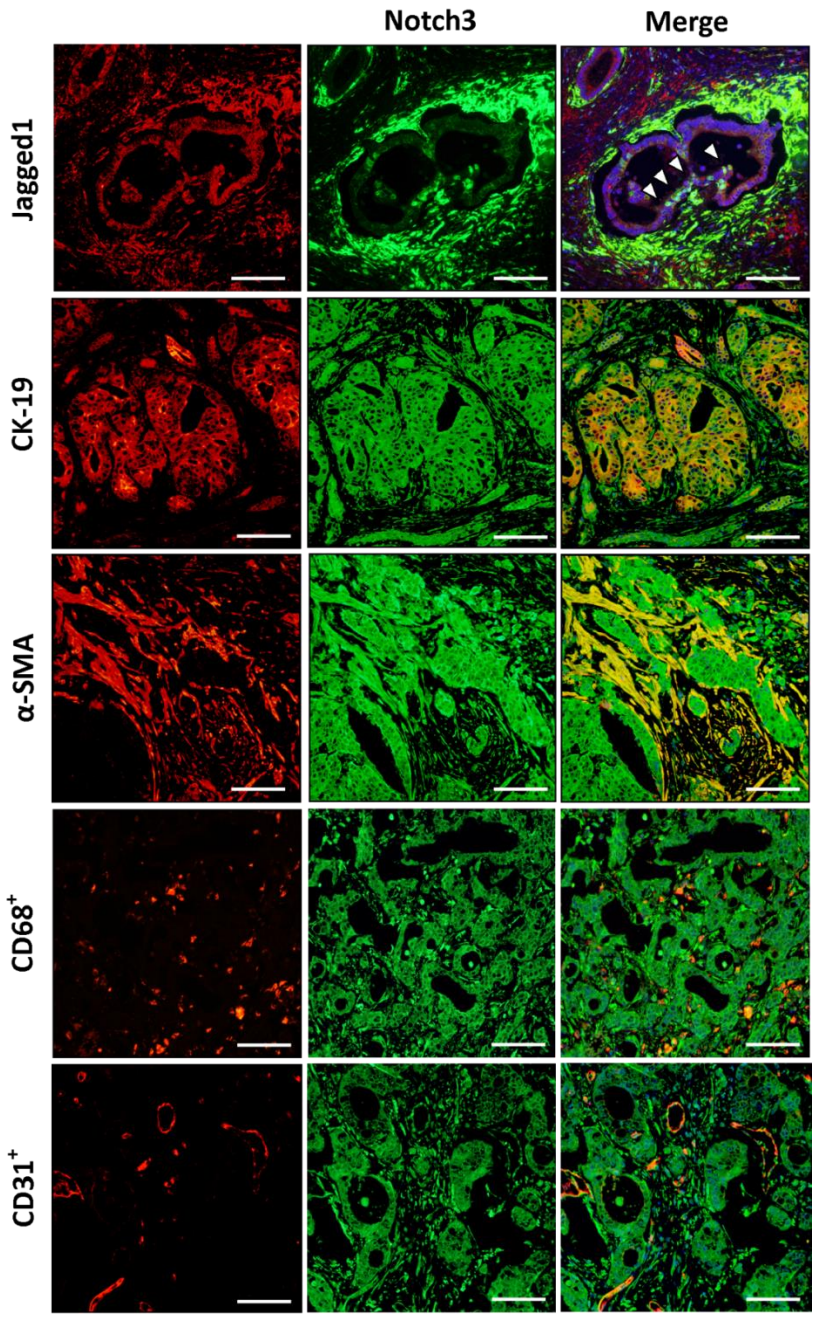

Figure 6.8 *Notch3 is expressed by malignant ductules and stromal myofibroblasts in human ICC but not other stromal cell types* Representative photomicrographs from human ICC showing co-immunofluorescent staining of Notch3 with Jagged1, CK19, αSMA, $CD68^+$ or $CD31^+$. Notch3 is expressed by both $CK19^+$ epithelia which exhibit nuclear

positivity, as well as stromal αSMA$^+$ myofibroblasts. Notch3 is not expressed by endothelia or inflammatory cells in the tumour stroma. Scalebars represent 100μm.

Immunostaining for the Hes/Hey target effectors was unsuccessful in paraffin-embedded, formalin-fixed tissue despite testing a number of antibodies. Therefore in order to determine whether activity through the Notch pathway was functional in human ICC, I performed a western blot for the Notch3 receptor using an antibody able to detect the intracellular domain of the protein (95kDa) (Figure 6.9).

Figure 6.9 N3-ICD is up-regulated in human ICC compared to distal non-cancerous liver.

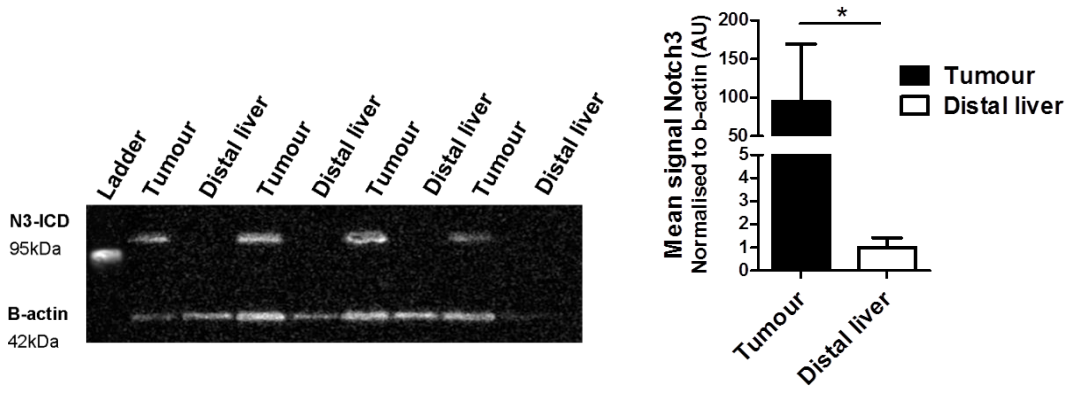

Figure 6.9 *N3-ICD is up-regulated in human ICC compared to distal non-cancerous liver.* On densitometric analysis of the 4 human ICC specimens and matched non-cancerous liver controls assayed with western blot, the intracellular domain of Notch3 is up-regulated 94.99 fold (p=0.0286).

Notch is progressively up-regulated during the natural history of disease progression in ICC

Recommended criteria for genetically engineered models of cancer include the use of the same mutations that occur in human tumours, preferably with silencing of mutations in embryogenesis and early postnatal development (except for paediatric tumours) (232). Even when transgenes are induced in adulthood however, these models will only truly represent that subset of patients with tumours carrying that defined genetic alteration and are often hindered by variability in tumour latency and penetrance (233). Chemically induced models of cancer, and in particular the thioacetamide (TAA) model of cholangiocarcinoma in rat have several advantages. Histologically tumours closely resemble those of human disease and exhibit a progression from chronic inflammation and fibrosis through to invasive adenocarcinoma accompanied by an intense desmoplastic stromal reaction. Given the similarities in this sequence, it is tempting to consider a similar mutagenic process may be occurring to that in human ICC; however despite this to date the mutational profile of this model has not been characterised. It is known however that these tumours in rat exhibit many of the phenotypic markers typical of human ICC including EGFR, MUC1, c-Met, erbB2, MMP2 and MMP9 (75, 234) and as such represents a suitable model to study ICC behaviour *in vivo.*

A timecourse of this rat model has been previously performed by a clinical research fellow in our laboratory Andrew Robson, whereby rats were administered 0.06% thioacetamide and harvested at the following time points: 8, 10, 12, 14, 16, 18, 20, 22, 24 and 26 weeks. Uninjured controls were also used however these were not time matched; all control animals were harvested at 26 weeks (n=3 at each time point; n=3 uninjured controls). I have stained this tissue with H&E and sought independent verification of the histological appearance from a specialist liver histopathologist: *"Livers from animals injured for 10-14 weeks show a HPC response around most portal tracts without portal-portal HPC bridging; this is associated with a sparse, mixed, neutrophil-rich inflammatory infiltrate. Pigment-laden macrophages are present in some*

larger portal tracts. At 14 weeks occasional large portal tracts are oedematous. There is no biliary epithelial or hepatocellular dysplasia or malignancy. After 16-18 weeks of injury the HPC response is more extensive, with widespread HPC portal-portal bridging and permeation into periportal sinusoids. In addition there are isolated (<4) and small (<5mm maximum diameter) foci of well-moderately differentiated adenocarcinoma in keeping with cholangiocarcinoma, focally showing mucin production; separate small foci of biliary dysplasia not definitely amounting to adenocarcinoma are also present. After 20 weeks, foci of cholangiocarcinoma are numerous, large and frequently coalescent."(Figure 6.10)

Figure 6.10 H&E staining of rat liver sections during the 26 week TAA timecourse.

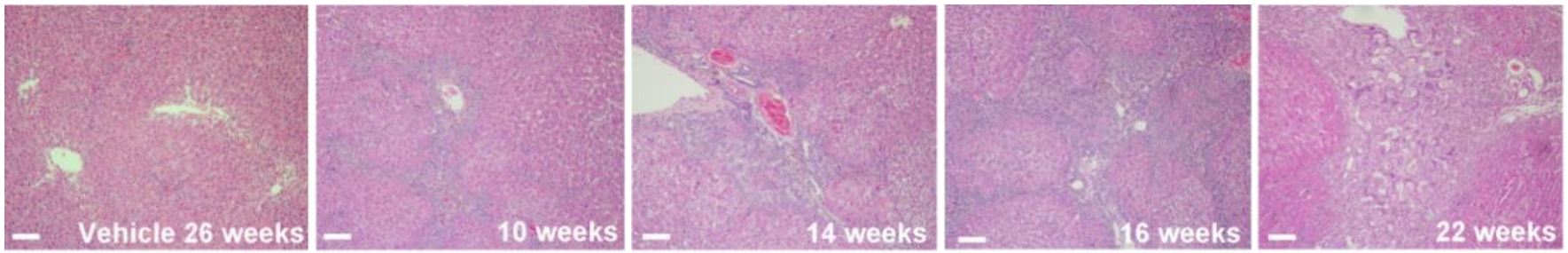

Figure 6.10 *H&E staining of rat liver sections during the 26 week TAA timecourse.* Representative photomicrographs from H&E stained timecourse of rat livers following treatment with TAA for up to 26 weeks with uninjured control. Scalebars represent 100μm.

This model therefore offers a suitable platform for studying how the Notch pathway behaves during disease progression in ICC. I firstly used Notch PCR arrays as used to look at pathway transcription in human ICC, to take a broad look at how the entire pathway is regulated during the course of disease development compared to uninjured controls. As tumours were multifocal and not always macroscopically visible, samples of whole fresh frozen liver were cut at random from TAA and vehicle treated rats. I pooled samples and categorised them according to histological diagnosis as follows: Inflamed 8 to 10 weeks TAA; Fibrotic 12 to 14 weeks ; Early malignant 16 to 20 weeks; Late malignant 22 to 26 weeks (n=3 at each timepoint). Each group was then compared to uninjured controls (RNA pooled from n=6). I observed a progressive up-regulation of the Notch pathway over time in response to injury with TAA. As seen in human ICC, the Notch3 receptor was the most up-regulated paralog (2.3 fold during the fibrotic stage; 5.7 fold in late malignancy) (See Appendix Table 2 for full list of genes and fold regulation). In advanced malignancy, Jag1 was the most highly up-regulated ligand (4.1 fold) and HeyL the most up-regulated target effector (6.6 fold) (Figure 6.11).

Figure 6.11 PCR Array of rat Notch pathway transcription during inflammation and invasive adenocarcinoma in the TAA model of ICC.

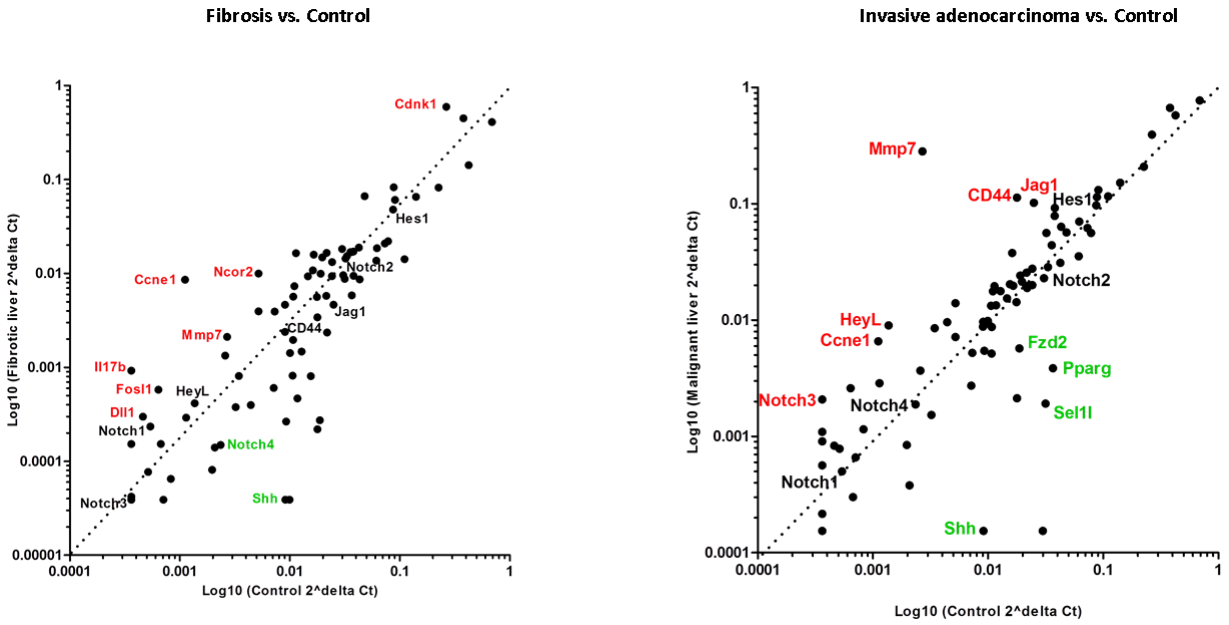

Figure 6.11 *PCR Array of rat Notch pathway transcription during inflammation and invasive adenocarcinoma in the TAA model of ICC.* Graphs showing progressive up-regulation of Notch pathway transcription in rat livers during fibrosis (12 to 14 weeks TAA) and advanced malignancy (22 to 26 weeks TAA) compared to uninjured control. *Notch3* was the most highly up-regulated receptor (2.3 fold during

fibrosis; 5.7 fold in invasive adenocarcinoma). Jag1 was the most highly up-regulated ligand (1.42 fold in fibrosis; 4.08 fold in adenocarcinoma) and HeyL the most up-regulated effector (1.46 fold in fibrosis; 6.58 fold in adenocarcinoma). A significant fold change in transcription was set at +/- 4 fold change in expression. Up-regulated genes are noted in red; down-regulated genes notated in green.

I then verified these data using rt-qPCR for key Notch pathway components using the same samples (Figure 6.12). Of the Notch receptors, *Notch3* was seen to be the most highly up-regulated paralog (52.0 fold ±30.2 p=0.0022) and *Jag1* the most up-regulated ligand (19.2 fold ±5.2 p=0.0022). *Notch1* was up-regulated 5.32 fold ±1.69 p=0.0411; *Notch2* 4.75 fold ±0.38 p=0.0022; *Notch 4* 9.67 fold ±3.78 p=0.0022 and *Jag2* 2.36 fold ±0.45 p=0.312). Interestingly in these samples from this model there was little change in transcription of the classical Notch effectors *Hes1* (1.0 fold ±0.20), *Hey1* (0.74 fold ±0.11), *Hey2* (0.88 fold ±0.18) or *HeyL* (1.61 fold ±0.38).

Figure 6.12 **Notch3** ***and*** **Jag1** ***transcription are most highly up-regulated during ICC progression in the TAA model in rat.***

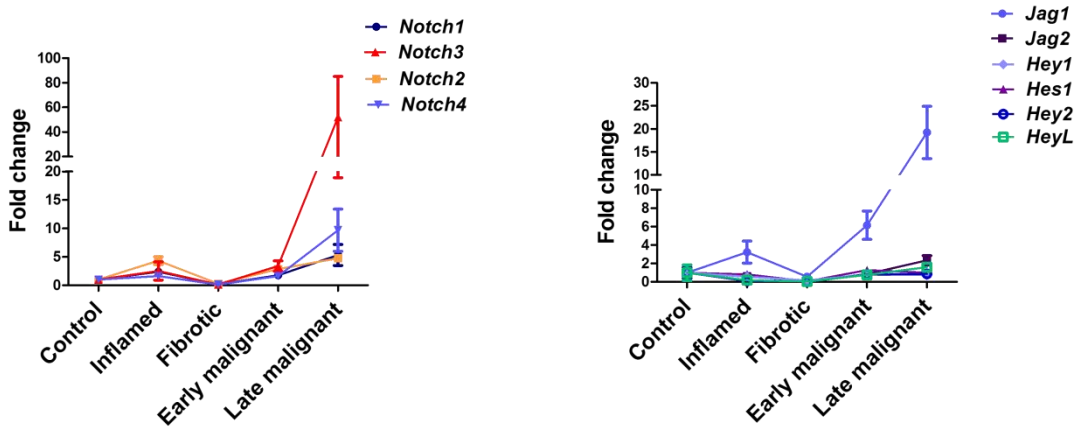

Figure 6.12 Notch3 *and* Jag1 *transcription are most highly up-regulated during ICC progression in the TAA model in rat.* qPCR data of the TAA timecourse in rat demonstrating *Notch3* is the most highly up-regulated Notch receptor during early and late stage ICC (52.0 fold ±30.2 p=0.0022) and *Jag1* the most up-regulated ligand (19.2 fold ±5.2 p=0.022). Data are represented as means ±S.E.M. As the animals receiving vehicle control in this experiment were not matched to the corresponding time points, I have used a Mann-Whitney U test to directly compare gene expression between rats receiving 26 weeks TAA and 'control' rats receiving 26 weeks normal drinking water.

To verify that these observed transcriptional changes were also recapitulated at the protein level within the tissue, I performed immunohistochemistry for the Notch3 receptor and Jagged 1 ligand on the TAA timecourse (Figure 6.13). As hyperplastic and ultimately malignant ducts appear (as demonstrated with CK19 staining), both Notch3 and Jagged1 are increasingly expressed. In the homeostatic adult rat liver Notch3 is expressed solely by smooth muscle surrounding the hepatic vasculature. During inflammation and then fibrosis fibroblasts infiltrating the parenchyma become positive for Notch3, as do proliferating biliary ductules. By early and late

malignancy Notch3 positivity is observed throughout regions of adenocarcinoma in both the cancerous epithelium and the surrounding desmoplastic stroma. Jagged1 is not expressed in the adult rat liver in homeostasis. As with Notch3, Jagged1 is up-regulated by infiltrating myofibroblasts in response to TAA damage, however its expression remains restricted to the mesenchymal compartment of the liver. In early and advanced adenocarcinoma Jagged1 is widely expressed throughout the tumour stroma on cancer associated fibroblasts investing the malignant ducts.

Figure 6.13 NOTCH3 and JAGGED1 proteins are increasingly expressed during the course of ICC development in a TAA rat model

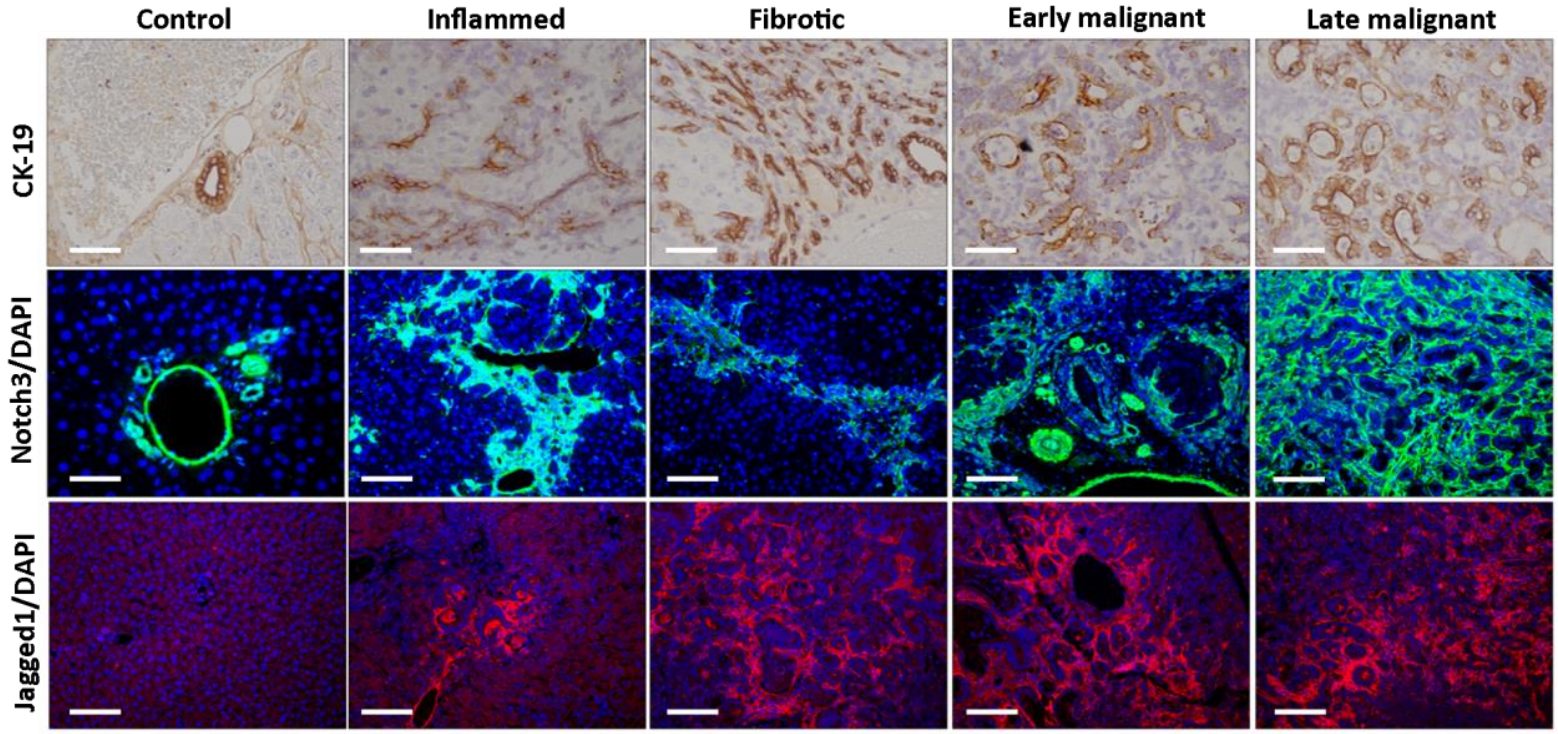

Figure 6.13 *NOTCH3 and JAGGED1 proteins are increasingly expressed during the course of ICC development in a TAA rat model.* In uninjured rat liver NOTCH3 is expressed in the smooth muscle surrounding the hepatic vasculature (middle panel). As inflammation and fibrosis develop NOTCH3 is up-regulated in the mesenchymal compartment of the liver as well as the biliary epithelium. By early and late malignancy, NOTCH3 can be observed on the malignant ductules as well as the surrounding desmoplastic stroma within areas of adenocarcinoma. JAGGED1 is not expressed in the healthy adult rat liver. It is progressively up-regulated by fibroblasts with increasing TAA damage, becoming florid in late malignancy. I observe no JAGGED1 expression within the epithelial compartment. Scalebars represent 100μm.

Notch3 is up-regulated in a mouse model of ICC

Finally I examined Notch pathway transcription in the murine model of ICC in which CK19CreYFPp53$^{flox/flox}$ mice underwent chronic liver injury with TAA for 26 weeks. I performed rt-qPCR on whole liver from CK19CreYFPp53$^{flox/flox}$ mice that developed tumours, CK19CreYFPp53$^{flox/flox}$ mice with no tumours, as well as CK19CreYFPp53$^{flox/wt}$, CK19CreYFPp53$^{wt/wt}$ mice and uninjured controls (Figure 6.14). In this model both Notch3 and Notch1 were up-regulated in CK19CreYFPp53$^{flox/flox}$ mice without tumours and further up-regulated in CK19CreYFPp53$^{flox/flox}$ mice with ICC (*Notch3* 85.92 fold ±67.66 p=0.0286; *Notch1* 17.09 fold ±9.04 p=0.0381). Neither the up-regulation of *Jag1* observed in CK19CreYFPp53$^{flox/flox}$ mice without tumours, nor that of *Jag2* in CK19CreYFPp53$^{flox/flox}$ mice with ICC reached statistical significance but this may be a result of the experiment being insufficiently powered . Of the Notch target genes, *Hey2* was the only gene that up-regulated (45.48 fold ±21.46 p=0.0286), and this was only observed in the mice with tumours.

Figure 6.14 Notch3 transcription is up-regulated in the CK19CreYFPp53$^{f/f}$ + TAA mouse model of ICC.

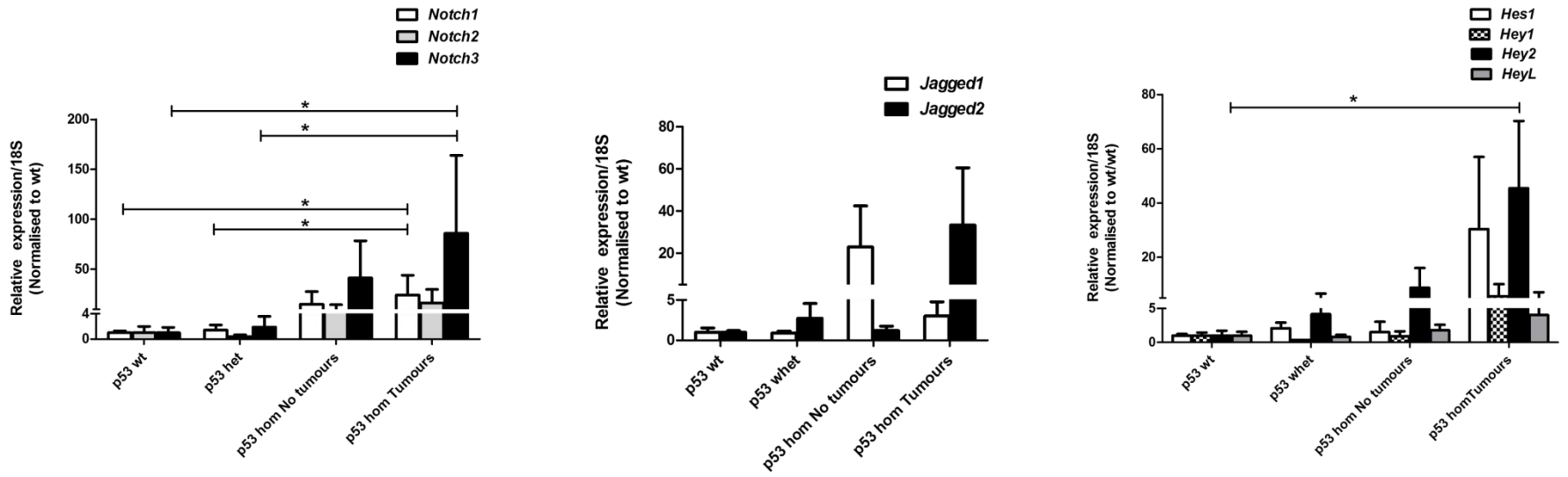

Figure 6.14 Notch3 *transcription is up-regulated in the CK19CreYFPp53$^{f/f}$ + TAA mouse model of ICC.* Rt-qPCR analysis of whole liver from CK19CreYFPp53 mice following 26 weeks of injury with TAA. When normalised to CK19CreYFPp53$^{fwt/wt}$ mice undergoing 26 weeks of TAA, *Notch3* is up-regulated 85.92 fold ±67.66 (p=0.0286) in CK19CreYFPp53$^{flox/flox}$ mice that developed ICC and 41.35 fold (p=0.0286) in CK19CreYFPp53$^{flox/flox}$ mice that did not. Similarly *Notch1*exhibited a 24.28 fold (p=0.0286) up-regulation in CK19CreYFPp53$^{flox/flox}$ mice with ICC and a 14.94 fold (p=0.0381) up-

regulation in CK19CreYFPp53$^{flox/flox}$ mice without tumours. The Notch target gene *Hey2* was also up-regulated 45.47 fold (p=0.0286) in CK19CreYFPp53$^{flox/flox}$ mice with tumours. Data are represented as mean ±S.E.M.

I confirmed with immunohistochemistry the tissue expression of Notch3 protein in this model and observed frequent co-localisation of Notch3 with the fluorescent reporter eYFP within tumours, indicating expression of Notch3 by CK19^{+} malignant ductules (Figure 6.15).

Figure 6.15 Notch3 protein is expressed by CK19^{+} epithelia in the CK19CreYFPp53$^{f/f}$ + TAA mouse model of ICC.

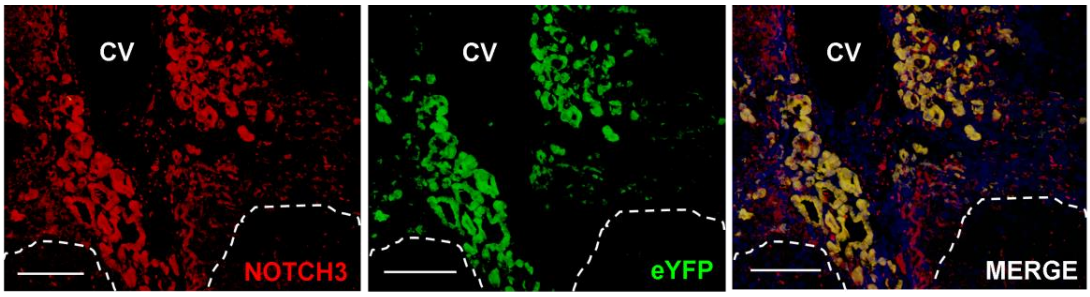

Figure 6.15 *Notch3 protein is expressed by CK19^{+} epithelia in the CK19CreYFPp53$^{f/f}$ + TAA mouse model of ICC.* Notch3 (red) is expressed on malignant ductules arising in CK19CreYFPp53$^{flox/flox}$ mice that have undergone 26 weeks of injury with TAA. In this lineage traced model Notch3 expression co-localises with the fluorescent reporter eYFP (green) driven by the CK19 promoter. CV: Central vein. Dashed line denotes tumour boundary. Scalebars represent 100μm.

Gamma secretase inhibition restricts tumour cell growth *in vitro* and *in vivo*

DAPT reduces cell viability and sphere formation in vitro

Before interrogating the effects of blocking signalling through the Notch pathway with γ-secretase inhibitors, I firstly confirmed that Notch pathway components are expressed in three intrahepatic cholangiocarcinoma cell lines (CC-SW-1; CC-LP-1;

SNU-1079) (Figure 6.16 (A)). Transcription of Notch receptors was detectable in all 3 lines, although CC-LP-1 expressed significantly higher levels than SNU-1079 and CC-SW-1. This pattern was recapitulated at the protein level (all photographs taken at same exposure) (Figure 6.15 (B)). Interestingly all 3 clonal lines also expressed Jagged1, suggesting signalling may be activated in these cells through autocrine provision of ligand.

Figure 6.16 Notch is expressed by human ICC cells

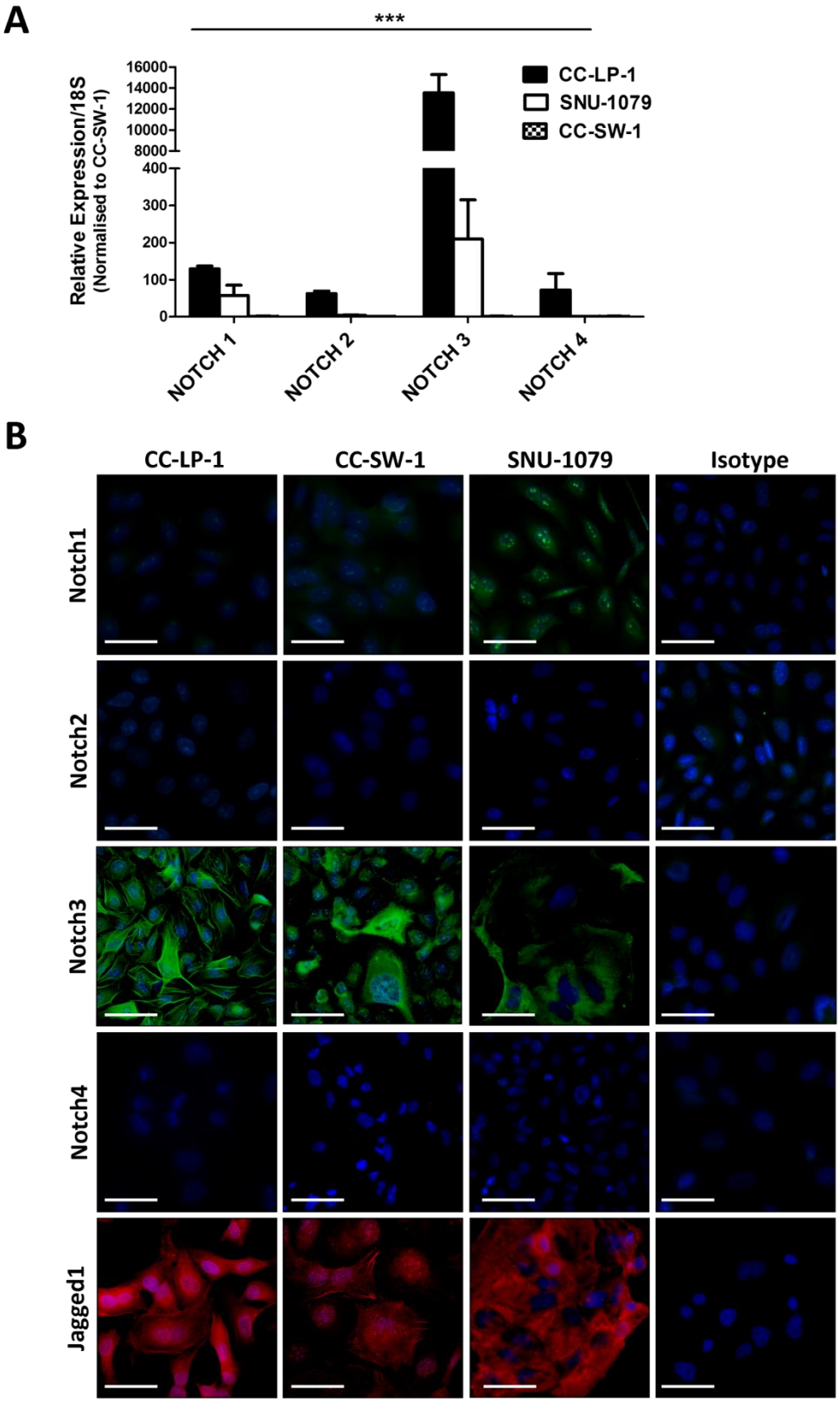

Figure 6.16 Notch is expressed by human ICC cells (**A**) rt-qPCR of Notch receptor transcription in human ICC lines CC-SW-1, CC-LP-1 and SNU-1079 (two way ANOVA p=<0.0001) (**B**) Immunocytochemistry for Notch 1, 2, 3, 4 and Jagged1 in the ICC lines CC-SW-1, CC-LP-1 and SNU-1079 with isotype controls. All photomicrographs were taken at the same exposure. Scalebars represent 50μm.

To determine an appropriate cell number for use in an assay of cell viability using the NADPH-dependent tetrazolium dye MTT, I plated cells at increasing densities in 96 well plates and cultured them for 48 hours before adding MTT and reading on a spectrophotometer. An absorbance of 1.0 was deemed to be an appropriate baseline for assessment of changes in viability, and therefore the following cell densities were subsequently used for all *in vitro* viability assays: SNU-1079 $3x10^3$ cells/well; CC-LP-1 $1.4x10^4$ cells/well; CC-SW-1 $1.75x10^4$ cells/well (Figure 6.17). Cell lines were then cultured in the presence of increasing concentrations of the γ-secretase inhibitor DAPT (3,5-Difluorophenacetyl)-L-alanyl]-S-phenylglycine t-butyl ester) or DMSO and viability measured after 48 hours. Cells were plated in triplicate and the experiment repeated three times. Cell viability decreases in a concentration dependent manner: at 50μM DAPT viability of the cell line SNU-1079 is reduced by 66.6%; CC-SW-1 by 42.6% and CC-LP-1 by 39.6% (Figure 6.17). To ensure treatment with DAPT had resulted in a reduction in Notch activity I measured Hes/Hey transcription in the 3 cell lines in response to 10μM DAPT. I observed a non-significant trend to reduction in transcription of Hes1, Hey1 and HeyL in SNU-1079 (Hes1 39.12% p=0.1; Hey1 17.62% p=0.4; HeyL 31.99% p=0.4); Hey1, Hey2 and HeyL in CC-LP-1 (Hey1 59.14% p=0.1; Hey2 54.74% p=0.1; HeyL 43.20% p=0.1) and Hes1 and Hey2 in CC-SW-1 (29.28% p=0.1; Hey2 51.66% p=0.1) (Figure 6.17).

***Figure 6.17 The γ-secretase inhibitor DAPT reduces cell viability* in vitro**

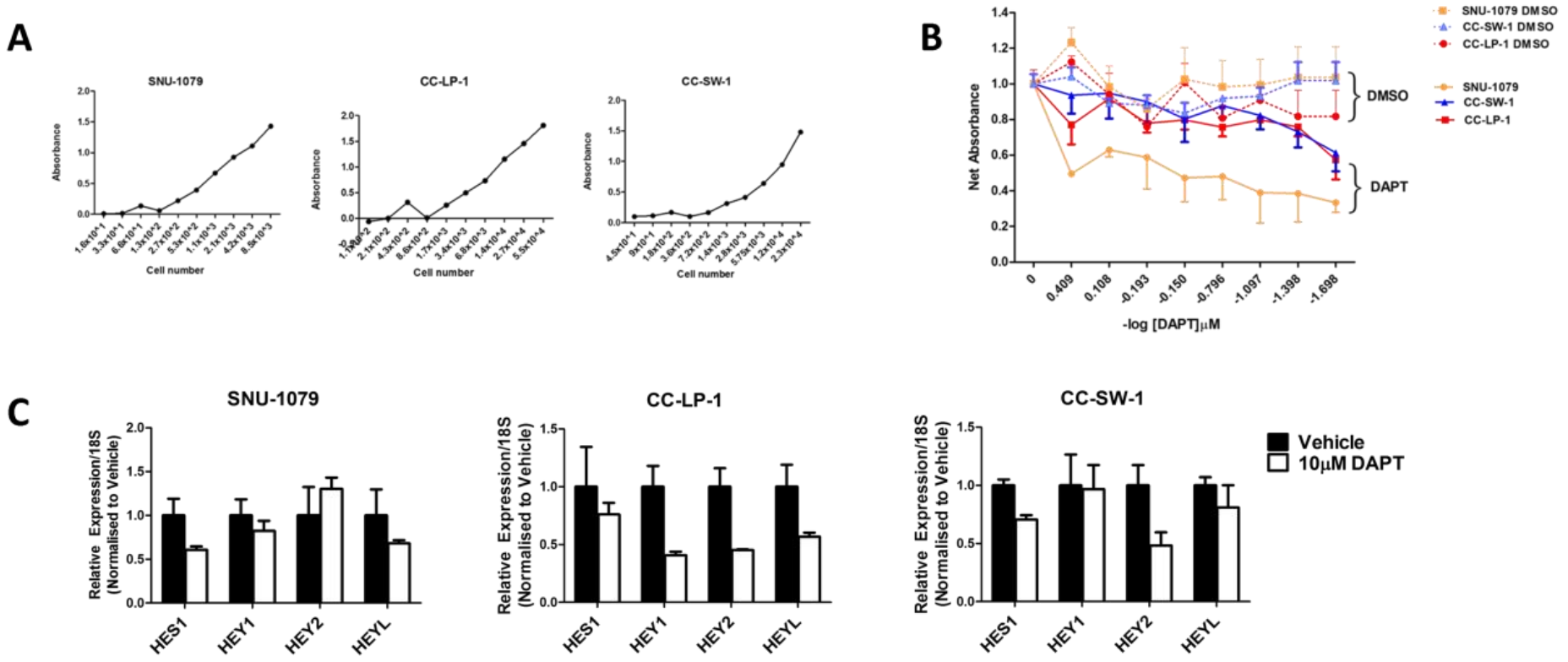

Figure 6.17 *The γ-secretase inhibitor DAPT reduces cell viability* in vitro (**A**) Determination of cell number for use in the MTT viability assay (using an absorbance of 1.0). (**B**) Concentration dependent reduction in cell viability in response to culture in 0 to 50μM DAPT. Data are represented as means ±S.E.M from 3 independent experiments. At 50μM DAPT cell viability was reduced in SNU-1079 by 66.6% (1.04 ±0.14 in control group; 0.33 ±0.04 in DAPT group), CC-SW-1 by 38.6% (1.02 ±0.08 in control group; 0.61 ± 0.08 in DAPT group) and CC-LP-1 by 42.6% (0.82 ±0.12 in control group; 0.57 ±0.09 in DAPT group). (**C**) rt-qPCR analysis of Hes/Hey gene transcription in ICC cells treated with 10μM DAPT. A non-significant trend to reduction was observed in transcription of Hes1, Hey1 and HeyL in SNU-1079 (Hes1 39.12% p=0.1; Hey1 17.62% p=0.4; HeyL 31.99% p=0.4); Hey1, Hey2 and HeyL in CC-LP-1 (Hey1 59.14% p=0.1; Hey2 54.74% p=0.1; HeyL 43.20% p=0.1) and Hes1 and Hey2 in CC-SW-1 (29.28% p=0.1; Hey2 51.66% p=0.1).

Tumour sphere culture is recognised to offer a more realistic representation of the 3-dimensional growth and organisation of *in vivo* tumours compared to traditional monolayer culture of cancer cell lines (235). The cell line CC-LP-1 was cultured on low adhesion plates in the presence of the same supplemented media used for culture in monolayer (see materials & methods). Tumour spheres were observed to form after 6 hours of culture and could be maintained and passaged (following cell dissociation) indefinitely. I found that the addition of the γ-secretase inhibitor DAPT to the culture media at the time of plating resulted in a significant reduction in the number of spheres (≥50μm diameter) formed after 48 hours of culture compared with DMSO control (Figure 6.18).

Figure 6.18 The γ-secretase inhibitor DAPT reduces* in vitro *tumour sphere formation.

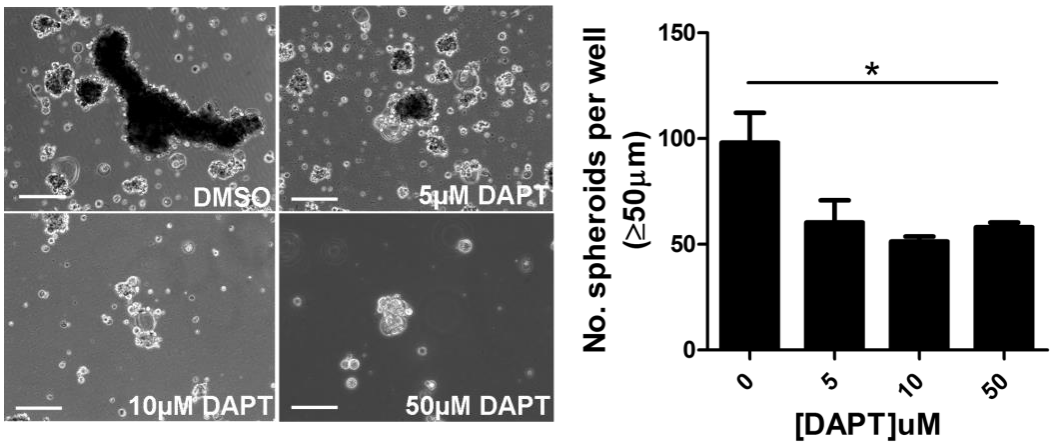

Figure 6.18 *The γ-secretase inhibitor DAPT reduces* in vitro *tumour sphere formation.* The addition of DAPT reduced the formation of tumour spheres after 48 hours of culture by 47.6% at 10μM DAPT (98 ±12 spheres/well with DMSO; 51 ±2 spheres/well with 10μM DAPT; one way ANOVA p=0.0238). Data are represented as means ±S.E.M. A significant difference between groups was demonstrated with the one-way analysis of variance test (n=3; p=0.0238). Scalebars represent 10μm.

DAPT enhances chemosensitivity of ICC cells *in vitro*

To examine whether Notch inhibition sensitises ICC cells to the cytotoxic effects of chemotherapeutic drugs, I cultured the 3 ICC cell lines in the presence of increasing concentrations of one of three chemotherapeutic agents: 5-fluorouracil, gemcitabine or cisplatin, either alone or in combination with 50μM DAPT. Cell viability was assessed after 72 hours of culture using MTT (Figure 6.19). I normalised data to the mean absorbance of no drug control wells and performed non-linear regression analyses on dose response curves of chemotherapy and chemotherapy in combination with DAPT. I then compared the differences in IC_{50} values using the Mann-Whitney U test. I observed a significant reduction in IC_{50} between 5-FU and 5-FU in combination with DAPT in the ICC cell line SNU-1079 (i.e. a chemosensitisation) (IC_{50} 5-FU alone 101.9μM ±31.3; IC_{50} 5-FU + DAPT 15.6μM ±1.5) (p=0.012). SNU-1079 also exhibited a trend to reduction in IC_{50} in response to the addition of DAPT with cisplatin but this was non-significant (IC_{50} Cisplatin alone 6.94μM ±4.98; IC_{50} Cisplatin + DAPT 0.67 ±0.52) (p=0.114), as did the cell line CC-SW-1 (IC_{50} Cisplatin alone 1.96μM ±0.54; IC_{50} Cisplatin + DAPT 0.32μM ±0.11) (p=0.10) (Figure 6.18). No chemosensitisation to gemcitabine was exhibited by any cell line in response to DAPT.

Figure 6.19 The γ-secretase inhibitor DAPT sensitises the ICC cell line SNU-1079 to treatment with 5-Fluorouracil.

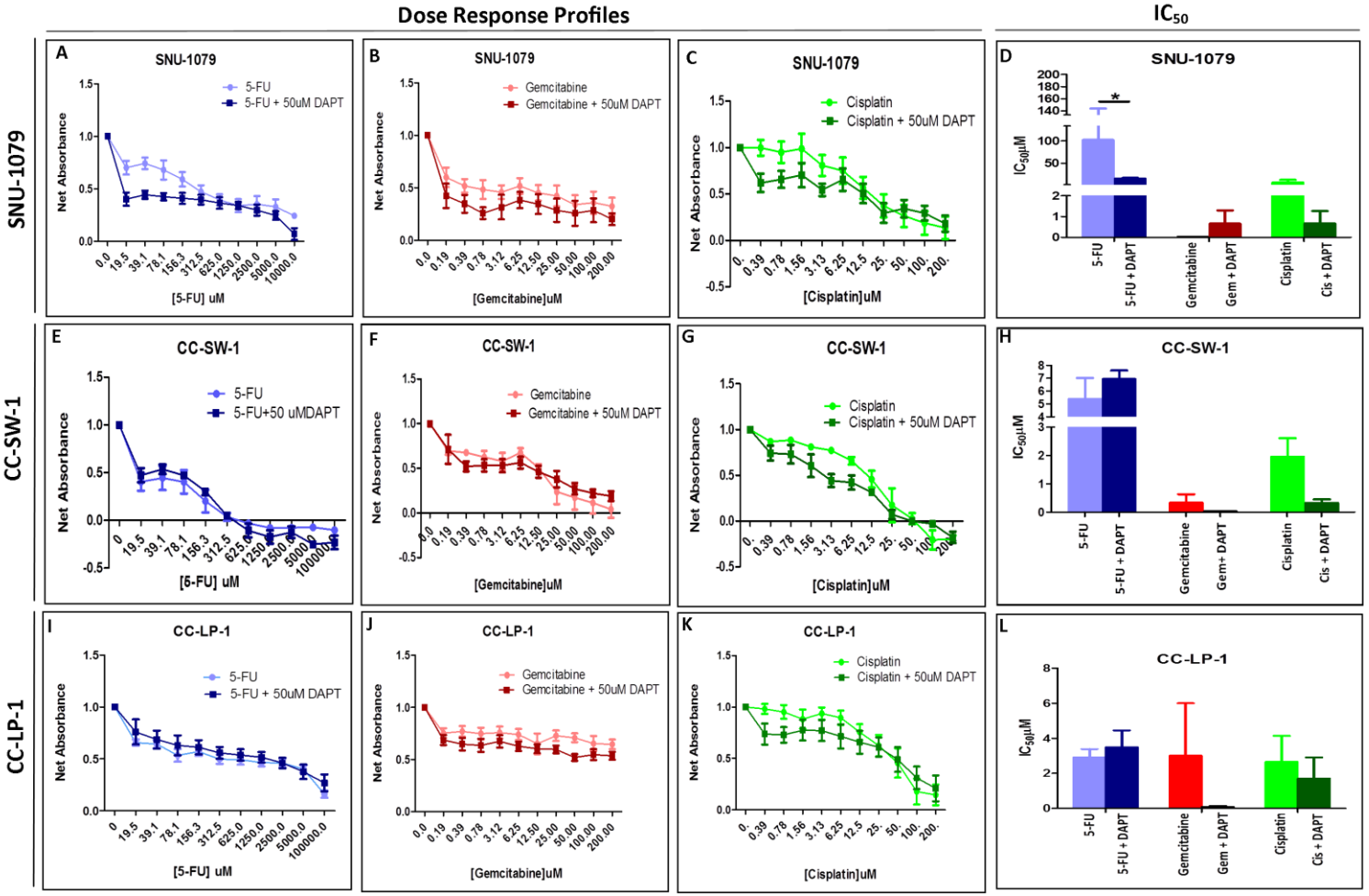

Figure 6.19 *The γ-secretase inhibitor DAPT sensitises the ICC cell line SNU-1079 to treatment with 5-Fluorouracil.* The ICC line SNU-1079 exhibited a significant reduction in IC_{50} in response to DAPT treatment in combination with 5-FU (IC_{50} 5-FU 101.9μM ±31.3; IC_{50} 5-FU + DAPT 15.6μM ±1.5 (p=0.012). SNU-1079 also exhibited a non-significant trend to reduction in IC_{50} (i.e. a chemosensitisation) in response to the addition of DAPT with cisplatin (IC_{50} Cisplatin alone 6.94μM ±4.98; IC_{50} Cisplatin + DAPT 0.67 ±0.52) (p=0.114), as did the cell line CC-SW-1 (IC_{50} Cisplatin alone 1.96μM ±0.54; IC_{50} Cisplatin + DAPT 0.32μM ±0.11) (p=0.10) (Figure 6.16). No chemosensitisation to gemcitabine was exhibited by any ICC line in response to Notch inhibition with DAPT. IC_{50}s are represented as means ±S.E.M.

DAPT reduces tumour growth in a xenograft model of ICC

To determine whether γ-secretase inhibitors have potential to restrict the progression of ICC *in vivo*, I established a xenograft model in which CC-LP-1 cells (were subcutaneously injected bilaterally into the flanks of immunocompromised mice and tumours allowed to engraft over a 28 day period. At 28 days all mice had palpable tumours bilaterally. Animals were then treated systemically with 40mg/kg DAPT i.p. or olive oil vehicle control 3 times a week for 3 weeks (Figure 6.20 (A)). Tumour mass was reduced by 47.7% in response to DAPT treatment (mean mass 115.96 ±10.6 mg vehicle group; 60.7 ±8.5 mg DAPT group), and tumour volume by 72.0% (mean volume 230.7±40.3 mm^3 vehicle group; 64.6 ±15.6 mm^3 DAPT group) (Figure 6.20 (B-C)). This reduction was associated with a non- significant trend to reduction in expression of the Notch target genes HES1, HEY1 and HEYL (fold change HES1 0.60 ±0.18 p=0.29; HEY1 0.87 ±0.22 p=0.56; HEYL 0.70 ±0.24 p=0.29) as well as genes involved in regulation of cell cycle; CYCLIN D1, CYCLIN D2 and CYCLIN E (fold change CYCLIN D1 0.66 ±0.25 p=0.41; CYCLIN D2 0.46 ±0.12 p=0.19; CYCLIN E 0.64 ±0.20 p=0.56) (Figure 6.20(D-E)).

Figure 6.20 The γ-secretase inhibitor DAPT reduces tumour growth in a xenograft model of ICC.

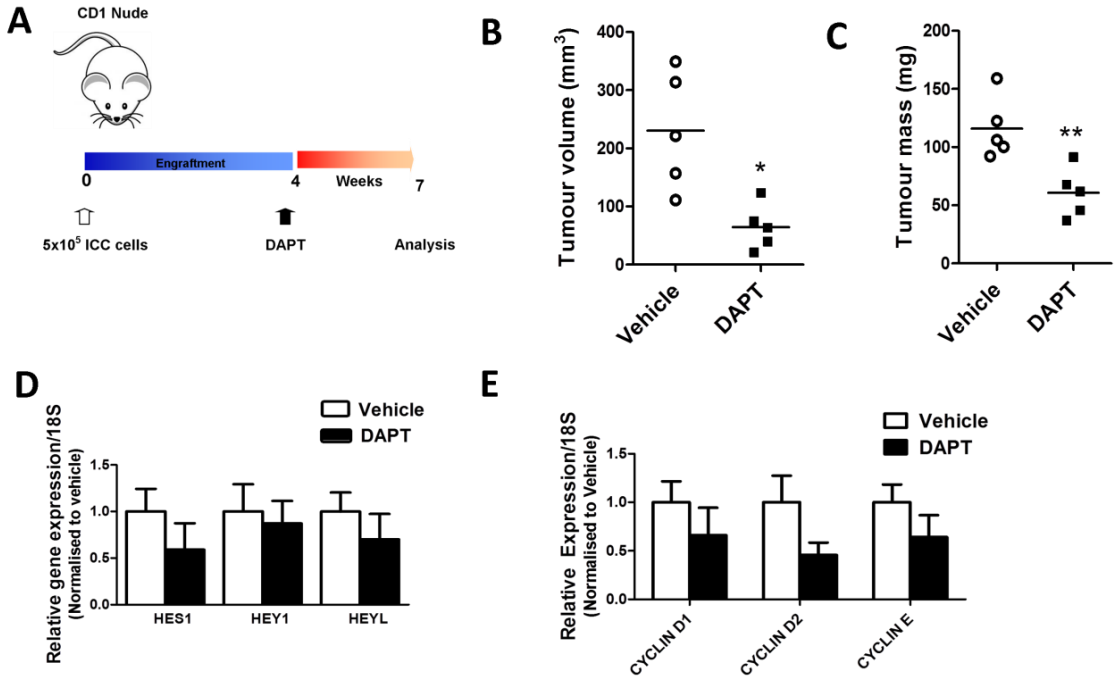

Figure 6.20 *The γ-secretase inhibitor DAPT reduces tumour growth in a xenograft model of ICC.* (A) Experimental schematic of xenograft model and treatment regime with DAPT. (B) Tumour mass is reduced by 47.7% in response to 40mg/kg DAPT (mean mass 115.96 ±10.6 mg vehicle group; 60.7 ±8.5 mg DAPT group). (C) Tumour volume is reduced by 72.0% in response to DAPT (mean volume 230.7±40.3 mm^3 vehicle group; 64.6 ±15.6 mm^3 DAPT group). (D) A non-significant trend to reduction in expression of Notch target genes HES1, HEY1 and HEYL was observed in response to DAPT. (E) A non-significant trend to reduction in expression of the cell cycle regulators CYCLIN D1, CYCLIN D2 and CYCLIN E was observed in response to DAPT treatment (fold change CYCLIN D1 0.66 ±0.25 p=0.41; CYCLIN D2 0.46 ±0.12 p=0.19; CYCLIN E 0.64 ±0.20 p=0.56). In both groups n=5 and all data were analysed using the Mann-Whitney U test. Data are represented as means ±S.E.M; *p≤0.05; **p≤0.01.

To determine whether this observed effect was a direct result on epithelial cell proliferation or rather secondary to an inhibition in neoangiogenesis, I performed immunohistochemistry for the endothelial marker $CD31^+$ on frozen sections from DAPT and vehicle treated xenografts. The ratio of mean rodamine to dapi pixels was quantified for the total area of each xenograft section using Adobe Photoshop. The mean ratio of rodamine to dapi pixels in DAPT treated tumours was 0.047 ±0.023 compared to 0.109 ±0.088 in vehicle treated i.e. there was no significant difference between the groups.

Figure 6.21 DAPT does not inhibit tumour growth through a reduction in neoangiogenesis.

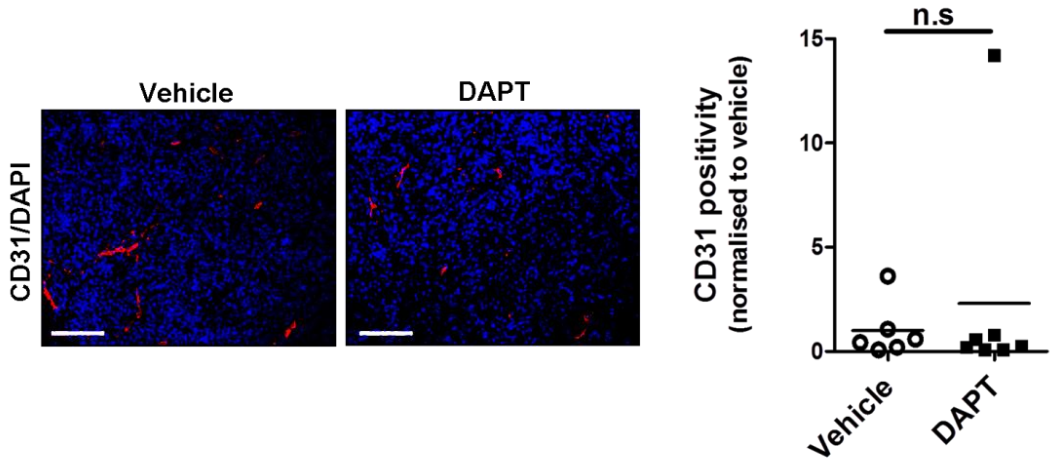

Figure 6.21 *DAPT does not inhibit tumour growth through a reduction in neoangiogenesis.* Representative immunofluorescent staining and quantification with pixel analysis showing no difference in expression of the endothelial marker $CD31^+$ in human ICC xenografts treated with 40mg/kg DAPT or olive oil control. The mean ratio of rodamine ($CD31^+$) to dapi pixels in DAPT treated tumours was 0.047 ±0.023 compared to 0.109 ±0.088 in vehicle treated. Data are represented as means ±S.E.M normalised to vehicle and the difference between groups was analysed using the Mann-Whitney U test.

DAPT reduces tumour growth in a chemically induced model of ICC in rat

To investigate how γ-secretase inhibition might affect *in situ* tumour growth in an *in vivo* model of ICC, I used the TAA model in rat. Sprague-Dawley rats were administered 0.06% TAA for a 26 week period with 10mg/kg DAPT (n=8) or olive oil control (n=10) i.p. 3 times a week between weeks 21 and 26. Tumours are reproducibly observed in 100% of animals by 20 weeks of TAA administration and therefore this experiment aimed to establish whether inhibition of the Notch pathway using γ-secretase inhibition would restrict the progression of an already

established tumour. Sera were taken from rats at the time of sacrifice to determine whether TAA induced injury was equivalent between the two groups (Figure 6.22).

Figure 6.22 *Serum biochemical markers of liver function are equivalent in rats treated with TAA and DAPT vs. TAA and vehicle.*

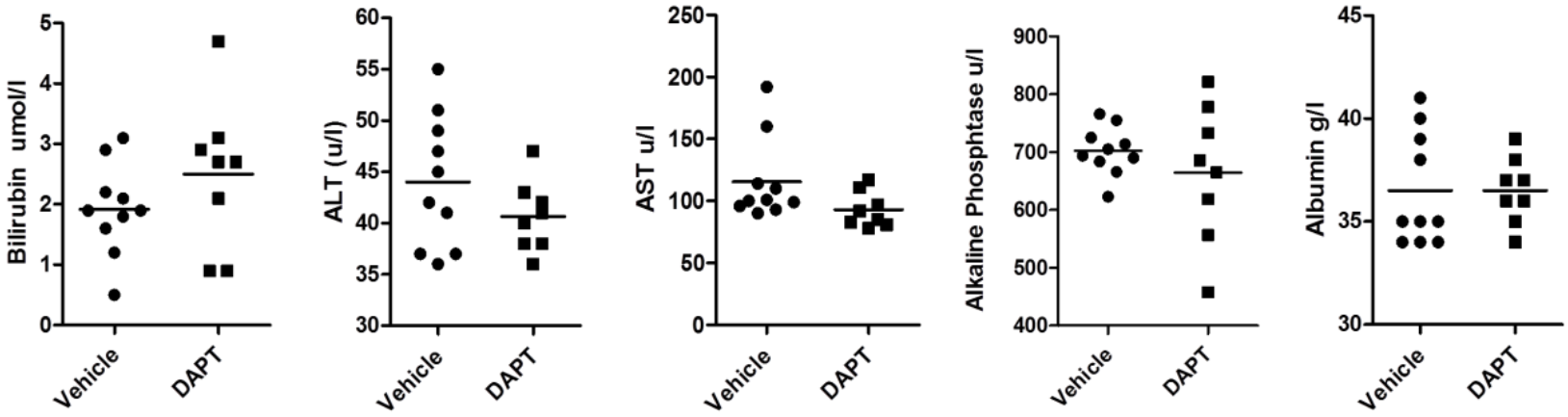

Figure 6.22 *Serum biochemical markers of liver function are equivalent in rats treated with TAA and DAPT vs. TAA and vehicle.* There is no difference in biochemical liver function tests between rats treated with TAA and DAPT and rats treated with TAA and vehicle. Data are represented as means ±S.E.M and analysed using the Mann-Whitney U test.

Figure 6.23 The γ-secretase inhibitor DAPT significantly reduces tumour growth in a TAA model of ICC.

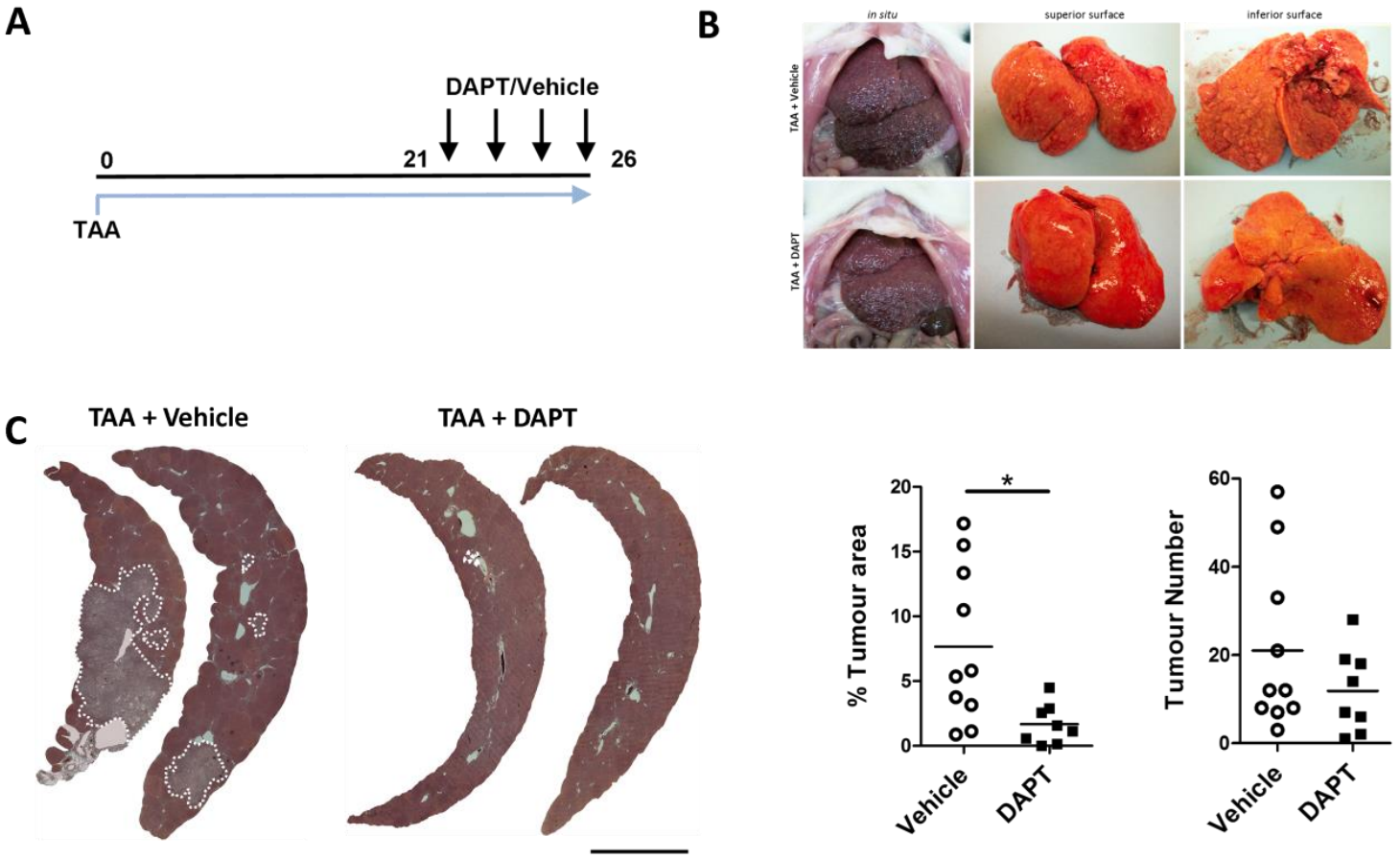

Figure 6.23 *The γ-secretase inhibitor DAPT significantly reduces tumour growth in a TAA model of ICC.* (A) 10mg/kg DAPT or vehicle was administered to rats undergoing 26 weeks of injury with 0.06% TAA (n=10 Vehicle group; n=8 DAPT group). (B) Representative photographs of rat livers from animals treated with TAA and Vehicle and animals treated with TAA and DAPT. (C) Tiled low-power photomicrographs of representative sections of livers from rats treated with TAA + vehicle or TAA + DAPT. Dashed white line represents tumour boundary. Scalebar represents 10mm. (D) There is a 78.2% reduction in % tumour area in response to treatment with DAPT p=0.0148 (mean % tumour area in TAA + Vehicle group 7.66% ±1.8; TAA + DAPT group 1.67% ±0.5). There is a no difference in the mean number of tumours per liver in response to treatment with DAPT (21 ±6 in TAA + Vehicle group; 12 ±3 in TAA + DAPT group). Data are represented as means ±S.E.M and passed the D'Agostino & Pearson omnibus test of normality of distribution. Differences between means were analysed using a two-tailed t test.

Discussion

During the course of this study two publications have described the capacity of transgenically activated Notch1 to induce development of biliary tumours in albumin-expressing cells (92, 230). In this thesis I aimed to characterise the activity of endogenous wild type Notch in ICC in human disease and rodent models in which Notch has not been genetically altered. These data demonstrate that in human disease, a chemically-induced model in rat and a transgenic murine model, the Notch pathway is indeed up-regulated in ICC. In particular I have observed specifically that transcription of the Notch3 receptor is induced most strongly in all three species and have demonstrated functionality through this receptor as evidenced by western blotting for its intracellular domain (Figure 6.8) and nuclear positivity within malignant epithelia with immunohistochemistry (Figure 6.7). Whilst Notch1 is very lowly expressed in the healthy adult liver, strong Notch3 positivity is consistently observed on the vascular smooth muscle, making the magnitude of the observed up-regulation of Notch3 transcription in cancer more remarkable. Immunostaining for Notch1 reveals weak positivity when compared with isotype control, but little difference in expression between healthy liver and cancer (Figure 6.6).

The TAA model of ICC in rat has enabled me to observe Notch activity during disease progression from healthy liver to inflammation, fibrosis and finally malignancy and I see that up-regulation of pathway transcription is a late event; occurring after initiation, during the process of tumour expansion. In both human disease and rodent models, Jagged1 ligand appears to be provided by the surrounding desmoplastic stroma with little epithelial expression; whereas Notch3 is observed both on myofibroblasts and malignant ductules (Figure 6.7). Further analyses using laser-capture microdissection of the epithelial and stromal compartments of tumours would be informative to confirm with a second technique that Jagged expression is confined to the desmoplastic stroma compared to Notch3 which appears to be up-regulated by both cancerous epithelia and myofibroblasts.

Quantification of stromal reaction in these animals would also clarify whether activity through this axis correlates to myofibroblast intensity.

The CK19YFPp53 + TAA murine model has enabled me to examine the differences in Notch expression between cancer and chronically injured liver. Up-regulation of Notch1 and more strikingly Notch3 occurs in CK19YFPp53$^{flox/flox}$ mice with and without ICC formation, with levels higher in animals with tumours (Figure 6.13). This finding is in contrast to reports in the literature where Notch2 is described as the dominant paralog in driving biliary differentiation of hepatoblasts during development and HPCs during biliary regeneration in the adult (135, 169). Furthermore there does appear to be activity through the canonical Notch pathway in this model, as a significant increase in transcription of the target effector *Hey2* is also observed in mice with ICC.

Activity through the Notch signalling pathway is dependent on the generation of N-ICD; that is cleavage of the intracellular fragment of the receptor to translocate to the nucleus and drive transcription. This cleavage event and hence pathway functionality is mediated by the protease complex γ-secretase: introduction of a single point mutation into Notch1 at the γ-secretase cleavage site leads to total loss of Notch signal and embryonic lethality (236). Due to the role of γ-secretase in the generation of Aβ peptide associated with Alzheimer's disease, a number of pharmacological agents have been developed that inhibit this interaction, blocking activity via all four receptors (237). Despite little success in clinical trials for Alzheimer's disease, many of these compounds have been tested for their anti-tumour efficacy; for example dibenzazepine (DBZ) has been shown to reduce epithelial proliferation and induce goblet cell transdifferentiation in the Apc(min) model of intestinal tumorigenesis (238). In the above experiments I aimed to establish whether pharmacological inhibition of γ-secretase with DAPT would reduce tumour cell growth of ICC *in vitro* and *in vivo*.

The anatomical complexity of resected BTC in man and vital importance of establishing the presence or absence of tumour at resection margins means that ICC specimens must be intact at the time of post-operative pathological examination. Furthermore at the time of pathological staging the clinical specimen is fixed in formalin and these issues have made it difficult to obtain fresh tissue for primary cell culture of human ICC in our department. It has therefore been necessary to use ICC cell lines in this work and I have selected three that have been derived from typical examples of moderately differentiated biliary adenocarcinoma with published characterisation of their cytogenetic and mutational profiles (239, 240). All three lines exhibited modest but dose-dependent reductions in viability in response to DAPT treatment (Figure 6.16). The non-significant trend to reduction in Hes/Hey gene transcription observed in these cells following treatment with a high dose (10μM) of DAPT suggests that these *in vitro* cell lines are not sensitive to the effects of GSIs. Although I have demonstrated presence of the Jagged1 protein on these cells with the implication of an autonomous signalling loop, it is possible that in the absence of an excess of ligand, these cells may not respond maximally to these agents. I therefore went on to test the effects of GSIs *in vivo*, where provision of ligand from surrounding stromal cells would be more abundant. Variation in the responsiveness of ICC lines to DAPT may also conceivably due to differences in gamma secretase activity at the membrane. Assays developed to quantitate this have so far principally relied on N-ICD generation, making it challenging to discriminate between gamma-secretase activity and Notch responsiveness.

My results similarly suggest that Notch inhibition reduces the sphere forming capacity of ICC cells. These data should be interpreted with caution however. Very few studies have been previously undertaken using tumour sphere culture as a model of cell behaviour in ICC, and hence little is known about the markers that define the sphere-forming population and how these might relate to self-renewal capacity. Furthermore the potential to form spheres is frequently used as a marker of a chemoresistant population in many cancer types and this hypothesis has not

been tested in ICC. Ideally it would be informative to perform an unbiased gene expression analysis on the sphere forming population of these cells to determine whether they represent a subpopulation enriched for markers of stemness or chemoresistance as a response to cell adhesion, along with experiments to test tumorigenicity *in vivo.* It must be considered that despite performing experiments at a low passage number, these cells do represent an immortalised cell line and are not primary cells newly derived from a patient.

In light of these sphere data, I decided to evaluate the potential for the γ-secretase inhibitor DAPT to sensitise ICC cells to chemotherapeutic agents *in vitro.* A significant *c*hemosensitisation to 5-FU was observed in response to treatment with DAPT by the ICC line SNU-1079, although this was not replicated across the other lines or with other chemotherapies (a non-significant trend to sensitisation was exhibited by all three lines to cisplatin). All three cell lines tested were relatively chemoresistant; requiring micromolar (and in the case of 5-FU millimolar) concentrations for maximal response.

These *in vitro* data were used however to inform subsequent *in vivo* experiments as discussed above. In comparison to orthotopic cell transplantation, xenograft models of cancer are limited by differences in the subcutaneous microenvironment, an altered immune response to tumorigenesis (due to the immunocompromised host), and differences arising due to species mismatch (232). They do however offer advantages over other models; in particular a rapid and effective platform for testing therapeutic response to drugs (genetically engineered murine models of cancer frequently have long tumour latencies). In response to systemic treatment with DAPT a significant reduction in the mass and volume of xenografted ICC was observed.

Gamma secretase is a high molecular weight multiprotein complex which cleaves not only Notch, but a number of other proteins including E-cadherin, $CD44^{+}$ and erbB-4 which are known modulators of new blood vessel formation (241). This is

likely to explain the non-significant reduction in Hes/Hey expression in DAPT-treated xenografts and it is likely that GSIs are reducing tumour size through blockade of other signalling pathways in addition to Notch. Mice lacking components of the γ-secretase complex including presenilin1 exhibit abnormal blood vessel development (242). I therefore sought to determine whether the observed reduction in tumour growth was a direct consequence of a change in cancer cell proliferation, apoptosis or death, or secondary to an inhibition of neoangiogenesis: no difference in $CD31^+$ positivity was observed between the two groups.

These xenograft experiments provided evidence that a longer, more expensive protocol to investigate the anti-tumour potential of GSIs to inhibit the development of ICC in the TAA rat model was worthwhile. A striking difference was seen in the macroscopic appearance of livers in rats following treatment with TAA and DAPT compared to rats treated with TAA and vehicle (Figure 6.22). Given the known role of Notch in progenitor mediated biliary regeneration after chronic injury, it would be anticipated that the observed reduction in macroscopic nodules is due to an attenuation of the regenerating parenchyma in addition to inhibition of tumour growth. This said, I observed no difference in serum biochemical markers of liver function, although these have poor correlation with tumour stage and therefore are difficult to interpret in this context. The observed 78% reduction in % tumour area in response to DAPT treatment suggests that γ-secretase inhibitors might offer a potential therapeutic role in the treatment of advanced ICC. No difference was observed in the number of tumours per liver, suggesting that Notch signalling plays a more prominent role in the promotion of tumour expansion and progression rather than its initiating molecular events.

It is important to recognise that despite the similarities in histological appearance and backgrounds of chronic liver disease, it is as yet uncertain as to whether the genetic alterations of TAA-induced ICC in the rat are truly representative of human disease. I have however demonstrated that the observed changes in Notch

signalling in this model do closely mimic those seen in human tumours. Further work is necessary to elucidate the mechanism of Notch up-regulation in ICC.

Since the commencement of this work, two publications have described anti-tumoural effects of GSIs in similar *in vitro* systems and human xenograft models of ICC (230, 243). These add further weight to the observations made here. Notch is however only one of a number of substrates for the γ-secretase complex which include amyloid precursor protein, $CD44^{+}$, E-cadherin and N-cadherin (244). This may contribute to the significant side effects that have been reported with these inhibitors (245). In particular cytotoxicity in the intestinal tract and transdifferentiation of enterocytes to a secretory, goblet cell phenotype secondary to loss of crypt-derived Notch, has led to scepticism about their clinical application (246). Despite this, combination of GSIs with glucocorticoids in T cell acute lymphoblastic leukaemia has not only reduced gut toxicity but also improved anti-tumoral efficacy (247). Phase I clinical trials in many other cancer types have now reported (248-251) and phase II studies are now well underway in tumours including melanoma, glioblastoma, non-small cell lung cancer, renal cell carcinoma and ovarian cancer (http://www.cancer.gov/clinicaltrials/search/results?protocolsearchid=8608408). In light of the lack of available therapeutic agents offering superior specificity profiles to GSIs, at the current time it is likely that this strategy holds the most translational potential for anti-Notch therapies in ICC.

The next key step in evaluating the utility of GSIs for down-staging ICC to increase the proportion of patients with surgically resectable disease will be to evaluate their *in vivo* efficacy both as a single agent in reducing tumour size, but also in sensitising tumours to existing chemotherapies. The $CK19CreYFPp53^{f/f}$ +TAA model in mouse and TAA model in rat would be ideal platforms for these pre-clinical studies. If the Notch positive population of cells within the tumour do represent a more naïve, stem-like phenotype, it may be that treating tumours with GSIs might eliminate this more chemoresistant population, thus sensitising tumours to conventional

therapies. Currently the mechanism or mechanisms through which Notch might drive chemoresistance (e.g. enhance drug efflux, defective apoptotic pathways, increased ability for DNA repair) are unknown and in fact given the mixed response of these three human ICC cell lines to GSI treatment, these *in vivo* animal studies are vital to establish whether GSIs can indeed chemosensitise tumours growing *in situ.*

Chapter 7: Investigating Notch3 as a non-redundant driver of ICC

Introduction

Given the up-regulation of Notch3 observed across three species in ICC (human, rat, mouse) using different modalities of cancer induction, I next sought to investigate whether Notch3 might represent a non-redundant driver of tumorigenesis.

Notch3 exhibits a number of structural differences to Notch1 and 2 in all three of its domains. In the extracellular region, Notch3 lacks EGF-like repeat 21 as well as a region corresponding to part of EGF-like repeats 2 and 3 in Notch1 and 2 (100) . Both the transmembrane domain (TMD) and RBPJκ-associated domain (RAM) have a much lower amino acid identity to Notch1 than that between Notch1 and 2 (99, 252). Most significantly Notch3 displays a significantly shorter region within the transactivation domain (TAD), which has been hypothesised to explain the weaker transactivational activity exhibited by N3-ICD compared to N1-ICD or N2-ICD (99).

The tissue distribution of Notch3 is more restricted than that of Notch1 or 2; expression being strong in arterial smooth muscle, the CNS, thymocytes and T-regulatory cells (100, 253-255). Arguably for this reason Notch3 null mutant mice are embryologically viable (unlike Notch1 knock outs), but do display structural arterial defects and altered arterial myogenic responses (256, 257). Interestingly embryos carrying double homozygous target mutations for both *Notch1* and *Notch3* exhibit defects ordinarily observed in *Notch1*-deficient embryos, but no synergistic effects compared to *Notch1* only mutants suggesting *Notch3* does not have a redundant function with *Notch1* during embryogenesis (257).

Spontaneous activating mutations of Notch3 results in CADASIL (cerebral autosomal dominant arteriopathy with subcortical infarcts and leukoencephalopathy); a late onset clinical syndrome of stroke and dementia characterised by recurrent subcortical ischaemic events (258). Here mutation results in an odd number of cysteine residues within the Notch3-ECD and accumulation of

ECD at the cell membrane leading to a lack of cerebrovascular reactivity (259, 260). Targeted transgenic overexpression of Notch3 in the developing lung results in a disruption of morphology with failure of type II pneumocyte differentiation and maturation (261).

Notch3 has been studied as a non-redundant driver of tumorigenesis in other cancer types. Overexpression of Notch3 has been observed in colorectal (262), ovarian (263, 264), cervical cancer (265), acute T-cell lymphoblastic leukaemia(266) and NSCLC (184) and mice carrying a thymocyte-specific activation of Notch3 exhibit increased number of thymocytes, particularly late CD4-CD8- cells and develop an aggressive multicentric T cell lymphoma (181). Suppression of cancer cell growth in response to γ-secretase inhibition and specific Notch3 blockade have both been described in NSCLC, and indeed in the lung cancer cell line HCC2429 (which expresses both the Notch1 and Notch3 receptors), deletion of Notch3 by siRNA abrogates the response to GSI treatment, suggesting that Notch3 but not Notch1 contributes to tumorigenesis (184, 267). More recently data also suggest Notch3 may play a particular role in cancer stem cell self-renewal (CSCs). Specific Notch3 inhibition with shRNA results in a decrease of aldehyde dehydrogenase positive lung CSCs (268) and NSCLC cell populations enriched for the three markers $CD24^{+}$, ITGB4 and Notch3 appear to represent a rare population capable of serial transplantation and resistance to chemotherapy (191). Furthermore enforced expression of N3-ICD in the T cell lineage is a potent inducer of T-cell lymphoma (181).

Notch3 drives cell survival and clonogenicity

To determine whether a unique role exists for Notch3 in driving cell survival in ICC, I took advantage of a spread of Notch3 positivity I had observed on flow cytometric analysis of the human ICC line CC-LP-1. Approximately 5% of the total cell population analysed stain positively for Notch3 compared to isotype control and therefore cells were gated at the upper and lower 5% limits of positivity and FACS sorted to establish whether these populations exhibited differences in phenotype or behaviour. Notch3 high, low and total CC-LP-1 populations were compared (Figure 7.2A). Although I observed no difference in cell cycle between the three populations after analysis with DAPT at the time of sorting (Figure 7.2B), after 48 hours in culture Notch3 high cells exhibited a mean absorbance 2.7 times greater than Notch3 low cells by MTT (Notch3 high population 1.00 ±0.01; Notch3 low population 0.37 ±0.01 $p=0.002$; $n=3$), and after 3 weeks in culture, a 57.1% increase in colony forming efficiency; although this did not reach significance (Notch3 high population mean colony forming efficiency 30.00% ±0.94; Notch3 low population 9.33% ±1.44 $n=3$; $p=0.10$) (Figure 7.2C-D).

Figure 7.2 Notch3 expressing ICC cells exhibit greater viability and clonogenicity.

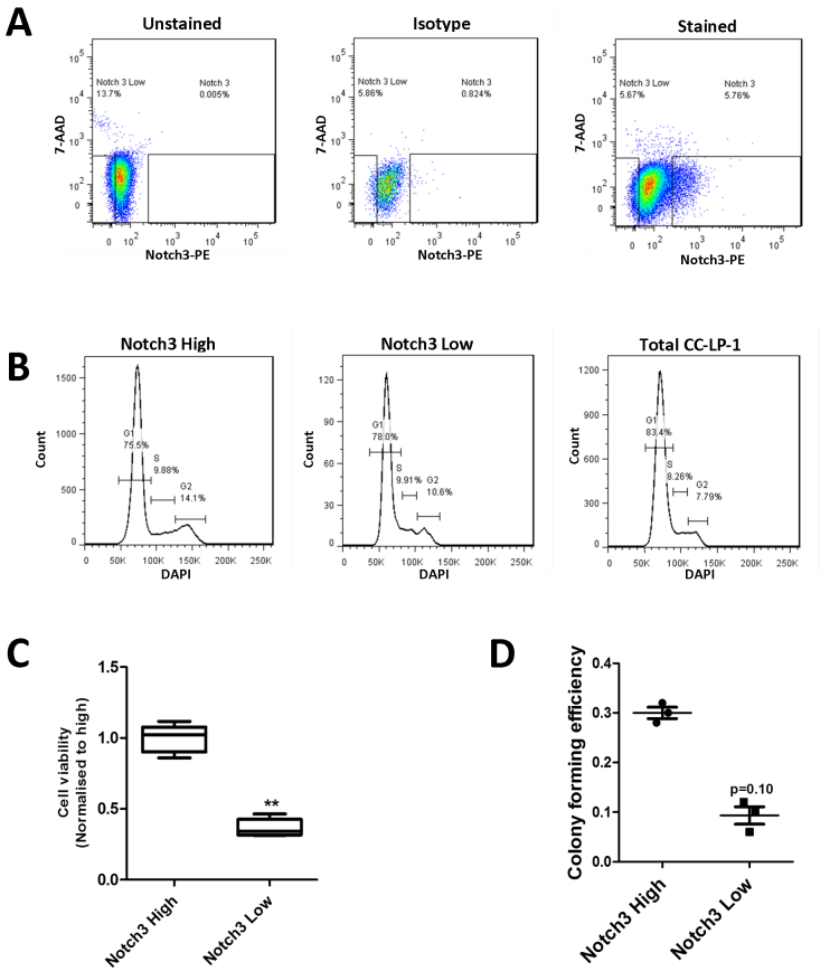

	% cells in G1	% cells in S phase	% cells in G2
Total CC-LP-1	75.50	9.88	14.10
Notch3 high	78.00	9.91	10.60
Notch3 low	83.40	8.26	7.76

Figure 7.2 *Notch3 expressing ICC cells exhibit greater viability and clonogenicity.* (A) The ICC line CC-LP-1 was stained for Notch3 or isotype control and analysed with flow cytometry. (B) No difference in cell cycle was observed between Notch3 high, low or total CC-LP-1 populations. (C) The Notch3 high population exhibited 63.45% greater viability than the low population following 48 hours in culture (MTT) ($p=0.0022$) ($n=3$). (D) The Notch3 high population exhibited a 68.89% better efficiency for forming colonies when plated at clonal density compared to the Notch3 low population although this was not statistically significant ($p=0.1000$). Data are represented as means ±S.E.M and differences analysed using the Mann-Whitney U test. * $p\leq0.05$; ** $p\leq0.01$; *** $p\leq0.001$.

The stability of the Notch3 protein is regulated by a balance of acetylation and deacetylation at the 1692^{Lys} and 1731^{Lys}residues in the RAM domain of the protein. Acetylation at this site reduces protein stability through ubiquitination, targeting its degradation by the proteosome and reducing N3-ICD mediated transcription (182). This balance is mediated by histone acetyltransferases (HAT) and histone deacetylases (HDAC) and as a consequence Notch3 stability can be disrupted by the use of histone deacetylase inhibitors (HDACi) including an inhibitor of HDAC1, Trichostatin A (TSA). TSA induces acetylation and proteosomal degradation of Notch3 in $N3^{IC}$ transgenic mice, thus inhibiting the development and progression of T-ALL ordinarily exhibited by these animals (182). Furthermore it has been shown that this compound does not alter signalling through the Notch1, 2 or 4 receptors and therefore I selected this small molecule as a second, corroborative approach to study the effects of selective Notch3 inhibition of the malignant phenotype of ICC *in vitro*.

I first established that signalling via N3-ICD was inhibited by Trichostatin A in this system by plating the ICC cell line CC-LP-1 in the presence of 500nM TSA or vehicle for 48 hours before performing western blotting for total Notch3 and N3-ICD (Figure 7.3(A)). Signal from N3-ICD was significantly reduced following treatment even with this low dose of TSA. I then went on to plate cells in increasing concentrations of TSA (0 to 10μM) and assessed viability with MTT. I observed a dose-dependent reduction in viability in all 3 ICC lines tested (Figure 7.3(B)); strongly suggesting Notch3 may itself be an independent driver of cell survival in ICC. The shape of the dose response curve suggests however that the effects of TSA on cell survival rapidly saturated in all three cell lines above a concentration of 1μM. On this basis I went on to test the effects of TSA *in vivo* in the xenograft model of ICC. Tumours were established subcutaneously using the ICC cell line CC-LP-1 in immunocompromised mice as previously described. Mice were then treated systemically with 1mg/kg TSA or vehicle daily for 14 days. Tumour mass was reduced by 38.8% in TSA treated mice (Vehicle mean mass 138.83mg ±9.03 (n=12);

TSA mean mass 84.90 ±13.49 (n=10); p=0.004) (Figure 7.3 (C)). Tumour volume was reduced by 33.7% in TSA treated mice (Vehicle mean volume 169.56mm^3 ±15.17 (n=12); TSA mean volume 112.50mm^3 ±17.36 (n=10) p=0.0296 (Figure 7.3(D)).

***Figure 7.3 The HDAC1 inhibitor Trichostatin A (TSA) disrupts N3-ICD mediated signalling in ICC and reduces tumour growth* in vitro *and* in vivo.**

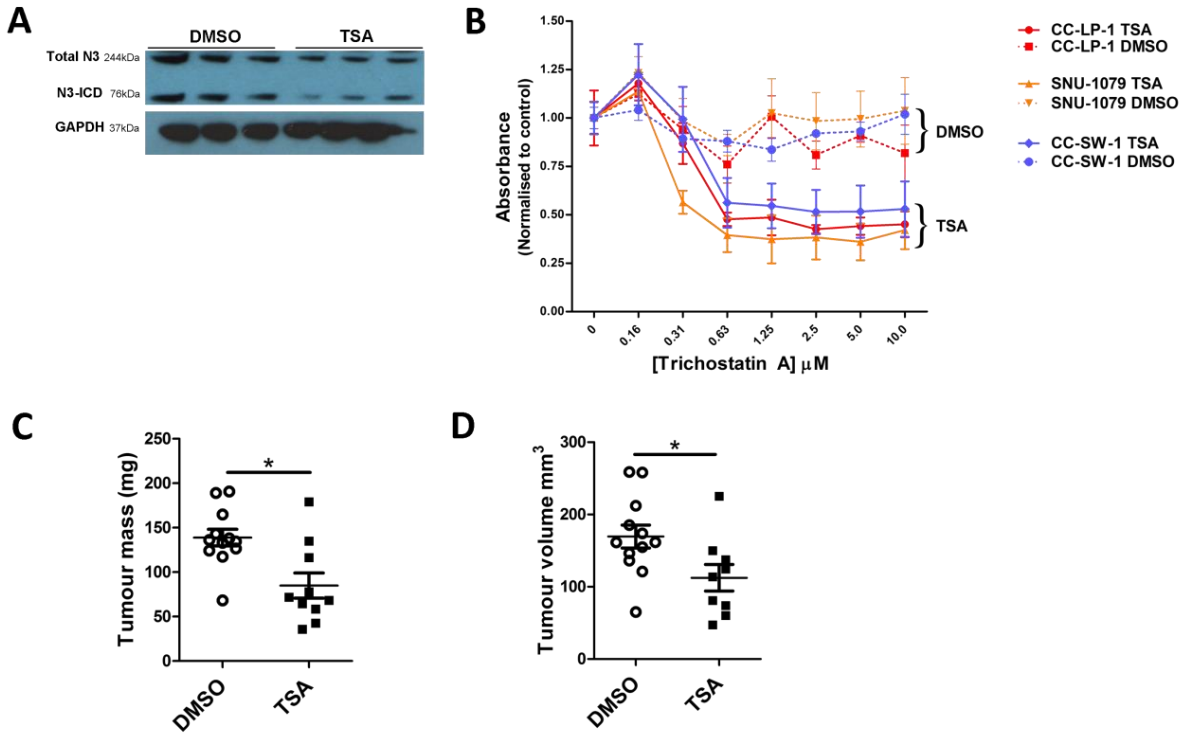

Figure 7.3 *The HDAC1 inhibitor Trichostatin A (TSA) disrupts N3-ICD mediated signalling in ICC and reduces tumour growth* in vitro *and* in vivo. (A) A reduction in expression of both total Notch3 and N3-ICD protein is observed on western blotting in the ICC line CC-LP-1 following 48 hours of treatment with 500nM TSA. GAPDH is used as a loading control. (B) A dose-dependent reduction in cell viability (MTT absorbance) is observed following 72 hours of treatment with TSA or vehicle in 3 ICC cell lines (CC-LP-1; SNU-1079; CC-SW-1). (C) A 38.8% reduction in tumour mass was observed following 14 days systemic treatment with 1mg/kg TSA (p=0.004) (Vehicle group n=12; TSA group n=9). (D) A 33.7% reduction in tumour volume was observed following 14 days systemic treatment with 1mg/kg TSA (p=0.0296) (Vehicle group n=12; TSA group n=9. Data are represented as means ±S.E.M. * p≤0.05; ** p≤0.01; ***p≤0.001.

Stable Notch3 silencing: Notch3 shRNA *in vitro* and *in vivo*

HDAC inhibitors bind a large number of substrates in addition to Notch3; in particular core histone proteins instrumental to the regulation of chromatin topology and hence gene transcription (269). I therefore sought a more targeted strategy to specifically and permanently silence Notch3 *in vitro* using shRNA. Three commercially available plasmids were obtained containing individual NOTCH3 (or scrambled control) shRNA sequences and puromycin resistance cassettes for stable selection and generation of cell lines with stable gene silencing (see Materials & Methods Figure 2.2). Briefly, *E.coli* were transformed with pDNA and colonies grown under ampicillin selection. Minipreparations were made for each shRNA sequence and plasmid DNA isolated with a yield of 0.5 to 2.5μg pDNA. To ensure purified plasmids contained the shRNA inset, a Pst1 restriction digestion was performed (Figure 7.4(A)). The ICC cell line CC-LP-1 was transfected with 0.5μg pDNA and grown under stable selection with puromycin until colonies appeared. These were picked, transferred to new culture plates for culture before rt-qPCR and western blotting performed to ensure silencing of NOTCH3 had occurred (Figure 7.4(B-C)).

Figure 7.4 Generation of a stably silenced* NOTCH3 *ICC cell line using shRNA.

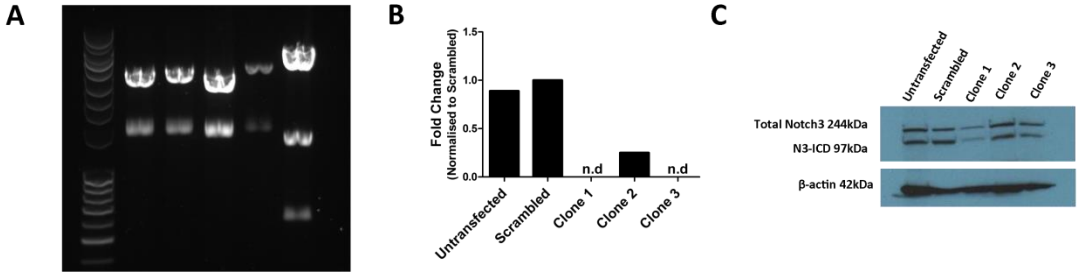

Figure 7.4 *Generation of a stably silenced* NOTCH3 *ICC cell line using shRNA.* (A) Pst-1 restriction digestion of isolated pDNA showing DNA fragments at 3209 and 1402bp. (Lane 1: 100kb ladder; Lane 2: N3_2 (Clone1); Lane 3: N3_3 (Clone2); Lane 4: N3_4 (Clone3); Lane 5: N3_OE (Note there is no uncut control on this gel)). (B) rt-PCR analysis of *NOTCH3* in CC-LP-1 clones transfected with pDNA containing NOTCH3 shRNA insert. (C) Western blot analysis of *NOTCH3* expression in CC-LP-1 clones transfected with pDNA containing NOTCH3 shRNA insert. Clone 1 was selected for use in further studies.

I firstly assessed the effect of Notch3 gene silencing on cell growth *in vitro*. Untransfected, scrambled control and N3 knock down (KD) cells were plated in standard conditions in 96 well plates and viability assessed after 48 hours. I observed a modest and non-significant reduction in viability (19.4%) was observed as measured by MTT assay (n=3; p=0.07) (Figure 7.5 (A)). In spite of this, I went on to evaluate whether silencing of Notch3 would have any effect of cell growth *in vivo* using the xenograft model of ICC. Notch3 KD or scrambled control cells were subcutaneously injected into the flanks of immunocompromised mice as previously described. Tumours were allowed to establish over 28 days at which time mice were culled and tumour mass and volume assessed. Tumours from Notch3 KD cells exhibited 76% less mass than scrambled controls (N3 KD: 138.12mg ±35.04 (n=10); Scrambled: 33.03mg ±8.23 (n=6)) and were 78% smaller in volume (N3 KD: 187.63mm^3 ±39.32; Scrambled: 40.54 ±9.83). To strengthen the likelihood that this

observed reduction was a consequence of loss of Notch activity, I performed rt-qPCR analysis for Hes/Hey Notch target gene transcription on the harvested tumours. A non-significant trend to reduction was observed in transcription of Hey1, Hey2 and HeyL (Hey1 fold change 0.936 p=0.1775; Hey2 0.869 p=0.0667; HeyL fold change 0.701 p=0.1775) and a significant reduction in Hes 4 (p=0.03) (Figure 7.5 (E)).

***Figure 7.5 Stable silencing of* NOTCH3 *with shRNA reduces tumour growth* in vivo.**

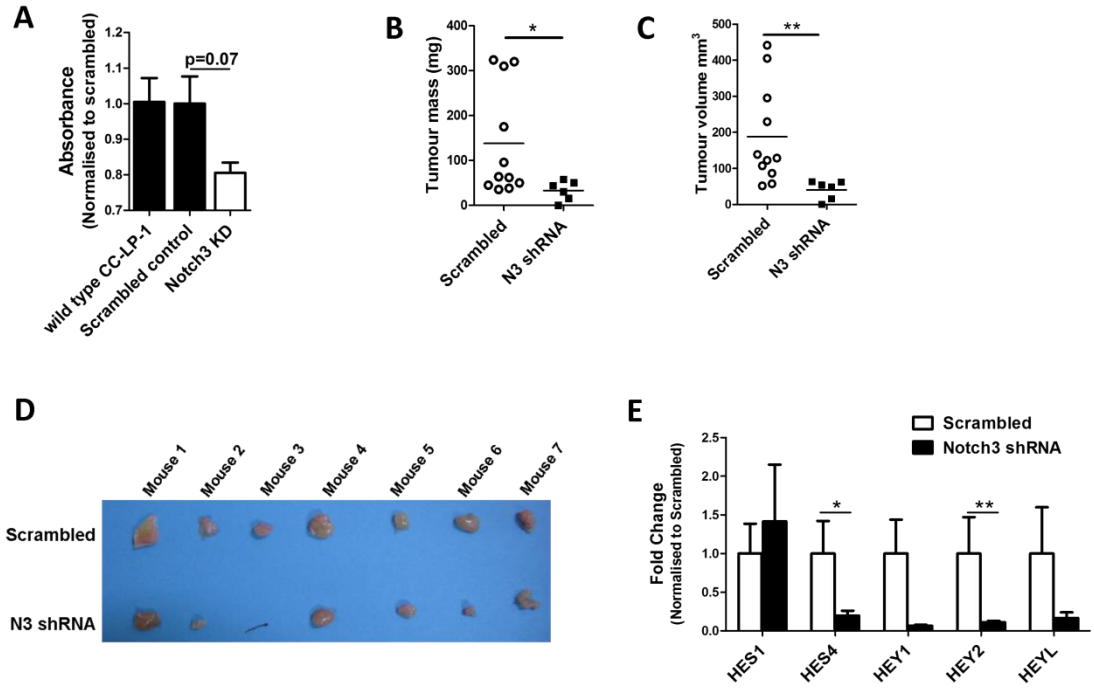

Figure 7.5 *Stable silencing of* NOTCH3 *with shRNA reduces tumour growth* in vivo. (A) A non-significant reduction in cell viability (MTT assay) was observed following re-plating and 48 hours of culture of Notch3 KD cells compared to scrambled controls (n=3; p=0.07). (B) Notch3 KD cells have significantly less tumour mass (76%; N3 KD 138.12mg ±35.04 (n=10)) compared to scrambled controls (33.03mg ±8.23 (n=6) p=0.0237). (C) Xenografted tumours from Notch3 KD cells exhibited 78% smaller volume tumours compared to scrambled control (N3 KD 187.63mm^3 ±39.32; Scrambled 40.54 ±9.83 p=0.0057). (D) Transcription of the Notch target genes Hes/Hey are significantly reduced in xenografted tumours with Notch3 KD compared to scrambled controls (Hes 1 fold change 1.42 p=0.792; Hes4 fold change 5.10 p=0.0303; Hey1 fold change 15.58 p=0.1775; Hey2 9.16 fold change p=0.0043; HeyL fold change 6.03 p=0.082). Data are represented as means ±S.E.M and differences calculated using the Mann-Whitney U test of significance. * p≤0.05; ** p≤0.01; ***p≤0.001.

To ensure that the observed effect was not due to a reduction in neoangiogenesis I performed immunohistochemistry for the endothelial marker CD31⁺ in these xenografts and found no difference between positivity in xenografts from scrambled sequence transfected cells and those from cell transfected with Notch3 shRNA (Figure 7.6).

Figure 7.6 Loss of Notch3 has no effect on neoangiogenesis in a xenograft model of ICC

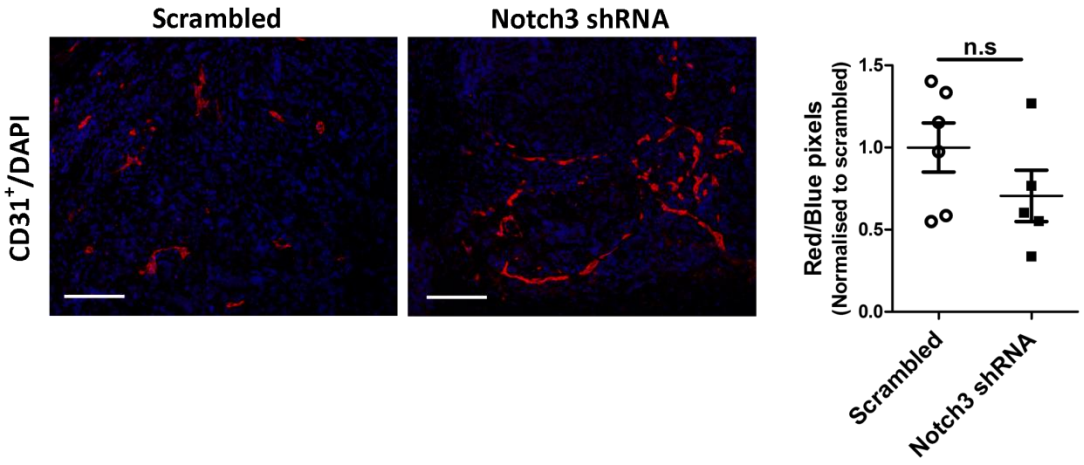

Figure 7.6 *Loss of Notch3 has no effect on neoangiogenesis in a xenograft model of ICC*

No significant difference in CD31 positivity was observed in tumours from xenografted ICC cells transfected with scrambled control (mean red/blue compared to those with Notch3 shRNA. The mean ratio of rodamine (CD31⁺) to dapi pixels in scrambled tumours was 0.051 ±0.007 compared to 0.036 ±0.007 in Notch3 knock down tumours. Data are represented as means ±S.E.M normalised to vehicle and the difference between groups was analysed using the Mann-Whitney U test.

Investigating the downstream mediators of Notch3 in ICC

To investigate the downstream mechanisms that might be mediating Notch3-driven cell survival in ICC, I sought to characterise the activity through signalling pathways already known to be dysregulated in primary hepatic carcinogenesis. Rather than analyse Notch3 KD cells maintained in culture for a number of weeks with the possibility of established adaptations in intracellular signalling activity; I sought to examine the consequent downstream effects of acute Notch3 silencing. Wild type CC-LP-1 cells were therefore transfected with siRNA targeted against either Notch3 or the downstream effector of canonical Notch, RBPJκ. Three independent siRNA sequences were used for each gene and expression levels compared to scrambled and untransfected controls. Knockdown efficiency was evaluated with rt-qPCR and western blotting for NOTCH3 and RBPJκ 36 hours after transfection. Cells with effective gene silencing from each sequence were taken forward for further analysis. In addition rt-qPCR of the Notch target genes Hes and Hey were performed to assess the functional effects of gene knock down (Figure 7.7).

Figure 7.7 Transfection with siRNA down-regulates transcription and protein expression of NOTCH3 and RBPJκ.

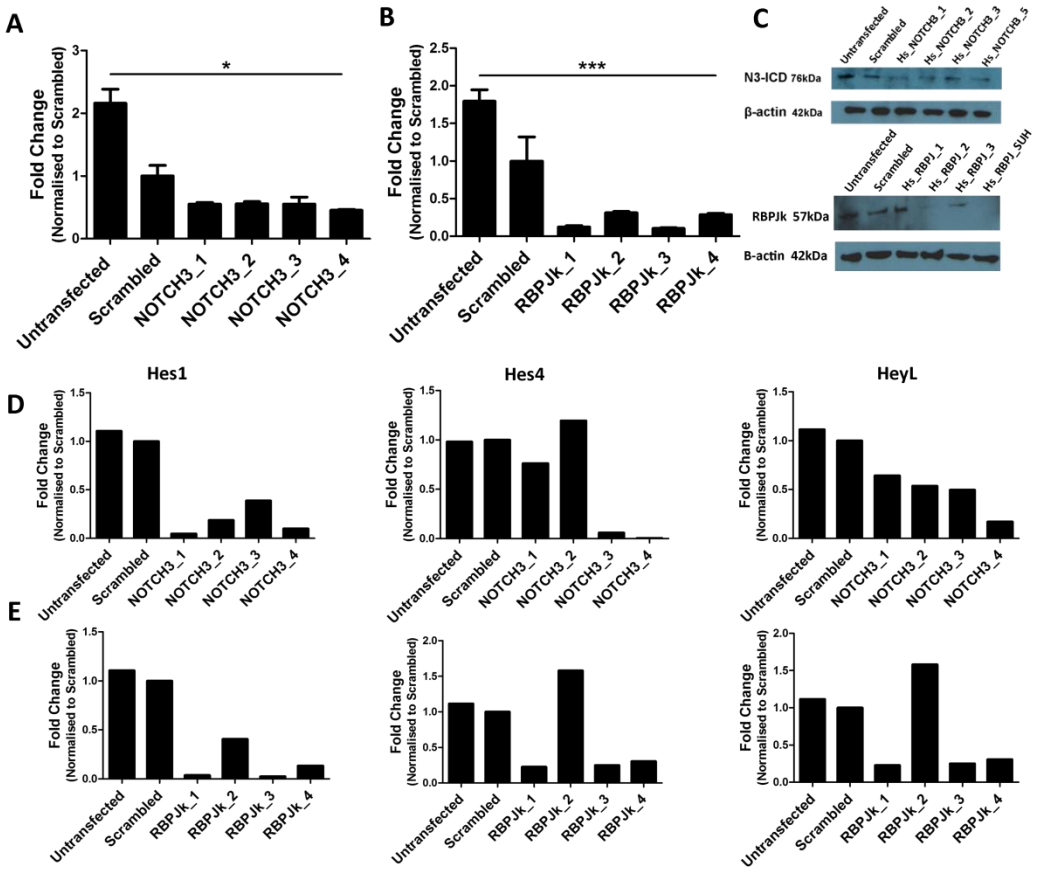

Figure 7.7 *Transfection with siRNA down-regulates transcription and protein expression of NOTCH3 and RBPJκ.* (A) rt-qPCR analysis showing inhibition of *NOTCH3* expression in CC-LP-1 cells 36 hours following transfection with *NOTCH3* siRNA compared with scrambled and untransfected controls. 18S was used as a housekeeping gene. Data are represented as means ±S.E.M. and normalised to scrambled control p=0.0175 (Kruskall Wallis test) (B) rt-qPCR analysis showing down-regulation of *RBPJκ* expression in CC-LP-1 cells 36 hours following transfection with *RBPJκ* siRNA compared with scrambled or untransfected controls. 18S was used as a housekeeping gene. Data are represented as means ±S.E.M. and normalised to scrambled control p=0.0008 (Kruskall Wallis test) (C) Western blots demonstrating down-regulation of NOTCH3 and RBPJκ protein in CC-LP-1 cells treated with

siRNA or scrambled control. β-actin is used as a loading control. (D) rt-qPCR analysis of Hes/Hey gene expression in CC-LP-1 cells 36 hours following transfection with siRNA targeted against *NOTCH3*. (E) rt-qPCR analysis of Hes/Hey gene expression in CC-LP-1 cells 36 hours following transfection with siRNA targeted against *RBPJκ*.

Gene expression analysis was carried out using the SA Biosciences Liver Cancer Quantitative RT² Profiler PCR array targeting 84 genes known to be dysregulated during progression of primary hepatocarcinogenesis (HCC and ICC). Results from samples transfected with siRNA sequences were compared to scrambled controls for analysis of changes in gene expression (using the delta delta Ct method). Changes in gene expression was defined as a change ≤ or ≥ 4 fold. In response to siRNA inhibition of *NOTCH3*, a number of genes were down-regulated across the different sequences: *MET*, *PTEN*, *FAS*, *FADD*, *IRS1*, *RAC1*, *RUNX3*, and *XIAP* (Figure 7.8 (A)) (see Appendix Table 3 for full list of gene changes in response to *NOTCH3* inhibition across different sequences). In contrast however, no changes in gene expression were observed in response to inhibition of the effector of canonical Notch, *RBPJκ* (see Appendix Table 4 for full list of gene changes) (Figure 7.8 (B)).

Figure 7.8 Inhibition of NOTCH3 but not RBPJκ in ICC down-regulates transcription of components of the PI3K-AKT signalling cascade.

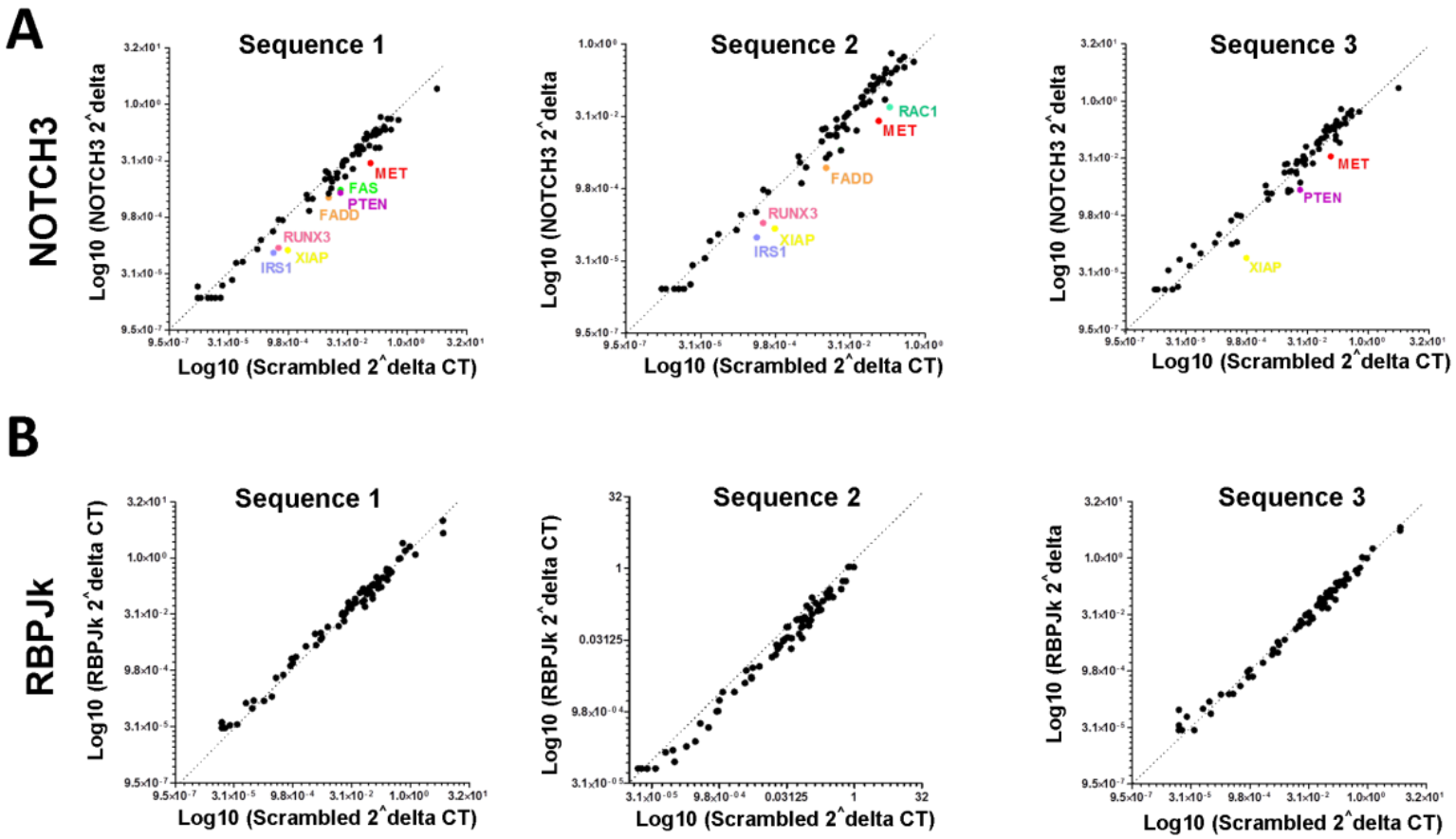

Figure 7.8 *Inhibition of NOTCH3 but not RBPJκ in ICC down-regulates transcription of components of the PI3K-AKT signalling cascade.* (A) *NOTCH3* inhibition with 3 independent siRNA sequences results in down-regulation of a number genes implicated in the PI3K/AKT signalling cascade including *MET*, *PTEN*, *FAS*, *FADD*, *IRS1*, *RAC1*, *RUNX3*, and *XIAP*. Genes represented in colour are down-regulated ≥ 4 fold. (B) Inhibition of the effector of canonical Notch, RBPJκ does not result in a significant change in gene expression.

Notch3 drives activity through the PI3K/AKT cascade in ICC *in vitro*

The genes in this system observed to down-regulate in response to Notch3 inhibition are linked via their participation in the PI3K/AKT signalling cascade. Highlighted genes are either key components of the pathway (PTEN), upstream drivers of AKT signalling (MET, IRS1, RUNX3) or downstream targets (XIAP, IRS1, FAS, FADD). I therefore sought to verify *in vitro* whether functional signalling through the PI3K/AKT cascade was indeed attenuated in response to Notch3 inhibition.

The FOXO transcription factors are a subfamily of the Forkhead box transcription factors and are direct targets of PI3K/AKT signalling. FOXO is directly phosphorylated and hence negatively regulated by AKT and therefore can be used as a surrogate marker of AKT activity: i.e. as activity through the AKT pathway increases, there is a reduction in FOXO activity (270). I consequently used a FOXO-responsive luciferase lentiviral vector to monitor the activity of FOXO in ICC cells in response to inhibition of NOTCH3.

CC-LP-1 cells previously transfected with shRNA against NOTCH3 and selected for puromycin resistance (N3 KD cells) and control cells (scrambled sequence) were transfected with FOXO-responsive lentiviral particles or positive or negative luciferase controls (see Materials & Methods). After 72 hours in culture, luminescence from both FOXO driven firefly and renilla luciferase were measured using a dual luciferase reporter assay and luminometer. An 88.9% increase in FOXO-driven luciferase activity was measured in N3 KD cells compared to scrambled controls (luminescence N3 shRNA cells 8.46 A.U. ±5.53 vs. scrambled control 0.93 A.U. ±0.04; p=0.10; n=3)

Figure 7.9 FOXO-responsive luciferase activity increases in response to stable inhibition of NOTCH3 with shRNA.

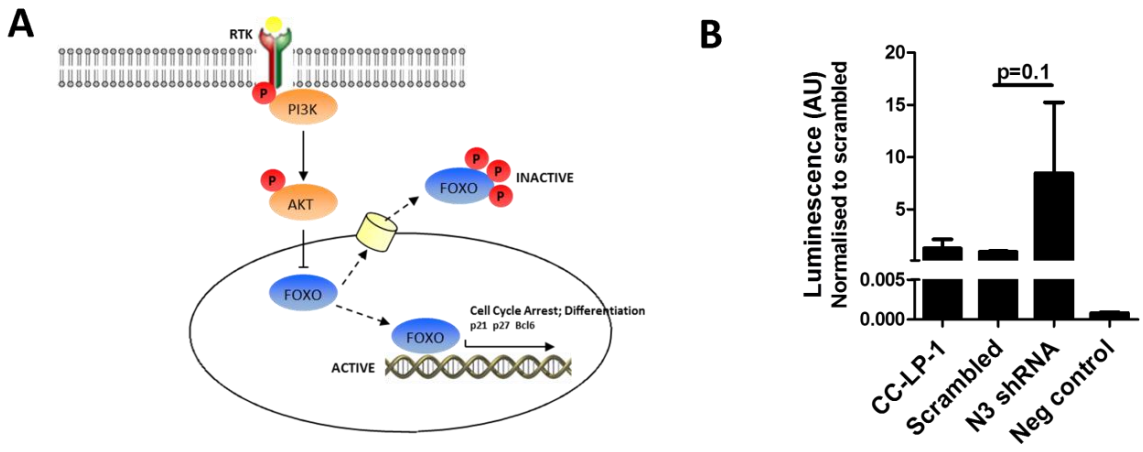

Figure 7.9 *FOXO-responsive luciferase activity increases in response to stable inhibition of NOTCH3 with shRNA.* (A) Schematic depicting the negative regulation of FOXO transcription factors by AKT. (B) A 9.10 fold increase in FOXO-driven luciferase activity was observed in response to inhibition of Notch3 activity in CC-LP-1 cells transfected with NOTCH3 shRNA compared to scrambled controls (mean luminescence N3 shRNA cells 8.46 A.U. ±5.53 vs. scrambled control 0.93 A.U. ±0.04; p=0.10). Cells were plated in triplicate and the assay was repeated three times. Positive controls not shown (luminescence off scale). Data are represented as means ±S.E.M. and differences analysed using the Mann-Whitney U test.

Notch3 drives activity through the PI3K/AKT cascade *in vivo*

I next sought to verify whether Notch3 was acting to promote PI3K/AKT-driven cell survival *in vivo.* Firstly I analysed the expression of genes previously highlighted by the Liver Cancer PCR array in the tumours that had been xenografted using N3 KD cells (NOTCH3 shRNA) and scrambled controls (Figure 7.5). I performed rt-qPCR for the genes *(PTEN*, *MET*, *IRS1*, *RAC1*, and *FAS*) and verified that expression of these genes was similarly decreased in tumours xenografted from N3 KD cells compared to scrambled controls (relative expression normalised to scrambled controls: *MET* scrambled 1.0 ±0.36, N3 KD 0.14 ±0.03; *IRS1* scrambled 1.0 ±0.41, N3 KD 0.46 ±0.20; *FAS1* scrambled 1.0 ±0.43, N3 KD 0.12 ±0.03; *RAC1* scrambled 1.0 ±0.48, N3 KD 0.02; *PTEN* scrambled 1.0 ±0.30, N3 KD 0.22 ±0.05) (Figure 7.9 (A)).

To determine whether this translated into a reduction in expression of AKT protein and its targets, I performed immunohistochemistry of phosphorylated AKT (pAKT473 and pAKT308) and its downstream targets pmTor and pS6. Quantification of these revealed that AKT phosphorylated at the threonine 308 residue, but not the serine 473 residue was reduced in response to inhibition of Notch3 in *in vivo* tumours. Similarly I observed a reduction in protein expression of the downstream targets of AKT; pmTor and pS6 in xenografted tumours originating from N3 KD cells (Figure 7.10 (B)).

***Figure 7.10 Notch3 drives activity through the PI3K/AKT cascade in ICC* in vivo.**

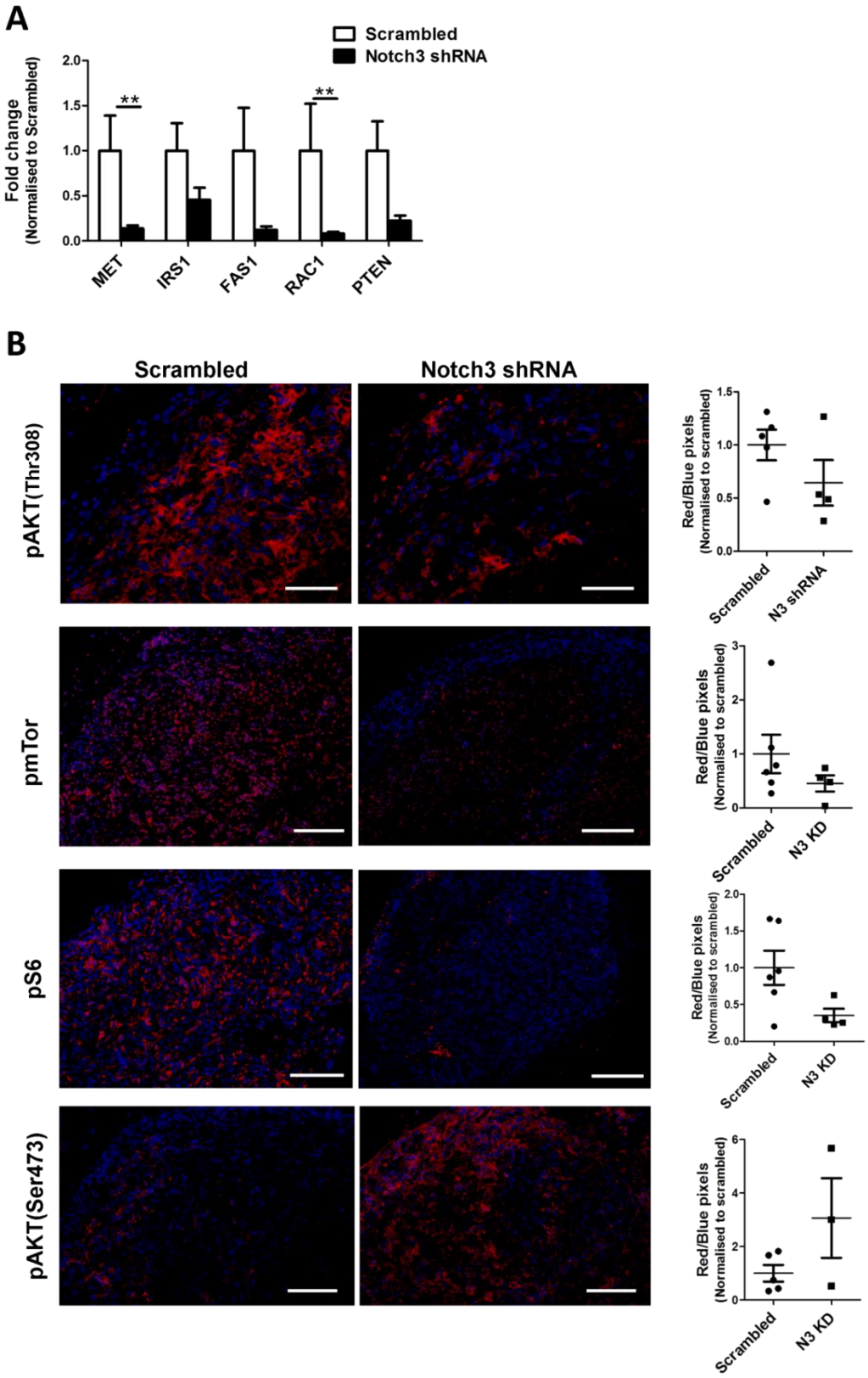

Figure 7.10 *Notch3 drives activity through the PI3K/AKT cascade in ICC* in vivo. (A) rt-qPCR analysis of the expression of genes previously identified on liver cancer PCR array, in xenografted tumours of N3 KD cells and scrambled controls. A significant reduction in gene expression was observed for *MET* and *RAC1* (*MET* scrambled 1.0 ±0.36, N3 KD 0.14 ±0.03 (p=0.009); *RAC1* scrambled 1.0 ±0.48, N3 KD 0.02 (p=0.009)), and a non-significant trend to reduction in the transcription of *IRS1*, FAS1 and *PTEN* (*IRS1* scrambled 1.0 ±0.41, N3 KD 0.46 ±0.20 (p0.329); *FAS1* scrambled 1.0 ±0.43, N3 KD 0.12 ±0.03 (p=0.519); *PTEN* scrambled 1.0 ±0.30, N3 KD 0.22 ±0.05 (p=0.519)). Data are expressed as means normalised to scrambled controls ±S.E.M. and differences were calculated using the Mann-Whitney U test. * p≤0.05; ** p≤0.01; ***p≤0.001.

Discussion

It is difficult to know whether correlations between mRNA levels of a gene of interest and tumour size and stage represent valid analyses. This cohort of tumours by definition represents end-stage disease and it is unclear how actively Notch3 is acting to drive tumour expansion in this context. In particular examining tumoural levels of Notch3 would seem unlikely to predict nodal status of resected tumours. If Notch3 is indeed acting as a driver of self-renewal in a limited population of cancer cells during tumour propagation, absolute levels of Notch3 would not be expected to correlate necessarily to tumour size.

The biggest challenge in elucidating a non-redundant role for Notch3 in ICC tumorigenesis is a paucity of specific molecular agonists or inhibitors to test this hypothesis. Soluble agonists of the Notch pathway not only act as receptor antagonists unless polymerised or fixed to plates, but also lack specificity for individual receptors (271). Efforts have been made to engineer agents including fusion proteins and neutralising antibodies to differentially inhibit Notch3 without disrupting signalling via the other Notch receptors (272, 273). Acquisition of these antibodies however has proven difficult and therefore I have endeavoured to design experiments that assess whether observed differences in Notch3 expression result in differences in phenotype or that use a more selective approach using RNA interference.

The principal limitation of these studies is their reliance on one ICC cell line that is known to be highly expressive of Notch3 (CC-LP-1). Although it is unknown how representative this system is of the spectrum of ICC, I have established that a measurable difference in cell survival and clonogenicity is demonstrable in cells with high and low levels of Notch3 protein. I have used an independent technique of inhibiting signalling via Notch3 using the HDAC1 inhibitor Trichostatin A (TSA) to corroborate this evidence both *in vitro* and a xenograft model; demonstrating that functional activity via Notch3 is reduced as evidenced by reduced expression of the

N3-ICD. Despite the potential therapeutic advantages of this experimental approach, HDAC inhibitors clearly will exert effects on many histone and non-histone proteins undergoing deacetylation and indeed HDACs are aberrantly expressed in many cancer types (274). Therefore I have substantiated these data using an independent approach to specifically target Notch3 using RNAi.

To this end I have generated a stably knocked-down human ICC cell line using shRNA against NOTCH3. When compared to cells carrying a scrambled sequence control insert, these cells demonstrated only a modest reduction in cell viability during culture in monolayer on plastic. Interestingly this mirrors similar observations made in the lung cancer cell line HCC2429 (275). When xenografted into immunodeficient mice however, a clear difference in tumour growth is seen between N3 KD cells and scrambled controls. Although I have demonstrated Jagged1 ligand to be expressed by wild type CC-LP-1 cells *in vitro*, the threshold levels required for activation of signalling through Notch3 and indeed requirement of ICC cells for other microenvironment or stromal derived factors for Notch3-driven cell survival are unknown and factors determining ligand availability may account for this observed difference of effect *in vivo*. Further investigation of this relationship should include experiments to co-culture Jagged1 expressing myofibroblasts with Notch3 deficient ICC cells within this xenograft system to assess whether excess of Notch ligand results in an exaggeration of these observed differences in phenotype.

To assess the effects of Notch3 inhibition on downstream signalling pathways I used a siRNA approach to examine acute Notch3 silencing, rather than screening cells with stable Notch3 knockdown that might have undergone adaptive transcriptional changes. In light of the limitations of using a single cell line for analysis in this screen, I selected as unbiased approach as was practicable, using a PCR array covering 84 known modulators of liver carcinogenesis. The same transcriptional changes were observed across independent siRNA sequences and were broadly grouped into members of the PI3K/AKT signalling cascade. This is not the first

description of such an interaction between Notch3 and the AKT cascade. Notch3 is overexpressed in the paediatric soft tissue tumour rhabdomyosarcoma and inhibition of Notch3 in this context results in induction of hyper-phosphorylation of p38 and AKT, causing differentiation of cancer cells into myotubes expressing myosin heavy chain i.e. Notch3 inhibition results in reversion back to the differentiated state (276). A larger body of evidence exists for Notch1 exerting its anti-apoptotic effects through PI3K/AKT signalling. In T cells for example, PI3K and the tyrosine kinase p56 are both required for the induction of IAP proteins (inhibitors of apoptosis) by Notch1(277). Furthermore Notch1 has been demonstrated to directly regulate transcription of PTEN and mutational loss of PTEN results in induction of resistance to Notch inhibition (278).

Experiments in the developing tracheal system of *Drosophila* where invasive growth and branching morphogenesis is Met dependent, have demonstrated that Hes1 is able to bind to the transcriptional promoter of *Met* and suppress its transcription. In this system the authors found that Notch-driven down-regulation of Met can also be induced by Met itself: i.e. *Met* activation results in transcriptional induction of the Notch ligand *Delta*, and that *Delta* acts to activate *Notch,* which in turn further down-regulates *Met*. In this way, the outcome of Notch activation here is an inhibition of HGF-dependent Ras activation (279). Although there are a number of core components of the Notch pathway that are conserved between *Drosophila* and vertebrates, in particular the DNA-binding protein Suppressor of Hairless (SuH) (known in mammals as RBPJκ), it is apparent that functionally Notch interactions have diverged and diversified across species with the result that this one pathway can regulate multicellular development through local cell interactions in pleiotropic contexts and species. Although I have used this example to illustrate that the Met/Hes1 interaction has been previously described, the functions observed in the *Drosophila* trachea are in contrast to my results, where I observe a down-regulation of Met transcription to Notch3 inhibition, and what adds further complexity to the relationship is that the transcriptional changes in AKT effectors in response to

Notch3 silencing are not observed in response to inhibition of the transcriptional effector of canonical Notch RBPJκ, suggesting that in this particular context, Notch3 may be driving AKT activity via a non-canonical mechanism. Certainly in the chemically-induced rat model, no increase in transcription of Notch target effectors was seen with tumour progression, suggesting either that the observed response to GSI therapy may be a result of non-Notch mediated effects of gamma secretase inhibition, or that the Hes/Hey gene family is not regulating this effect.

The first evidence for the existence of a non-canonical (CSL-independent) Notch pathway came from studies of the developing muscle in *Drosophila* mesoderm, where Notch mutants exhibit twice the number of muscle precursor cells, but mutants lacking Notch ligands or downstream effectors do not (280, 281). Subsequently such CSL-independent functions have been described in a range of systems and species, can be ligand-dependent or independent, but principally are observed in stem or embryonic cells with capacity for differentiation and expansion; it has therefore been suggested that this indicates an interaction between this pathway and known cell regulators, in particular the Wnt pathway (282). Canonical Notch and Wnt signalling frequently co-operate throughout development, for example in the imaginal wing disc of *Drosophila*, or in the developing and regenerating mammalian intestinal crypt (151, 283). In contrast however non-canonical Notch appears more frequently to antagonise Wnt, in particular through regulation of β-catenin activity (284). Recently it has been demonstrated that uncleaved, membrane-bound Notch and not just N-ICD, is able to exert functional activity within the cell, and that this form of receptor is able to physically interact and negatively regulate β-catenin in *Drosophila*, acting as a membrane-tethered transcription factor (285). It has also been shown that Notch is able to act post-translationally to phosphorylate and hence de-activate β-catenin (286). Furthermore other components of the β-catenin destruction complex, Axin and Apc, participate in this process by regulating endocytosis and trafficking of Notch receptor (287). It is unclear in this system and further work is required to determine how Notch3

might be acting in this non-canonical manner to drive ICC growth. Given such frequently described effects of membrane-tethered Notch on activated β-catenin in other contexts, it would be desirable to examine the consequence of Notch3 silencing on phosphorylated β-catenin here. In light of the observed down-regulation in transcription in PI3K/AKT signalling components, it would similarly be interesting to investigate whether any physical interaction is able to occur between these targets and Notch3.

Should this paradigm of Notch acting in a non-canonical fashion prove to also hold true in ICC *in vivo*, there may be important implications for Notch-targeted therapies in ICC as RBPJκ-directed inhibitors may prove to be inefficacious. The murine model I have described in this study offers an appropriate tool for addressing this question. Mice carrying targeted deletion of the Notch3 gene ($N3^{-/-}$) (257) have been bred with $CK19YFPp53^{f/f}$ mice. The tumour burden from ICC in these mice following 26 weeks of injury with TAA will be compared to that occurring in $CK19YFPp53^{f/f}$ mice bred with those carrying tamoxifen inducible floxed alleles of RBPJκ ($RBPJ\kappa^{f/f}$). These experiments will not only determine definitively whether Notch3 is a critical and non-redundant driver of ICC tumorigenesis, but will assess the requirement for integrity of the canonical Notch pathway in this process.

This apparent divergence of the role of Notch3 in ICC away from that of Notch1 or the canonical Notch cascade presents an exciting opportunity for therapy. The ubiquitous requirement for Notch in such a plethora of fundamental developmental and adult systems has made targeting this pathway in disease states particularly challenging, and an approach that bypasses such key components of the canonical system is highly desirable. Notch3 as a target however presents particular challenges to the development of both therapeutic neutralising antibodies and small molecule inhibitors. The structural differences that distinguish Notch3 from the other receptors are principally found within the transmembrane and intracellular portions of the protein and as such are inaccessible to the local environment (99,

252). Consequently neutralising antibodies have been targeted against EGF-like repeats 7-10 and 21-22, or the NRR region of the protein (272, 273), but this process has proven to be highly complex: Li and colleagues found that antibodies exhibiting the most potent activating and inhibitory activity actually shared overlapping epitopes within the NRR; a region that protects the receptor from proteolysis and autoactivation in its resting autoinhibited state (273). A further obstacle to the development of Notch3 specific inhibitors is the lack of a paralog-specific read out of receptor blockade: RBPJκ-driven reporter activity would screen compounds affecting canonical activity through all four receptors; N-ICD-RBPJκ reporters would be more specific, but the mechanisms of downstream target activation are very similar between receptors and so to date these have not been developed. Much work is currently focussed on characterising individual receptor-ligand interactions using structural studies, as the development of receptor-specific Notch inhibitors continues to be highly desirable.

Individualised neutralising monoclonal antibodies targeted against Notch ligands are under development although currently are not active against Jagged1 and 2 (288). The overexpression of stromal ligand makes this an alternative attractive strategy for therapeutic development; although it is not known to what degree established invasive tumours remain ligand-dependent and further work would be required. Equally enticing is the prospect of the application of Notch components as disease biomarkers. Although the majority of ICC arises sporadically and is in general detected at a late, often inoperable stage, there exists a discrete cohort of patients, particularly those with PSC undergoing liver transplantation, who are at an especially high risk of tumour development, and in whom graft surveillance is highly challenging. The temporal increase in Notch expression with progression of disease observed in the TAA rat model timecourse suggests that Notch3 and to a lesser extent Jagged1 may represent potential biomarkers of ICC development. Further analysis in premalignant models is required to assess its discriminatory potential from PSC as well as its sensitivity.

CONCLUSIONS AND FUTURE PERSPECTIVES

ICC is a highly aggressive malignancy that is diagnosed late and currently has few effective treatment options. If we are to increase the proportion of patients who might be potential candidates for curative resectional surgery, new strategies to improve early detection diagnosis are urgently required. This project aimed to determine whether targeting Notch signalling represents a new therapeutic strategy in ICC.

I have described how the Notch pathway is up-regulated across three species in ICC (human, rat and mouse) and how the Notch3 paralog in particular is strikingly up-regulated during the process of tumour expansion. I have demonstrated functional activity through the Notch cascade and how Notch transcription is activated during the natural history of disease progression. I have characterised the spatial and cellular expression of Notch components within the tumour-stromal microenvironment and observed that stromal derived ligands, in particular Jagged1 and Jagged2, appear to activate epithelial Notch3 receptor.

I have used γ-secretase inhibitors to demonstrate significant reductions in tumour burden in response to pharmacological pan-Notch blockade both in a human xenograft model and a chemically induced model in rat, and have preliminary *in vitro* data to suggest these agents warrant further investigation as to their potential for chemosensitisation in ICC. Finally, I have used multiple independent methods to specifically inhibit the Notch3 receptor and demonstrate a significant attenuation in tumour burden in xenografted immunodeficient mice.

The data presented in this study regarding the potential for γ-secretase inhibitors to sensitise ICC cells to chemotherapeutic agents are preliminary. Further work using a broader range of human cell lines as well as *in vivo* testing using animal models is required. My data have suggested, although not proven, that Notch3 may represent a more naïve, stem-like population of cells within ICC. If these cells can be targeted with anti-Notch therapies, it is tempting to speculate that a consequence might be

sensitisation of the residual tumour mass to conventional agents allowing neoadjuvant shrinkage of tumours to permit resection or even transplantation. The pre-clinical models are now available to determine this and this will be a crucial step if anti-Notch treatments are to be translated to the clinical setting.

A further aim of this thesis was to establish a novel murine model of ICC to permit inducible, tumour-specific genetic alterations and hence enable interrogation of specific signalling pathways during disease pathogenesis. I have described a model that combines transgenesis with chronic injury using the hepatotoxin TAA, to induce ICC that closely mimics human disease histologically and has an acceptable tumour latency and penetrance. In particular, and in contrast to other published models, no concomitant occurrence of HCC or extra-hepatic tumours were observed. Tamoxifen induction of Cre will enable concomitant deletion or activation of floxed alleles in conjunction with p53 deletion at the start of injury with TAA, allowing future assessment of genetic contributions to disease development.

The next phase of this work will involve cross-breeding of this model with a N3 null mouse to establish genetically the extent to which Notch3 drives progression of *in situ* developing tumours. This will be essential for determining whether the potential benefits warrant the investment to overcome the challenges of developing a drug with anti-Notch3 efficacy. To further elucidate whether Notch3 does indeed act to stimulate AKT via a non-canonical mechanism *in vivo*, models will be similarly engineered to carry floxed alleles for Notch1 and the effector of canonical Notch, RBPJκ. It will be interesting to evaluate these data in light of the results from the current trials of GSIs in other solid organ tumours as this class of agents may still represent an alternative therapeutic strategy in ICC, particularly if issues with toxicity can be overcome.

The development of a Notch3 specific small molecule antagonist will be challenging. In the absence of a stereotypical Hes/Hey transcriptional response following activity through Notch3, an *in vitro* assay would be required to reproducibly detect the

presence of N3-ICD, in order to assess Notch3 signalling during for example screening of small molecule libraries for anti-tumoral efficacy.

Many unanswered questions still remain regarding the role of Notch in driving the malignant phenotype in ICC. The mechanisms through which Notch is up-regulated are yet to be determined. One compelling hypothesis is that the infiltrating stroma might act to induce epithelial Notch, acting as a bridge between chronic inflammation and cancer. My data in the rat do demonstrate that Jagged1 up-regulates during the late inflammatory/early malignancy stage of disease progression, in contrast to Notch3 which appears to be a late event occurring in line with tumour expansion. In order to test this, stromally-driven Cre-loxP systems such as the PDGFRβ-Cre (289)could be used to delete Notch ligand and assess the subsequent effects on tumour formation. It is also unknown how Notch activity changes according to epithelial mutation in ICC and whether certain oncogenic events may act as drivers for Notch up-regulation. This will be able to be addressed as more disease models are developed employing different genetic aberrations. In light of the data presented here it would be of interest to assess the role played by Notch in PTEN deleted models of ICC in particular.

Finally, the data in this study have demonstrated that the cell of origin of ICC can be the $CK19^{+}$ cholangiocyte or progenitor cell and that this cell population in the liver should not be ruled out as a target for future drug development. These lineage tracing data combined with recently published hepatocyte tracing experiments make it desirable to concomitantly trace both liver cell types during different injury models to assess the contributions of both populations *in vivo*. Our lab has currently replicated data demonstrating that during chronic biliary injury, hepatocytes are able to contribute both to ductule formation during regeneration and malignancy during carcinogenesis. It would seem likely therefore that during the progression from chronic inflammation to cancer both cell types may make contributions to the same tumour. The transgenic technology necessary for concomitant dual labelling does not currently exist and viral labelling of cell types can be flawed. These data

do suggest however that in contrast to the traditional paradigm of a mutated epithelial clone expanding to form a tumour, niche-derived signals may possess potential to recruit multiple cell types and induce de-differentiation as part of the tumorigenic process.

APPENDICES

Appendix 1: Clarification of Notch homolog nomenclature

Pathway component	***Drosophila***	***Caenorhabditis elegans***	**Mammals**
Receptors	Notch	LIN-12, GLP-1	Notch 1,2,3,4
Ligands	Delta, Serrate		Dll 1,3,4, Jagged 1, 2
DNA-binding transcription factor	Su(H)*	LAG-1*	RBPJκ/CBF-1*
Transcriptional co-activator	Mastermind	LAG-3	MAML1-3
Transcriptional co-repressors	Hairless, SMRTR		Mint/SHRP/SPEN, NCoR/SMRT/KyoT2/SKIP
Furin covertase (S2 cleavage)			PC5,6,Furin
Metalloproteases (S2 cleavage)	Kuzbanian, Kubanian-like, TACE	SUP-17/Kuzbanian, ADM-4/TACE	ADAM10/Kuzbanian, ADAM17/TACE
Gamma secretase (S3 cleavage)	Presenilin, Nicastrin, APH-1, PEN-2	SEL-12, APH-1, APH-2, PEN-2	Presenilin 1 and 2, Nicastrin, APH-1 a-c, PEN-2
O-fucosyl transferase	OFUT-1	O-FUT-1	PO-FUT-1
O-glucosyl transferase	RUMI		
B1,3-GlcNAc-transferase	Fringe		Lunatic, Manic, Radical Fringe
E3 ubiquitin ligase (ligand endocytosis)	Mindbomb 1-2, Neuralized		Mindbomb, skeletrophin, Neuralized 1-2
E3 ubiquitin ligase (receptor endocytosis)	Deltex		Deltex 1-4, SEL10
Canonical bHLH repressor genes	*E(spl)*	*REF-1*	*HES/ESR/HEY*

*CSL (CBF-1/SuH/LAG-1) Alternative nomenclature for the canonical Notch binding protein

Appendix 2: Normal liver development

Transplantation studies have determined that hepatoblasts develop from the definitive endoderm lining the putative ventral foregut near the developing heart. At embryonic day 9 in the mouse (7-8 somite stage) foregut endoderm is in contact with cardiac mesoderm (and therefore receptive to FGF signalling (290)) and begins to proliferate more rapidly before firstly α-fetoprotein (αFP) and then albumin mRNA become detectable. By day 9.5 the hepatic endoderm migrates into the posterior mesenchyme of the septum transversum and begins to form the liver bud in response to BMP signalling (291). Endothelial cells are critical in this process in delimiting the mesenchymal domain into which the bud grows (292). At this point haemopoietic cells migrate into the liver bud and proliferate whilst concomitantly providing growth factors including Oncostatin M to the developing liver (293). Specification of endoderm into a hepatic fate occurs in response to a number of cues including expression of FoxA and GATA4, which are able to bind to the albumin enhancer before the onset of albumin expression, and HNF1β (294-296).

Once the hepatic endoderm has been specified and the liver bud is growing, epithelia within the bud become known as hepatoblasts. It is important to note that at this stage, even before commitment into hepatocyte and cholangiocyte lineages has occurred, these bipotential hepatoblasts will activate transcription of genes which will later be thought of as stereotypical hepatocyte genes including albumin, transthyretin, α-fetoprotein (αFP) and retinal binding protein (RBP) (297). It is at this point that a subpopulation of hepatoblasts will initiate transcription of biliary-specific genes including Sox9 and some cytokeratins, whereas the remaining hepatoblasts remain cytokeratin-negative and will go on to become hepatocytes (145). The cytokeratin-positive population become known as biliary progenitor cells before differentiating further into biliary epithelial cells (BECs). Once specified, these will organise into a single-layered sheet surrounding the portal vein, known as the ductal plate (E15.5-16.5). Polarisation of the liver bud occurs to create canaliculi and venous sinusoids.

After E16.5 a second ductal plate layer begins to form from hepatoblasts on the parenchymal side of the plate, in which *in situ* asymmetrical dilatations begin to appear; precursors of mature, lumenised intrahepatic bile ducts. This process continues into the post-natal period until the second postnatal week, by which time all unincorporated biliary precursor cells have disappeared. Following the commencement of duct formation, asymmetric expression of biliary and hepatocyte genes can be observed to occur along the tubule; CK19 gets expressed along the portal side of the plate, whereas HNF4α appears only on the parenchymal side (145). Hepatocyte maturation is regulated through expression and cross-regulation of a set of transcription factors which include HNF1α HNF1β, FoxA2, HNF4α1, HNF6 and LRH-1 (298). Hepatic zonation and the positioning of hepatocytes within the liver lobule is controlled at least in part via Wnt/β-catenin signalling(299).

The large extrahepatic bile ducts arise through branching of a gut-derived diverticulum containing pancreatobiliary precursors coexpressing PDX1 and SOX17 (300). Expression of SOX17 is regulated by Hes1 and mutant studies have shown that the absence of Hes1 results in accelerated development of pancreatic endocrine precursors and re-direction of bile ducts to a pancreatic phenotype (301).

Appendix Table 1

Unigene	Refseq	Symbol	Fold Change	p Value
Hs.8546	NM_000435	**NOTCH3**	18.202	0.000025
Hs.433445	NM_002226	**JAG2**	12.5846	0.003088
Hs.653700	NM_007129	**ZIC2**	12.2213	0.014216
Hs.234434	NM_012258	**HEY1**	10.2518	0.016558
Hs.244723	NM_001238	**CCNE1**	9.1662	0.08289
Hs.728907	NM_000214	**JAG1**	8.4314	0.000426
Hs.173859	NM_003507	**FZD7**	7.5751	0.01193
Hs.472566	NM_014571	**HEYL**	6.0241	0.000829
Hs.525198	NM_003035	**STIL**	5.9598	0.005442
Hs.563344	NM_006186	**NR4A2**	5.0864	0.178302
Hs.159142	NM_001040167	**LFNG**	4.5722	0.172785
Hs.142912	NM_001466	**FZD2**	4.5159	0.125445
Hs.502328	NM_000610	**CD44**	3.3175	0.058305
Hs.386567	NM_004120	**GBP2**	3.1529	0.020033
Hs.492974	NM_003882	**WISP1**	2.8781	0.669151
Hs.137510	NM_006312	**NCOR2**	2.8553	0.078323
Hs.94234	NM_003505	**FZD1**	2.5179	0.251392
Hs.517603	NM_002405	**MFNG**	2.4929	0.086738
Hs.591863	NM_003506	**FZD6**	2.3132	0.155446
Hs.664706	NM_024015	**HOXB4**	2.264	0.078899
Hs.149261	NM_001754	**RUNX1**	2.1419	0.279567
Hs.446352	NM_004448	**ERBB2**	1.9708	0.099765
Hs.495473	NM_017617	**NOTCH1**	1.9332	0.105153
Hs.504096	NM_005188	**CBL**	1.8568	0.068651
Hs.487360	NM_024408	**NOTCH2**	1.8422	0.136808
Hs.2256	NM_002423	**MMP7**	1.8389	0.318428
Hs.728902	NM_203458	**NOTCH2NL**	1.838	0.076917
Hs.437922	NM_005376	**MYCL1**	1.7638	0.372321
Hs.390736	NM_003879	**CFLAR**	1.7396	0.122128
Hs.728776	NM_012423	**RPL13A**	1.6804	0.123115
Hs.716382	NM_004210	**NEURL**	1.6387	0.309506
Hs.404914	NM_003183	**ADAM17**	1.6198	0.142189
Hs.436100	NM_004557	**NOTCH4**	1.5761	0.076371
Hs.73090	NM_002502	**NFKB2**	1.546	0.503839
Hs.404089	NM_016169	**SUFU**	1.5366	0.575025
Hs.349094	NM_002351	**SH2D1A**	1.4657	0.332305
Hs.517517	NM_001429	**EP300**	1.3542	0.953128
Hs.592082	NM_003502	**AXIN1**	1.329	0.521975
Hs.251680	NM_000427	**LOR**	1.2918	0.284098
Hs.445498	NM_012245	**SNW1**	1.2895	0.300704
Hs.578508	NM_001110	**ADAM10**	1.214	0.384552
Hs.88556	NM_004964	**HDAC1**	1.2073	0.401968
Hs.34560	NM_005574	**LMO2**	1.2055	0.58369
Hs.515053	NM_001130	**AES**	1.1931	0.320549
Hs.283565	NM_005438	**FOSL1**	1.0615	0.468063

Unigene	Refseq	Symbol	Fold Change	p Value
Hs.654408	NM_003998	**NFKB1**	1.0525	0.878895
Hs.445733	NM_002093	**GSK3B**	0.9903	0.997244
Hs.520640	NM_001101	**ACTB**	0.9579	0.676272
Hs.272367	NM_018411	**HR**	0.9513	0.745327
Hs.534255	NM_004048	**B2M**	0.9409	0.754207
Hs.3260	NM_000021	**PSEN1**	0.9259	0.957733
Hs.25363	NM_000447	**PSEN2**	0.9211	0.719164
Hs.437846	NM_005631	**SMO**	0.9192	0.917649
Hs.250666	NM_005524	**HES1**	0.9042	0.687197
Hs.632702	NM_005269	**GLI1**	0.9019	0.726693
Hs.534465	NM_172341	**PSENEN**	0.8563	0.643321
Hs.654609	NM_003744	**NUMB**	0.8241	0.916316
Hs.655331	NM_021961	**TEAD1**	0.7914	0.665451
Hs.459691	NM_002613	**PDPK1**	0.7708	0.465492
Hs.379912	NM_005618	**DLL1**	0.7449	0.389426
Hs.476018	NM_001904	**CTNNB1**	0.7301	0.341752
Hs.374127	NM_003903	**CDC16**	0.718	0.168774
Hs.654464	NM_016734	**PAX5**	0.7176	0.503075
Hs.531754	NM_145185	**MAP2K7**	0.7174	0.605296
Hs.728789	NM_005252	**FOS**	0.6793	0.425548
Hs.472409	NM_172236	**POFUT1**	0.6762	0.402127
Hs.523852	NM_053056	**CCND1**	0.6041	0.178436
Hs.198998	NM_001278	**CHUK**	0.589	0.010609
Hs.412707	NM_000194	**HPRT1**	0.5764	0.23416
Hs.11392	NM_004469	**FIGF**	0.5699	0.213409
Hs.569700	NM_002917	**RFNG**	0.539	0.264641
Hs.40735	NM_017412	**FZD3**	0.4341	0.35265
Hs.6347	NM_002335	**LRP5**	0.4239	0.358288
Hs.197320	NM_005077	**TLE1**	0.4125	0.084711
Hs.80828	NM_006121	**KRT1**	0.4108	0.178684
Hs.370771	NM_000389	**CDKN1A**	0.396	0.150495
Hs.156979	NM_014443	**IL17B**	0.3786	0.3182
Hs.162646	NM_015869	**PPARG**	0.3637	0.001923
Hs.181300	NM_005065	**SEL1L**	0.3378	0.201228
Hs.856	NM_000619	**IFNG**	0.3377	0.903416
Hs.19545	NM_012193	**FZD4**	0.3148	0.242607
Hs.533055	NM_003884	**KAT2B**	0.2946	0.049651
Hs.108219	NM_004626	**WNT11**	0.176	0.251588
Hs.372152	NM_004416	**DTX1**	0.1495	0.011557
Hs.164537	NM_000193	**SHH**	0.0625	0.180074
Hs.524518	NM_003153	**STAT6**	1.1651	0.155658
Hs.592355	NM_002046	**GAPDH**	1.1455	0.476017
Hs.231367	NM_000417	**IL2RA**	1.0872	0.71911
Hs.169002	NM_138296	**PTCRA**	1.0858	0.453129

Appendix Table 1 *(relating to Table 6.1):* Full list of Notch pathway genes and their fold transcriptional change in human ICC vs. patient-matched, non-cancerous distal liver (n=5) as measured with the Notch pathway RT^2 Profiler™ PCR array (SABiosciences).

Appendix Table 2

	Fold change			
Symbol	Inflamed (8-10weeks)	Fibrotic (12-14weeks)	Early malignant (16-20weeks)	Advanced malignancy (21-26weeks)
Mmp7	0.9658	2.4933	9.5454	104.8512
Heyl	0.3739	1.4555	2.4446	6.5823
Cd44	0.2347	0.9341	1.4094	6.3304
Ccne1	9.4719	12.3632	6.122	5.8848
Notch3	0.131	2.8114	1.269	5.7307
Jag1	0.2286	1.4154	1.1896	4.0773
Fosl1	1.1151	1.5161	0.9916	4.062
Il17b	3.1246	4.4388	3.7048	3.0122
Ncor2	2.355	4.9988	2.7228	2.6779
hr	0.3141	2.3182	1.4387	2.5085
Neurl	0.5173	1.9776	1.1683	2.4982
Fzd1	0.2892	0.8235	0.7968	2.475
Fos	0.3056	1.0761	0.6038	2.4218
Nfkb1	0.8177	1.2992	1.3289	2.3251
Mycl1	0.1105	0.5385	0.7352	2.1658
Map1b	0.5557	2.1614	1.4026	2.0793
Dll1	0.7969	3.0818	1.445	1.7991
Ccnd1	1.4515	2.4019	1.4937	1.7516
Psen1	0.5517	1.013	1.1565	1.7456
Tle1	1.7781	3.357	2.2917	1.7171
Nfkb2	0.8156	1.5006	1.05	1.6006
Hprt1	1.3644	1.1395	1.8796	1.566
Gli1	0.131	1.2467	0.358	1.5506
Smo	0.184	2.9473	0.6858	1.5199
Cdkn1a	2.755	3.1557	2.9396	1.4803
Gbp2	0.2465	0.265	0.3446	1.4688
Ctnnb1	0.8229	1.1203	0.8046	1.4456
Fzd3	0.6346	0.5179	0.7967	1.4208
Il2ra	0.0963	2.3574	0.8523	1.3875
Hoxb4	0.141	0.8742	0.7024	1.3791
Fzd7	0.9339	1.3145	1.5592	1.3746
Hdac1	0.4119	0.7379	0.9512	1.3587
Runx1	0.0638	0.1163	0.2109	1.3097
Cdc16	1.1533	1.8708	1.228	1.2955
Ep300	0.6419	1.5713	0.8289	1.2646
Erbb2	0.0945	0.5952	0.522	1.2505
Gsk3b	0.5827	0.7904	1.4263	1.2334
Supt6h	1.179	2.7661	1.5787	1.1925
Pdpk1	0.9428	1.4195	1.0594	1.1796
Chuk	1.6998	2.7608	1.3433	1.1771
Map2k7	0.6696	2.5015	0.9001	1.1423
Nr4a2	0.049	0.599	0.9597	1.1419
Ldha	3.7554	2.616	1.4337	1.1323
Stat6	0.3678	0.7935	1.0264	1.1321

	Fold change			
Symbol	Inflamed (8-10weeks)	Fibrotic (12-14weeks)	Early malignant (16-20weeks)	Advanced malignancy (21-26weeks)
Sufu	0.3248	0.912	0.9442	1.0668
Axin1	0.7851	2.291	0.9233	1.0499
Lmo2	0.1582	0.2616	0.491	1.0446
Jag2	0.0048	0.0455	0.2216	0.9878
Rplp1	2.7966	2.9224	0.9466	0.9875
Lrp5	0.6323	2.3288	0.71	0.9696
Rpl13a	1.2381	1.2937	0.8515	0.935
Wisp1	0.0671	0.6386	0.1834	0.9306
Figf	0.1737	1.0062	0.4602	0.9263
Notch1	0.5341	0.8383	0.7734	0.9254
Aes	0.4479	1.1824	1.1767	0.9229
Fzd6	0.3298	1.1423	0.7095	0.9089
Lfng	0.132	0.227	0.3168	0.863
Notch2	0.5683	2.0499	0.8686	0.8612
Cflar	0.35	0.7758	0.4303	0.845
Psen2	0.4754	1.5348	0.5839	0.8249
Rfng	0.6476	1.2304	0.6965	0.811
Cbl	0.3906	0.3242	0.5618	0.8054
Notch4	0.0778	0.1924	0.3379	0.7989
Adam17	0.3842	0.4657	0.4597	0.7486
Numb	0.5473	1.531	0.7815	0.732
Fzd5	0.6628	1.6935	1.1146	0.7159
Tead1	0.3454	0.6381	0.6177	0.7157
Actb	0.1576	0.2593	0.4358	0.6032
Ptcra	0.1411	1.2467	0.3787	0.5943
Wnt11	0.0351	0.0488	0.1646	0.5863
Pcaf	0.2744	0.6128	0.5401	0.5769
Rbpjl	0.225	0.4805	0.3876	0.4806
Krt1	0.1442	0.6017	0.6005	0.4756
Pofut1	0.2798	1.7287	0.1935	0.4483
Mfng	0.0504	0.2298	0.2023	0.4287
Ifng	0.131	1.2467	0.358	0.4251
Zic2	0.131	1.2467	0.358	0.4251
Fzd4	0.1043	0.3493	0.2346	0.3815
Fzd2	0.018	0.1664	0.1184	0.3046
Hes5	0.0827	0.6452	0.1198	0.1818
Hey1	0.0151	0.0254	0.0484	0.1194
Pparg	0.1967	0.1586	0.2157	0.1053
Sel1l	0.3418	1.1946	0.5706	0.0606
Shh	0.0052	0.0496	0.0142	0.0169
Adam10	0.7499	0.763	0.3217	0.0052
Psenen	0.7293	0.9997	1.1626	1.1192
Hes1	0.6774	0.7625	1.1288	1.1116
Ncstn	0.9243	1.7537	0.787	1.0836
Il6st	0.5737	1.0788	0.7305	1.0779

Appendix Table 2 *(relating to Figure 6.10):* Full list of Notch pathway genes and their fold transcriptional change during a timecourse of ICC development in rat using the chemical carcinogen TAA, as measured by a Notch pathway RT^2 Profiler™ PCR array (SABiosciences). Comparison was made between pooled RNA from whole rat liver exposed to 8 to 10 weeks (inflamed) (n=3), 12 to 14 weeks (fibrotic) (n=3), 16 to 20 weeks (early malignant) (n=3) and 22 to 26weeks (late malignant) (n=3) to uninjured controls (n=6).

Appendix Table 3

Gene Symbol	Compared to Scrambled control								
	NOTCH3 1		NOTCH3 2		NOTCH3 3		Untransfected		Scrambled
	Ct	Fold Change	Ct	Fold Change	Ct	Fold Change	Ct	Fold Change	Ct
ADAM17	26.13	1.31	26.50	1.47	26.57	1.09	26.00	1.21	25.37
AKT1	20.04	0.75	20.00	0.63	20.47	0.62	20.57	1.09	20.09
ANGPT2	20.82	0.67	20.80	0.57	21.09	0.49	21.17	0.86	21.03
BAX	19.06	0.76	19.08	0.67	19.58	0.67	19.53	1.07	19.08
BCL2	26.15	1.00	26.16	0.88	26.51	0.79	26.25	1.09	25.77
BCL2L1	22.71	0.83	22.84	0.79	23.59	0.93	23.49	1.44	22.61
BID	23.06	0.89	23.55	1.08	23.78	0.90	23.13	0.94	22.86
BIRC2	25.66	2.40	25.86	2.40	26.26	2.23	23.50	0.54	24.02
BIRC5	25.21	2.04	25.60	2.32	26.31	2.68	23.58	0.67	23.81
CASP8	29.79	0.82	29.80	0.71	30.16	0.65	29.79	0.83	29.71
CCL5	31.81	0.78	31.59	0.58	31.13	0.30	31.37	0.58	31.80
CCND1	19.16	1.54	19.20	1.38	19.43	1.14	18.52	1.00	18.16
CCND2	27.99	0.65	28.06	0.60	28.46	0.55	28.67	1.06	28.23
CDH1	0.00	0.77	40.00	7.39E+11	0.00	0.47	40.00	8.59E+11	0.00
CDH13	36.52	7.60E+10	0.00	0.67	0.00	0.47	0.00	0.78	0.00
CDKN1A	20.37	0.84	20.36	0.73	20.74	0.67	21.53	1.91	20.24
CDKN1B	24.23	1.42	24.23	1.24	24.68	1.19	24.61	1.87	23.35
CDKN2A	22.18	1.25	22.17	1.08	22.69	1.09	22.08	1.18	21.48
CFLAR	23.90	1.15	23.18	0.61	23.97	0.74	24.15	1.38	23.33
CTNNB1	22.74	0.89	22.75	0.78	22.48	0.45	23.08	1.14	22.54
CXCR4	33.34	1.79	32.77	1.05	32.89	0.80	31.38	0.46	32.13
DAB2IP	23.70	0.52	23.88	0.51	24.04	0.40	23.78	0.56	24.27
DLC1	20.30	1.08	20.67	1.21	20.63	0.83	20.20	1.02	19.82
E2F1	21.51	0.89	21.22	0.64	21.77	0.66	21.66	1.00	21.30
EGF	0.00	0.00	0.00	0.00	40.00	42.22	0.00	0.00	33.52
EGFR	20.55	0.82	20.35	0.62	20.80	0.60	21.36	1.46	20.46
EP300	21.92	0.95	22.12	0.95	22.20	0.71	22.63	1.57	21.62
FADD	26.02	3.09	26.54	3.85	26.46	2.57	24.95	1.49	24.02
FAS	25.34	3.85	25.32	3.31	25.61	2.85	23.28	0.94	23.02
FHIT	34.96	1.35	36.92	4.58	37.64	5.31	34.00	0.70	34.15
FLT1	0.00	0.77	38.40	2.44E+11	0.00	0.47	0.00	0.78	0.00
FZD7	23.85	0.66	23.80	0.55	23.98	0.44	24.13	0.81	24.08
GADD45B	20.20	0.76	20.46	0.79	20.96	0.79	20.63	1.04	20.22
GSTP1	20.01	1.80	19.58	1.16	19.80	0.95	19.18	1.02	18.79
HGF	24.63	1.42	24.27	0.96	24.60	0.85	24.55	1.36	23.75
HHIP	34.92	2.78	34.66	2.02	34.69	1.45	34.66	2.35	33.07
HRAS	20.15	1.08	19.97	0.83	20.51	0.85	21.23	2.30	19.67
IGF2	40.00	1.19	40.00	1.03	40.00	0.73	39.95	1.16	39.38
IRS1	30.93	3.72	31.35	4.33	31.01	2.41	28.59	0.74	28.66
ITGB1	21.63	2.24	21.82	2.23	21.86	1.61	20.14	0.81	20.09
KDR	0.00	0.77	0.00	0.67	0.00	0.47	0.00	0.78	0.00
LEF1	30.61	1.16	30.84	1.19	30.89	0.86	30.48	1.07	30.02
MCL1	20.02	1.29	19.62	0.85	20.46	1.07	19.67	1.02	19.28
MET	22.98	4.28	23.29	4.61	23.34	3.36	20.83	0.98	20.51
MSH2	23.49	2.18	23.96	2.63	23.95	1.84	21.86	0.71	21.99
MSH3	23.24	1.00	23.66	1.16	23.68	0.83	23.48	1.19	22.87
MTDH	19.77	1.03	19.75	0.88	20.02	0.75	19.78	1.05	19.36
MYC	19.06	0.92	18.86	0.70	19.31	0.67	19.42	1.19	18.81
NFKB1	22.81	0.79	23.02	0.80	23.31	0.69	23.62	1.41	22.77
NRAS	20.73	0.71	20.84	0.67	20.97	0.52	20.91	0.82	20.84
OPCML	0.00	0.77	0.00	0.67	0.00	0.47	0.00	0.78	0.00
PDGFRA	33.90	0.19	0.00	0.00	35.69	0.40	0.00	0.00	35.94
PIN1	20.37	0.56	20.22	0.44	20.70	0.43	20.62	0.67	20.84
PTEN	25.60	4.58	25.33	3.31	26.25	4.41	24.00	1.53	23.03
PTGS2	36.09	1.99	0.00	0.00	0.00	0.00	34.88	0.87	34.72
PTK2	21.89	1.04	22.05	1.01	22.14	0.76	21.85	1.02	21.46
PYCARD	31.72	1.08	31.12	0.62	31.81	0.70	31.51	0.94	31.24
RAC1	21.62	2.78	22.34	3.99	22.13	2.43	19.94	0.88	19.77
RASSF1	27.21	2.24	27.60	2.56	27.10	1.27	26.63	1.52	25.67

Gene Symbol	Compared to Scrambled control								
	NOTCH3 1		NOTCH3 2		NOTCH3 3		Untransfected		Scrambled
	Ct	Fold Change	Ct	Fold Change	Ct	Fold Change	Ct	Fold Change	Ct
RHOA	20.83	0.75	21.16	0.82	21.55	0.75	20.37	0.55	20.88
RUNX3	30.48	3.65	30.36	2.92	30.82	2.83	28.97	1.30	28.24
SFRP2	0.00	0.77	0.00	0.67	0.00	0.47	0.00	0.78	0.00
SMAD4	24.18	2.26	23.87	1.59	24.05	1.27	23.22	1.18	22.63
SMAD7	29.03	0.96	29.60	1.24	28.93	0.55	29.48	1.33	28.71
SOCS1	28.03	0.84	28.22	0.84	28.54	0.74	28.29	1.02	27.90
SOCS3	24.30	1.51	24.35	1.36	24.83	1.34	23.52	0.89	23.33
STAT3	21.75	1.20	21.96	1.21	21.74	0.73	21.83	1.29	21.11
TCF4	21.53	0.71	21.66	0.68	22.20	0.69	21.74	0.83	21.65
TERT	25.79	0.73	25.75	0.62	25.88	0.48	25.91	0.80	25.87
TGFA	33.85	1.44	33.25	0.83	32.33	0.31	33.58	1.21	32.95
TGFB1	18.90	0.46	18.61	0.32	19.20	0.34	19.06	0.52	19.66
TGFBR2	20.01	0.76	19.69	0.53	20.21	0.54	20.29	0.94	20.03
TLR4	40.00	8.48E+11	0.00	0.67	0.00	0.47	0.00	0.78	0.00
TNFRSF10B	24.41	0.82	24.71	0.88	24.74	0.63	24.89	1.16	24.32
TNFSF10	35.78	2.94	35.77	2.54	33.29	0.32	27.63	0.01	33.85
TP53	24.28	1.01	24.28	0.88	24.67	0.81	24.19	0.96	23.89
VEGFA	22.24	0.91	22.36	0.86	23.00	0.94	22.37	1.00	22.01
WT1	35.94	5.09E+10	0.00	0.67	0.00	0.47	0.00	0.78	0.00
XIAP	30.69	7.24	30.74	6.53	32.21	12.73	27.09	0.60	27.46
YAP1	21.47	0.72	21.62	0.70	22.03	0.66	21.50	0.75	21.56

Appendix Table 3 *(Relating to Figure 7.7): Complete table of gene changes following silencing of NOTCH3 with siRNA in ICC cells.* CC-LP-1 cells transfected with siRNA against NOTCH3 down-regulated a number of genes in response to transfection with 3 independent siRNA sequences. Down-regulation is defined as ≥4 fold reduction in gene expression.

Appendix Table 4

Gene Symbol	Compared to Scrambled control								
	RBPJκ 1		RBPJκ 2		RBPJκ 3		Untransfected		Scrambled
	Ct	Fold Change	Ct	Fold Change	Ct	Fold Change	Ct	Fold Change	Ct
ADAM17	24.32	1.77	26.06	1.21	24.81	1.17	25.19	0.98	24.29
AKT1	22.3	1.62	23.09	2.13	23.17	0.82	22.85	1.12	22.14
ANGPT2	23.12	0.98	24.66	0.77	23.04	0.96	22.83	1.22	22.24
BAX	21.31	1.3	22.52	1.27	21.59	0.99	21.78	0.95	20.83
BCL2	28.82	2.21	30.99	1.12	30.29	0.74	29.67	1.24	29.11
BCL2L1	24.74	1.54	26.46	1.06	25.52	0.83	25.53	0.91	24.51
BID	22.57	2.47	24.58	1.39	23.31	1.37	23.3	1.51	23.02
BIRC2	22.56	1.03	24.02	0.85	23.43	0.52	22.78	0.89	21.74
BIRC5	24.19	0.72	25.92	0.5	24.18	0.68	24.46	0.61	22.87
CASP8	32.57	0.83	33.47	1.01	31.82	1.3	32.32	1	31.45
CCL5	33.26	1.03	33.72	1.71	32.45	1.68	32.48	1.8	32.45
CCND1	18.85	2.09	20.96	1.1	19.76	1.03	19.97	0.98	19.06
CCND2	29.2	1.59	30.25	1.74	29.64	1.08	30.1	0.86	29.01
CDH1	37.3	1.81	37.62	4.11	36.74	1.68	37.07	1.84	36.18
CDH13	40	1.81	40	4.11	40	1.68	40	1.84	39.97
CDKN1A	22.52	1.76	24.68	0.9	22.8	1.34	22.87	1.4	22.48
CDKN1B	24.04	1.97	25.99	1.16	24.7	1.15	25	1.03	24.16
CDKN2A	23.76	1.14	25.62	0.71	23.66	1.13	23.88	1.06	23.09
CFLAR	25.48	1	26.47	1.15	25.52	0.91	25.87	0.78	24.63
CTNNB1	24.35	1.44	25.14	1.89	25.5	0.6	25.63	0.6	24.02
CXCR4	32.53	1.56	34.54	0.88	33.53	0.72	36.32	0.29	32.32
DAB2IP	26.94	1.36	27.98	1.51	27.44	0.89	27.65	0.84	26.53
DLC1	21.7	1.17	22.8	1.24	21.79	1.02	22.3	0.78	21.07
E2F1	22.96	2.28	24.64	1.61	23.95	1.06	24.58	0.75	23.29
EGF	34.76	1.36	37.16	2.62	33.79	2.47	35.87	1.17	34.35
EGFR	21.57	2.23	23.47	1.36	22.58	1.03	22.92	0.89	21.87
EP300	23.05	1.39	24.55	1.12	23.71	0.82	24.16	0.65	22.67
FADD	23.81	2.49	26.11	1.15	24.78	1.18	25.04	1.08	24.27
FAS	22.87	1.9	25.17	0.88	23.59	1.07	23.91	0.94	22.94
FHIT	35.77	1.81	37.26	4.11	34.99	1.69	37.17	1.84	35.83
FLT1	0	1.81	0	4.11	0	1.68	0	1.84	0
FZD7	27.12	1.3	28.63	1.04	27.18	1.15	27.66	0.91	26.64
GADD45B	22.5	1.81	24.63	0.94	22.92	1.25	23.1	1.21	22.5
GSTP1	19.22	2.12	20.96	1.44	19.69	1.42	19.92	1.33	19.45
HGF	25.99	1.87	27.88	1.15	26.98	0.87	26.99	0.95	26.04
HHIP	34.67	0.94	36.76	1.71	35.35	0.7	36.78	0.76	33.73
HRAS	22.18	1.77	24.23	0.97	22.57	1.25	22.63	1.32	22.15
IGF2	40	1.81	40	4.11	40	1.68	40	1.84	40
IGFBP1	40	1.81	40	4.11	40	1.68	0	1.84	40
IGFBP3	27.72	2.04	29.67	1.2	29.01	0.77	28.72	1.03	27.89
IRS1	26.61	2.56	29.04	1.08	28.3	0.74	28.45	0.72	27.11
ITGB1	18.53	3.96	21.93	0.85	20.61	0.87	20.79	0.84	19.66
KDR	38.12	1.81	40	4.11	38.42	1.68	40	1.84	38.39
LEF1	32.19	0.68	33.11	0.82	31.78	0.84	32.14	0.71	30.78
MCL1	22.44	0.93	23.94	0.75	22.2	1.02	22.08	1.21	21.48
MET	19.89	1.77	21.93	0.98	21.1	0.71	21.52	0.58	19.86
MSH2	21.94	1.51	23.59	1.09	21.94	1.4	22.01	1.46	21.68
MSH3	24.01	1.76	25.86	1.11	24.57	1.11	24.88	0.98	23.97
MTDH	21.59	1.52	23.33	1.04	21.85	1.18	21.66	1.47	21.34
MYC	20.91	1.71	22.65	1.16	21.16	1.33	21.15	1.47	20.83
NFKB1	25.92	1.03	27.24	0.94	26.04	0.88	26.05	0.96	25.11
NRAS	22.86	1.75	25.07	0.86	23.6	0.97	23.07	1.53	22.81
OPCML	40	1.81	40	4.11	40	1.68	39.5	1.84	40
PDGFRA	35.99	1.81	40	4.11	36.64	1.68	37.86	1.84	35.98
PIN1	22.96	1.2	25.05	0.64	24.19	0.48	23.71	0.72	22.37
PTEN	23.49	2.08	26.65	0.53	24.99	0.68	24.55	1.01	23.69
PTGS2	0	1.81	26.34	1663.49	0	1.68	0	1.84	0
PTK2	22.31	1.8	23.86	1.39	23.06	0.99	23.33	0.9	22.3
PYCARD	32.77	2.08	33.88	2.19	33.1	1.53	33.47	1.3	32.97
RAC1	19.95	1.86	22.5	0.72	20.83	0.94	20.6	1.2	19.99
RASSF1	26.53	1.94	28.71	0.97	28.12	0.6	28.51	0.5	26.63

Gene Symbol	Compared to Scrambled control								
	RBPJκ 1		RBPJκ 2		RBPJκ 3		Untransfected		Scrambled
	Ct	Fold Change	Ct	Fold Change	Ct	Fold Change	Ct	Fold Change	Ct
RHOA	21.11	1.27	23.06	0.75	21.59	0.84	20.53	1.93	20.6
RUNX3	30.26	1.33	32.15	0.81	31.07	0.7	30.96	0.83	29.81
SFRP2	36.7	1.81	40	4.11	33.18	5.92	37.88	1.84	36.54
SMAD4	23.84	1.6	25.92	0.86	25.11	0.61	24.7	0.89	23.66
SMAD7	29.46	1.51	31.02	1.16	29.81	1.1	30.59	0.7	29.2
SOCS1	30.53	1.68	31.85	1.53	31.76	0.66	31.47	0.89	30.42
SOCS3	23.92	1.8	25.13	1.77	24.92	0.83	25.26	0.72	23.91
STAT3	22.99	1.32	23.66	1.88	23.25	1.02	23	1.33	22.53
TCF4	23.63	1.1	24.74	1.16	23.83	0.89	23.53	1.19	22.91
TERT	28.67	1.91	29.67	2.17	30.24	0.6	30.14	0.7	28.75
TGFA	35.79	1.53	38.68	3.48	35.55	1.42	34.55	2.12	34.76
TGFB1	21.07	1.74	22.94	1.08	21.77	0.99	21.55	1.26	21.01
TGFBR2	21.82	1	23.08	0.95	22.17	0.72	22.26	0.75	20.96
TLR4	34.47	2.61	36.03	4.11	34.57	2.26	35.05	1.84	35.64
TNFRSF10B	24.75	1.84	26.38	1.35	25.79	0.83	26.66	0.5	24.77
TNFSF10	34.53	2.51	37.86	4.11	34.54	2.31	37.62	1.84	35.91
TP53	27.61	1.2	28.16	1.87	27.83	0.96	28.2	0.81	27.02
VEGFA	24.99	1.46	26.66	1.04	25.29	1.1	25.94	0.77	24.68
WT1	37.28	1.81	40	4.11	36.12	1.68	40	1.84	40
XIAP	24.89	1.75	27.07	0.88	25.73	0.91	25.71	1	24.84
YAP1	20.82	2.08	22.75	1.24	22.08	0.8	22.1	0.87	21.02

Appendix Table 4 *(Relating to Figure 7.7): Complete table of gene changes following silencing of NOTCH3 with siRNA in ICC cells.* CC-LP-1 cells transfected with siRNA against RBPJκ down-regulated a number of genes in response to transfection with 3 independent siRNA sequences.

Publications arising from this thesis

Published OnlineFirst December 5, 2013; DOI: 10.1158/0008-5472.CAN-13-1911

Cancer Research

Priority Report

Cell Lineage Tracing Reveals a Biliary Origin of Intrahepatic Cholangiocarcinoma

Rachel V. Guest[1], Luke Boulter[1,2], Timothy J. Kendall[2], Sarah E. Minnis-Lyons[1], Robert Walker[1], Stephen J. Wigmore[3], Owen J. Sansom[4], and Stuart J. Forbes[1]

Abstract

Intrahepatic cholangiocarcinoma is a treatment refractory malignancy with a high mortality and an increasing incidence worldwide. Recent studies have observed that activation of Notch and AKT signaling within mature hepatocytes is able to induce the formation of tumors displaying biliary lineage markers, thereby raising the suggestion that it is hepatocytes, rather than cholangiocytes or hepatic progenitor cells that represent the cell of origin of this tumor. Here, we use a cholangiocyte-lineage tracing system to target p53 loss to biliary epithelia and observe the appearance of labeled biliary lineage tumors in response to chronic injury. Consequent to this, upregulation of native functional Notch signaling is observed to occur spontaneously within cholangiocytes and hepatocytes in this model as well as in human intrahepatic cholangiocarcinoma. These data prove that in the context of chronic inflammation and p53 loss, frequent occurrences in human disease, biliary epithelia are a target of transformation and an origin of intrahepatic cholangiocarcinoma. *Cancer Res; 74(4); 1005–10. ©2013 AACR.*

Introduction

The unexplained increase in incidence of intrahepatic cholangiocarcinoma (1, 2), coupled with its poor response to chemotherapeutics and high mortality, necessitates a greater understanding of the biology of this aggressive malignancy, in which the cell of origin remains unclear. The historic assumption that these tumors arise from the oncogenic transformation of mature biliary epithelia has been based on a glandular histologic morphology, location within and adjacent to the biliary network, and expression of cholangiocyte-specific proteins, including mucin and biliary cytokeratins 7 and 19 (3). Substantive evidence for this origin, however, has been lacking. Patients with primary sclerosing cholangitis and liver fluke infection, diseases characterized by chronic biliary inflammation and epithelial proliferation, are up to 161 and 27 times more likely to develop biliary tract cancers compared with the general population (4, 5). Bipotential hepatic progenitor cells (HPC) have also been considered as a cellular source of intrahepatic cholangiocarcinoma in light of the existence of combined hepatocellular cholangiocarcinoma (6), tumors with features of both cholangiocarcinoma and hepatocellular carcinoma, as well as cholangiolocellular carcinoma, characterized by ductular reaction and cords resembling the Canals of Hering (7).

Interestingly, the incidence of intrahepatic cholangiocarcinoma is increased in chronic hepatocellular injury such as hepatitis C virus and heptatitis B virus (8) infection, indicating a more complex cellular origin of these cancers. Recent work has demonstrated that mature hepatocytes possess potential for transdifferentiation into intrahepatic cholangiocarcinoma, a phenomenon dependent on intracellular Notch signaling (9, 10). This concurs with the known role of Notch in the specification of hepatoblasts during ontogeny as well as observations that Notch is able to reprogram postnatal and terminally differentiated hepatocytes into biliary epithelia with the capacity to form ductular structures (11–13).

In recent fate-tracing experiments, chemically induced tumors were established in transgenic mice carrying an inducible heritable label for either hepatocyte (Alb-CreER^{T2}) or biliary (CK19-CreER^{T2}) lineages. Unexpectedly, in the absence of transgenic Notch overexpression, labeled neoplastic nodules positive for epithelial cell adhesion molecule were observed in tumors arising in Alb-CreER^{T2} but not CK19-CreER^{T2} animals, which suggested that intrahepatic cholangiocarcinoma arose from hepatocytes rather than cholangiocytes in that model (10). Given the unexpected nature of these findings within the clinical context of this disease and their implications for the development of future therapy, we set out to assess whether targeted loss of tumor suppressor function within cholangiocytes can precipitate intrahepatic cholangiocarcinoma formation using an independent transgenic strategy and, hence, whether biliary epithelia should still be considered a cell of origin of intrahepatic cholangiocarcinoma.

Authors' Affiliations: [1]MRC Centre for Regenerative Medicine; [2]Human Genetics Unit, University of Edinburgh; [3]Department of Surgery and Transplantation Medicine, Royal Infirmary of Edinburgh, Edinburgh; and [4]Beatson Institute for Cancer Research, Glasgow, Scotland, United Kingdom

Note: Supplementary data for this article are available at Cancer Research Online (http://cancerres.aacrjournals.org/).

Corresponding Author: Stuart J Forbes, MRC Centre for Regenerative Medicine, 5 Little France Drive, Edinburgh bioQuarter, Edinburgh EH16 4UU, Scotland, United Kingdom. Phone: 44-0131-6519-569; Fax: 44-0131-6519-501; E-mail: stuart.forbes@ed.ac.uk

doi: 10.1158/0008-5472.CAN-13-1911

Published OnlineFirst December 5, 2013; DOI: 10.1158/0008-5472.CAN-13-1911

Materials and Methods

Mice

CK19CreER^{T}R26ReYFP mice on a mixed genetic background (a kind gift from Guoqiang Gu, Vanderbilt University Medical Center, Nashville, TN) and Trp53^{tm1Brn} (The Jackson Laboratory) were used in this study.

Experimental protocol

For induction of Cre activity, 6-week-old CK19CreER^{T}eYFPp53$^{f/f}$ mice were administered three intraperitoneal injections of 4 mg tamoxifen (Sigma) reconstituted in olive oil (Sigma) at a concentration of 30 mg/mL on alternate days. Mice were harvested 72 hours following tamoxifen administration to assess efficiency of Cre recombination. A separate cohort went on to receive 600 mg/mL thioacetamide (TAA; Sigma) in drinking water for 26 weeks to induce tumor formation. To assess noncarcinogenic injury models, mice received 1 μL/g carbon tetrachloride (Sigma) or olive oil (Sigma) intraperitoneally for 16 weeks or 3,5-diethoxycarbonyl-1,4-dihydro-collidine (DDC; Sigma) diet (0.1% Purina 5015 Mouse chow) for 14 days.

Immunohistochemistry

Livers were fixed overnight in 4% aqueous buffered formalin, embedded in paraffin, and cut into 5-μm sections. The tissue underwent microwave antigen retrieval using Tris-EDTA with 0.1% Tween20 (Sigma) and blocked with H_20_2 and Protein Block (Invitrogen). Sections were incubated overnight with the following primary antibodies: GFP, CK19, Cyp2D6, Sox9 and Notch1 (Abcam), Nanog (eBiosciences), or Oct4 (Santa Cruz Biotechnology). After washing in PBS, the directly conjugated Alexa 488 and Alexa 555/564–conjugated secondary antibodies (Invitrogen) were used according to species with DAPI (4′,6-diamidino-2-phenylindole)-Fluoromount (SouthernBiotech). Day-8.5 mouse embryos and the murine epistem cell line C2 were used as positive controls for Oct4 and Nanog immunostaining.

Study approval

All animal experiments were approved by the University of Edinburgh animal ethics committee and conducted with the U.K. Home Office approval. Human specimens were collected prospectively from patients undergoing hepatic resection at the Royal Infirmary of Edinburgh with local ethical approval and informed patient consent.

Results and Discussion

Up to 26% of patients with intrahepatic cholangiocarcinoma carry mutations in the *TRP53* gene [up to 44.4% in fluke-associated intrahepatic cholangiocarcinoma (14)], primarily single-base substitutions at CpG sites, resulting in loss of tumor suppressor function (15). In our tamoxifen inducible experimental system, we have, therefore, targeted functional loss of p53 in CK19-expressing cells that are synchronously labeled with a Cre inducible eYFP reporter (CK19-CreERT; R26ReYFP;Trp53loxP), in which Cre recombination induces excision of exons 2 to 10 of the *Trp53* gene, and also the stop locus upstream of eYFP (Fig. 1A). In the healthy and injured mouse liver, CK19 expression is found on cholangiocytes lining medium and large-sized bile ducts as well as terminal ductules in the Canals of Hering, but not in hepatocytes (Fig. 1B). In the absence of Cre or tamoxifen, no eYFP expression was seen in either healthy or injured liver, but following induction with tamoxifen at 6 weeks old, eYFP positivity was observed in 14% of all cholangiocytes (Fig. 1C). No cell types other than biliary epithelia were labeled.

One week following Cre induction, mice were initiated on TAA to induce tumor formation (Fig. 2A; ref. 16). After 26 weeks, multifocal tumors were observed in the livers of CK19CreER^{T}eYFPp53$^{-/-}$ (80%) but not CK19CreER^{T}eYFPp53$^{+/-}$ (0%) or CK19CreER^{T}eYFPp53$^{+/+}$ (0%) animals (Fig. 2B). eYFP positivity was observed in all histologically identified neoplastic nodules, and this colocalized with expression of the ductular markers CK19 and Sox9. No cells were dually positive for eYFP and the mature hepatocyte marker Cyp2D6 (Fig. 2C).

In light of the emerging role for Notch in driving cholangiocarcinogenesis, we then looked to identify the cellular expression of the Notch 1 receptor within this model. Membranous and nuclear positivity of activated Notch1 was observed widely in the epithelium of the malignant ducts and frequently colocalized with eYFP staining (Fig. 3A). Interestingly, positivity was also seen to occur within nuclei of hepatocytes, particularly those located adjacent to the cancerous stroma (Fig. 3B). We went on to assess whether Notch1 was also expressed in nonmalignant models of liver injury and observed strong ductular positivity in the context of the DDC biliary injury dietary model, but none during chronic hepatocyte regeneration with carbon tetrachloride or in the uninjured mouse liver (Fig. 3C). Furthermore, this pattern of Notch activity is recapitulated in human resected intrahepatic cholangiocarcinoma specimens, in which the strongest positivity is observed within malignant ducts, as well as in hepatocytes adjacent to the invasive front of the tumors (Fig. 3D). Hepatic lineage-tracing experiments have proved problematic; indeed the CK19CreER^{T}R26R^{YFP} mouse has hitherto not been widely adopted for cell-specific gene deletion experiments due to poor efficiency. p53 deletion at the point of tamoxifen administration does not result in increased labeling efficiency, but is likely to cause a preferential expansion of the eYFP^{+} compartment in response to TAA-induced injury, making it more probable that a transforming event will occur in this population of cells compared with labeled cells in a similar fate-tracing system without p53 deletion. We believe this to be a robust and representative model of biliary carcinogenesis, given the frequent combination of p53 loss and chronic biliary inflammation observed in human disease. eYFP positivity was observed in all animals in which tumors arose as well as in each and every focus of malignancy. We observed colocalization between eYFP and the M3 acetylcholine receptor, a marker of mature cholangiocytes, occasional colocalization with CD44 and no colocalization with the stem cell markers Nanog and Oct 4 (17; Supplementary Fig. S1). A likely cell of origin is, therefore, the mature cholangiocyte, although we cannot eliminate the possibility of stem cells, progenitors or

Published OnlineFirst December 5, 2013; DOI: 10.1158/0008-5472.CAN-13-1911

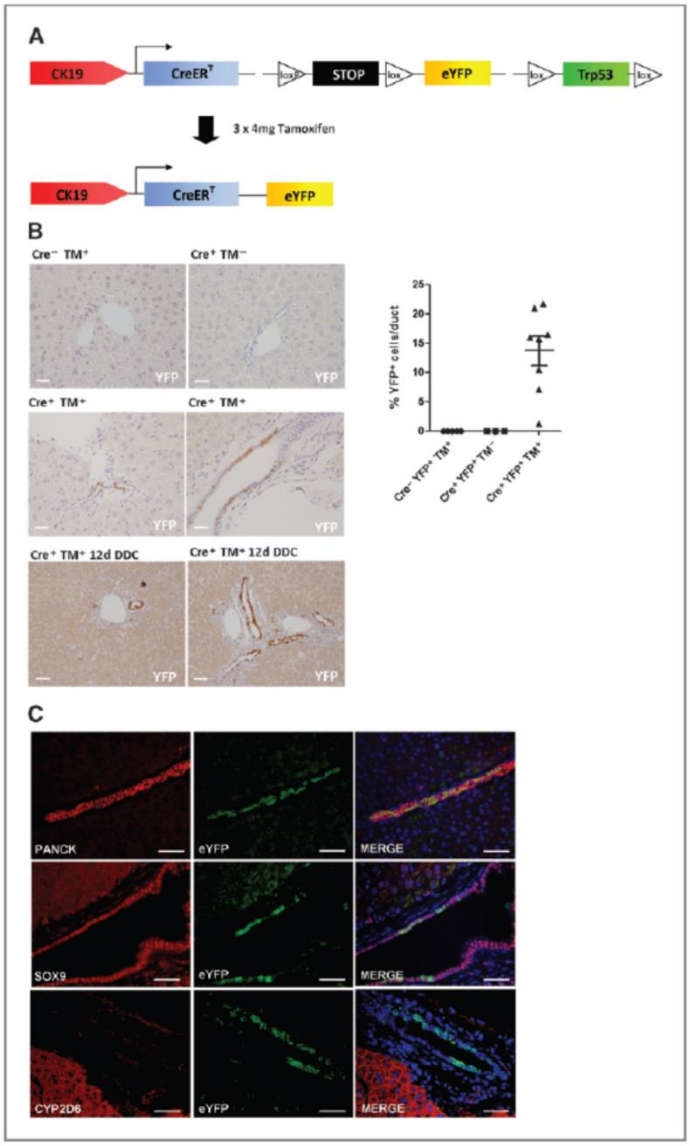

Figure 1. Transgenic system of tamoxifen-inducible, Cre-mediated cell tracking with Trp53 deletion in CK19CreER^T eYFP^{R26}p53f/f mice. A, transgenic construct of fluorescent labeling and tumor suppressor deletion in CK19$^+$ cells in response to tamoxifen in 6-week-old mice. B, in the presence of Cre and tamoxifen (TM), eYFP activity is seen within small ductules as well as large bile ducts. The eYFP$^+$ population expands following 14 days of dietary DDC; scale bars, 50 μm. Quantitative analysis of Cre efficiency 72 hours post injection in Cre$^-$ mice exposed to tamoxifen ($n = 5$), Cre$^+$ mice without tamoxifen ($n = 3$), and Cre$^+$ mice exposed to tamoxifen ($n = 8$). C, following tamoxifen injection, eYFP positivity is seen only in CK19-expressing cells. These are cholangiocytes that also express the biliary markers Sox9. No colocalization is seen with the mature hepatocyte marker Cyp2D6; scale bars, 50 μm.

intermediates as targets of transformation. Interestingly, given the lineage-tracing system used here, these would be CK19$^+$ cells. Given the CK19CreER^{T}R26R^{YFP} mouse has not hitherto exhibited lineage labeling of hepatocytes, we can conclude that the eYFP$^+$ tumor cells here, arise from cholangiocytes rather than hepatocytes. It is unclear why

Published OnlineFirst December 5, 2013; DOI: 10.1158/0008-5472.CAN-13-1911

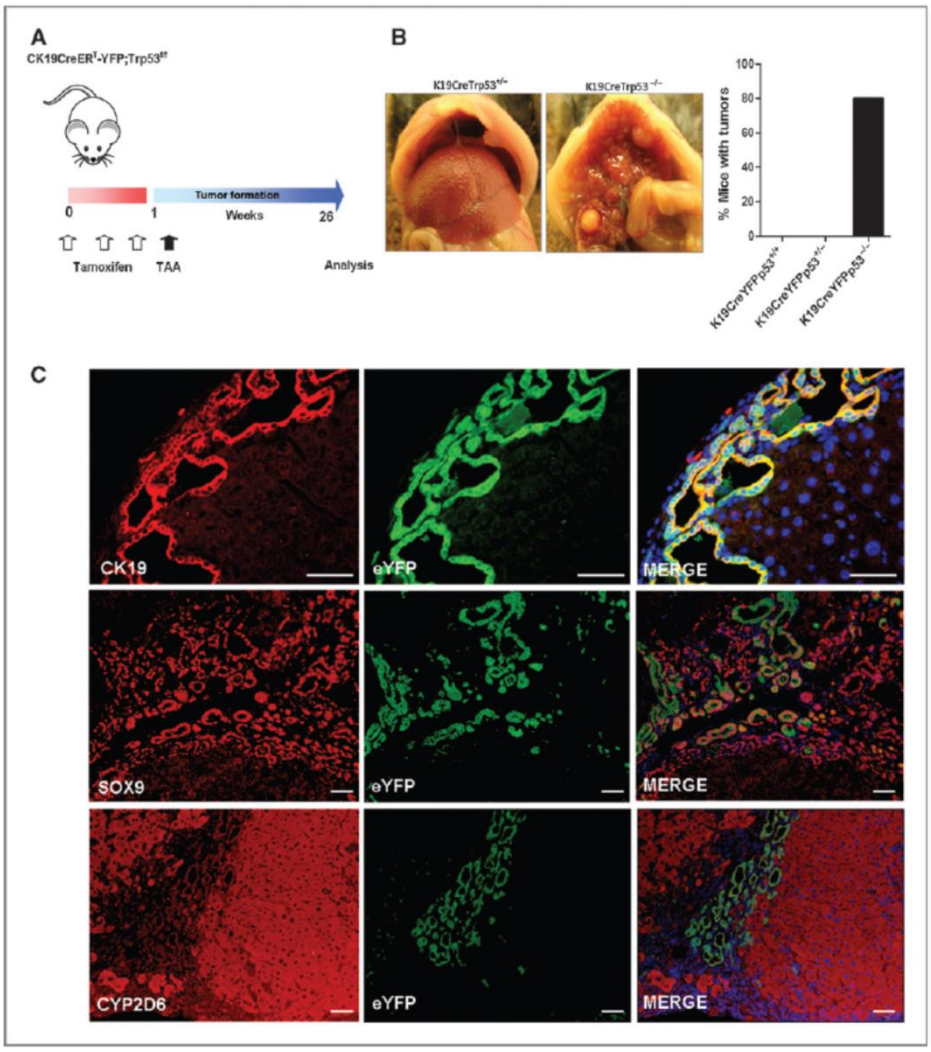

Figure 2. Intrahepatic cholangiocarcinoma is derived from CK19$^+$ cholangiocytes. A, experimental strategy of tamoxifen induction in CK19CreER^T eYFP^{R26}p53$^{f/f}$ mice followed by oral administration of 600 mg/mL TAA for 26 weeks. B, multifocal tumors developed only in CK19CreER^{T}eYFPp53$^{-/-}$ (homozygous for p53 deletion; $n = 5$) and not CK19CreER^{T}eYFP^{R26}p53$^{+/-}$ ($n = 14$) or CK19CreER^{T}eYFP^{R26}p53$^{+/+}$ ($n = 5$) animals, and only following TAA administration. C, coimmunofluorescent staining of eYFP with the biliary lineage markers CK19 and Sox9. All eYFP$^+$ cells were seen to be CK19$^+$. eYFP positivity did not overlap with the mature hepatocyte marker Cyp2D6. Nuclei are stained with DAPI; scale bars, 50 μm.

labeled tumors were not observed after 30 weeks of TAA administration in the CK19CreER^{T2}R26R^{YFP} system published by Sekiya and colleagues; however, our data clearly and definitively attest that biliary epithelia can be a cell of origin of intrahepatic cholangiocarcinoma in an independent CK19-based transgenic system.

Published OnlineFirst December 5, 2013; DOI: 10.1158/0008-5472.CAN-13-1911

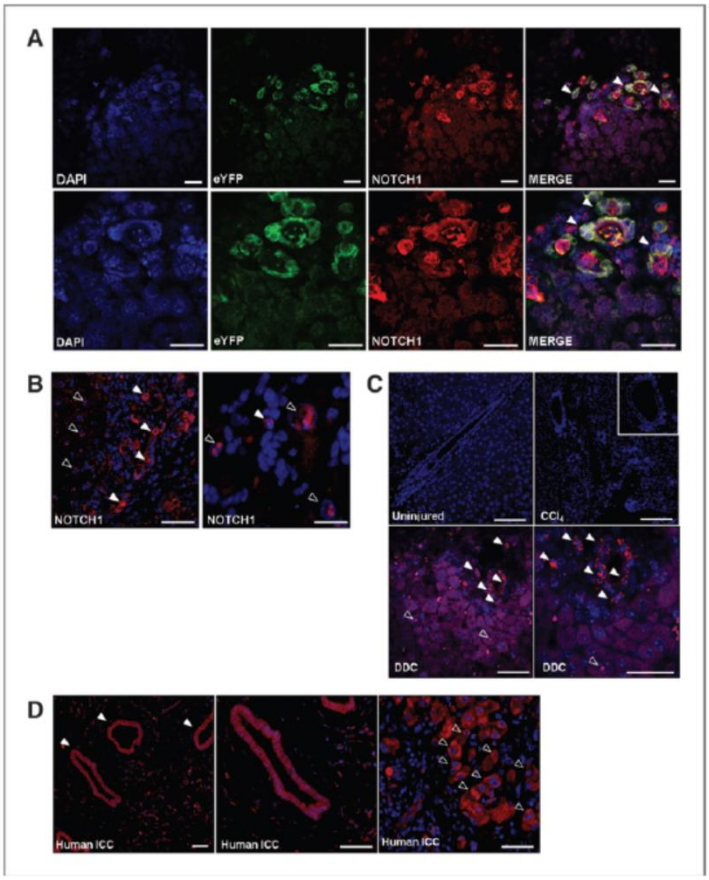

Figure 3. Native Notch signaling is activated in intrahepatic cholangiocarcinoma (ICC). A, immunofluorescent staining of activated Notch1 in the membranes of malignant ductules of TAA-induced intrahepatic cholangiocarcinoma in CK19CreER^{T}eYFPp53$^{-/-}$ mice frequently colocalizes with eYFP positivity (filled arrowheads; scale bars, 50 μm). B, immunostaining of activated Notch1 within nuclei of peritumoral hepatocytes [open arrowheads; scale bars, 50 μm and 125 μm (second photomicrograph taken under oil)]. C, activated Notch1 immunostaining in uninjured mouse liver; CCl_4 induced fibrosis (16 weeks) and DDC diet; scale bars, 50 μm). D, activated Notch1 immunostaining in human intrahepatic cholangiocarcinoma specimens. Staining in malignant biliary epithelia (filled arrowheads) and peritumoral hepatocytes (open arrowheads); scale bars, 50 μm.

Primary liver cancers are a phenotypically and molecularly heterogeneous group of malignancies without a stereotypical mutational signature. It has been suggested that such heterogeneity reflects in part the diversity of the underlying cells of origin (17), although this remains unproved. What is evident, however, is the plasticity of hepatic lineages. Following oncogenic transduction, mature hepatocytes, HPCs, and hepatoblasts all have potential for reprogramming into tumor-initiating cells with acquisition of CD133^{+} expression, side population fractions as well as tumor-forming and metastatic capacity (18). Cellular differentiation seems to trigger distinct transcriptional programs in response to the same oncogenic stimulus; however, all transduced cells independent of origin, are able to form tumors of multiple lineages.

Our data support the published evidence for Notch as driver of biliary oncogenesis (19) by demonstrating active signaling within the ductular epithelium in intrahepatic cholangiocarcinoma in both human and mouse. The observation of strong Notch1 intracellular domain expression within hepatocyte nuclei adjacent to the desmoplastic stroma substantiates previous experiments that have shown Notch1 activation within these cells acts as a transdifferentiating factor (9, 10). Moreover, this model of reprogramming is further strengthened by the capacity of constitutively activated Notch2 in albumin-expressing cells to induce intrahepatic cholangiocarcinoma formation and accelerate DEN-induced hepatocellular carcinoma, which is less differentiated than wild-type controls (20). This Notch high state, able to prime the peritumoral parenchyma for transdifferentiation, has significant therapeutic implications for the many patients who develop intrahepatic cholangiocarcinoma on a background of chronic hepatocellular injury (8). We believe that these findings unify and

Published OnlineFirst December 5, 2013; DOI: 10.1158/0008-5472.CAN-13-1911

clarify previous reports and explain how chronic biliary damage can lead to cholangiocarcinoma arising from biliary epithelium. In conclusion, we have definitively shown that even in the absence of transgenic Notch activation, intrahepatic cholangiocarcinoma can arise from the biliary epithelia. Future therapeutic strategies should target the Notch pathway as a driver of tumorigenesis in this aggressive malignancy.

Disclosure of Potential Conflicts of Interest

No potential conflicts of interest were disclosed.

Authors' Contributions

Conception and design: R.V. Guest, L. Boulter, S.E. Minnis-Lyons, S.J. Wigmore, O.J. Sansom, S.J. Forbes
Development of methodology: R.V. Guest
Acquisition of data (provided animals, acquired and managed patients, provided facilities, etc.): R.V. Guest, T.J. Kendall, R. Walker, S.J. Wigmore
Analysis and interpretation of data (e.g., statistical analysis, biostatistics, computational analysis): R.V. Guest, L. Boulter, T.J. Kendall, S.J. Wigmore, S.J. Forbes
Writing, review, and/or revision of the manuscript: R.V. Guest, L. Boulter, S.E. Minnis-Lyons, S.J. Wigmore, S.J. Forbes
Administrative, technical, or material support (i.e., reporting or organizing data, constructing databases): R. Walker, S.J. Wigmore
Study supervision: S.J. Wigmore, S.J. Forbes

Acknowledgments

The authors thank Guoqiang Gu, Vanderbilt University Medical Center, Nashville, TN for the provision of mice.

Grant Support

This work was supported by the MRC Centre for Regenerative Medicine, University of Edinburgh, United Kingdom. Funding was provided by the Wellcome Trust, the Medical Research Council, and Cancer Research UK. R.V. Guest is supported by a Wellcome Trust Clinical Research Training Fellowship; L. Boulter is supported by a Cancer Research UK project grant and an MRC research grant; T.J. Kendall is supported by a Wellcome Trust Intermediate Clinical Fellowship; S.E. Minnis-Lyons is supported by an MRC Scottish Clinical Pathology Fellowship; R. Walker is supported by a Cancer Research UK project grant; S.J. Wigmore is supported by the Scottish Higher Education Funding Council; O.J. Sansom is supported by Cancer Research UK and the European Research Council; and S.J. Forbes is supported by the MRC and a Cancer Research UK project grant.

Received July 9, 2013; revised October 31, 2013; accepted November 20, 2013; published OnlineFirst December 5, 2013.

References

1. Taylor-Robinson SD, Toledano MB, Arora S, Keegan TJ, Hargreaves S, Beck A, Khan SA, et al. Increase in mortality rates from intrahepatic cholangiocarcinoma in England and Wales 1968–1998. Gut 2001;48:816–20.
2. Witjes CDM, Karim-Kos HE, Visser O, de Vries E, Ijzermans JNM, de Man RA, et al. Intrahepatic cholangiocarcinoma in a low endemic area: rising incidence and improved survival. HPB 2012;14:777–81.
3. Ishak KG, Anthony PP, Sobin LH. Histological typing of tumours of the liver. WHO International Classification of Tumours. Berlin: Springer Verlag; 1994.
4. Bergquist A, Ekbom A, Olsson R, Kornfeldt D, Loof L, Danielsson A, et al. Hepatic and extrahepatic malignancies in primary sclerosing cholangitis. J Hepatol 2002;36:321–7.
5. Sripa B, Kaewkes S, Sithithaworn P, Mairiang E, Laha T, Smout M, et al. Liver fluke induces cholangiocarcinoma. PloS Med 2007;4:e201.
6. Goodman ZD, Ishak KG, Langloss JM, Sesterhenn IA, Rabin L. Combined hepatocellular-cholangiocarcinoma. A histologic and immunohistochemical study. Cancer 1985;55:124–35.
7. Komuta M, Spee B, Vander Borght S, De Vos R, Verslype C, Aerts R, et al. Clinicopathological study on cholangiolocellular carcinoma suggesting hepatic progenitor cell origin. Hepatology 2008;47:1544–56.
8. Palmer WC, Patel T. Are common factors involved in the pathogenesis of primary liver cancers? A meta-analysis of risk factors for intrahepatic cholangiocarcinoma. J Hepatol 2012;57:69–76.
9. Fan B, Malato Y, Calvisi DF, Naqvi S, Razumilava N, Ribback S, et al. Cholangiocarcinomas can originate from hepatocytes in mice. J Clin Investig 2012;122:2911–5.
10. Sekiya S, Suzuki A. Intrahepatic cholangiocarcinoma can arise from Notch-mediated conversion of hepatocytes. J Clin Investig 2012;122:3914–8.
11. Zong Y, Panikkar A, Xu J, Antoniou A, Raynaud P, Lemaigre F, et al. Notch signaling controls liver development by regulating biliary differentiation. Development 2009;136:1727–39.
12. Yanger K, Zong Y, Maggs LR, Shapira SN, Maddipati R, Aiello NM, et al. Robust cellular reprogramming occurs spontaneously during liver regeneration. Genes Dev 2013;27:719–24.
13. Boulter L, Govaere O, Bird TG, Radulescu S, Aucott RL, Van Rooijen N, et al. Macrophage derived Wnt signalling opposes Notch signalling in a NUMB mediated manner to specify HPC fate in chronic liver disease in liver and mouse. Nat Med 2012;18:572–9.
14. Ong CK, Subimerb C, Pairojkul C, Wongkham S, Cutcutache I, Yu W, et al. Exome sequencing of liver fluke-associated cholangiocarcinoma. Nat Genet 2012;44:690–3.
15. Khan SA, Thomas HC, Toledano MB, Cox IJ, Taylor-Robinson SD. p53 Mutations in human cholangiocarcinoma: a review. Liver Int 2005;25:704–16.
16. Yeh C-N, Maitra A, Lee K-F, Jan Y-Y, Chen M-F. Thioacetamide-induced intestinal-type cholangiocarcinoma in rat: an animal model recapitulating the multi-stage progression of human cholangiocarcinoma. Carcinogenesis 2004;25:631–6.
17. Komuta M, Govaere O, Vandecaveye V, Akiba J, Van Steenbergen W, Verslype C, et al. Histological diversity in cholangiocellular carcinoma reflects the different cholangiocyte phenotypes. Hepatology 2012;55:1876–88.
18. Holczbauer A, Factor VM, Andersen JB, Marquardt JU, Kleiner D, Raggi C, et al. Modeling pathogenesis of primary liver cancer in lineage-specific mouse cell types. Gastroenterology 2013;145:221–31.
19. Zender S, Nickeleit I, Wuestefeld T, Sorensen I, Dauch D, Bozko P, et al. A critical role for notch signaling in the formation of cholangiocellular carcinomas. Cancer Cell 2013;23:784–95.
20. Dill MT, Tornillo L, Fritzius T, Terracciano L, Semela D, Bettler B, et al. Constitutive notch2 signaling induces hepatic tumors in mice. Hepatology 2013;57:1607–19.

BIBLIOGRAPHY

1. Blechacz, B.R., Sanchez, W., and Gores, G.J. 2009. A conceptual proposal for staging ductal cholangiocarcinoma. *Curr Opin Gastroenterol* 25:238-239.
2. Nakeeb, A., Pitt, H.A., Sohn, T.A., Coleman, J., Abrams, R.A., Piantadosi, S., Hruban, R.H., Lillemoe, K.D., Yeo, C.J., and Cameron, J.L. 1996. Cholangiocarcinoma. A spectrum of intrahepatic, perihilar, and distal tumors. *Ann Surg* 224:463-473; discussion 473-465.
3. Klatskin, G. 1965. Adenocarcinoma of the Hepatic Duct at Its Bifurcation within the Porta Hepatis. An Unusual Tumor with Distinctive Clinical and Pathological Features. *Am J Med* 38:241-256.
4. Khan, S.A., Emadossadaty, S., Ladep, N.G., Thomas, H.C., Elliott, P., Taylor-Robinson, S.D., and Toledano, M.B. 2012. Rising trends in cholangiocarcinoma: is the ICD classification system misleading us? *J Hepatol* 56:848-854.
5. Komuta, M., Govaere, O., Vandecaveye, V., Akiba, J., Van Steenbergen, W., Verslype, C., Laleman, W., Pirenne, J., Aerts, R., Yano, H., et al. 2012. Histological diversity in cholangiocellular carcinoma reflects the different cholangiocyte phenotypes. *Hepatology* 55:1876-1888.
6. Vauthey, J.N., and Blumgart, L.H. 1994. Recent advances in the management of cholangiocarcinomas. *Semin Liver Dis* 14:109-114.
7. Shaib, Y.H., Davila, J.A., McGlynn, K., and El-Serag, H.B. 2004. Rising incidence of intrahepatic cholangiocarcinoma in the United States: a true increase? *J Hepatol* 40:472-477.
8. Vatanasapt, V., Martin, N., Sriplung, H., Chindavijak, K., Sontipong, S., Sriamporn, H., Parkin, D.M., and Ferlay, J. 1995. Cancer incidence in Thailand, 1988-1991. *Cancer Epidemiol Biomarkers Prev* 4:475-483.
9. Khan SA, T.-R.S., Toledano MB, Beck A, Elliott P, Thomas HC. 2002. Changing international trends in mortality rates for liver, biliary and pancreatic tumours. *Journal of Hepatology* 37:806-813.

10. Bertuccio, P., Bosetti, C., Levi, F., Decarli, A., Negri, E., and La Vecchia, C. 2013. A comparison of trends in mortality from primary liver cancer and intrahepatic cholangiocarcinoma in Europe. *Ann Oncol* 24:1667-1674.

11. Witjes CDM, K.-K.H., Visser O, de Vries E, Ijzermans JNM, de Man RA, Coebergh JWW, Verhoed C. 2012. Intrahepatic cholangiocarcinoma in a low endemic area: rising incidence and improved survival. *HPB* 14:777-781.

12. Taylor-Robinson SD, T.M., Arora S, Keegan TJ, Hargreaves S, Beck A, Khan SA, Elliott P, Thomas HC. 2001. Increase in mortality rates from intrahepatic cholangiocarcinoma in England and Wales 1968-1998. *Gut* 48:816-820.

13. Khan, S.A., Thomas, H.C., Davidson, B.R., and Taylor-Robinson, S.D. 2005. Cholangiocarcinoma. *Lancet* 366:1303-1314.

14. Patel, T. 2001. Increasing incidence and mortality of primary intrahepatic cholangiocarcinoma in the United States. *Hepatology* 33:1353-1357.

15. Patel, T. 2002. Worldwide trends in mortality from biliary tract malignancies. *BMC Cancer* 2:10.

16. Shaib YH, D.J., Henderson L, McGlynn KA, El-Serag HB. 2007. Endoscopic and surgical therapy for intrahepatic cholangiocarcinoma in the united states: a population-based study. *Journal of Clinical Gastroenterology* 41:911-917.

17. Valle, J., Wasan, H., Palmer, D.H., Cunningham, D., Anthoney, A., Maraveyas, A., Madhusudan, S., Iveson, T., Hughes, S., Pereira, S.P., et al. 2010. Cisplatin plus gemcitabine versus gemcitabine for biliary tract cancer. *N Engl J Med* 362:1273-1281.

18. Broome, U., Olsson, R., Loof, L., Bodemar, G., Hultcrantz, R., Danielsson, A., Prytz, H., Sandberg-Gertzen, H., Wallerstedt, S., and Lindberg, G. 1996. Natural history and prognostic factors in 305 Swedish patients with primary sclerosing cholangitis. *Gut* 38:610-615.

19. Pitt, H.A., Dooley, W.C., Yeo, C.J., and Cameron, J.L. 1995. Malignancies of the biliary tree. *Curr Probl Surg* 32:1-90.

20. Kubo, S., Kinoshita, H., Hirohashi, K., and Hamba, H. 1995. Hepatolithiasis associated with cholangiocarcinoma. *World J Surg* 19:637-641.

21. Sripa B, K.S., Sithithaworn P, Mairiang E, laha T, Smout M, Pairojkul C, Bhudhisawasdi V, Tesana S, Thinkamrop B, Bethony JM, Loukas A, Brindley P. 2007. Liver fluke induces cholangiocarcinoma. *Plos Medicine* 4:e201.

22. Hakamada, K., Sasaki, M., Endoh, M., Itoh, T., Morita, T., and Konn, M. 1997. Late development of bile duct cancer after sphincteroplasty: a ten- to twenty-two-year follow-up study. *Surgery* 121:488-492.

23. Tanaka, K., Ikoma, A., Hamada, N., Nishida, S., Kadono, J., and Taira, A. 1998. Biliary tract cancer accompanied by anomalous junction of pancreaticobiliary ductal system in adults. *Am J Surg* 175:218-220.

24. Palmer, W.C., and Patel, T. 2012. Are common factors involved in the pathogenesis of primary liver cancers? A meta-analysis of risk factors for intrahepatic cholangiocarcinoma. *J Hepatol* 57:69-76.

25. Kobayashi, M., Ikeda, K., Saitoh, S., Suzuki, F., Tsubota, A., Suzuki, Y., Arase, Y., Murashima, N., Chayama, K., and Kumada, H. 2000. Incidence of primary cholangiocellular carcinoma of the liver in japanese patients with hepatitis C virus-related cirrhosis. *Cancer* 88:2471-2477.

26. Claessen, M.M., Vleggaar, F.P., Tytgat, K.M., Siersema, P.D., and van Buuren, H.R. 2009. High lifetime risk of cancer in primary sclerosing cholangitis. *J Hepatol* 50:158-164.

27. Kuper, H., Ye, W., Broome, U., Romelsjo, A., Mucci, L.A., Ekbom, A., Adami, H.O., Trichopoulos, D., and Nyren, O. 2001. The risk of liver and bile duct cancer in patients with chronic viral hepatitis, alcoholism, or cirrhosis. *Hepatology* 34:714-718.

28. Shaib, Y.H., Davila, J.A., Henderson, L., McGlynn, K.A., and El-Serag, H.B. 2007. Endoscopic and surgical therapy for intrahepatic cholangiocarcinoma in the united states: a population-based study. *J Clin Gastroenterol* 41:911-917.

29. Bismuth, H., Nakache, R., and Diamond, T. 1992. Management strategies in resection for hilar cholangiocarcinoma. *Ann Surg* 215:31-38.

30. Greene FL, P.D., Fleming ID, Fritz AG, Balch CM, Haller DG, Morrow M, editor. 2002. *AJCC cancer staging manual*. Berlin Heidelberg New York: Springer.

31. Jarnagin, W.R., Fong, Y., DeMatteo, R.P., Gonen, M., Burke, E.C., Bodniewicz, B.J., Youssef, B.M., Klimstra, D., and Blumgart, L.H. 2001. Staging, resectability, and outcome in 225 patients with hilar cholangiocarcinoma. *Ann Surg* 234:507-517; discussion 517-509.

32. Burke, E.C., Jarnagin, W.R., Hochwald, S.N., Pisters, P.W., Fong, Y., and Blumgart, L.H. 1998. Hilar Cholangiocarcinoma: patterns of spread, the importance of hepatic resection for curative operation, and a presurgical clinical staging system. *Ann Surg* 228:385-394.

33. Jarnagin, W.R., Bowne, W., Klimstra, D.S., Ben-Porat, L., Roggin, K., Cymes, K., Fong, Y., DeMatteo, R.P., D'Angelica, M., Koea, J., et al. 2005. Papillary phenotype confers improved survival after resection of hilar cholangiocarcinoma. *Ann Surg* 241:703-712; discussion 712-704.

34. Takada, T., Amano, H., Yasuda, H., Nimura, Y., Matsushiro, T., Kato, H., Nagakawa, T., and Nakayama, T. 2002. Is postoperative adjuvant chemotherapy useful for gallbladder carcinoma? A phase III multicenter prospective randomized controlled trial in patients with resected pancreaticobiliary carcinoma. *Cancer* 95:1685-1695.

35. Gores, G.J., Darwish Murad, S., Heimbach, J.K., and Rosen, C.B. 2013. Liver transplantation for perihilar cholangiocarcinoma. *Dig Dis* 31:126-129.

36. Darwish Murad, S., Kim, W.R., Therneau, T., Gores, G.J., Rosen, C.B., Martenson, J.A., Alberts, S.R., and Heimbach, J.K. 2012. Predictors of pretransplant dropout and posttransplant recurrence in patients with perihilar cholangiocarcinoma. *Hepatology* 56:972-981.

37. Duignan, S., Maguire, D., Ravichand, C.S., Geoghegan, J., Hoti, E., Fennelly, D., Armstrong, J., Rock, K., Mohan, H., and Traynor, O. 2014. Neoadjuvant chemoradiotherapy followed by liver transplantation for unresectable

cholangiocarcinoma: a single-centre national experience. *HPB (Oxford)* 16:91-98.

38. Glimelius, B., Hoffman, K., Sjoden, P.O., Jacobsson, G., Sellstrom, H., Enander, L.K., Linne, T., and Svensson, C. 1996. Chemotherapy improves survival and quality of life in advanced pancreatic and biliary cancer. *Ann Oncol* 7:593-600.

39. Rao, S., Cunningham, D., Hawkins, R.E., Hill, M.E., Smith, D., Daniel, F., Ross, P.J., Oates, J., and Norman, A.R. 2005. Phase III study of 5FU, etoposide and leucovorin (FELV) compared to epirubicin, cisplatin and 5FU (ECF) in previously untreated patients with advanced biliary cancer. *Br J Cancer* 92:1650-1654.

40. Ducreux, M., Van Cutsem, E., Van Laethem, J.L., Gress, T.M., Jeziorski, K., Rougier, P., Wagener, T., Anak, O., Baron, B., and Nordlinger, B. 2005. A randomised phase II trial of weekly high-dose 5-fluorouracil with and without folinic acid and cisplatin in patients with advanced biliary tract carcinoma: results of the 40955 EORTC trial. *Eur J Cancer* 41:398-403.

41. Gebbia, V., Giuliani, F., Maiello, E., Colucci, G., Verderame, F., Borsellino, N., Mauceri, G., Caruso, M., Tirrito, M.L., and Valdesi, M. 2001. Treatment of inoperable and/or metastatic biliary tree carcinomas with single-agent gemcitabine or in combination with levofolinic acid and infusional fluorouracil: results of a multicenter phase II study. *J Clin Oncol* 19:4089-4091.

42. Lee, J., Park, S.H., Chang, H.M., Kim, J.S., Choi, H.J., Lee, M.A., Jang, J.S., Jeung, H.C., Kang, J.H., Lee, H.W., et al. 2012. Gemcitabine and oxaliplatin with or without erlotinib in advanced biliary-tract cancer: a multicentre, open-label, randomised, phase 3 study. *Lancet Oncol* 13:181-188.

43. Sohal, D.P., Mykulowycz, K., Uehara, T., Teitelbaum, U.R., Damjanov, N., Giantonio, B.J., Carberry, M., Wissel, P., Jacobs-Small, M., O'Dwyer, P.J., et al. 2013. A phase II trial of gemcitabine, irinotecan and panitumumab in advanced cholangiocarcinoma. *Ann Oncol* 24:3061-3065.

44. Borad, M.J., Champion, M.D., Egan, J.B., Liang, W.S., Fonseca, R., Bryce, A.H., McCullough, A.E., Barrett, M.T., Hunt, K., Patel, M.D., et al. 2014. Integrated genomic characterization reveals novel, therapeutically relevant drug targets in FGFR and EGFR pathways in sporadic intrahepatic cholangiocarcinoma. *PLoS Genet* 10:e1004135.

45. Lubner, S.J., Mahoney, M.R., Kolesar, J.L., Loconte, N.K., Kim, G.P., Pitot, H.C., Philip, P.A., Picus, J., Yong, W.P., Horvath, L., et al. 2010. Report of a multicenter phase II trial testing a combination of biweekly bevacizumab and daily erlotinib in patients with unresectable biliary cancer: a phase II Consortium study. *J Clin Oncol* 28:3491-3497.

46. Bowling, T.E., Galbraith, S.M., Hatfield, A.R., Solano, J., and Spittle, M.F. 1996. A retrospective comparison of endoscopic stenting alone with stenting and radiotherapy in non-resectable cholangiocarcinoma. *Gut* 39:852-855.

47. Ong CK, S.C., Pairojkul, Wongkham S, Cutcutache I, Yu W, McPherson JR, Allen GE, Ng CCY, Wong BH, Myint SS, Rajasegaran V, Heng HL, Gan A, Zang ZJ, Wu Y, Wu J, Lee MH, Huang D, Ong P, Chan-on W, Cao Y, Qian C-N, Lim KH, Ooi A, Dykema K, Furge K, Kukongviriyapan V, Sripa B, Wongkham C, Yongvanit P, Futreal PA, Bhudhisawasdi V, Rozen S, Tan P, Teh BT. 2012. Exome sequencing of liver fluke-associated cholangiocarcinoma. *Nature Genetics* 44:690-693.

48. Chan-On, W., Nairismagi, M.L., Ong, C.K., Lim, W.K., Dima, S., Pairojkul, C., Lim, K.H., McPherson, J.R., Cutcutache, I., Heng, H.L., et al. 2013. Exome sequencing identifies distinct mutational patterns in liver fluke-related and non-infection-related bile duct cancers. *Nat Genet* 45:1474-1478.

49. Sia, D., Hoshida, Y., Villanueva, A., Roayaie, S., Ferrer, J., Tabak, B., Peix, J., Sole, M., Tovar, V., Alsinet, C., et al. 2013. Integrative molecular analysis of intrahepatic cholangiocarcinoma reveals 2 classes that have different outcomes. *Gastroenterology* 144:829-840.

50. Andersen JB, S.B., Blechacz BR, Avital I, Komuta M, Barbour A, Conner EA, Gillen MC, Roskams T, Roberts LR, Factor VM, Thorgiersson S. 2012.

Genomic and genetic characterization of cholangiocarcinoma identifies therapeutic targets for tyrosine kinase inhibitors. *Gastroenterology* 142:1021-1031.

51. Robertson, S., Hyder, O., Dodson, R., Nayar, S.K., Poling, J., Beierl, K., Eshleman, J.R., Lin, M.T., Pawlik, T.M., and Anders, R.A. 2013. The frequency of KRAS and BRAF mutations in intrahepatic cholangiocarcinomas and their correlation with clinical outcome. *Hum Pathol* 44:2768-2773.
52. Voss, J.S., Holtegaard, L.M., Kerr, S.E., Fritcher, E.G., Roberts, L.R., Gores, G.J., Zhang, J., Highsmith, W.E., Halling, K.C., and Kipp, B.R. 2013. Molecular profiling of cholangiocarcinoma shows potential for targeted therapy treatment decisions. *Hum Pathol* 44:1216-1222.
53. Borger, D.R., Tanabe, K.K., Fan, K.C., Lopez, H.U., Fantin, V.R., Straley, K.S., Schenkein, D.P., Hezel, A.F., Ancukiewicz, M., Liebman, H.M., et al. 2012. Frequent mutation of isocitrate dehydrogenase (IDH)1 and IDH2 in cholangiocarcinoma identified through broad-based tumor genotyping. *Oncologist* 17:72-79.
54. Wang, P., Dong, Q., Zhang, C., Kuan, P.F., Liu, Y., Jeck, W.R., Andersen, J.B., Jiang, W., Savich, G.L., Tan, T.X., et al. 2013. Mutations in isocitrate dehydrogenase 1 and 2 occur frequently in intrahepatic cholangiocarcinomas and share hypermethylation targets with glioblastomas. *Oncogene* 32:3091-3100.
55. Kipp, B.R., Voss, J.S., Kerr, S.E., Barr Fritcher, E.G., Graham, R.P., Zhang, L., Highsmith, W.E., Zhang, J., Roberts, L.R., Gores, G.J., et al. 2012. Isocitrate dehydrogenase 1 and 2 mutations in cholangiocarcinoma. *Hum Pathol* 43:1552-1558.
56. Goeppert, B., Konermann, C., Schmidt, C.R., Bogatyrova, O., Geiselhart, L., Ernst, C., Gu, L., Becker, N., Zucknick, M., Mehrabi, A., et al. 2013. Global alterations of DNA methylation in cholangiocarcinoma targets the Wnt signaling pathway. *Hepatology*.

57. Kajiyama, K., Maeda, T., Takenaka, K., Sugimachi, K., and Tsuneyoshi, M. 1999. The significance of stromal desmoplasia in intrahepatic cholangiocarcinoma: a special reference of 'scirrhous-type' and 'nonscirrhous-type' growth. *Am J Surg Pathol* 23:892-902.

58. Chuaysri, C., Thuwajit, P., Paupairoj, A., Chau-In, S., Suthiphongchai, T., and Thuwajit, C. 2009. Alpha-smooth muscle actin-positive fibroblasts promote biliary cell proliferation and correlate with poor survival in cholangiocarcinoma. *Oncol Rep* 21:957-969.

59. Campbell, D.J., Dumur, C.I., Lamour, N.F., Dewitt, J.L., and Sirica, A.E. 2012. Novel organotypic culture model of cholangiocarcinoma progression. *Hepatol Res* 42:1119-1130.

60. Mertens, J.C., Fingas, C.D., Christensen, J.D., Smoot, R.L., Bronk, S.F., Werneburg, N.W., Gustafson, M.P., Dietz, A.B., Roberts, L.R., Sirica, A.E., et al. 2013. Therapeutic effects of deleting cancer-associated fibroblasts in cholangiocarcinoma. *Cancer Res* 73:897-907.

61. Aishima, S., Nishihara, Y., Iguchi, T., Taguchi, K., Taketomi, A., Maehara, Y., and Tsuneyoshi, M. 2008. Lymphatic spread is related to VEGF-C expression and D2-40-positive myofibroblasts in intrahepatic cholangiocarcinoma. *Mod Pathol* 21:256-264.

62. Utispan, K., Thuwajit, P., Abiko, Y., Charngkaew, K., Paupairoj, A., Chau-in, S., and Thuwajit, C. 2010. Gene expression profiling of cholangiocarcinoma-derived fibroblast reveals alterations related to tumor progression and indicates periostin as a poor prognostic marker. *Mol Cancer* 9:13.

63. Aishima, S., Taguchi, K., Terashi, T., Matsuura, S., Shimada, M., and Tsuneyoshi, M. 2003. Tenascin expression at the invasive front is associated with poor prognosis in intrahepatic cholangiocarcinoma. *Mod Pathol* 16:1019-1027.

64. Dai, R., Li, J., Fu, J., Chen, Y., Wang, R., Zhao, X., Luo, T., Zhu, J., Ren, Y., Cao, J., et al. 2012. The tyrosine kinase c-Met contributes to the pro-

tumorigenic function of the p38 kinase in human bile duct cholangiocarcinoma cells. *J Biol Chem* 287:39812-39823.

65. Terada, T., Okada, Y., and Nakanuma, Y. 1996. Expression of immunoreactive matrix metalloproteinases and tissue inhibitors of matrix metalloproteinases in human normal livers and primary liver tumors. *Hepatology* 23:1341-1344.
66. Chen, Y., Sasatomi, E., Satoh, T., Miyazaki, K., and Tokunaga, O. 2000. Abnormal distribution of collagen type IV in extrahepatic bile duct carcinoma. *Pathol Int* 50:884-890.
67. Kawahara, N., Ono, M., Taguchi, K., Okamoto, M., Shimada, M., Takenaka, K., Hayashi, K., Mosher, D.F., Sugimachi, K., Tsuneyoshi, M., et al. 1998. Enhanced expression of thrombospondin-1 and hypovascularity in human cholangiocarcinoma. *Hepatology* 28:1512-1517.
68. Benckert, C., Jonas, S., Cramer, T., Von Marschall, Z., Schafer, G., Peters, M., Wagner, K., Radke, C., Wiedenmann, B., Neuhaus, P., et al. 2003. Transforming growth factor beta 1 stimulates vascular endothelial growth factor gene transcription in human cholangiocellular carcinoma cells. *Cancer Res* 63:1083-1092.
69. Hasita, H., Komohara, Y., Okabe, H., Masuda, T., Ohnishi, K., Lei, X.F., Beppu, T., Baba, H., and Takeya, M. 2010. Significance of alternatively activated macrophages in patients with intrahepatic cholangiocarcinoma. *Cancer Sci* 101:1913-1919.
70. Subimerb, C., Pinlaor, S., Lulitanond, V., Khuntikeo, N., Okada, S., McGrath, M.S., and Wongkham, S. 2010. Circulating CD14(+) CD16(+) monocyte levels predict tissue invasive character of cholangiocarcinoma. *Clin Exp Immunol* 161:471-479.
71. Ling, H., Roux, E., Hempel, D., Tao, J., Smith, M., Lonning, S., Zuk, A., Arbeeny, C., and Ledbetter, S. 2013. Transforming growth factor beta neutralization ameliorates pre-existing hepatic fibrosis and reduces cholangiocarcinoma in thioacetamide-treated rats. *PLoS One* 8:e54499.

72. Shimizu T, Y.S., Mizuguchi Y, Kawahigashi Y, Arima Y, Taniai N, Mamada Y, Yoshida H, Akimaru K, Tajiri T. 2006. Effect of transforming growth factor-β1 on human intrahepatic cholangiocarcinoma cell growth. *World Journal of Gastroenterology* 21:6316-6324.

73. Meng, F., Yamagiwa, Y., Ueno, Y., and Patel, T. 2006. Over-expression of interleukin-6 enhances cell survival and transformed cell growth in human malignant cholangiocytes. *J Hepatol* 44:1055-1065.

74. Wehbe H, H.R., Meng F, Mize-Berge J, and Patel T. 2006. Interleukin-6 Contributes to Growth in Cholangiocarcinoma Cells by Aberrant Promoter Methylation and Gene Expression. *Cancer Research* 66:10517-10524.

75. Yeh C-N, M.A., Lee K-F,Jan Y-Y, Chen M-F. 2004. Thioacetamide-induced intestinal-type cholangiocarcinoma in rat: an animal model recapitulating the multi-stage progression of human cholangiocarcinoma. *Carcinogenesis* 25:631-636.

76. Morley CG, B.J. 1977. Stimulation of hepatocellular proliferation by a serum factor from thioacetamide-treated rats. *Biochim Biophys Acta.* 477:165-176.

77. Barker, E.A., and Smuckler, E.A. 1972. Altered microsome function during acute thioacetamide poisoning. *Mol Pharmacol* 8:318-326.

78. Elmore LW, S.A. 1992. Sequential appearance of intestinal mucosal cell types in the right and caudate liver lobes of furan-treated rats. *Hepatology* 16:1220-1226.

79. Lu JP, M.J., Li MS, Lu SL, Hu XQ, Zhu SN, Nomura S. 2003. In situ detection of TGF betas, TGF beta receptor II mRNA and telomerase activity in rat cholangiocarcinogenesis. *World Journal of Gastroenterology* 9:590-594.

80. Yuan ST, H.X., Lu J-P, Keiki H, Zhai WR, Zhang YE. 2000. Changes of integrin expression in rat hepatocarcinogenesis induced b 3'-Me-DAB. *World Journal of Gastroenterology* 6:231-233.

81. Sirica AE, Z.Z., Lai GH, Asano T, Shen X-N, Ward DJ,, and Mahatme A, a.D.J. 2008. A Novel "Patient-like" Model of Cholangiocarcinoma

Progression Based on Bile Duct Inoculation of Tumorigenic Rat Cholangiocyte Cell Lines. *Hepatology* 47:1178-1190.

82. Lai G-H, Z.Z., Shen X-N, Ward DJ, Dewitt JL, Holt SE, Rozich RA, Hixson DC and Sirica AE. 2005. erbB-2/neu Transformed Rat Cholangiocytes Recapitulate Key Cellular and Molecular Features of Human Bile Duct Cancer. *Gastroenterology* 129:2047-2057.
83. Thamavit W, B.N., Sahaphong S, Vajrasthira S, Angskubhakorn S. 1978. Effects of dimethylnitrosamine on induction of cholangiocarcinoma in *Opisthorchis viverrini*-infected Syrina golden hamsters. *Cancer Research* 38:4634-4639.
84. Kiguchi K, C.S., Chan K, Beltra´n L, Ruffino L, Shen J, Matsumoto T, Yoshimi N,and DiGiovanni J. 2001. Constitutive Expression of ErbB-2 in Gallbladder Epithelium Results in Development of Adenocarcinoma. *Cancer Research* 61:6971-6976.
85. Xu X, K.S., Qiao W,Li C,Xiao C,Radaeva S, Stiles B,Wang R-H,Nobuya Ohara N,Yoshino T,LeRoith D, Torbenson MS, Gores GJ, Wu H,4 Gao B and Deng C-X. 2006. Induction of intrahepatic cholangiocellular carcinoma by liver-specific disruption of Smad4 and Pten in mice. *Journal of Clinical Investigation* 116:1843-1852.
86. O'Dell MR, H.J.-L., Whitney-Miller CL, Deshpande V, Rothberg P, Grose V, Rossi RM, Zhu AX, Land H, Bardeesy N, Hezel AF. 2012. $Kras^{G12D}$ and p53 mutation causes primary intra-hepatic cholangiocarcinoma. *Cancer Research*.
87. Marsh, V., Davies, E.J., Williams, G.T., and Clarke, A.R. 2013. PTEN loss and KRAS activation cooperate in murine biliary tract malignancies. *J Pathol* 230:165-173.
88. Ishak KG, A.P., Sobin LH. 1994. Histological typing of tumours of the liver. WHO International Classification of Tumours. *Berlin: Springer Verlag*.
89. Bergquist A, E.A., Olsson R, Kornfeldt D, Loof L, Danielsson A, Hultcrantz R, Lindgren S, Prytz H, Sandberg-Gertzen H, Almer S, Granath F, Broome U.

2002. Hepatic and extrahepatic malignancies in primary sclerosing cholangitis. *Journal of Hepatology* 36:321-327.

90. Goodman ZD, I.K., Langloss JM, Sesterhenn IA, Rabin L. 1985. Combined Hepatocellular-Cholangiocarcinoma. A histologic and immunohistochemical study. *Cancer* 55:124-135.
91. Komuta M, S.B., Vander Borght S, De Vos R, Verslype C, Aerts R, Yano H, Suzuki T, Matsuda M, Fuiji H, Desmet VI, Kojiro M, Roskams T. 2008. Clinicopathological study on cholangiolocellular carcinoma suggesting hepatic progenitor cell origin. *Hepatology* 47:1544-1556.
92. Fan B, M.Y., Calvisi DF, Naqvi S, Razumilava N, Ribback S, Gores GJ, Dombowski F, Evert M, Chen X, Willenbring H. 2012. Cholangiocarcinomas can originate from hepatocytes in mice. *Journal of Clinical Investigation* 122:2911-2915.
93. Sekiya S, S.A. 2012. Intrahepatic cholangiocarcinoma can arise from Notch-mediated conversion of hepatocytes. *Journal of Clinical Investigation* 122:3914-3918.
94. Pires-daSilva A, S.R. 2003. The evolution of signalling pathways in animal development. *Nature Reviews Genetics* 4:39-49.
95. Bellavia, D., Checquolo, S., Campese, A.F., Felli, M.P., Gulino, A., and Screpanti, I. 2008. Notch3: from subtle structural differences to functional diversity. *Oncogene* 27:5092-5098.
96. Sharma, A., Rangarajan, A., and Dighe, R.R. 2013. Antibodies against the extracellular domain of human Notch1 receptor reveal the critical role of epidermal-growth-factor-like repeats 25-26 in ligand binding and receptor activation. *Biochem J* 449:519-530.
97. Yamamoto, S., Charng, W.L., Rana, N.A., Kakuda, S., Jaiswal, M., Bayat, V., Xiong, B., Zhang, K., Sandoval, H., David, G., et al. 2012. A mutation in EGF repeat-8 of Notch discriminates between Serrate/Jagged and Delta family ligands. *Science* 338:1229-1232.

98. Fitzgerald, K., Wilkinson, H.A., and Greenwald, I. 1993. glp-1 can substitute for lin-12 in specifying cell fate decisions in Caenorhabditis elegans. *Development* 119:1019-1027.

99. Beatus, P., Lundkvist, J., Oberg, C., Pedersen, K., and Lendahl, U. 2001. The origin of the ankyrin repeat region in Notch intracellular domains is critical for regulation of HES promoter activity. *Mech Dev* 104:3-20.

100. Lardelli, M., Dahlstrand, J., and Lendahl, U. 1994. The novel Notch homologue mouse Notch 3 lacks specific epidermal growth factor-repeats and is expressed in proliferating neuroepithelium. *Mech Dev* 46:123-136.

101. Parks, A.L., Stout, J.R., Shepard, S.B., Klueg, K.M., Dos Santos, A.A., Parody, T.R., Vaskova, M., and Muskavitch, M.A. 2006. Structure-function analysis of delta trafficking, receptor binding and signaling in Drosophila. *Genetics* 174:1947-1961.

102. Le Borgne, R., Remaud, S., Hamel, S., and Schweisguth, F. 2005. Two distinct E3 ubiquitin ligases have complementary functions in the regulation of delta and serrate signaling in Drosophila. *PLoS Biol* 3:e96.

103. Lai, E.C., Bodner, R., Kavaler, J., Freschi, G., and Posakony, J.W. 2000. Antagonism of notch signaling activity by members of a novel protein family encoded by the bearded and enhancer of split gene complexes. *Development* 127:291-306.

104. Ladi, E., Nichols, J.T., Ge, W., Miyamoto, A., Yao, C., Yang, L.T., Boulter, J., Sun, Y.E., Kintner, C., and Weinmaster, G. 2005. The divergent DSL ligand Dll3 does not activate Notch signaling but cell autonomously attenuates signaling induced by other DSL ligands. *J Cell Biol* 170:983-992.

105. Weng, A.P., Ferrando, A.A., Lee, W., Morris, J.P.t., Silverman, L.B., Sanchez-Irizarry, C., Blacklow, S.C., Look, A.T., and Aster, J.C. 2004. Activating mutations of NOTCH1 in human T cell acute lymphoblastic leukemia. *Science* 306:269-271.

106. Girard, L., Hanna, Z., Beaulieu, N., Hoemann, C.D., Simard, C., Kozak, C.A., and Jolicoeur, P. 1996. Frequent provirus insertional mutagenesis of Notch1

in thymomas of MMTVD/myc transgenic mice suggests a collaboration of c-myc and Notch1 for oncogenesis. *Genes Dev* 10:1930-1944.

107. Demehri, S., Liu, Z., Lee, J., Lin, M.H., Crosby, S.D., Roberts, C.J., Grigsby, P.W., Miner, J.H., Farr, A.G., and Kopan, R. 2008. Notch-deficient skin induces a lethal systemic B-lymphoproliferative disorder by secreting TSLP, a sentinel for epidermal integrity. *PLoS Biol* 6:e123.
108. Lee, J., Basak, J.M., Demehri, S., and Kopan, R. 2007. Bi-compartmental communication contributes to the opposite proliferative behavior of Notch1-deficient hair follicle and epidermal keratinocytes. *Development* 134:2795-2806.
109. Fryer, C.J., White, J.B., and Jones, K.A. 2004. Mastermind recruits CycC:CDK8 to phosphorylate the Notch ICD and coordinate activation with turnover. *Mol Cell* 16:509-520.
110. Wilkinson, H.A., Fitzgerald, K., and Greenwald, I. 1994. Reciprocal changes in expression of the receptor lin-12 and its ligand lag-2 prior to commitment in a C. elegans cell fate decision. *Cell* 79:1187-1198.
111. Rhyu, M.S., Jan, L.Y., and Jan, Y.N. 1994. Asymmetric distribution of numb protein during division of the sensory organ precursor cell confers distinct fates to daughter cells. *Cell* 76:477-491.
112. Zhao, C., Guo, H., Li, J., Myint, T., Pittman, W., Yang, L., Zhong, W., Schwartz, R.J., Schwarz, J.J., Singer, H.A., et al. 2013. Numb family proteins are essential for cardiac morphogenesis and progenitor differentiation. *Development*.
113. Le Borgne, R., and Schweisguth, F. 2003. Unequal segregation of Neuralized biases Notch activation during asymmetric cell division. *Dev Cell* 5:139-148.
114. Cheng, Y.C., Amoyel, M., Qiu, X., Jiang, Y.J., Xu, Q., and Wilkinson, D.G. 2004. Notch activation regulates the segregation and differentiation of rhombomere boundary cells in the zebrafish hindbrain. *Dev Cell* 6:539-550.
115. Irvine, K.D. 1999. Fringe, Notch, and making developmental boundaries. *Curr Opin Genet Dev* 9:434-441.

116. de Celis, J.F., Garcia-Bellido, A., and Bray, S.J. 1996. Activation and function of Notch at the dorsal-ventral boundary of the wing imaginal disc. *Development* 122:359-369.

117. Oda, T., Elkahloun, A.G., Pike, B.L., Okajima, K., Krantz, I.D., Genin, A., Piccoli, D.A., Meltzer, P.S., Spinner, N.B., Collins, F.S., et al. 1997. Mutations in the human Jagged1 gene are responsible for Alagille syndrome. *Nat Genet* 16:235-242.

118. Li, L., Krantz, I.D., Deng, Y., Genin, A., Banta, A.B., Collins, C.C., Qi, M., Trask, B.J., Kuo, W.L., Cochran, J., et al. 1997. Alagille syndrome is caused by mutations in human Jagged1, which encodes a ligand for Notch1. *Nat Genet* 16:243-251.

119. Alagille, D., Estrada, A., Hadchouel, M., Gautier, M., Odievre, M., and Dommergues, J.P. 1987. Syndromic paucity of interlobular bile ducts (Alagille syndrome or arteriohepatic dysplasia): review of 80 cases. *J Pediatr* 110:195-200.

120. Alagille, D., Odievre, M., Gautier, M., and Dommergues, J.P. 1975. Hepatic ductular hypoplasia associated with characteristic facies, vertebral malformations, retarded physical, mental, and sexual development, and cardiac murmur. *J Pediatr* 86:63-71.

121. Warthen, D.M., Moore, E.C., Kamath, B.M., Morrissette, J.J., Sanchez-Lara, P.A., Piccoli, D.A., Krantz, I.D., and Spinner, N.B. 2006. Jagged1 (JAG1) mutations in Alagille syndrome: increasing the mutation detection rate. *Hum Mutat* 27:436-443.

122. McDaniell, R., Warthen, D.M., Sanchez-Lara, P.A., Pai, A., Krantz, I.D., Piccoli, D.A., and Spinner, N.B. 2006. NOTCH2 mutations cause Alagille syndrome, a heterogeneous disorder of the notch signaling pathway. *Am J Hum Genet* 79:169-173.

123. Spinner, N.B., Colliton, R.P., Crosnier, C., Krantz, I.D., Hadchouel, M., and Meunier-Rotival, M. 2001. Jagged1 mutations in alagille syndrome. *Hum Mutat* 17:18-33.

124. Kamath, B.M., Krantz, I.D., Spinner, N.B., Heubi, J.E., and Piccoli, D.A. 2002. Monozygotic twins with a severe form of Alagille syndrome and phenotypic discordance. *Am J Med Genet* 112:194-197.

125. Fabris, L., Cadamuro, M., Guido, M., Spirli, C., Fiorotto, R., Colledan, M., Torre, G., Alberti, D., Sonzogni, A., Okolicsanyi, L., et al. 2007. Analysis of liver repair mechanisms in Alagille syndrome and biliary atresia reveals a role for notch signaling. *Am J Pathol* 171:641-653.

126. Todani, T., Watanabe, Y., Narusue, M., Tabuchi, K., and Okajima, K. 1977. Congenital bile duct cysts: Classification, operative procedures, and review of thirty-seven cases including cancer arising from choledochal cyst. *Am J Surg* 134:263-269.

127. Desmet, V.J. 1992. Congenital diseases of intrahepatic bile ducts: variations on the theme "ductal plate malformation". *Hepatology* 16:1069-1083.

128. Dayton, M.T., Longmire, W.P., Jr., and Tompkins, R.K. 1983. Caroli's Disease: a premalignant condition? *Am J Surg* 145:41-48.

129. Furubo, S., Sato, Y., Harada, K., and Nakanuma, Y. 2013. Roles of myofibroblasts and notch and hedgehog signaling pathways in the formation of intrahepatic bile duct lesions in polycystic kidney rats. *Pediatr Dev Pathol* 16:177-190.

130. Xue, Y., Gao, X., Lindsell, C.E., Norton, C.R., Chang, B., Hicks, C., Gendron-Maguire, M., Rand, E.B., Weinmaster, G., and Gridley, T. 1999. Embryonic lethality and vascular defects in mice lacking the Notch ligand Jagged1. *Hum Mol Genet* 8:723-730.

131. Ryan, M.J., Bales, C., Nelson, A., Gonzalez, D.M., Underkoffler, L., Segalov, M., Wilson-Rawls, J., Cole, S.E., Moran, J.L., Russo, P., et al. 2008. Bile duct proliferation in Jag1/fringe heterozygous mice identifies candidate modifiers of the Alagille syndrome hepatic phenotype. *Hepatology* 48:1989-1997.

132. McCright, B., Lozier, J., and Gridley, T. 2002. A mouse model of Alagille syndrome: Notch2 as a genetic modifier of Jag1 haploinsufficiency. *Development* 129:1075-1082.

133. Gessler, M., Knobeloch, K.P., Helisch, A., Amann, K., Schumacher, N., Rohde, E., Fischer, A., and Leimeister, C. 2002. Mouse gridlock: no aortic coarctation or deficiency, but fatal cardiac defects in Hey2 -/- mice. *Curr Biol* 12:1601-1604.

134. Donovan, J., Kordylewska, A., Jan, Y.N., and Utset, M.F. 2002. Tetralogy of fallot and other congenital heart defects in Hey2 mutant mice. *Curr Biol* 12:1605-1610.

135. Geisler, F., Nagl, F., Mazur, P.K., Lee, M., Zimber-Strobl, U., Strobl, L.J., Radtke, F., Schmid, R.M., and Siveke, J.T. 2008. Liver-specific inactivation of Notch2, but not Notch1, compromises intrahepatic bile duct development in mice. *Hepatology* 48:607-616.

136. Lozier, J., McCright, B., and Gridley, T. 2008. Notch signaling regulates bile duct morphogenesis in mice. *PLoS One* 3:e1851.

137. Ishibashi, M., Ang, S.L., Shiota, K., Nakanishi, S., Kageyama, R., and Guillemot, F. 1995. Targeted disruption of mammalian hairy and Enhancer of split homolog-1 (HES-1) leads to up-regulation of neural helix-loop-helix factors, premature neurogenesis, and severe neural tube defects. *Genes Dev* 9:3136-3148.

138. Kodama, Y., Hijikata, M., Kageyama, R., Shimotohno, K., and Chiba, T. 2004. The role of notch signaling in the development of intrahepatic bile ducts. *Gastroenterology* 127:1775-1786.

139. Jeliazkova, P., Jors, S., Lee, M., Zimber-Strobl, U., Ferrer, J., Schmid, R.M., Siveke, J.T., and Geisler, F. 2013. Canonical Notch2 signaling determines biliary cell fates of embryonic hepatoblasts and adult hepatocytes independent of Hes1. *Hepatology* 57:2469-2479.

140. Sparks, E.E., Huppert, K.A., Brown, M.A., Washington, M.K., and Huppert, S.S. 2010. Notch signaling regulates formation of the three-dimensional architecture of intrahepatic bile ducts in mice. *Hepatology* 51:1391-1400.

141. Vanderpool, C., Sparks, E.E., Huppert, K.A., Gannon, M., Means, A.L., and Huppert, S.S. 2012. Genetic interactions between hepatocyte nuclear factor-6

and Notch signaling regulate mouse intrahepatic bile duct development in vivo. *Hepatology* 55:233-243.

142. Hofmann, J.J., Zovein, A.C., Koh, H., Radtke, F., Weinmaster, G., and Iruela-Arispe, M.L. 2010. Jagged1 in the portal vein mesenchyme regulates intrahepatic bile duct development: insights into Alagille syndrome. *Development* 137:4061-4072.

143. Lorent, K., Yeo, S.Y., Oda, T., Chandrasekharappa, S., Chitnis, A., Matthews, R.P., and Pack, M. 2004. Inhibition of Jagged-mediated Notch signaling disrupts zebrafish biliary development and generates multi-organ defects compatible with an Alagille syndrome phenocopy. *Development* 131:5753-5766.

144. Lorent, K., Moore, J.C., Siekmann, A.F., Lawson, N., and Pack, M. 2010. Reiterative use of the notch signal during zebrafish intrahepatic biliary development. *Dev Dyn* 239:855-864.

145. Zong Y, P.A., Xu J, Antoniou A, Raynaud P, Lemaigre F and Stanger1 BZ. 2009. Notch signaling controls liver development by regulating biliary differentiation. *Development* 136:1727-1739.

146. Costa, R.H., Kalinichenko, V.V., Holterman, A.X., and Wang, X. 2003. Transcription factors in liver development, differentiation, and regeneration. *Hepatology* 38:1331-1347.

147. Tanimizu, N., and Miyajima, A. 2004. Notch signaling controls hepatoblast differentiation by altering the expression of liver-enriched transcription factors. *J Cell Sci* 117:3165-3174.

148. Sumazaki, R., Shiojiri, N., Isoyama, S., Masu, M., Keino-Masu, K., Osawa, M., Nakauchi, H., Kageyama, R., and Matsui, A. 2004. Conversion of biliary system to pancreatic tissue in Hes1-deficient mice. *Nat Genet* 36:83-87.

149. Sansom, O.J., Reed, K.R., Hayes, A.J., Ireland, H., Brinkmann, H., Newton, I.P., Batlle, E., Simon-Assmann, P., Clevers, H., Nathke, I.S., et al. 2004. Loss of Apc in vivo immediately perturbs Wnt signaling, differentiation, and migration. *Genes Dev* 18:1385-1390.

150. Sato, T., van Es, J.H., Snippert, H.J., Stange, D.E., Vries, R.G., van den Born, M., Barker, N., Shroyer, N.F., van de Wetering, M., and Clevers, H. 2011. Paneth cells constitute the niche for Lgr5 stem cells in intestinal crypts. *Nature* 469:415-418.

151. Fre, S., Huyghe, M., Mourikis, P., Robine, S., Louvard, D., and Artavanis-Tsakonas, S. 2005. Notch signals control the fate of immature progenitor cells in the intestine. *Nature* 435:964-968.

152. Pellegrinet, L., Rodilla, V., Liu, Z., Chen, S., Koch, U., Espinosa, L., Kaestner, K.H., Kopan, R., Lewis, J., and Radtke, F. 2011. Dll1- and dll4-mediated notch signaling are required for homeostasis of intestinal stem cells. *Gastroenterology* 140:1230-1240 e1231-1237.

153. Croquelois, A., Blindenbacher, A., Terracciano, L., Wang, X., Langer, I., Radtke, F., and Heim, M.H. 2005. Inducible inactivation of Notch1 causes nodular regenerative hyperplasia in mice. *Hepatology* 41:487-496.

154. Haller, O., Staeheli, P., and Kochs, G. 2007. Interferon-induced Mx proteins in antiviral host defense. *Biochimie* 89:812-818.

155. Nijjar, S.S., Wallace, L., Crosby, H.A., Hubscher, S.G., and Strain, A.J. 2002. Altered Notch ligand expression in human liver disease: further evidence for a role of the Notch signaling pathway in hepatic neovascularization and biliary ductular defects. *Am J Pathol* 160:1695-1703.

156. Flynn, D.M., Nijjar, S., Hubscher, S.G., de Goyet Jde, V., Kelly, D.A., Strain, A.J., and Crosby, H.A. 2004. The role of Notch receptor expression in bile duct development and disease. *J Pathol* 204:55-64.

157. Nijjar, S.S., Crosby, H.A., Wallace, L., Hubscher, S.G., and Strain, A.J. 2001. Notch receptor expression in adult human liver: a possible role in bile duct formation and hepatic neovascularization. *Hepatology* 34:1184-1192.

158. Boulter L, G.O., Bird TG, Radulescu S, Aucott RL, Van Rooijen N, Sansom OJ, Iredale JP, Lowell S, Roskams T, Forbes SJ. 2012. Macrophage derived Wnt signalling opposes Notch signalling in a NUMB mediated manner to

specify HOC fate in chronic liver disease in liver and mouse. *Nature Medicine*.

159. Higgins GM, A.R. 1931. Restoration of the liver of the white rat following partial surgical removal. *Archives of Pathology* 12:186-202.

160. Stocker, E., Wullstein, H.K., and Brau, G. 1973. [Capacity of regeneration in liver epithelia of juvenile, repeated partially hepatectomized rats. Autoradiographic studies after continous infusion of 3H-thymidine (author's transl)]. *Virchows Arch B Cell Pathol* 14:93-103.

161. Dorrell, C., Erker, L., Schug, J., Kopp, J.L., Canaday, P.S., Fox, A.J., Smirnova, O., Duncan, A.W., Finegold, M.J., Sander, M., et al. 2011. Prospective isolation of a bipotential clonogenic liver progenitor cell in adult mice. *Genes Dev* 25:1193-1203.

162. Espanol-Suner, R., Carpentier, R., Van Hul, N., Legry, V., Achouri, Y., Cordi, S., Jacquemin, P., Lemaigre, F., and Leclercq, I.A. 2012. Liver progenitor cells yield functional hepatocytes in response to chronic liver injury in mice. *Gastroenterology* 143:1564-1575 e1567.

163. Roskams, T.A., Theise, N.D., Balabaud, C., Bhagat, G., Bhathal, P.S., Bioulac-Sage, P., Brunt, E.M., Crawford, J.M., Crosby, H.A., Desmet, V., et al. 2004. Nomenclature of the finer branches of the biliary tree: canals, ductules, and ductular reactions in human livers. *Hepatology* 39:1739-1745.

164. Lowes, K.N., Brennan, B.A., Yeoh, G.C., and Olynyk, J.K. 1999. Oval cell numbers in human chronic liver diseases are directly related to disease severity. *Am J Pathol* 154:537-541.

165. Bird, T.G., Lorenzini, S., and Forbes, S.J. 2008. Activation of stem cells in hepatic diseases. *Cell Tissue Res* 331:283-300.

166. Eleazar, J.A., Memeo, L., Jhang, J.S., Mansukhani, M.M., Chin, S., Park, S.M., Lefkowitch, J.H., and Bhagat, G. 2004. Progenitor cell expansion: an important source of hepatocyte regeneration in chronic hepatitis. *J Hepatol* 41:983-991.

167. Spee, B., Carpino, G., Schotanus, B.A., Katoonizadeh, A., Vander Borght, S., Gaudio, E., and Roskams, T. 2010. Characterisation of the liver progenitor cell niche in liver diseases: potential involvement of Wnt and Notch signalling. *Gut* 59:247-257.

168. Shackel, N.A., McGuinness, P.H., Abbott, C.A., Gorrell, M.D., and McCaughan, G.W. 2001. Identification of novel molecules and pathogenic pathways in primary biliary cirrhosis: cDNA array analysis of intrahepatic differential gene expression. *Gut* 49:565-576.

169. Boulter, L., Govaere, O., Bird, T.G., Radulescu, S., Ramachandran, P., Pellicoro, A., Ridgway, R.A., Seo, S.S., Spee, B., Van Rooijen, N., et al. 2012. Macrophage-derived Wnt opposes Notch signaling to specify hepatic progenitor cell fate in chronic liver disease. *Nat Med* 18:572-579.

170. Sawitza, I., Kordes, C., Reister, S., and Haussinger, D. 2009. The niche of stellate cells within rat liver. *Hepatology* 50:1617-1624.

171. Chen, Y., Zheng, S., Qi, D., Guo, J., Zhang, S., and Weng, Z. 2012. Inhibition of Notch signaling by a gamma-secretase inhibitor attenuates hepatic fibrosis in rats. *PLoS One* 7:e46512.

172. Lorenzini, S., Bird, T.G., Boulter, L., Bellamy, C., Samuel, K., Aucott, R., Clayton, E., Andreone, P., Bernardi, M., Golding, M., et al. 2010. Characterisation of a stereotypical cellular and extracellular adult liver progenitor cell niche in rodents and diseased human liver. *Gut* 59:645-654.

173. Preisegger, K.H., Factor, V.M., Fuchsbichler, A., Stumptner, C., Denk, H., and Thorgeirsson, S.S. 1999. Atypical ductular proliferation and its inhibition by transforming growth factor beta1 in the 3,5-diethoxycarbonyl-1,4-dihydrocollidine mouse model for chronic alcoholic liver disease. *Lab Invest* 79:103-109.

174. Fiorotto, R., Raizner, A., Morell, C.M., Torsello, B., Scirpo, R., Fabris, L., Spirli, C., and Strazzabosco, M. 2013. Notch signaling regulates tubular morphogenesis during repair from biliary damage in mice. *J Hepatol* 59:124-130.

175. Yanger, K., Zong, Y., Maggs, L.R., Shapira, S.N., Maddipati, R., Aiello, N.M., Thung, S.N., Wells, R.G., Greenbaum, L.E., and Stanger, B.Z. 2013. Robust cellular reprogramming occurs spontaneously during liver regeneration. *Genes Dev* 27:719-724.

176. Ellisen, L.W., Bird, J., West, D.C., Soreng, A.L., Reynolds, T.C., Smith, S.D., and Sklar, J. 1991. TAN-1, the human homolog of the Drosophila notch gene, is broken by chromosomal translocations in T lymphoblastic neoplasms. *Cell* 66:649-661.

177. Radtke F, W.A., Stark G, Bauer M, van Meerwijk J, MacDonald HR, Aguet M. 1999. Deficient T cell fate specification in mice with an induced inactivation of *Notch1*. *Immunity* 10:547-558.

178. Wolfer, A., Wilson, A., Nemir, M., MacDonald, H.R., and Radtke, F. 2002. Inactivation of Notch1 impairs VDJbeta rearrangement and allows pre-TCR-independent survival of early alpha beta Lineage Thymocytes. *Immunity* 16:869-879.

179. Aster, J.C., Xu, L., Karnell, F.G., Patriub, V., Pui, J.C., and Pear, W.S. 2000. Essential roles for ankyrin repeat and transactivation domains in induction of T-cell leukemia by notch1. *Mol Cell Biol* 20:7505-7515.

180. Rohn, J.L., Lauring, A.S., Linenberger, M.L., and Overbaugh, J. 1996. Transduction of Notch2 in feline leukemia virus-induced thymic lymphoma. *J Virol* 70:8071-8080.

181. Bellavia, D., Campese, A.F., Alesse, E., Vacca, A., Felli, M.P., Balestri, A., Stoppacciaro, A., Tiveron, C., Tatangelo, L., Giovarelli, M., et al. 2000. Constitutive activation of NF-kappaB and T-cell leukemia/lymphoma in Notch3 transgenic mice. *EMBO J* 19:3337-3348.

182. Palermo, R., Checquolo, S., Giovenco, A., Grazioli, P., Kumar, V., Campese, A.F., Giorgi, A., Napolitano, M., Canettieri, G., Ferrara, G., et al. 2012. Acetylation controls Notch3 stability and function in T-cell leukemia. *Oncogene* 31:3807-3817.

183. Westhoff, B., Colaluca, I.N., D'Ario, G., Donzelli, M., Tosoni, D., Volorio, S., Pelosi, G., Spaggiari, L., Mazzarol, G., Viale, G., et al. 2009. Alterations of the Notch pathway in lung cancer. *Proc Natl Acad Sci U S A* 106:22293-22298.

184. Haruki, N., Kawaguchi, K.S., Eichenberger, S., Massion, P.P., Olson, S., Gonzalez, A., Carbone, D.P., and Dang, T.P. 2005. Dominant-negative Notch3 receptor inhibits mitogen-activated protein kinase pathway and the growth of human lung cancers. *Cancer Res* 65:3555-3561.

185. Maraver, A., Fernandez-Marcos, P.J., Herranz, D., Canamero, M., Munoz-Martin, M., Gomez-Lopez, G., Mulero, F., Megias, D., Sanchez-Carbayo, M., Shen, J., et al. 2012. Therapeutic effect of gamma-secretase inhibition in KrasG12V-driven non-small cell lung carcinoma by derepression of DUSP1 and inhibition of ERK. *Cancer Cell* 22:222-234.

186. Donnem, T., Andersen, S., Al-Shibli, K., Al-Saad, S., Busund, L.T., and Bremnes, R.M. 2010. Prognostic impact of Notch ligands and receptors in nonsmall cell lung cancer: coexpression of Notch-1 and vascular endothelial growth factor-A predicts poor survival. *Cancer* 116:5676-5685.

187. Singh, S.K., Hawkins, C., Clarke, I.D., Squire, J.A., Bayani, J., Hide, T., Henkelman, R.M., Cusimano, M.D., and Dirks, P.B. 2004. Identification of human brain tumour initiating cells. *Nature* 432:396-401.

188. O'Brien, C.A., Pollett, A., Gallinger, S., and Dick, J.E. 2007. A human colon cancer cell capable of initiating tumour growth in immunodeficient mice. *Nature* 445:106-110.

189. Hermann, P.C., Huber, S.L., Herrler, T., Aicher, A., Ellwart, J.W., Guba, M., Bruns, C.J., and Heeschen, C. 2007. Distinct populations of cancer stem cells determine tumor growth and metastatic activity in human pancreatic cancer. *Cell Stem Cell* 1:313-323.

190. Al-Hajj, M., Wicha, M.S., Benito-Hernandez, A., Morrison, S.J., and Clarke, M.F. 2003. Prospective identification of tumorigenic breast cancer cells. *Proc Natl Acad Sci U S A* 100:3983-3988.

191. Zheng, Y., de la Cruz, C.C., Sayles, L.C., Alleyne-Chin, C., Vaka, D., Knaak, T.D., Bigos, M., Xu, Y., Hoang, C.D., Shrager, J.B., et al. 2013. A Rare Population of CD24(+)ITGB4(+)Notch(hi) Cells Drives Tumor Propagation in NSCLC and Requires Notch3 for Self-Renewal. *Cancer Cell* 24:59-74.

192. Plentz, R., Park, J.S., Rhim, A.D., Abravanel, D., Hezel, A.F., Sharma, S.V., Gurumurthy, S., Deshpande, V., Kenific, C., Settleman, J., et al. 2009. Inhibition of gamma-secretase activity inhibits tumor progression in a mouse model of pancreatic ductal adenocarcinoma. *Gastroenterology* 136:1741-1749 e1746.

193. Mazur PK, E.H., Lee M, Sipos B, Nakhai H, Rad R, Zimber-Strobl U, Strobl LJ, Radtke F, Kloppel G, Schimd RM, Siveke JT. 2010. Notch2 is required for progression of pancreatic intraepithelial neoplasia and development of pancreatic ductal adenocarcinoma. *PNAS* 107:13438-13443.

194. Bouras, T., Pal, B., Vaillant, F., Harburg, G., Asselin-Labat, M.L., Oakes, S.R., Lindeman, G.J., and Visvader, J.E. 2008. Notch signaling regulates mammary stem cell function and luminal cell-fate commitment. *Cell Stem Cell* 3:429-441.

195. Yamamoto, M., Taguchi, Y., Ito-Kureha, T., Semba, K., Yamaguchi, N., and Inoue, J. 2013. NF-kappaB non-cell-autonomously regulates cancer stem cell populations in the basal-like breast cancer subtype. *Nat Commun* 4:2299.

196. Xing F, O.H., Watabe M, Kobayashi A, Pai SK, Liu W, Pandey PR, Fukuda K, Hirota S, Sugai T, Wakabayshi G, Koeda K, Kashiwaba , Suzuki K, Chiba T, Endo M, Mo Y-Y and Watabe K. 2011. Hypoxia-induced Jagged2 promotes breast cancer metastasis and self-renewal of cancer stem-like cells. *Oncogene* 30:4075-4086.

197. Sethi N, D.X., Winter CG, Kang Y. 2011. Tumor-Derived Jagged1 Promotes Osteolytic Bone Metastasis of Breast Cancer by Engaging Notch Signaling in Bone Cells. *Cancer Cell* 19:192-205.

198. Sonoshita, M., Aoki, M., Fuwa, H., Aoki, K., Hosogi, H., Sakai, Y., Hashida, H., Takabayashi, A., Sasaki, M., Robine, S., et al. 2011. Suppression of colon

cancer metastasis by Aes through inhibition of Notch signaling. *Cancer Cell* 19:125-137.

199. Fujita H, O.K., Mizumoto K,Egami T,Miyoshi K,Moriyama T, Cui L,Yu J, Zhao M, Manabe T and Tanaka M. 2009. Tumor–stromal interactions with direct cell contacts enhance proliferation of human pancreatic carcinoma

cells. *Cancer Science* 100:2309-2317.

200. Kabashima-Niibe, A., Higuchi, H., Takaishi, H., Masugi, Y., Matsuzaki, Y., Mabuchi, Y., Funakoshi, S., Adachi, M., Hamamoto, Y., Kawachi, S., et al. 2013. Mesenchymal stem cells regulate epithelial-mesenchymal transition and tumor progression of pancreatic cancer cells. *Cancer Sci* 104:157-164.

201. Umiel, T., Friedman, S., Zaizov, R., Cohen, I.J., Gozes, Y., Epstein, N., Kobiler, D., and Zipori, D. 1986. Long-term culture of infant leukemia cells: dependence upon stromal cells from the bone marrow and bilineage differentiation. *Leuk Res* 10:1007-1013.

202. Nwabo Kamdje, A.H., Mosna, F., Bifari, F., Lisi, V., Bassi, G., Malpeli, G., Ricciardi, M., Perbellini, O., Scupoli, M.T., Pizzolo, G., et al. 2011. Notch-3 and Notch-4 signaling rescue from apoptosis human B-ALL cells in contact with human bone marrow-derived mesenchymal stromal cells. *Blood* 118:380-389.

203. Dill, M.T., Tornillo, L., Fritzius, T., Terracciano, L., Semela, D., Bettler, B., Heim, M.H., and Tchorz, J.S. 2013. Constitutive Notch2 signaling induces hepatic tumors in mice. *Hepatology* 57:1607-1619.

204. Mazur, P.K., Riener, M.O., Jochum, W., Kristiansen, G., Weber, A., Schmid, R.M., and Siveke, J.T. 2012. Expression and clinicopathological significance of notch signaling and cell-fate genes in biliary tract cancer. *Am J Gastroenterol* 107:126-135.

205. Weijzen S, R.P., Braid M, Vaishnav R, Jonkheer SM, Zlobin A, Osborne BA, Gottipati S, Aster JC, Hahn WC, Rudolf M, Siziopikou K, Kast WM, Miele L.

2002. Activation of Notch-1 signaling maintains the neoplastic phenotype in human Ras-transformed cells. *Nature Medicine* 8:979-986.

206. Price, J.V., Savenye, E.D., Lum, D., and Breitkreutz, A. 1997. Dominant enhancers of Egfr in Drosophila melanogaster: genetic links between the Notch and Egfr signaling pathways. *Genetics* 147:1139-1153.

207. Berset, T., Hoier, E.F., Battu, G., Canevascini, S., and Hajnal, A. 2001. Notch inhibition of RAS signaling through MAP kinase phosphatase LIP-1 during C. elegans vulval development. *Science* 291:1055-1058.

208. Fitzgerald K, H.A.a.L.P. 2000. Ras pathway signals are required for notch-mediated oncogenesis. *Oncogene* 19:4191-4198.

209. Rangarajan A, S.R., Selvarajah S, Chakrabarti O, Sarin A, and Krishna S. 2001. Activated Notch1 Signaling Cooperates with Papillomavirus Oncogenes in Transformation and Generates Resistance to Apoptosis on Matrix Withdrawal through PKB/Akt. *Virology* 286:23-30.

210. Miyamoto, Y., Maitra, A., Ghosh, B., Zechner, U., Argani, P., Iacobuzio-Donahue, C.A., Sriuranpong, V., Iso, T., Meszoely, I.M., Wolfe, M.S., et al. 2003. Notch mediates TGF alpha-induced changes in epithelial differentiation during pancreatic tumorigenesis. *Cancer Cell* 3:565-576.

211. Millar, T., Walker, R., Arango, J.C., Ironside, J.W., Harrison, D.J., MacIntyre, D.J., Blackwood, D., Smith, C., and Bell, J.E. 2007. Tissue and organ donation for research in forensic pathology: the MRC Sudden Death Brain and Tissue Bank. *J Pathol* 213:369-375.

212. Shimizu Y, D.A., Gollin SM, Storto PD, Bedford HM, Altarac S, Iwatsuki S, Herberman RB, Whiteside T. 2006. Two new human cholangiocarcinoma cell lines and their cytogenetics and responses to growth factors, hormones, cytokines or immunologic effector cells. *International Journal of Cancer* 52:252-260.

213. Coulon, A., Flahaut, M., Muhlethaler-Mottet, A., Meier, R., Liberman, J., Balmas-Bourloud, K., Nardou, K., Yan, P., Tercier, S., Joseph, J.M., et al. 2011.

Functional sphere profiling reveals the complexity of neuroblastoma tumor-initiating cell model. *Neoplasia* 13:991-1004.

214. Debnath, J., and Brugge, J.S. 2005. Modelling glandular epithelial cancers in three-dimensional cultures. *Nat Rev Cancer* 5:675-688.

215. Jacks, T., and Weinberg, R.A. 2002. Taking the study of cancer cell survival to a new dimension. *Cell* 111:923-925.

216. O'Brien, L.E., Zegers, M.M., and Mostov, K.E. 2002. Opinion: Building epithelial architecture: insights from three-dimensional culture models. *Nat Rev Mol Cell Biol* 3:531-537.

217. Farazi P, Z.M., Glickman J, Zhang Y, Kalluri R, DePinho RA. 2006. Chronic bile duct injury associated with fibrotic matrix microenvironment provokes cholangiocarcinoma in p53-deficient mice. *Cancer Research* 66:6622-6627.

218. Means AL, X.Y.X., Zhao A, Ray KC, Gu G. 2008. A CK19^{CreERT} Knockin mouse line allows for conditional DNA recombination in epithelial cells in multiple endodermal organs. *Genesis* 46:318-232.

219. Shimonishi, T., Miyazaki, K., and Nakanuma, Y. 2000. Cytokeratin profile relates to histological subtypes and intrahepatic location of intrahepatic cholangiocarcinoma and primary sites of metastatic adenocarcinoma of liver. *Histopathology* 37:55-63.

220. Koo, S.H., Ihm, C.H., Kwon, K.C., Park, J.W., Kim, J.M., and Kong, G. 2001. Genetic alterations in hepatocellular carcinoma and intrahepatic cholangiocarcinoma. *Cancer Genet Cytogenet* 130:22-28.

221. Rubin, E., Hutterer, F., and Popper, H. 1963. Cell proliferation and fiber formation in chronic carbon tetrachloride intoxication. A morphologic and chemical study. *Am J Pathol* 42:715-728.

222. Fujii, T., Fuchs, B.C., Yamada, S., Lauwers, G.Y., Kulu, Y., Goodwin, J.M., Lanuti, M., and Tanabe, K.K. 2010. Mouse model of carbon tetrachloride induced liver fibrosis: Histopathological changes and expression of CD133 and epidermal growth factor. *BMC Gastroenterol* 10:79.

223. Tannapfel, A., Benicke, M., Katalinic, A., Uhlmann, D., Kockerling, F., Hauss, J., and Wittekind, C. 2000. Frequency of p16(INK4A) alterations and K-ras mutations in intrahepatic cholangiocarcinoma of the liver. *Gut* 47:721-727.

224. Tannapfel, A., Sommerer, F., Benicke, M., Katalinic, A., Uhlmann, D., Witzigmann, H., Hauss, J., and Wittekind, C. 2003. Mutations of the BRAF gene in cholangiocarcinoma but not in hepatocellular carcinoma. *Gut* 52:706-712.

225. Deshpande, V., Nduaguba, A., Zimmerman, S.M., Kehoe, S.M., Macconaill, L.E., Lauwers, G.Y., Ferrone, C., Bardeesy, N., Zhu, A.X., and Hezel, A.F. 2011. Mutational profiling reveals PIK3CA mutations in gallbladder carcinoma. *BMC Cancer* 11:60.

226. Rosenthal, N., and Brown, S. 2007. The mouse ascending: perspectives for human-disease models. *Nat Cell Biol* 9:993-999.

227. de Groen, P.C., Gores, G.J., LaRusso, N.F., Gunderson, L.L., and Nagorney, D.M. 1999. Biliary tract cancers. *N Engl J Med* 341:1368-1378.

228. Sripa, B., Kaewkes, S., Sithithaworn, P., Mairiang, E., Laha, T., Smout, M., Pairojkul, C., Bhudhisawasdi, V., Tesana, S., Thinkamrop, B., et al. 2007. Liver fluke induces cholangiocarcinoma. *PLoS Med* 4:e201.

229. Sparks E, P.D., Huppert KA, Peterson TE, Huppert SS. 2011. Defects in hepatic Notch signalling result in disruption of the communicating intrahepatic bile duct network in mice. *Disease Models & Mechanisms* 4:359-367.

230. Zender, S., Nickeleit, I., Wuestefeld, T., Sorensen, I., Dauch, D., Bozko, P., El-Khatib, M., Geffers, R., Bektas, H., Manns, M.P., et al. 2013. A Critical Role for Notch Signaling in the Formation of Cholangiocellular Carcinomas. *Cancer Cell*.

231. Murphy, D.J., Junttila, M.R., Pouyet, L., Karnezis, A., Shchors, K., Bui, D.A., Brown-Swigart, L., Johnson, L., and Evan, G.I. 2008. Distinct thresholds govern Myc's biological output in vivo. *Cancer Cell* 14:447-457.

232. Richmond, A., and Su, Y. 2008. Mouse xenograft models vs GEM models for human cancer therapeutics. *Dis Model Mech* 1:78-82.

233. Abate-Shen, C., Brown, P.H., Colburn, N.H., Gerner, E.W., Green, J.E., Lipkin, M., Nelson, W.G., and Threadgill, D. 2008. The untapped potential of genetically engineered mouse models in chemoprevention research: opportunities and challenges. *Cancer Prev Res (Phila)* 1:161-166.

234. Jan Y-Y, Y.T.-S., Yeh J-N, Yang H-R, and Chen M-F. 2004. Expression of Epidermal Growth Factor Receptor, Apomucins, Matrix Metalloproteinases, and p53 in Rat and Human Cholangiocarcinoma. *Annals of Surgery* 240:89-94.

235. Weiswald, L.B., Guinebretiere, J.M., Richon, S., Bellet, D., Saubamea, B., and Dangles-Marie, V. 2010. In situ protein expression in tumour spheres: development of an immunostaining protocol for confocal microscopy. *BMC Cancer* 10:106.

236. Huppert, S.S., Le, A., Schroeter, E.H., Mumm, J.S., Saxena, M.T., Milner, L.A., and Kopan, R. 2000. Embryonic lethality in mice homozygous for a processing-deficient allele of Notch1. *Nature* 405:966-970.

237. Shih Ie, M., and Wang, T.L. 2007. Notch signaling, gamma-secretase inhibitors, and cancer therapy. *Cancer Res* 67:1879-1882.

238. van Es, J.H., van Gijn, M.E., Riccio, O., van den Born, M., Vooijs, M., Begthel, H., Cozijnsen, M., Robine, S., Winton, D.J., Radtke, F., et al. 2005. Notch/gamma-secretase inhibition turns proliferative cells in intestinal crypts and adenomas into goblet cells. *Nature* 435:959-963.

239. Shimizu, Y., Demetris, A.J., Gollin, S.M., Storto, P.D., Bedford, H.M., Altarac, S., Iwatsuki, S., Herberman, R.B., and Whiteside, T.L. 1992. Two new human cholangiocarcinoma cell lines and their cytogenetics and responses to growth factors, hormones, cytokines or immunologic effector cells. *Int J Cancer* 52:252-260.

240. Ku J-L, Y.K.-A., Kim I-J, Kim W-H, Jang J-Y, Suh K-S, Kim S-W, Park Y-H, Hwang J-H, Yoon Y-B, Park J-G. 2002. Establishment and characterisation of six human biliary tract cancer cell lines. *British Journal of Cancer* 87:187-193.

241. Blaschuk, O.W., and Rowlands, T.M. 2000. Cadherins as modulators of angiogenesis and the structural integrity of blood vessels. *Cancer Metastasis Rev* 19:1-5.

242. Nakajima, M., Yuasa, S., Ueno, M., Takakura, N., Koseki, H., and Shirasawa, T. 2003. Abnormal blood vessel development in mice lacking presenilin-1. *Mech Dev* 120:657-667.

243. El Khatib, M., Bozko, P., Palagani, V., Malek, N.P., Wilkens, L., and Plentz, R.R. 2013. Activation of Notch signaling is required for cholangiocarcinoma progression and is enhanced by inactivation of p53 in vivo. *PLoS One* 8:e77433.

244. McCarthy, J.V. 2005. Involvement of presenilins in cell-survival signalling pathways. *Biochem Soc Trans* 33:568-572.

245. Barten, D.M., Meredith, J.E., Jr., Zaczek, R., Houston, J.G., and Albright, C.F. 2006. Gamma-secretase inhibitors for Alzheimer's disease: balancing efficacy and toxicity. *Drugs R D* 7:87-97.

246. Milano, J., McKay, J., Dagenais, C., Foster-Brown, L., Pognan, F., Gadient, R., Jacobs, R.T., Zacco, A., Greenberg, B., and Ciaccio, P.J. 2004. Modulation of notch processing by gamma-secretase inhibitors causes intestinal goblet cell metaplasia and induction of genes known to specify gut secretory lineage differentiation. *Toxicol Sci* 82:341-358.

247. Real, P.J., Tosello, V., Palomero, T., Castillo, M., Hernando, E., de Stanchina, E., Sulis, M.L., Barnes, K., Sawai, C., Homminga, I., et al. 2009. Gamma-secretase inhibitors reverse glucocorticoid resistance in T cell acute lymphoblastic leukemia. *Nat Med* 15:50-58.

248. Tolcher, A.W., Messersmith, W.A., Mikulski, S.M., Papadopoulos, K.P., Kwak, E.L., Gibbon, D.G., Patnaik, A., Falchook, G.S., Dasari, A., Shapiro, G.I., et al. 2012. Phase I study of RO4929097, a gamma secretase inhibitor of Notch signaling, in patients with refractory metastatic or locally advanced solid tumors. *J Clin Oncol* 30:2348-2353.

249. Krop, I., Demuth, T., Guthrie, T., Wen, P.Y., Mason, W.P., Chinnaiyan, P., Butowski, N., Groves, M.D., Kesari, S., Freedman, S.J., et al. 2012. Phase I pharmacologic and pharmacodynamic study of the gamma secretase (Notch) inhibitor MK-0752 in adult patients with advanced solid tumors. *J Clin Oncol* 30:2307-2313.

250. Strosberg, J.R., Yeatman, T., Weber, J., Coppola, D., Schell, M.J., Han, G., Almhanna, K., Kim, R., Valone, T., Jump, H., et al. 2012. A phase II study of RO4929097 in metastatic colorectal cancer. *Eur J Cancer* 48:997-1003.

251. Fouladi, M., Stewart, C.F., Olson, J., Wagner, L.M., Onar-Thomas, A., Kocak, M., Packer, R.J., Goldman, S., Gururangan, S., Gajjar, A., et al. 2011. Phase I trial of MK-0752 in children with refractory CNS malignancies: a pediatric brain tumor consortium study. *J Clin Oncol* 29:3529-3534.

252. Kopan, R., and Weintraub, H. 1993. Mouse notch: expression in hair follicles correlates with cell fate determination. *J Cell Biol* 121:631-641.

253. Joutel, A., Andreux, F., Gaulis, S., Domenga, V., Cecillon, M., Battail, N., Piga, N., Chapon, F., Godfrain, C., and Tournier-Lasserve, E. 2000. The ectodomain of the Notch3 receptor accumulates within the cerebrovasculature of CADASIL patients. *J Clin Invest* 105:597-605.

254. Felli, M.P., Maroder, M., Mitsiadis, T.A., Campese, A.F., Bellavia, D., Vacca, A., Mann, R.S., Frati, L., Lendahl, U., Gulino, A., et al. 1999. Expression pattern of notch1, 2 and 3 and Jagged1 and 2 in lymphoid and stromal thymus components: distinct ligand-receptor interactions in intrathymic T cell development. *Int Immunol* 11:1017-1025.

255. Anastasi, E., Campese, A.F., Bellavia, D., Bulotta, A., Balestri, A., Pascucci, M., Checquolo, S., Gradini, R., Lendahl, U., Frati, L., et al. 2003. Expression of activated Notch3 in transgenic mice enhances generation of T regulatory cells and protects against experimental autoimmune diabetes. *J Immunol* 171:4504-4511.

256. Domenga, V., Fardoux, P., Lacombe, P., Monet, M., Maciazek, J., Krebs, L.T., Klonjkowski, B., Berrou, E., Mericskay, M., Li, Z., et al. 2004. Notch3 is

required for arterial identity and maturation of vascular smooth muscle cells. *Genes Dev* 18:2730-2735.

257. Krebs, L.T., Xue, Y., Norton, C.R., Sundberg, J.P., Beatus, P., Lendahl, U., Joutel, A., and Gridley, T. 2003. Characterization of Notch3-deficient mice: normal embryonic development and absence of genetic interactions with a Notch1 mutation. *Genesis* 37:139-143.

258. Joutel, A., Corpechot, C., Ducros, A., Vahedi, K., Chabriat, H., Mouton, P., Alamowitch, S., Domenga, V., Cecillion, M., Marechal, E., et al. 1996. Notch3 mutations in CADASIL, a hereditary adult-onset condition causing stroke and dementia. *Nature* 383:707-710.

259. Monet, M., Domenga, V., Lemaire, B., Souilhol, C., Langa, F., Babinet, C., Gridley, T., Tournier-Lasserve, E., Cohen-Tannoudji, M., and Joutel, A. 2007. The archetypal R90C CADASIL-NOTCH3 mutation retains NOTCH3 function in vivo. *Hum Mol Genet* 16:982-992.

260. Lacombe, P., Oligo, C., Domenga, V., Tournier-Lasserve, E., and Joutel, A. 2005. Impaired cerebral vasoreactivity in a transgenic mouse model of cerebral autosomal dominant arteriopathy with subcortical infarcts and leukoencephalopathy arteriopathy. *Stroke* 36:1053-1058.

261. Dang, T.P., Eichenberger, S., Gonzalez, A., Olson, S., and Carbone, D.P. 2003. Constitutive activation of Notch3 inhibits terminal epithelial differentiation in lungs of transgenic mice. *Oncogene* 22:1988-1997.

262. Serafin, V., Persano, L., Moserle, L., Esposito, G., Ghisi, M., Curtarello, M., Bonanno, L., Masiero, M., Ribatti, D., Sturzl, M., et al. 2011. Notch3 signalling promotes tumour growth in colorectal cancer. *J Pathol* 224:448-460.

263. Jung, S.G., Kwon, Y.D., Song, J.A., Back, M.J., Lee, S.Y., Lee, C., Hwang, Y.Y., and An, H.J. 2010. Prognostic significance of Notch 3 gene expression in ovarian serous carcinoma. *Cancer Sci* 101:1977-1983.

264. Park, J.T., Li, M., Nakayama, K., Mao, T.L., Davidson, B., Zhang, Z., Kurman, R.J., Eberhart, C.G., Shih Ie, M., and Wang, T.L. 2006. Notch3 gene amplification in ovarian cancer. *Cancer Res* 66:6312-6318.

265. Yeasmin, S., Nakayama, K., Rahman, M.T., Rahman, M., Ishikawa, M., Iida, K., Otsuki, Y., Kobayashi, H., Nakayama, S., and Miyazaki, K. 2010. Expression of nuclear Notch3 in cervical squamous cell carcinomas and its association with adverse clinical outcomes. *Gynecol Oncol* 117:409-416.

266. Bellavia, D., Campese, A.F., Checquolo, S., Balestri, A., Biondi, A., Cazzaniga, G., Lendahl, U., Fehling, H.J., Hayday, A.C., Frati, L., et al. 2002. Combined expression of pTalpha and Notch3 in T cell leukemia identifies the requirement of preTCR for leukemogenesis. *Proc Natl Acad Sci U S A* 99:3788-3793.

267. Konishi, J., Kawaguchi, K.S., Vo, H., Haruki, N., Gonzalez, A., Carbone, D.P., and Dang, T.P. 2007. Gamma-secretase inhibitor prevents Notch3 activation and reduces proliferation in human lung cancers. *Cancer Res* 67:8051-8057.

268. Sullivan, J.P., Spinola, M., Dodge, M., Raso, M.G., Behrens, C., Gao, B., Schuster, K., Shao, C., Larsen, J.E., Sullivan, L.A., et al. 2010. Aldehyde dehydrogenase activity selects for lung adenocarcinoma stem cells dependent on notch signaling. *Cancer Res* 70:9937-9948.

269. Minucci, S., and Pelicci, P.G. 2006. Histone deacetylase inhibitors and the promise of epigenetic (and more) treatments for cancer. *Nat Rev Cancer* 6:38-51.

270. Zhang, X., Tang, N., Hadden, T.J., and Rishi, A.K. 2011. Akt, FoxO and regulation of apoptosis. *Biochim Biophys Acta* 1813:1978-1986.

271. Sun, X., and Artavanis-Tsakonas, S. 1997. Secreted forms of DELTA and SERRATE define antagonists of Notch signaling in Drosophila. *Development* 124:3439-3448.

272. Wu, Y., Cain-Hom, C., Choy, L., Hagenbeek, T.J., de Leon, G.P., Chen, Y., Finkle, D., Venook, R., Wu, X., Ridgway, J., et al. 2010. Therapeutic antibody targeting of individual Notch receptors. *Nature* 464:1052-1057.

273. Li, K., Li, Y., Wu, W., Gordon, W.R., Chang, D.W., Lu, M., Scoggin, S., Fu, T., Vien, L., Histen, G., et al. 2008. Modulation of Notch signaling by antibodies

specific for the extracellular negative regulatory region of NOTCH3. *J Biol Chem* 283:8046-8054.

274. West, A.C., and Johnstone, R.W. 2014. New and emerging HDAC inhibitors for cancer treatment. *J Clin Invest* 124:30-39.

275. Lin, L., Mernaugh, R., Yi, F., Blum, D., Carbone, D.P., and Dang, T.P. 2010. Targeting specific regions of the Notch3 ligand-binding domain induces apoptosis and inhibits tumor growth in lung cancer. *Cancer Res* 70:632-638.

276. Raimondi, L., Ciarapica, R., De Salvo, M., Verginelli, F., Gueguen, M., Martini, C., De Sio, L., Cortese, G., Locatelli, M., Dang, T.P., et al. 2012. Inhibition of Notch3 signalling induces rhabdomyosarcoma cell differentiation promoting p38 phosphorylation and p21(Cip1) expression and hampers tumour cell growth in vitro and in vivo. *Cell Death Differ* 19:871-881.

277. Sade, H., Krishna, S., and Sarin, A. 2004. The anti-apoptotic effect of Notch-1 requires p56lck-dependent, Akt/PKB-mediated signaling in T cells. *J Biol Chem* 279:2937-2944.

278. Palomero, T., Sulis, M.L., Cortina, M., Real, P.J., Barnes, K., Ciofani, M., Caparros, E., Buteau, J., Brown, K., Perkins, S.L., et al. 2007. Mutational loss of PTEN induces resistance to NOTCH1 inhibition in T-cell leukemia. *Nat Med* 13:1203-1210.

279. Stella, M.C., Trusolino, L., Pennacchietti, S., and Comoglio, P.M. 2005. Negative feedback regulation of Met-dependent invasive growth by Notch. *Mol Cell Biol* 25:3982-3996.

280. Rusconi, J.C., and Corbin, V. 1998. Evidence for a novel Notch pathway required for muscle precursor selection in Drosophila. *Mech Dev* 79:39-50.

281. Shawber, C., Nofziger, D., Hsieh, J.J., Lindsell, C., Bogler, O., Hayward, D., and Weinmaster, G. 1996. Notch signaling inhibits muscle cell differentiation through a CBF1-independent pathway. *Development* 122:3765-3773.

282. Andersen, P., Uosaki, H., Shenje, L.T., and Kwon, C. 2012. Non-canonical Notch signaling: emerging role and mechanism. *Trends Cell Biol* 22:257-265.

283. Hing, H.K., Sun, X., and Artavanis-Tsakonas, S. 1994. Modulation of wingless signaling by Notch in Drosophila. *Mech Dev* 47:261-268.

284. Rangarajan, A., Talora, C., Okuyama, R., Nicolas, M., Mammucari, C., Oh, H., Aster, J.C., Krishna, S., Metzger, D., Chambon, P., et al. 2001. Notch signaling is a direct determinant of keratinocyte growth arrest and entry into differentiation. *EMBO J* 20:3427-3436.

285. Hayward, P., Brennan, K., Sanders, P., Balayo, T., DasGupta, R., Perrimon, N., and Martinez Arias, A. 2005. Notch modulates Wnt signalling by associating with Armadillo/beta-catenin and regulating its transcriptional activity. *Development* 132:1819-1830.

286. Kwon, C., Qian, L., Cheng, P., Nigam, V., Arnold, J., and Srivastava, D. 2009. A regulatory pathway involving Notch1/beta-catenin/Isl1 determines cardiac progenitor cell fate. *Nat Cell Biol* 11:951-957.

287. Munoz-Descalzo, S., Tkocz, K., Balayo, T., and Arias, A.M. 2011. Modulation of the ligand-independent traffic of Notch by Axin and Apc contributes to the activation of Armadillo in Drosophila. *Development* 138:1501-1506.

288. Ridgway, J., Zhang, G., Wu, Y., Stawicki, S., Liang, W.C., Chanthery, Y., Kowalski, J., Watts, R.J., Callahan, C., Kasman, I., et al. 2006. Inhibition of Dll4 signalling inhibits tumour growth by deregulating angiogenesis. *Nature* 444:1083-1087.

289. Henderson, N.C., Arnold, T.D., Katamura, Y., Giacomini, M.M., Rodriguez, J.D., McCarty, J.H., Pellicoro, A., Raschperger, E., Betsholtz, C., Ruminski, P.G., et al. 2013. Targeting of alphav integrin identifies a core molecular pathway that regulates fibrosis in several organs. *Nat Med* 19:1617-1624.

290. Jung, J., Zheng, M., Goldfarb, M., and Zaret, K.S. 1999. Initiation of mammalian liver development from endoderm by fibroblast growth factors. *Science* 284:1998-2003.

291. Rossi, J.M., Dunn, N.R., Hogan, B.L., and Zaret, K.S. 2001. Distinct mesodermal signals, including BMPs from the septum transversum

mesenchyme, are required in combination for hepatogenesis from the endoderm. *Genes Dev* 15:1998-2009.

292. Matsumoto, K., Yoshitomi, H., Rossant, J., and Zaret, K.S. 2001. Liver organogenesis promoted by endothelial cells prior to vascular function. *Science* 294:559-563.

293. Kamiya, A., Kinoshita, T., Ito, Y., Matsui, T., Morikawa, Y., Senba, E., Nakashima, K., Taga, T., Yoshida, K., Kishimoto, T., et al. 1999. Fetal liver development requires a paracrine action of oncostatin M through the gp130 signal transducer. *EMBO J* 18:2127-2136.

294. Bossard, P., and Zaret, K.S. 1998. GATA transcription factors as potentiators of gut endoderm differentiation. *Development* 125:4909-4917.

295. Lokmane, L., Haumaitre, C., Garcia-Villalba, P., Anselme, I., Schneider-Maunoury, S., and Cereghini, S. 2008. Crucial role of vHNF1 in vertebrate hepatic specification. *Development* 135:2777-2786.

296. Gualdi, R., Bossard, P., Zheng, M., Hamada, Y., Coleman, J.R., and Zaret, K.S. 1996. Hepatic specification of the gut endoderm in vitro: cell signaling and transcriptional control. *Genes Dev* 10:1670-1682.

297. Shiojiri, N., Lemire, J.M., and Fausto, N. 1991. Cell lineages and oval cell progenitors in rat liver development. *Cancer Res* 51:2611-2620.

298. Kyrmizi, I., Hatzis, P., Katrakili, N., Tronche, F., Gonzalez, F.J., and Talianidis, I. 2006. Plasticity and expanding complexity of the hepatic transcription factor network during liver development. *Genes Dev* 20:2293-2305.

299. Benhamouche, S., Decaens, T., Godard, C., Chambrey, R., Rickman, D.S., Moinard, C., Vasseur-Cognet, M., Kuo, C.J., Kahn, A., Perret, C., et al. 2006. Apc tumor suppressor gene is the "zonation-keeper" of mouse liver. *Dev Cell* 10:759-770.

300. Spence, J.R., Lange, A.W., Lin, S.C., Kaestner, K.H., Lowy, A.M., Kim, I., Whitsett, J.A., and Wells, J.M. 2009. Sox17 regulates organ lineage segregation of ventral foregut progenitor cells. *Dev Cell* 17:62-74.

301. Fukuda, A., Kawaguchi, Y., Furuyama, K., Kodama, S., Horiguchi, M., Kuhara, T., Koizumi, M., Boyer, D.F., Fujimoto, K., Doi, R., et al. 2006. Ectopic pancreas formation in Hes1 -knockout mice reveals plasticity of endodermal progenitors of the gut, bile duct, and pancreas. *J Clin Invest* 116:1484-1493.